
Università degli Studi di Cagliari

DIPARTIMENTO DI FISICA

Scuola di Dottorato di Ricerca in Fisica
XIX Ciclo

# Aspects of Black Hole Physics:
## Scalar Sources, Holography and Gravitational Wave Emission

Settore scientifico disciplinare di afferenza: FIS/02

Presentata da:
Edgardo Franzin

Coordinatore Dottorato:
Prof. Alessandro de Falco

Tutor:
Prof. Mariano Cadoni

Esame finale anno accademico 2015–2016

# Aspects of Black Hole Physics:

## Scalar Sources, Holography and Gravitational Wave Emission

# Abstract

We investigate several aspects of black hole physics. First, we consider models of gravity minimally coupled to scalar fields. We derive a new class of asymptotically flat black holes sourced by a non-trivial asymptotically massless scalar field; we discuss their relationship with known solutions and standard no-hair theorems and their thermodynamics. We derive exact neutral and charged brane solutions sourced by a scalar field with vanishing potential, which are conformal to the Lifšic spacetime; we discuss the symmetries and their holographic application for hyperscaling violation; we also give a quite general classification of brane solutions sourced by scalar fields useful for holographic applications. We study an inflationary model inspired by the domain wall/cosmology correspondence in which inflation is driven by a scalar with a two-exponential potential; we derive its phenomenological consequences in the slow-roll approximation and compare its predictions with the Planck 2015 data. Second, we investigate ultra-compact astrophysical objects which can act as black hole mimickers, in particular boson stars and wormholes. We discuss the existence and the stability of boson stars in higher dimensions and boson stars built with multiple scalars. We compute tidal Love numbers for various mimickers and discuss how to distinguish black holes from their possible mimickers with gravitational-wave data. We study the gravitational radiation emitted by a particle falling into an exotic compact object and show that the initial ringdown signal cannot be use distinguish between a black hole and a black hole mimicker.

Key words: black holes; scalar fields; hairy black holes; black branes; holography; inflation; black hole mimickers; boson stars; wormholes; tidal Love numbers; gravitational waves.

# Contents

# Preface

The work presented in this thesis was mainly carried out at the Physics Department of the University of Cagliari in the triennium 2014–2016 and at the Centro Multidisciplinar de Astrofísica (CENTRA) of the Instituto Superior Técnico in Lisbon from September 2015 to May 2016.

## List of papers included in this thesis

Chapter 2 is the result of a collaboration with Mariano Cadoni. It is based on the following paper:

> M. Cadoni and E.F. 'Asymptotically flat black holes sourced by a massless scalar field'. *Phys. Rev.* D91 (2015), 104011. arXiv: 1503.04734.

Chapter 3 is the result of a collaboration with Mariano Cadoni and Matteo Serra. It is based on the following paper:

> M. Cadoni, E.F., and M. Serra. 'Brane solutions sourced by a scalar with vanishing potential and classification of scalar branes'. *J. High Energy Phys.* 1601 (2016), 125. arXiv: 1511.03986.

Chapter 4 is the result of a collaboration with Mariano Cadoni and Salvatore Mignemi. It is based on the following paper:

> M. Cadoni, E.F., and S. Mignemi. 'Inflation as de Sitter instability'. *Eur. Phys. J.* C76 (2016), 483. arXiv: 1510.04030.

Chapter 7 is the result of a collaboration with Vítor Cardoso, Andrea Maselli, Paolo Pani and Guilherme Raposo. It is based on the following paper:

> V. Cardoso, E.F., A. Maselli, P. Pani, and G. Raposo. 'Testing strong-field gravity with tidal Love numbers'. (2017). arXiv: 1701.01116.

Chapter 8 is the result of a collaboration with Vítor Cardoso and Paolo Pani. It is based on the following letter:

> V. Cardoso, E.F., and P. Pani. 'Is the gravitational-wave ringdown a probe of the event horizon?' *Phys. Rev. Lett.* 116 (2016), 171101. arXiv: 1602.07309. Erratum: *ibid.* 117 (2016), 089902.

# Notation and Acronyms

In this work we mainly use natural units $c = G = 1$ and we adopt the $(-,+,+,+)$ convention for the signature of the metric. At the beginning of each chapter we remind the adopted conventions. In general, a dot represents derivation with respect to time and a prime derivation with respect to the radial coordinate.
We tried to avoid acronyms as much as possible. Some of them belong to every physicist dictionary, e.g. AdS (anti de Sitter) and QFT (quantum field theory). Others may appear in same plots and equations.

ADM Arnowitt-Deser-Misner

BH Black hole

CFT Conformal field theory

GW Gravitational wave

QNM Quasi-normal mode

WH Wormhole

Colophon: Typeset by the author in EB Garamond using XeLaTeX and BibLaTeX.

# Introduction and Summary

The triennium during which we worked on this thesis has been abundant of discoveries and anniversaries: the discovery of gravitational waves by the LIGO and Virgo collaborations [1, 2], the centenary of Einstein's general theory of relativity [3–6], the centenary of the Schwarzschild solution [7], the constraints on inflation put by the Planck collaboration [8]. They have been important years for the research on gravity and, in particular, for Einstein's general relativity[1] which has got further experimental and theoretical confirmations of its validity as classical theory of gravity. Einstein theory is described by the action

$$\mathcal{A} = \frac{1}{16\pi G}\int \mathrm{d}^4x\,\sqrt{-g}\,(\mathcal{R}-2\Lambda) + \mathcal{A}_{\mathrm{m}}\,(g_{\mu\nu},\psi)\,, \tag{1}$$

where $g$ is the spacetime metric, $\mathcal{R}$ is the scalar curvature, $\Lambda$ is a (possible) cosmological constant and $\mathcal{A}_{\mathrm{m}}$ is the matter action that depends generically on the metric and all matter fields $\psi$.

The classical theoretical predictions of general relativity have been tested with high accuracy and on scales ranging from the millimeter up to galactic scales, from the historical ones — precession of planetary orbits, bending of light, gravitational redshift — to the very recent detection of gravitational waves produced by the coalescence of a black hole binary [9].

Yet, general relativity is a classical theory and needs corrections at short distances, where quantum effects become important. Until now, all the attempts to unificate general relativity with quantum mechanics are not completely satisfactory. From a quantum field theory point of view, general relativity is non-renormalisable,[2] and it has been argued that general relativity is an effective theory that necessitates an ultraviolet completion, if not before, at least when we reach energies of the order of the Planck mass, e.g. string theory or loop quantum gravity.

There are also strong arguments, both theoretical and experimental, for high-energy corrections to general relativity. For instance, high-energy, or high-curvature corrections, might also prevent the formation of singularities, which has been shown to be unavoidable in classical general relativity [11].

Cosmological measurements of the galaxy rotation curves and gravitational lensing observations have taught us that also in the far infrared, at large scales, there is some tension between general relativity and observations. This tension can be solved by assuming that in the Universe there exists

1. See e.g. the Classical and Quantum Gravity Focus Issue on 'Milestones of General Relativity' and the American Physical Society 'General Relativity's Centennial'.

2. Stelle showed that terms quadratic in the curvature tensor make gravity renormalisable [10].

something that is invisible to electromagnetic instruments but interacts *only* gravitationally: dark matter. Dark matter is now also a necessary ingredient in models of structure formations and to explain the current composition of our Universe. Cosmological observations provide as well evidence for the (accelerated) expansion of the Universe, and general relativity cannot explain what drives this acceleration, unless we introduce a mysterious form of energy: dark energy. In quantum field theory, the vacuum energy is not zero, and it might drive accelerated expansion. But we have a naturalness problem: according to quantum field theory, the value of the vacuum energy — the cosmological constant — is at least sixty order of magnitude bigger than the observed value!

Despite these problems at very small and very large distances, general relativity works incredibly well at intermediate distances. Solar system test and binary pulsar experiments verify Einstein's equivalence principle, set the parametrised post-Newtonian parameters [12] very close to those of general relativity and give stringent bounds on, for instance, scalar-tensor theories and Lorentz-violating theories. Hence, any modified theory of gravity which introduces new degrees of freedom and/or new interaction terms in the gravitational sector must modify the theory at low and high energies but reproduce general relativity at intermediate energies.

There exists a large number of modified theories of gravity. In scalar-tensor theories, such as Brans-Dicke [13] or Horndeski [14], gravity is non-minimally coupled with scalar field(s). These theories arise from string theory to cosmology and they are useful for phenomenological aspects [15, 16]. Another possible way to modify general relativity without introducing other fields is to substitute the scalar curvature in Eq. (1) with a generic function of it, to obtain $f(\mathcal{R})$ gravity [17–19]. A famous application of such a theory has been used by Starobinky in his groundbreaking paper on inflation. Other extensions include Lorentz-violating theories, massive gravity theories, and theories involving non-dynamical fields — for some reviews, see e.g. Refs. [20–23].

Nevertheless, except for binary pulsar observations, all tests of general relativity were in the weak-field regime. Fortunately, the first direct gravitational-wave detection of a compact binary coalescence, has opened up the possibility of testing gravity in strong regimes [24–26]. Already, the differences between the prediction of general relativity and the signal detected by Advanced LIGO put constraints on non-standard mechanisms (e.g. the activation of scalar fields, gravitational leakage into large extra dimensions, the variability of Newton's constant, the speed of gravity, a modified dispersion relation, gravitational Lorentz violation and the strong equivalence principle) that could be responsible for such anomalies [27].

Gravitational-wave events can also constrain or rule out exotic alternatives to Kerr black holes.[3] Even without adducing exotic alternatives, the Kerr metric — which describes a rotating black hole — appears as a vacuum solution in many modified theories of gravity, but the details of the dynamics and the gravitational-wave emission might be able to discriminate among theories. Black holes (and

3. Notice that, however, to perform such an analysis we would need a complete understanding of the full evolution of an exotic binary, while the current templates are based on general relativity.

neutron stars) are indeed the best laboratory to study gravity in extreme regimes. It will also be possible to test the strange property of black holes of being described only by few parameters, the so-called no-hair conjecture. To do so, it is important to study the dynamics of fields in black holes backgrounds.

It has been argued that the gravitational waves signals may also be an indirect effect of dark matter, i.e. LIGO observed the merge of two primordial black holes rather than two stellar black holes [28, 29].

In recent years, the theoretical research on gravity has seen exciting developments in a rather different perspective, namely that of the holographic character of the gravitational interaction. In the last two decades, the AdS/CFT correspondence and the holographic principle had increased both the knowledge on strongly coupled quantum field theories and condensed matter systems (e.g. holographic superconductors [30–33] and the universality of the shear viscosity to entropy density ratio [34, 35]), and the understanding of gravity itself (e.g. the microscopic origin of the black hole entropy [36], the information puzzle [37–40] and entanglement entropy [41, 42]).

It is more than desirable that both the more phenomenological and the more speculative research areas could communicate and cross-fertilise themselves. For instance, choosing an example that we will discuss in detail in this thesis, gravitational solutions sourced by scalar fields play a fundamental role in cosmological models, the uniqueness of black holes, and act as order parameters breaking symmetry and generating phase transitions in holographically dual quantum field theories. This is a very interesting point showing that most of the recent progress in the holographic applications of gravity is essentially based on the violation of old no-hair theorems. This cross-fertilisation appears even more compelling if one considers that shortly, gravitational-wave observations could open an observational window in the quantum regime of gravity, e.g. through quantum signatures of a black hole horizons.

This thesis represents an attempt in this direction. We will focus the research on two concepts that play a fundamental role in different parts of black hole physics and more generally in gravitational physics: scalar sources and black hole perturbation theory. We will investigate several topics, which, in some sense, represent a bridge between different research areas. Concerning the first concept, we will investigate the implications of the no-hair theorem, holographically dual quantum field theories and cosmological inflation. The second concept will be used to study the stability and the tidal deformations of black hole mimickers; we will also give a critical discussion on gravitational-wave data from black hole merging.

In Part I, we discuss several gravitational systems coupled with scalar fields. We will derive and discuss a variety of gravitational solutions sourced by non-trivial scalar field configurations: black holes, black branes and cosmological solutions describing inflation. This might allow checking if the no-hair conjecture is correct and will allow putting constraints on alternative theories of gravity. If

these scalars imply different black hole spacetimes from those of general relativity or if they predict new phenomena, they could be detected. Also, black hole spacetimes are a perfect laboratory to test and detect fundamental scalar fields [43, 44]. Massive scalar or pseudo-scalars are a theoretically appealing candidate of dark matter and dark energy, which are predicted to arise in a variety of scenarios [45]. Complex scalar fields coupled to general relativity give rise to self-gravitating bosonic configurations, known as boson stars. On the experimental side, the study of scalar fields is strongly supported by the recent discovery of the Higgs particle at Large Hadron Collider [46, 47]. Moreover, scalar particles can drive inflation. This has been corroborated by the observations of the Planck 2015 satellite which give a striking confirmation of cosmological inflation. Eventually, gravity coupled to matter fields, and in particular scalars, are of special interest for their holographic applications, where hairy black holes can be used to describe symmetry breaking or phase transitions in the dual quantum field theory. In Chapter 2, we derive asymptotically flat black hole solutions with scalar hair using a solution generating technique developed in the holographic context. We discuss their relation with standard no-hair theorems and already known solutions, and we also investigate their thermodynamics. In Chapter 3, we derive exact brane solutions of minimally coupled Einstein-Maxwell-scalar gravity with a vanishing scalar potential and we show that these solutions are conformal to the Lifšic spacetime whose dual quantum field theory is characterised by hyperscaling violation. We also give a quite general classification of brane solutions sourced by scalar fields in the general relativity context, which may be very useful for holographic applications. In Chapter 4, inspired by holography, we study the most general model of hilltop inflation in which the potential is written as the sum of two exponentials. In the slow-roll approximation, our model can correctly reproduce the most recent Planck data and it predicts inflation at energy scales of four to five orders of magnitude below the Planck scale.

In Part II, we take a critical look at the new gravitational-wave data. To assure the scientificity of a theory, its verifiability, i.e. the capacity to predict testable phenomena, is not a sufficient criterion. The theory must also be falsifiable, i.e. it can be proven wrong. This approach might both individuate fallacies in general relativity and exclude or constrain alternative theories. For instance, black holes are the most feasible candidate for dark compact objects, but this cannot be turned into a paradigm. Data will allow testing the models to discriminate among black holes and other possible compact objects and to shed light on their nature and internal structure. Here, numerical simulations of binary systems not being black holes or neutron stars are indispensable. In Chapter 6, we study mini boson stars in five spacetime dimensions and boson stars built with various scalars. We show that the former are always dynamically unstable, while the latter are stable for a broad range of the parameters space. In Chapter 7, we compute axial and polar tidal Love numbers for boson stars, wormholes and gravastars and we discuss their possible detection. In Chapter 8, we investigate the gravitational radiation emitted by a point particle in radial motion towards a traversable wormhole and we compare it to that of a Schwarzschild black hole. We show that, if the wormhole is compact enough, the distinction in the initial ringdown signal of the emitted gravitational wave is irrelevant.

# Part I

# Scalar Hair, Holography and Cosmology

# Chapter 1

*Introduction to Part I*

# Scalar Fields Coupled to Gravity

Gravity coupled to scalar fields is interesting for several reasons. First, in order to verify the no-hair conjecture — the fact that black holes are characterised only by their asymptotic charges: mass, electric charge and angular momentum — it is important to study the dynamics of scalar fields in black hole backgrounds. Second, in the context of the AdS/CFT correspondence, the holographic interpretation of scalar fields allows for the description of various phenomena. And finally, a simple scalar field could drive inflation and solve fundamental problems in standard cosmology. The first part of this thesis is devoted to the investigation of these three issues.

## 1.1 Black Holes

Black holes are what is left after a complete gravitational collapse and they are a fascinating subject for physicists and not [48]. They are extreme-curvature regions of the spacetime from which not even light can escape. Although in the beginning they were considered simply as mathematical solutions to the Einstein's field equations, nowadays although we do not have yet a direct evidence of an event horizon, there is a huge observational evidence of their existence. and they found applications in the most different branches of physics, e.g. in mathematical physics as solutions to the Einstein's equations; in astrophysics, where along with neutron stars, they represent the best laboratory to test strong gravity; in holographic applications.

The Schwarzschild metric [7]

$$\mathrm{d}s^2 = -\left(1-\frac{2M}{r}\right)\mathrm{d}t^2 + \left(1-\frac{2M}{r}\right)^{-1}\mathrm{d}r^2 + r^2\left(\mathrm{d}\vartheta^2 + \sin^2\vartheta\,\mathrm{d}\varphi^2\right), \tag{1.1}$$

describes a black hole of mass $M$ but also, for $r > 2M$, the exterior geometry of any object with the same mass. Most of the experimental tests of general relativity are based on this simple geometry.

The Kerr metric [49], discovered almost fifty years later, decribes the spacetime outside a massive

and spinning black hole. In Boyer-Lindquist coordinates, the metric is

$$\begin{aligned} \mathrm{d}s^2 = &- \left(1 - \frac{2Mr}{\Sigma}\right) \mathrm{d}t^2 - \frac{4Mra\sin^2\vartheta}{\Sigma}\,\mathrm{d}t\,\mathrm{d}\phi + \frac{\Sigma}{\Delta}\,\mathrm{d}r^2 + \Sigma\,\mathrm{d}\vartheta^2 \\ &+ \left(\frac{2Mra^2\sin^2\vartheta}{\Sigma} + r^2 + a^2\right)\sin^2\vartheta\,\mathrm{d}\phi^2\,, \end{aligned} \tag{1.2}$$

where $a = J/M$ is the total angular momentum per unit mass, $\Delta = r^2 - 2Mr + a^2$ and $\Sigma = r^2 + a^2\cos^2\vartheta$.

Both the Schwarzschild and the Kerr solutions have been generalised to the charged case, respectively, by Reissner and Nordström [50, 51] and Newman et al. [52]. Astrophysical black holes are very unlikely charged because they would attract opposite charges and get neutral. In any case, the black hole metric depends — at most — on its mass, electric charge and angular momentum, and in case on other charges associated with other internal global symmetries. All the details about the matter that composes the black hole are lost and no observer could distinguish two black holes generated by the collapse of different matter if they turn out to have the same mass and angular momentum. This characteristic and the following formulation of no-hair theorems will be discussed in Section 1.2.

Another curious feature of black holes is that the laws of black hole dynamics resemble those of thermodynamics, which is characterised by a small number of parameters as well [53, 54]. The event horizon surface area always increases when the black hole undergoes any transformation [55], but this general theorem of differential geometry is nothing more than an analogy with the second law of thermodynamics which has a statistical origin. On the one hand, when a body falls into a black hole, the information is irretrievably lost and Bekenstein [56] conjectured that a suitable multiple of the black hole event horizon area might be interpreted as its entropy (in physical units),

$$S_{\mathrm{BH}} = \frac{k_B c^3 A}{4\hbar G}\,. \tag{1.3}$$

On the other hand, classical black holes are perfect absorbers but they do not emit anything, so their physical temperature is absolute zero and it would make no physical sense in associating an entropy to a black hole. However, these formal correspondences become physical when we turn classical general relativity into semi-classical and we consider quantum effects. The physical temperature of a black hole is no longer absolute zero, but rather the Hawking temperature [57], which for the Schwarzschild black hole is (in physical units)

$$T_{\mathrm{H}} = \frac{\hbar c^3}{8\pi G k_B M}\,. \tag{1.4}$$

This equation contains almost all the fundamental physical constants and for this reason we could say that black holes are 'meeting point' of gravity, quantum mechanics and statistical mechanics.

## 1.2 No-Hair Theorems

At the turn of the Seventies, the issue of the uniqueness of the Schwarzschild and Kerr black holes and their charged extensions [58–62], has motivated the formulation of no-hair theorems [63, 64]. Black holes are characterised only by three parameters — the mass, the electric charge and the angular momentum — and they cannot have other 'hairs', i.e. the external description of a stationary black hole cannot depend on other fields or quantum numbers.

During the Nineties, several stable hairy black hole solutions have been discovered [65–70], for a review, see e.g. Ref. [71]. The peculiarity of these solutions is that the hairs are non-Abelian gauge fields. Nevertheless, Abelian and scalar fields are different and this has led to the formulation of no-scalar-hair theorems. Originally, they forbid regular hairy black hole solutions in the case of a convex and, more generally, semi-positive definite potential scalar potential [72–74].

Later, it was discovered that also some low-energy string models allow for black hole solutions with scalar hair [75–79]. Nevertheless, the existence of these solutions remains limited to gravity theories with non-minimal couplings between the scalar and the electromagnetic fields. This has led to recent no-hair theorems [80, 81] that state the absence of regular hairy black hole solutions if the scalar-gravity theory satisfies the positive energy theorem [82, 83], i.e. the ADM energy is positive definite. In spite of these advances on the side of hairy black hole solutions with AdS asymptotics, progress in the search for asymptotically flat black holes with scalar hair has been achieved only recently [84–90].

What about astrophysical black holes? In order to test whether the spacetime around a black hole is described by the Kerr geometry, we need to observe stars orbiting around a black hole or the gravitational-wave emission due to the coalescence of two black holes. The first is a non-dynamical test that allows probing the background spacetime in the weak-field regime, while the second, which involves a dynamical event, could tell us about the dynamics of the spacetime, and then to probe different theories [25, 91–94].

The existence of no-hair theorems is a particularly puzzling issue in view of the huge entropy (1.3) associated with the black hole. If we assume that Eq. (1.3) has a statistical interpretation *à la* Boltzmann, it must correspond to a huge degeneration of the black hole considered as a thermodynamical system. It is still a mystery why such a system characterised by a bunch of charges could be so degenerate. It is likely that answering to this question would require understanding quantum gravity and the holographic nature of gravity.

## 1.3 The Holographic Principle and the AdS/CFT Correspondence

In a quantum theory of gravity, the holographic principle is an idea of 't Hooft [95] that states that the information contained in spacetime region is encoded on its boundary. The current name is due to Susskind who promoted such an idea with a catchier name [96].

The argument of 't Hooft is fundamentally based on unitarity. Trying to conciliate gravitational collapse, i.e. the formation of a black hole, with the postulates of quantum mechanics, one finds that the spacetime at the Planck scale cannot be (3+1)-dimensional. Instead, the observables can be better described by a two-dimensional lattice evolving with time. This principle is closely related to the thermodynamics of black holes and in particular to the Bekenstein-Hawking formula (1.3), which relates the entropy of a black hole to the area of its horizon.

The AdS/CFT correspondence is probably the most famous realisation of the holographic principle and it is a conjectured equivalence between a higher-dimensional gravitational theory and a quantum field theory in less spacetime dimensions without gravity [97–99]. In Maldacena's original formulation [100], AdS is the gravitational theory and means type IIB string theory with $\mathrm{AdS}_5 \times \mathrm{S}^5$ boundary conditions, while CFT is a four-dimensional $\mathcal{N} = 4$ supersymmetric Yang-Mills quantum field theory. He considered a low energy limit of some branes in string theory where the field theory on the brane decouples from the bulk. Soon after, it has been formulated a precise correspondence between correlation functions in the gauge theory and those of supergravity on the boundary conditions [101, 102]. Alternatively, the duality can be formulated in terms of the partition function on the gravitational and field theory side.

One of the most remarkable features of this correspondence is that it is a strong/weak duality, i.e. strongly coupled gauge theories correspond to weakly interacting gravitational theories — which are easier to study for instance in perturbation theory. Thus, black holes and black branes (their planar counterparts) can unveil features and properties of apparently uncorrelated systems and vice-versa.

However, the gauge theory dual to $\mathrm{AdS}_5 \times \mathrm{S}^5$ is at zero temperature. A non-zero temperature would introduce an energy scale responsible of the conformal symmetry breaking and make standard calculations very complicated. Here is the power of the correspondence: the holographic dual of a quantum field theory at finite temperature is a black hole in the bulk with a given Hawking temperature. The other way round, a black hole is dual to a hot gas of fermions and gauge bosons. As a consequence, many problems in condensed matter physics and nuclear physics have been translated into problems of gravitational physics and string theory.

A simple extension of this correspondence introduces other fields in the bulk spacetime. Consider, for definiteness, Einstein-Maxwell-scalar gravity in $d + 2$ spacetime dimensions ($d \geqslant 2$). In its most general setting, this theory is characterised by three coupling functions: the self-interaction scalar potential $V(\phi)$, the gauge coupling function $Z(\phi)$, and the coupling function $S(\phi)$ responsible for the mass of the Maxwell field,

$$\mathcal{A} = \int \mathrm{d}^{d+2}x \sqrt{-g} \left( \mathcal{R} - Z(\phi)\, F^2 - S(\phi)\, A^2 - 2(\partial\phi)^2 - V(\phi) \right), \tag{1.5}$$

where $\mathcal{R}$ is the scalar curvature of the spacetime, $F$ is the electromagnetic tensor, $A$ is the 4-potential and $\phi$ a scalar field with scalar potential $V(\phi)$.

Using the rules of the AdS/CFT correspondence, and with the possibility of circumvent stan-

dard no-hair theorems owing to the AdS asymptotics,[1] plenty of black hole and black brane solutions — both analytical and numerical — in $d+2$ dimensions with various forms of the coupling functions have been discovered [104–114]. This strategy has allowed to uncover a very rich phenomenology for condensed matter systems, e.g. superconductors [30–33], holographic phase transitions [115, 116], quantum criticality [117–119], hyperscaling violation in critical systems [120–137], hydrodynamic regime of strongly coupled quantum field theories [138, 139] and entanglement entropy [140–143].

It is important to stress that the existence of solutions endowed with scalar hairs is a crucial ingredient to have this rich phenomenology in the dual QFT. In fact, the scalar field acts in the dual QFT has an order parameter generating through a non-vanishing vacuum expectation value of a scalar operator symmetry breaking and phase transitions. In the bulk, this corresponds to a non-trivial scalar field profile. This is a very interesting point showing that the recent progress in the holographic applications of gravity is essentially based on the violation of old no-hair theorems.

However, the essential qualitative features of the dual QFT are not pertinent to the presence of non-trivial coupling functions $Z(\phi)$ and $S(\phi)$ but are basically determined by the presence of a non-constant scalar field. In the dual QFT, the non-trivial profile of the scalar field plays the crucial role of an order parameter triggering symmetry breaking and/or phase transitions. For this reason, in the next chapters, we investigate solutions to the simplest theory, namely *minimally coupled* Einstein-Maxwell-scalar gravity, which is characterised by a single coupling function, the potential $V(\phi)$, whereas the other two are trivial, i.e. $Z(\phi) = 1$ and $S(\phi) = 0$.

Solitonic solutions interpolating between AdS vacua and domain wall solutions with scale-covariant symmetries in Einstein-scalar gravity are naturally related to cosmological solutions by the so-called domain wall/cosmology duality, a sort of analytic continuation which maps the soliton in a Friedmann-Robertson-Lamaître-Walker solution [144–146]. For example, the cosmological duals of solitons which interpolate between an AdS spacetime at large distances of the bulk theory (the ultraviolet of the dual QFT) and a scale-covariant geometry at small distances in the bulk theory (the infrared of the dual QFT) are natural candidates for describing dark energy [147]. As a second example, the cosmological duals of solitons interpolating between AdS in the infrared and scale-covariant geometries in the ultraviolet may be relevant for describing inflation [148]. This latter model has been generalised in Chapter 4.

## 1.4 Inflation

The last application that we briefly discuss in this chapter about scalars and gravity is cosmological inflation. In few words, inflation is a period in the early Universe during which the expansion was accelerated, which can be successful described by coupling a real scalar field (the inflaton) with gravity, i.e. quantum field theory in de Sitter space.

1. In the AdS spacetime, differently from the flat case, a scalar field may have tachyonic excitations, without destabilizing the vacuum [103].

Inflation has been introduced to solve some problems in the standard Friedmann-Robertson-Lamaître-Walker cosmology, such as the horizon and flatness problems [149–153], but it also explains why the universe *is* and *was not* homogeneous. However, the original models were plagued by some fundamental issues [154], and the solution came with the chaotic model [155]. In this scenario, inflation may start even if the early Universe was not in equilibrium, and does not demand any particular scalar potential. The only requirement is that the potential has a *plateau* allowing for the existence of the slow-roll regime.

According to Friedman's equation, to have accelerated expansion one needs negative pressure. The simplest field that can produce inflation is a scalar field, whose equation of state is $p = -\rho/3$. The discussion of the perturbations of this field is a nice exercise of quantum mechanics, but it will not be tackled here — see e.g. Refs. [156, 157]. The quantum fluctuations of the inflaton are responsible for the large-scale structures in the Universe.

The existence of an inflationary epoch in the cosmological evolution of the Universe driven by a single scalar field has been greatly supported by the recent Planck 2015 results. In particular, the stringent bounds on non-gaussianity and the spectral index of cosmic microwave background strongly sustain inflation driven by a single scalar field with an exponential potential, e.g. like that of the Starobinsky model. These are exactly the kind of potentials for the scalar field that are motivated by our holographic arguments and we will discuss in detail in this thesis.

Chapter 2

# Asymptotically Flat Black Holes Sourced by a Massless Scalar Field

We derive exact, asymptotically flat black hole solutions of Einstein-scalar gravity sourced by a non-trivial scalar field with harmonic asymptotic behaviour. Using an ansatz for the scalar field profile, we calculate, together with the metric functions, the corresponding form of the scalar self-interaction potential. Near to the singularity, the black hole behaves as the Janis-Newmann-Winicour-Wyman solution. The thermodynamical description of our black hole solutions satisfies the first principle and it is the same of the Schwarzschild black hole for large masses.

Units: $c = 1; G = 1/16\pi$; the kinetic scalar term is non-standard.

This chapter is mainly based on: M. Cadoni and E.F. 'Asymptotically flat black holes sourced by a massless scalar field'. *Phys. Rev.* D91 (2015), 104011. arXiv: 1503.04734.

## 2.1 Introduction

In this chapter, we study solutions to minimally coupled Einstein-scalar gravity in four spacetime dimensions. In particular, we look for spherically symmetric, asymptotically flat black holes sourced by an asymptotically massless scalar field. The general action of this theory contains general relativity and a real scalar field with an appropriate self-interaction scalar potential,

$$\mathcal{A} = \int \mathrm{d}^4x \sqrt{-g} \left( \mathcal{R} - 2(\partial\phi)^2 - V(\phi) \right) . \tag{2.1}$$

The existence of asymptotically flat (or AdS), spherically symmetric, black hole solutions in such a theory with a non-trivial scalar field is strongly constrained by the no-hair theorems discussed in Section 1.2. On the one hand, old no-hair theorems forbid regular hairy black hole solutions in the case of a convex and, more generally, semi-positive definite potential $V(\phi)$. On the other hand, recent no-hair theorems state the absence of regular hairy black hole solutions if the scalar-gravity theory satisfies the positive energy theorem, i.e. the ADM energy is positive definite.

For a null potential, $V(\phi) = 0$, but with a non-trivial scalar field, there exists a simple solution of Einstein-scalar gravity which describes a static, spherically symmetric, asymptotically flat spacetime with no event horizon. It was discovered back in 1968 by Janis, Newman, and Winicour [158] and later by Wyman [159] in 1981. It is known as the Janis-Newmann-Winicour-Wyman solution [160], and consistently with old no-hair theorems, it describes a naked singularity.

To find asymptotically flat hairy black hole solutions, one has to relax the condition $V(\phi) = 0$. In this chapter, we investigate the case of a non-trivial massless scalar whose potential is zero only asymptotically. This corresponds to probe the short-scale behaviour of the theory, as at high energies the mass term can be neglected with respect to the kinetic term. In order to keep the scalar massless, we impose the asymptotic $r \to \infty$ fall-off behaviour for the scalar, which constrains in a highly non-trivial way the asymptotic $\phi \to 0$ behaviour of the potential. More precisely, the potential turns out to be unbounded from below, violating the no-hair theorems and hence allowing for black hole solutions.

If we assume the spacetime to be static and spherically symmetric, following the notations and conventions of Appendix A, the field equations for the action (2.1) are given by Eqs. (A.8) with $d = 2, \varepsilon = 1$, and $Q = 0$,

$$Y' + Y^2 + \phi'^2 = 0\,, \tag{2.2a}$$

$$(u\phi')' - \frac{1}{4}\frac{\mathrm{d}V}{\mathrm{d}\phi}\,\mathrm{e}^{2\int Y} = 0\,, \tag{2.2b}$$

$$u'' - 4(uY)' + 2 = 0\,, \tag{2.2c}$$

$$u'' - 2 + 2V\,\mathrm{e}^{2\int Y} = 0\,. \tag{2.2d}$$

Even with simple expressions for the potential $V(\phi)$, it might be very difficult to find exact solutions of the field equations sourced by a non-trivial scalar. Nevertheless, we can improve the situation by imposing asymptotic boundary condition on the scalar field. Knowing the fall-off behaviour of the scalar field, we can use the general method described in Appendix A to solve the field equations.

Here, we investigate the simplest case of an asymptotically massless scalar field, therefore the most natural boundary condition is that the scalar field behaves asymptotically as a harmonic function,

$$\phi \sim 1/r\,, \tag{2.3}$$

and we will therefore consider the class of potentials satisfying

$$V|_{\phi=0} = \left.\frac{\mathrm{d}V}{\mathrm{d}\phi}\right|_{\phi=0} = \left.\frac{\mathrm{d}^2V}{\mathrm{d}\phi^2}\right|_{\phi=0} = 0\,. \tag{2.4}$$

## 2.2 The Janis-Newmann-Winicour-Wyman solution

The Janis-Newmann-Winicour-Wyman solution is a particular solution to the field equations (2.2) with the scalar potential identically zero. This spherically symmetric solution represents a naked singularity, but, despite that, it has several interesting features: it is stable under scalar perturbations [161], it appears as the extremal limit of charged dilatonic black hole solutions [76], and it has

been used to construct traversable wormholes [162]. The Janis-Newmann-Winicour-Wyman solution also appears as the extremal limit of the exact black hole solutions we will derive in Section 2.4.

The parametrisation (2.2) allows a simple rederivation of the Janis-Newmann-Winicour-Wyman solution. Following the recipe described in Appendix A, we first solve the linear equation (2.2d) giving $u$ as a quadratic function of $r$, then we solve (2.2c) for $Y$. Finally, we use (2.2b) to determine $\phi$. We find:

$$U = \left(1 - \frac{r_0}{r}\right)^{2w-1}, \quad R^2 = r^2 \left(1 - \frac{r_0}{r}\right)^{2(1-w)}, \quad \phi = -\gamma \log\left(1 - \frac{r_0}{r}\right) + \phi_0 \,. \tag{2.5}$$

The Riccati equation (2.2a) simply constrains the integration constants $w$ and $\gamma$, $w(1-w) = \gamma^2$, therefore $0 \leqslant w \leqslant 1$. Actually, the range of $w$ can be restricted to $1/2 \leqslant w \leqslant 1$ because of the invariance of the solution under $w \to 1 - w$ together with the coordinate translation $r \to r_0 - r$.

If we ignore the physically irrelevant constant shift of the scalar, Eq. (2.5) gives a two-parameter family of solutions, parametrized by the length scale $r_0$ and the dimensionless parameter $w$. As expected, the scalar field $\phi$ has the harmonic behaviour (2.3) for $r \to \infty$. The solution (2.5) with $r_0$ being a generic real number is therefore the most general solution. For $w = 1$ we get the usual Schwarzschild black hole solution (with constant scalar field) which reduces to the usual Minkowski vacuum solution in the $r_0 \to 0$ limit. For $w \neq 1$ and $r_0$ positive, $r = r_0$ is a curvature singularity, whereas for $r_0$ negative, the curvature singularity is at $r = 0$. The solution (2.5) has no event horizon, it interpolates between the Minkowski spacetime at $r = \infty$ and a naked singularity with power-law metric near $r = r_0$. For $r_0 > 0$ after shifting $r \to r + r_0$, the metric behaves near the singularity as

$$U = \left(\frac{r}{r_0}\right)^{2w-1}, \quad R^2 = r_0^2 \left(\frac{r}{r_0}\right)^{2-2w}, \quad \phi = -\gamma \log \frac{r}{r_0} \,, \tag{2.6}$$

whereas for $r_0 < 0$ we have

$$U = \left(\frac{r}{|r_0|}\right)^{1-2w}, \quad R^2 = r_0^2 \left(\frac{r}{|r_0|}\right)^{2w}, \quad \phi = \gamma \log \frac{r}{|r_0|} \,. \tag{2.7}$$

### 2.2.1 Energy of the Solution

We now calculate the total energy $M$ of the solution, which tells us whether the solution will be stable with respect to the Minkowski vacuum. In general, the total energy could have a contribution coming both from the metric and the scalar field [163, 164], as in the Euclidean action formalism, the variation of the boundary terms of the action has both a gravitational and a scalar contribution

$$\delta M = 8\pi \left(U' R \delta R - R R' \delta U - 2 U R \delta R'\right)\big|^{\infty} - 16\pi \, R^2 U \phi' \delta\phi \big|^{\infty}. \tag{2.8}$$

The total energy can be calculated by expanding the metric functions and the scalar field (2.5) up to terms proportional to $1/r$,

$$U \approx 1 - \frac{(2w-1) r_0}{r} \,, \quad R \approx r - (1-w) r_0 - \frac{\gamma^2 r_0^2}{2r} \,, \quad \phi \approx \phi_0 + \frac{\gamma r_0}{r} \,. \tag{2.9}$$

The contribution of the scalar field to (2.8) as well as the second and third term behave like $1/r$ and therefore they vanish as $r \to \infty$. Only the first term gives a non-vanishing contribution leading to

$$M = 8\pi(2w-1)r_0\,, \tag{2.10}$$

which coincides with the gravitational mass $M_0$, proportional to the $1/r$ term of $U$ in (2.9),

$$M_0 = 8\pi(2w-1)r_0\,, \tag{2.11}$$

meaning that the total energy of the solution is of purely gravitational origin.

We see from Eq. (2.10) that for $r_0 > 0$ the energy of the solution is positive (negative) for $w > 1/2$ ($w < 1/2$) and it vanishes for $w = 1/2$; the exactly opposite holds for $r_0 < 0$. This means that for $r_0 > 0$ solutions with $w < 1/2$ are stable with respect to the Minkowski vacuum, whereas solutions with $w = 1/2$ are degenerate with respect to the same vacuum. However, it has to be stressed that the Janis-Newmann-Winicour-Wyman solutions represent naked singularities, therefore they can be ruled out by means of a cosmic censorship principle. Another interesting feature of the Janis-Newmann-Winicour-Wyman solutions is that their mass can be positive or zero even in the presence of a naked singularity. This is rather unusual and it is due to the back-reaction of the metric to the presence of a non-trivial scalar field.

It should be noted that because the total energy of the solution is not positive definite the positive energy theorem is not satisfied. However, violation of the positive energy theorem is a necessary but not sufficient condition for the existence of regular hairy black hole solutions.

From the asymptotic expansion of the scalar field in Eq. (2.9) one can read off the scalar charge, $\sigma = \gamma\, r_0$. Thus, mass and scalar charge are not independent, consistently with no-hair theorems, which forbid solutions with independent scalar hair.

### 2.2.2 Zero Mass and Charge Limit of Dilatonic Black Hole Solutions

The solution (2.5) also appears as limiting case of dilatonic, black hole solutions, i.e. solutions of *non*-minimally coupled Einstein-Maxwell-dilaton gravity. For instance, the Janis-Newmann-Winicour-Wyman solution can be obtained in the zero charge limit of the Garfinkle-Horowitz-Strominger black hole [76] and also in a particular limit of the S-duality model investigated in Ref. [78]. The latter model considers a Lagrangian as in (2.1) with $V(\phi) = 0$ plus the term $-\cosh 2\phi\, F^2$ and allows for charged, scalar-dressed, asymptotically flat black hole solutions with the metric functions and scalar field given by,

$$U = \frac{(r-r_-)(r-r_+)}{r(r-r_0)}\,, \quad R^2 = r^2\left(1-\frac{r_0}{r}\right), \quad \phi = \phi_0 + \frac{1}{2}\log\left(1-\frac{r_0}{r}\right). \tag{2.12}$$

The constants $r_\pm$ are related to the mass $M$, the magnetic charge $Q$ and the scalar charges $\sigma = -r_0/2$, $\phi_0$, trough

$$r_\pm = M + \frac{r_0}{2} \pm \sqrt{M^2 + \frac{r_0^2}{4} - Q^2\cosh 2\phi_0}\,, \quad r_0 = -\frac{Q^2}{M}\sinh 2\phi_0\,. \tag{2.13}$$

The solution (2.12) represents a three-parameter family of black hole solutions generalizing the well-known Reissner-Nordström solution of general relativity for $M^2 + \frac{r_0^2}{4} - Q^2 \cosh 2\phi_0 \geqslant 0$. The extremal limit is reached when the previous inequality is saturated.

One can easily realise that the solutions (2.5) with $w = 1/2$ can be obtained from the dilatonic black hole solution (2.12) in the limit $M \to 0$, $Q \to 0$ keeping $Q^2/M$ finite. In this limit, the inner horizon at $r = r_-$ is pushed to $r = 0$ whereas the outer horizon at $r = r_+$ coincides with the singularity at $r = r_0$.

### 2.2.3 The Charged Janis-Newmann-Winicour-Wyman Solution

In this subsection, we generalise the Janis-Newmann-Winicour-Wyman solutions by switching on an electric field as in (A.6), characterized by an electric charge $Q$. The field equations are given by Eqs. (2.2) with $V(\phi) = 0$, substituting Eq. (2.2c) with

$$u'' - 4(uY)' + 2 - 4Q^2\, \mathrm{e}^{-2\int Y} = 0\,. \tag{2.14}$$

We find the solution by determining first $u$ and $\phi$, and then by solving the Riccati equation. Finally, we use Eq. (2.14) to express $Q$ in terms of the integration constants. We have[1]

$$U = \left(1 + \frac{r_0}{r}\right)^{2w-1} \left[1 - \frac{Q^2}{r_0^2(1-2w)^2}\left(1 + \frac{r_0}{r}\right)^{2w-1}\right]^{-2}, \tag{2.15a}$$

$$R^2 = r^2\left(1 + \frac{r_0}{r}\right)^{2(1-w)} \left[1 - \frac{Q^2}{r_0^2(1-2w)^2}\left(1 + \frac{r_0}{r}\right)^{2w-1}\right]^{2}, \tag{2.15b}$$

$$\phi = -\gamma \log\left(1 + \frac{r_0}{r}\right) + \phi_0\,. \tag{2.15c}$$

with $w(1-w) = \gamma^2$. For $w \neq 0, 1$, these solutions can be considered as the charged generalisation of the Janis-Newmann-Winicour-Wyman solutions and describe a spacetime with a naked singularity at

$$r = r_0 \left[\left(\frac{Q}{r_0(1-2w)}\right)^{2/(1-2w)} - 1\right]^{-1}. \tag{2.16}$$

The scalar curvature of the spacetime is:

$$\mathcal{R} = \frac{2\gamma^2 r_0^2}{r^4}\left(1 + \frac{r_0}{r}\right)^{2w-3} \left[1 - \frac{Q^2}{r_0^2(1-2w)^2}\left(1 + \frac{r_0}{r}\right)^{2w-1}\right]^{-2}. \tag{2.17}$$

For $w = 0, 1$ the solution (2.15) gives the usual Reissner-Nordström black hole with a constant scalar field, which can be put in its standard form by rescaling and translating the radial coordinate $r$.

For the rest of the chapter, we focus on the $Q = 0$ case.

1. Notice that Eqs. (2.15) are not normalised such that $U \to 1$ as $r \to \infty$.

## 2.3 Asymptotic Behaviours

Eq. (2.5) represents the most general, static, spherically symmetric solutions sourced by a scalar field with an identically vanishing potential. Consistently with no-hair theorems, they do not describe black holes but naked singularities, therefore to have black hole solutions sourced by a non-trivial scalar either we violate the positive energy theorem or/and we consider a non-convex scalar potential. An easy way to achieve this is to consider a potential which is zero only asymptotically but becomes non-zero and negative in the bulk spacetime. Focusing on black hole solutions sourced by an asymptotically massless scalar, we have to impose the conditions (2.4) on the potential and the boundary condition (2.3) on the scalar field.

The conditions (2.4) imply that asymptotically, near $\phi = 0$, the potential must behave at leading order as $V(\phi) = \mu\,\phi^n$ where $\mu$ is a constant and $n \geqslant 3$. The corresponding asymptotic behaviour of the scalar field for $r \to \infty$ can be determined by using the field equation for the scalar (2.2b) written in the form

$$(u\phi')' = n\mu\, R^2 \phi^{n-1}\,, \tag{2.18}$$

and the conditions for asymptotic flatness of the spacetime: $u = r^2$, $R^2 = r^2$. Using these conditions, Eq. (2.18) gives the fall-off behaviour of $\phi$. For $n = 3$ we have a scalar field decaying asymptotically as $\phi = 2/(3\mu r^2)$. For $n = 4$ the theory corresponds to a conformal field theory in flat spacetime, which allows for time-dependent meron solutions $\phi \sim 1/\sqrt{r^2 - t^2}$. The most interesting case is however obtained for $n = 5$. In this case the scalar field behaves asymptotically as in Eq. (2.5), i.e. as a harmonic function in three dimensions,

$$\phi = \frac{\beta}{r} + \mathcal{O}\left(1/r^2\right), \tag{2.19}$$

where $\beta$ is a constant. It is important to stress that the presence of a term $\mathcal{O}\left(1/r^2\right)$ is necessary to cancel the contribution of the $1/r$ term in the right hand side of Eq. (2.18).

We have reached an important result. Compatibility of condition (2.3) with conditions (2.4) require a quintic asymptotic behaviour of potential $V(\phi)$. This condition translates immediately in a condition for the existence of asymptotically flat black hole solutions sourced by a scalar field behaving asymptotically as massless, i.e. decaying as a harmonic function.

## 2.4 Black Hole Solutions

In this section, we derive asymptotically flat black hole solutions sourced by a scalar field with $1/r$ asymptotic behaviour. We expect these solutions to be closely related to solution (2.5), and, given the results of Section 2.3 we also expect the potential to behave asymptotically as $V(\phi) \sim \phi^5$.

We start with the scalar field profile one obtains in the case of a vanishing potential

$$\phi = -\gamma \log\left(1 - \frac{r_0}{r}\right), \tag{2.20}$$

and we determine the metric functions and the potential using the method described in Appendix A. The solution for $R$ is obtained by integrating the Riccati equation (2.2a) and it can be read directly from Eq. (2.5),

$$R^2 = r^2\left(1 - \frac{r_0}{r}\right)^{2(1-w)}, \quad w(1-w) = \gamma^2 . \tag{2.21}$$

The metric function $u$ and the potential $V$ are given by

$$\frac{u}{R^4} = -\int \mathrm{d}r \left(\frac{2r + C_1}{R^4}\right) + C_2 , \quad V = \frac{1}{R^2}\left(1 - \frac{u''}{2}\right). \tag{2.22}$$

For generic values of the integration constants $C_1$ and $C_2$ the corresponding solutions are not asymptotically flat. For $w \neq 1/4,\ 1/2,\ 3/4$ we get asymptotically flat solutions by choosing

$$C_2 = \frac{C_1 - r_0 + 4r_0 w}{r_0^3(2w-1)(4w-3)(4w-1)}, \tag{2.23}$$

and the metric function $U$ reads

$$U(r) = X^{2w-1}\left[1 - \Lambda(r^2 + (4w-3)rr_0 + (2w-1)(4w-3)r_0^2)\right] + \Lambda r^2 X^{2(1-w)}, \tag{2.24}$$

where $X = 1 - r_0/r$ and $\Lambda = C_2$. Using Eq. (2.22) and inverting $\phi = \phi(r)$ given by Eq. (2.20) we are now able to write down the corresponding potential $V(\phi)$,[2]

$$V(\phi) = 4\Lambda\left[-w(1-4w)\sinh\frac{(2w-2)\phi}{\gamma} + 8\gamma^2\sinh\frac{(2w-1)\phi}{\gamma} + (1-w)(3-4w)\sinh\frac{2w\phi}{\gamma}\right]. \tag{2.25}$$

Similarly to the $V(\phi) = 0$ case, the solutions (2.20), (2.21) and (2.24) and the potential (2.25) are invariant under the transformation $w \to 1 - w$ and $r \to r_0 - r$, so we can restrict the range of $w$ to $1/2 \leqslant w \leqslant 1$.

We now show that the metric function (2.24) has an event horizon and hence it describes a black hole. Let $\lambda = 1/(r_0^2\Lambda)$, then the position of the event horizon $r_h$ is given by the zeros with $0 \leqslant X < 1$ of the following equation

$$f(X) := \left\{[\lambda - (2w-1)(4w-3)](1-X)^2 - (4w-3)(1-X) - 1\right\}X^{4w-3} + 1 . \tag{2.26}$$

The solutions of this equation can be found graphically by determining for which values of the parameter $\lambda$ the function $f(X)$ intersects the $X$ axis at $0 \leqslant X < 1$. We have to distinguish between the two cases $1/2 < w < 3/4$ and $3/4 < w < 1$.

2. The potential (2.25) arises also from the study of a general class of Petrov type D solutions [84, 85] and the solution (2.24), albeit in a different form, had already been derived in Ref. [85].

$1/2 < w < 3/4$. Taking into account that $f'(1) = 0$, necessary conditions for the existence of the solution are $f(X) \to +\infty$ for $X \to 0^+$ and $f(X) \to -\infty$ for $X \to +\infty$, requiring $(2w-1)(4w-3) < \lambda \leqslant (2w-1)(4w-1)$. On the other hand $f(X)$ has a local minimum for

$$X = X_2 = \frac{(4w-3)[\lambda - (2w-1)(4w-1)]}{(4w-1)[\lambda - (2w-1)(4w-3)]}\,. \tag{2.27}$$

$f(X)$ intersects the $X$-axis at $0 < X < 1$ only if $0 \leqslant X_2 < 1$, which in turn implies $\lambda > 0$. Thus Eq. (2.26) admits a solution only for $0 < \lambda \leqslant (2w-1)(4w-1)$. We will see that this case is similar to the $w = 1/2$ case.

Black hole solutions exist only for

$$r_0^2 \geqslant \frac{1}{(2w-1)(4w-1)\Lambda}\,. \tag{2.28}$$

The black hole mass is given by

$$M = (2w-1)8\pi r_0 \left[1 - \frac{(4w-3)(4w-1)}{3\lambda}\right], \tag{2.29}$$

whereas the scalar charge is determined by the mass. We have large black holes for $\lambda \to 0$ and a naked singularity for $\lambda = (2w-1)(4w-1)$. Owing to Eq. (2.28) the black hole mass has a lower bound given by

$$M_{\text{min}} = \frac{16\pi}{3\sqrt{\Lambda}} \frac{w}{\sqrt{(4w-1)(2w-1)}}\,. \tag{2.30}$$

$3/4 < w < 1$. In this case we always have $f(0) = 1$, so that a necessary condition for a solution to Eq. (2.26) to exist is $f(X) \to -\infty$ for $X \to +\infty$, requiring $\lambda < (2w-1)(4w-1)$. On the other hand, $0 \leqslant X < 1$ implies $\lambda < 0$. It follows that solutions always exist for $\lambda < 0$. We will see that it is analogous to the $w = 3/4$ case.

There is no lower bound on $\lambda$ nor the black hole mass (2.29). Black holes exist for arbitrarily small values of the mass (corresponding to $\lambda \to -\infty$), while the mass of the solution which describes the naked singularity is zero.

### 2.4.1 Black Hole Solutions for $w = 1/2$

For $w = 1/2$ the solutions are asymptotically flat when

$$C_2 = -\frac{2}{r_0^2}\,. \tag{2.31}$$

The solutions and the potential read

$$U(r) = \frac{r^2}{r_0^2} X \left[ \left(1 + r_0^2 \Lambda\right) X - 2 r_0^2 \Lambda \log X + \left(1 - r_0^2 \Lambda\right) X^{-1} - 2 \right], \tag{2.32}$$

$$V(\phi) = 4\Lambda \left[ 3 \sinh 2\phi - 2\phi \left( \cosh 2\phi + 2 \right) \right], \quad \Lambda = -\frac{C_1 + r_0}{r_0^3}. \tag{2.33}$$

The solution of the transcendental equation

$$X \log X = \frac{1+\lambda}{2} X^2 - \lambda X - \frac{1-\lambda}{2}, \tag{2.34}$$

gives the position of the event horizon $r_h$ of the metric function (2.32). For $0 < \lambda \leqslant 1$, corresponding to $r_0^2 \geqslant 1/\Lambda$, Eq. (2.34) has always an acceptable solution, i.e. a solution $0 \leqslant X(r_h) < 1$, corresponding to $r_0 \leqslant r_h < \infty$.

The spacetime represents a black hole with event horizon at $r = r_h$ and a curvature singularity at $r = r_0$. For $X(r_h) \to 1$ (corresponding to $r_h \to \infty$), $\lambda \to 0$ and then we have large black holes. Conversely, for $X(r_h) = 0$ (corresponding to $r_h = r_0$) the horizon disappears and we are left with a naked singularity.

The black hole mass can be easily evaluated from the coefficient of the $1/r$ term in the asymptotic expansion of the metric function $U$,

$$M = \frac{8\pi r_0}{3\lambda}. \tag{2.35}$$

Because of the bound $r_0^2 \geqslant 1/\Lambda$, there is a minimum value for the black hole mass,

$$M_{\text{min}} = \frac{8\pi}{3\sqrt{\Lambda}}, \tag{2.36}$$

under which black hole solutions cannot exist. The continuous part of the black hole mass spectrum is separated from the Minkowski vacuum, attained for $r_0 = 0$, by a mass gap.

### 2.4.2 Black Hole Solutions for $w = 3/4$

For $w = 3/4$ we have asymptotically flat solutions for

$$C_2 = -\frac{3C_1}{2r_0^3} - \frac{2}{r_0^2}. \tag{2.37}$$

The solutions and the potential take the form

$$U(r) = \frac{r^2}{r_0^2} X^{1/2} \left[ \left( 1 + \frac{r_0^2 \Lambda}{2} \right) X^2 - 2 \left( 1 + r_0^2 \Lambda \right) X + r_0^2 \Lambda \log X + 1 + \frac{3 r_0^2 \Lambda}{2} \right], \tag{2.38}$$

$$V(\phi) = \Lambda \left( 8\sqrt{3}\phi \cosh \frac{2\phi}{\sqrt{3}} - 9 \sinh \frac{2\phi}{\sqrt{3}} - \sinh 2\sqrt{3}\phi \right), \quad \Lambda = -\frac{C_1 + 2r_0}{r_0^3}. \tag{2.39}$$

In this case, the position of the event horizon $r_h$ is given by the solutions of the equation

$$\log X = -\left(\lambda + \frac{1}{2}\right) X^2 + 2(\lambda+1)X - \lambda - \frac{3}{2}\,. \tag{2.40}$$

Solutions of this equation with $0 \leqslant X(r_h) < 1$ always exist for $\lambda \geqslant 0$. Also in this case we have large black holes ($X(r_h) \to 1$) when $\lambda \to 0$ and naked singularities ($X(r_h) = 0$) for $\lambda \to \infty$.

The black hole mass is

$$M = 4\pi r_0 \left(1 + \frac{2}{3\lambda}\right). \tag{2.41}$$

Since $\lambda$ has no upper bound, differently from the previous case, black holes exist for arbitrarily small values of the mass whereas the naked singularity has zero mass.

## 2.5 Thermodynamics

In this section, we investigate the thermodynamics of the black hole solutions we have found in the previous section. The masses have already been calculated, while the temperature $T$ and the entropy $S$ will be calculated using the well-known formulæ involving the surface gravity and the area law:

$$T = \left.\frac{U'}{4\pi}\right|_{r=r_h}, \quad S = \left. 16\pi^2 R^2\right|_{r=r_h}. \tag{2.42}$$

We will also show that consistently with the non-existence of an independent scalar hair the thermodynamical parameters $M$, $T$ and $S$ satisfy the first principle $\mathrm{d}M = T\,\mathrm{d}S$.[3] As usual we discuss separately the three cases $1/2 < w < 1$, $w = 1/2$, and $w = 3/4$.

Let us define the dimensionless parameter $\omega \equiv r_0/r_h$, with $0 < \omega \leqslant 1$, and let us begin with generic $1/2 < w < 1$, $w \neq 3/4$. Then, Eq. (2.26) evaluated at the horizon can be solved for $\lambda$,

$$\lambda(\omega) = \frac{1-(1-\omega)^{3-4w}}{\omega^2} + \frac{4w-3}{\omega} + (2w-1)(4w-3)\,. \tag{2.43}$$

The functions $T(\omega)$ and $S(\omega)$ are given by

$$T(\omega) = \frac{\sqrt{\Lambda}}{4\pi\sqrt{\lambda}}\left[\left(\frac{2}{\omega} + \frac{3-4w}{1-\omega}\right)(1-\omega)^{2-2w} - \left(\frac{2}{\omega} + 4w - 3\right)(1-\omega)^{2w-1}\right], \tag{2.44}$$

$$S(\omega) = \frac{16\pi^2}{\Lambda\lambda}\frac{(1-\omega)^{2-2w}}{\omega^2}\,, \tag{2.45}$$

The general thermodynamical relations $M(T)$, $S(T)$ characterising the black hole cannot be found analytically. However, one can easily check by differentiating $\lambda(\omega)$ and $M(\omega)$ the validity

3. The same results can be derived using the Euclidean action formalism, but we omit the calculations here.

of the first law of thermodynamics. This is a rather non-trivial consistency check, because the scalar charge of the solution is not independent, therefore we cannot have a thermodynamical potential associated with it.

The large mass limit can be discussed expanding $T$, $S$, $M$ and $\lambda$ about $\omega = 0$. At leading order one gets from (2.43), $\lambda = \frac{1}{3}\omega(1-2w)(3-4w)(1-4w)$ which inserted into the expansion of (2.44) and (2.45) gives

$$T \approx \frac{\sqrt{\Lambda}\omega^{3/2}}{4\sqrt{3}\pi}\frac{1}{(1-2w)(3-4w)(1-4w)}\,, \tag{2.46}$$

$$S \approx \frac{48\pi^2}{\Lambda\omega^3}(1-2w)^2(3-4w)^2(1-4w)^2\,. \tag{2.47}$$

The leading term for the mass (2.29) is

$$M \approx \frac{8\sqrt{3}\pi}{\sqrt{\Lambda}\omega^{3/2}}(1-2w)(3-4w)(1-4w)\,. \tag{2.48}$$

From these equations one easily finds the thermodynamical potentials

$$M = \frac{2}{T}\,, \qquad S = \frac{1}{T^2}\,, \qquad F = M - TS = \frac{1}{T}\,, \tag{2.49}$$

where $F$ is the free energy. The previous thermodynamical relations are exactly those satisfied by the Schwarzschild black hole. Thus, for large masses, our scalar dressed black hole is thermodynamically indistinguishable from a Schwarzschild one at the same temperature. This is an interesting result, particularly if one considers that for the model under consideration, the Schwarzschild solution sourced by a constant scalar is unstable.

### 2.5.1 The $w = 1/2$ case

The temperature and the entropy (2.42) can be easily written as functions of $\omega$ and $\lambda$,

$$T(\omega) = \frac{\sqrt{\Lambda}}{4\pi\sqrt{\lambda}}\left[2\left(1-\frac{2}{\omega}\right)\log(1-\omega)-4\right], \quad S(\omega) = \frac{16\pi^2}{\Lambda\lambda}\left(\frac{1}{\omega^2}-\frac{1}{\omega}\right). \tag{2.50}$$

where $\lambda$ is obtained by solving Eq. (2.34) evaluated at the horizon,

$$\lambda(\omega) = \frac{2(1-\omega)\log(1-\omega)}{\omega^2} + \frac{2}{\omega} - 1\,. \tag{2.51}$$

In Section 2.4.1 we have found that $0 < \lambda \leqslant 1$, meaning that the temperature, the mass and the entropy are always positive. For $\omega = \lambda = 1$ we have an extremal state with zero entropy and infinite temperature saturating the inequality $r_0^2 \geqslant 1/\Lambda$. Near to the singularity, the temperature diverges logarithmically $T \sim -\log(1-\omega)$. For this state, the horizon coincides with the singularity.

Nevertheless, the mass is not zero but it is given by the minimum value $M_{\rm min} = 8\pi/(3\sqrt{\Lambda})$. The behaviour of this singular extremal state has to be compared with that of the Schwarzschild black hole, for which the extremal, infinite temperature state has zero mass.

Using Eqs. (2.35), (2.50) and (2.51) one can check the validity of the first law of thermodynamics, hence the absence of a thermodynamical potential associated with the scalar charge. We can derive the explicit form of the thermodynamical potentials in the limit of large black holes, $\lambda, \omega \to 0$ corresponding to $r_0^2 \gg 1/\Lambda$. In this limit, the mass and entropy diverge whereas the temperature tends to zero. Expanding Eq. (2.51) about $\omega = 0$ we get $\lambda = \omega/3 + \mathcal{O}(\omega^2)$, which inserted in Eqs. (2.35) and (2.50) gives at leading order

$$M = \frac{8\sqrt{3}\pi}{\sqrt{\Lambda}\omega^{3/2}}\,, \qquad T = \frac{\sqrt{\Lambda}}{4\sqrt{3}\pi}\omega^{3/2}\,, \qquad S = \frac{48\pi^2}{\Lambda\omega^3}\,. \tag{2.52}$$

Using these equations one can easily get the thermodynamical potentials (2.49).

### 2.5.2 The $w = 3/4$ case

Also in this case we begin writing the temperature and the entropy as functions of the dimensionless parameters $\omega$ and $\lambda$,

$$T(\omega) = \frac{\sqrt{\Lambda}}{4\pi\sqrt{\lambda}}\frac{(1+2\lambda)\omega^2 - 2\lambda\omega}{\sqrt{1-\omega}}\,, \quad S(\omega) = \frac{16\pi^2}{\Lambda\lambda}\frac{\sqrt{1-\omega}}{\omega^2}\,. \tag{2.53}$$

where $\lambda(\omega)$ is obtained solving Eq. (2.40) evaluated at the horizon with respect to $\lambda$,

$$\lambda(\omega) = -\frac{\omega(\omega+2) + 2\log(1-\omega)}{2\omega^2}\,, \tag{2.54}$$

where now $\lambda > 0$ from Section 2.4.2.

Although the explicit general form of $M(T)$ and $S(T)$ cannot be found analytically, one can quickly check, using the same procedure as before, the validity of the first principle.

The extremal, singular, black hole state is obtained for $\omega = 1, \lambda = \infty$. We now have an extremal state with $M = S = 0$ and $T = \infty$. In this state the horizon coincides with the singularity and the mass is zero analogously to the Schwarzschild black hole. Conversely, large black holes are obtained for $\lambda, \omega \to 0$ when the mass and entropy diverge whereas the temperature tends to zero. In this limit we get again approximate solution for $\lambda = \omega/3$, at leading order in $\omega$, the temperature and the entropy satisfy the same relations as in Eq. (2.52) and we have the same thermodynamical potentials (2.49).

## 2.6 Summary and Conclusions

In this chapter, we have derived exact, asymptotically flat, spherically symmetric, black hole solutions sourced by a non-trivial scalar field behaving asymptotically as a harmonic function. The expressions

for the metric function (2.24), (2.32) and (2.38), together with, respectively, the potentials (2.25), (2.33) and (2.39) represent a two-parameter family of solutions of the Einstein-scalar gravity theory (2.1) sourced by a non-trivial scalar field given by Eq. (2.20).

The solutions (2.24), (2.32) and (2.38) have a curvature singularity at $r = r_0$ (for $r_0 > 0$) or at $r = 0$ (for $r_0 < 0$), and it can be easily shown that near the singularity they have the same scaling behaviour of the Janis-Newmann-Winicour-Wyman solution given in Eqs. (2.6) and (2.7). Hence, our solutions share the same singularity structure with the Janis-Newmann-Winicour-Wyman solution and, similarly to the latter, they interpolate between an asymptotically flat spacetime and a power-law metric near to the singularity, typical of hyperscaling violation.

In view of the results of Section 2.3, for $\phi \to 0$, the potentials (2.25), (2.33) and (2.39) and their $n$-order derivatives vanish till $n = 5$, i.e. the potential behaves near $\phi = 0$ respectively for $w$ generic, $w = 1/2$ and $w = 3/4$ as

$$V(\phi \approx 0) = -32\Lambda \, \frac{(2w-1)(4w-1)(4w-3)}{(w-w^2)^{3/2}} \, \phi^5 + \mathcal{O}\left(\phi^7\right), \tag{2.55}$$

$$V(\phi \approx 0) = -256\Lambda \, \phi^5 + \mathcal{O}\left(\phi^7\right), \tag{2.56}$$

$$V(\phi \approx 0) = -\frac{1856\Lambda}{3\sqrt{3}} \, \phi^5 + \mathcal{O}\left(\phi^7\right). \tag{2.57}$$

For all values of the parameter $1/2 \leqslant w < 1$ the potential is always antisymmetric under $\phi \to -\phi$ and diverges for $\phi \to -\infty$, which means that it is always not limited from below. Since the first derivative of the potential evaluated at $\phi = 0$ vanishes, all the three models allow for the Schwarzschild black hole solution endowed with a identically trivial scalar, $\phi = 0$. However, $\phi = 0$ is not a minimum of the potential so that we naturally expect this solution to be unstable. Moreover, because $\phi = 0$ is an inflection point for $V(\phi)$, the potential is not convex and according to old no-scalar hair theorems, black hole solutions with non-trivial scalar profile are in principle allowed.

The masses of these solutions, given by, respectively, expressions (2.29), (2.36) and (2.41) are not positive definite, and therefore the positive energy theorem is therefore violated, i.e. our solutions do not satisfy the conditions of recent no-hair theorems.

In our model, although characterised by a non-trivial scalar field profile, the corresponding scalar charge is not independent, implying the absence of a corresponding thermodynamical potential. Nevertheless, the thermodynamics of our solutions shows several interesting features. In the large mass limit, they have the same thermodynamical behaviour of the Schwarzschild solution, whereas the infrared behaviour of the mass spectrum of the black hole solutions with $1/2 \leqslant w < 3/4$ is characterised by the presence of a mass gap. The behaviour near the singular state is different for the two cases $1/2 < w < 3/4$ and $3/4 < w < 1$. The first one is very similar to the $w = 1/2$ case: we have a singular extremal state with zero entropy, infinite temperature, but non-vanishing mass given by the minimal mass (2.30) for $\lambda = (2w-1)(4w-1)$, corresponding to $\omega = 1$. The second case is akin to the $w = 3/4$ case: we have a singular extremal state with zero entropy, infinite temperature, and vanishing mass for $\lambda \to -\infty$.

On the other hand, the model has some troublesome features, related to the behaviour of the potential $V(\phi)$ both at $\phi \to 0$ and $\phi \to \infty$. Because $\phi = 0$ is not a minimum of the potential but only an inflexion point, the $\phi = 0$ Schwarzschild black hole, although solution of the field equation, is most likely unstable. Moreover, the potential is unlimited from below, $V(\phi) \to -\infty$ for $\phi \to -\infty$, and behaves near $\phi = 0$ as $V(\phi) \sim \phi^5$, hence it is not renormalisable from the quantum field theory point of view. For these reasons our model cannot be fundamental but can give only an effective description valid in the region $\phi \geqslant 0$. It is well-known that the renormalisation group flow may drive the scalar field potential in regions of instability. An important example of this kind of behaviour is given by the coefficient of the quartic term in the Higgs potential, which at short distances could become negative making the usual Higgs vacuum unstable [165, 166].

A rather intriguing possibility comes into the play if we consider the parameter $\Lambda$ in the potentials (2.25), (2.33) and (2.39) as dynamical. This can be the case if we regard the model as an effective description (e.g. resulting from some renormalisation group flow) of some fundamental microscopic theory. If this is the case, focusing on the case $w = 1/2$, the vacuum can be obtained at $\Lambda = 0$, corresponding to $r_0 = \infty$. For $\lambda = 0$ we get the solution (2.5) for a massless field with the value $w = 1/2$, i.e. a solution with zero mass, endowed with a non-trivial scalar field.

An important point we have not addressed in this chapter is the stability of the black hole solutions we have found. For all our models we have the Minkowski vacuum solution for $\phi = 0$. On the other hand, we have already argued about the instability of the Schwarzschild solution. The stability of solution (2.24) has been investigated in Ref. [86], where it has been shown that it presents mode instability against linear radial perturbations.

Chapter 3

# Brane Solutions Sourced by a Scalar with Vanishing Potential

We derive exact brane solutions of minimally coupled Einstein-Maxwell-scalar gravity in $d+2$ dimensions with a vanishing scalar potential and we show that these solutions are conformal to the Lifšic spacetime whose dual quantum field theory is characterised by hyperscaling violation. These solutions, together with the AdS brane and the domain wall sourced by an exponential potential, give the complete list of scalar branes sourced by a generic potential having simple (scale-covariant) scaling symmetries not involving Galilean boosts. This allows us to give a classification of both elementary and interpolating brane solution of minimally coupled Einstein-Maxwell-scalar gravity having no Schrödinger isometries, which may be very useful for holographic applications.

Units: $c = 1; G = 1/16\pi$; the kinetic scalar term is non-standard.

This chapter is based on: M. Cadoni, E.F., and M. Serra. 'Brane solutions sourced by a scalar with vanishing potential and classification of scalar branes'. *J. High Energy Phys.* 1601 (2016), 125. arXiv: 1511.03986.

## 3.1 Introduction

In this chapter, we study brane solutions of minimally coupled Einstein-Maxwell-scalar gravity. As briefly discussed in Section 1.3, these solutions are of particular interest in the holographic context, where we can identify three different types of solutions.

1. *Black branes*, i.e. solutions with a singularity shielded by an event horizon. These solutions correspond to a field theory at finite temperature $T$ and they are crucial in the description of dual quantum field theories at finite temperature. In particular they may give rise to phase transitions.

2. *Scale-covariant branes*, i.e. elementary solutions that transform covariantly under scale transformations. They represent a generalisation of the usual Minkowski or AdS vacua to spacetimes with non-standard asymptotics. They are sourced by a scalar field with $\log r$ behaviour, have no horizon and in the dual QFT typically correspond to a $T = 0$ ground state exhibiting hyperscaling violation. The AdS brane, which is characterised by full conformal invariance and is sourced by a constant scalar, appears as the limiting case of this class of solutions. In

general, scale-covariant solutions have a curvature singularity at $r = 0$ and need therefore an infrared regularisation.

3. *Interpolating branes*, i.e. solutions that interpolate between two elementary branes at $r = 0$ (the infrared of the dual QFT) and $r = \infty$ (the ultraviolet of the dual QFT). They are $T = 0$ solutions describing the flow of the dual QFT from the infrared to the ultraviolet regime, in which the solution behaves as an elementary, scale-covariant, solution.

The presence of a given type of brane solution in the spectrum of minimally coupled Einstein-Maxwell-scalar gravity theories depends on the specific form of the scalar potential. For a constant potential we obtain AdS branes; elementary, scale-covariant branes require an exponential potential; black or interpolating branes typically require a more complicated potential with different behaviour in the $r = 0$ and $r = \infty$ region. Notice that the known no-hair theorems only apply to asymptotically flat or AdS solutions. Thus, solutions with non-standard asymptotics do not necessarily satisfy no-hair theorems. Although several solutions of minimally coupled Einstein-Maxwell-scalar gravity theories are known, presently it is not clear if the scale-covariant geometries found until now exhaust all the possible solutions of this kind of theory. Clearly, this lack of knowledge prevents a complete classification of the possible interpolating geometries.

In this chapter we present two results. First, we derive the exact solutions of minimally coupled Einstein-Maxwell-scalar gravity in the case of a vanishing scalar potential, which are the brane counterpart of the Janis-Newmann-Winicour-Wyman solutions discussed in Chapter 2. We show that these solutions belong to the class of scale-covariant solutions generating hyperscaling violation in the dual QFT. Second, we demonstrate that these solutions complete the list of the possible scale-covariant solutions of the theory having isometries not involving Galilean boosts. This will allow us to give an exhaustive classification of the interpolating brane solutions of minimally coupled Einstein-Maxwell-scalar gravity with no Schrödinger isometries.

## 3.2 Scaling Symmetries and Hyperscaling Violation

The $d+2$ dimensional metric for a brane whose dual QFT is characterised by hyperscaling violation is usually written as [122]

$$\mathrm{d}s^2 = r^{-2(d-\vartheta)/d}\left(-r^{-2(z-1)}\,\mathrm{d}t^2 + \mathrm{d}r^2 + \mathrm{d}x_i\,\mathrm{d}x^i\right), \tag{3.1}$$

where $\mathrm{d}x_i\,\mathrm{d}x^i$ is the line element of the $d$ dimensional transverse spacetime with planar topology, $\vartheta$ is the hyperscaling violation parameter and $z$ is the dynamic scaling exponent characterizing the anisotropic scaling of the time and space coordinates, which breaks Lorentz invariance in the dual QFT. The scaling symmetries of the metric (3.1) are

$$t \to \lambda^z t\,, \quad r \to \lambda\, r\,, \quad x_i \to \lambda\, x_i\,, \quad \mathrm{d}s \to \lambda^{\vartheta/d}\,\mathrm{d}s\,. \tag{3.2}$$

A non-zero value of $\vartheta$ makes the metric (3.1) not scale-invariant, but only *scale-covariant*, in the sense that the metric transforms with a definite weight under a scale transformation. Notice that in this chapter we consider simple scaling symmetries (3.2), which do not involve Galilean boosts.[1]

It is useful to distinguish between the two effects of hyperscaling violation ($\vartheta \neq 0$) and anisotropic scaling ($z \neq 1$) introducing four different subclasses:

| | $\vartheta = 0$ | $\vartheta \neq 0$ |
|---|---|---|
| $z = 1$ | AdS branes | Domain Walls |
| $z \neq 1$ | Lifšic branes | Conformal-Lifšic branes |

Table 3.1: Brane classification according to their (violation of) hyperscaling violation parameter and anisotropic scaling exponent.

AdS branes. The metric (3.1) gives the $AdS_{d+2}$ spacetime, the scaling (3.2) is isotropic and the dual QFT is a conformal field theory.

Lifšic branes. Because $\vartheta = 0$, the metric is not only covariant but also invariant under the scale transformation (3.2). On the other hand, because $z \neq 1$ the scaling is not isotropic in the $t$ and $x_i$ coordinates and the dual $d+1$ dimensional QFT is not invariant under the $d+1$ dimensional Lorentz group.

Domain Walls. The scaling (3.2) is isotropic but being $\vartheta \neq 0$, the full scale invariance is broken and only scale covariance survives. The metric is conformal to the AdS spacetime, the dual QFT is Lorentz-invariant and one can still formulate a DW/QFT correspondence [173, 174]. Notice that the Minkowski spacetime in $d+2$ dimensions is a particular case of this class of solutions, obtained for $\vartheta = d$.

Conformal-Lifšic branes. The scaling (3.2) is anisotropic and hyperscaling is violated. In this case the metric (3.1) is conformal to the Lifšic spacetime [111].

Hyperscaling violation can be realised both for positive and negative values of $\vartheta$, and the two cases are qualitatively different. The scaling transformation determines the following scaling behaviour for the free energy of the dual QFT, given in terms of $\vartheta$ and $z$:

$$F \sim T^{(d+z-\vartheta)/z} . \tag{3.3}$$

1. Holography has also been investigated for non-relativistic quantum field theories, which allows for boosts in addition to the simple scaling geometries (3.1), and it is known as Schrödinger holography [167–172]. A complete and exhaustive classification of all non-relativistic holographic models, in particular of the important case $z = 2$, would require a separate classification also involving the Schrödinger symmetries which we do not study here.

The effect of a positive hyperscaling violation parameter $\vartheta$ is a 'lowering' of the effective dimensionality of the dual system from $d$ to $d - \vartheta$, whereas for $\vartheta < 0$ this dimensionality increases to $d + |\vartheta|$. For typical condensed matter critical systems $\vartheta$ is always positive. However, in the context of holographically generated hyperscaling violation, negative values of $\vartheta$ have been found in a number of cases, see e.g. Refs. [120, 121] and references therein.

## 3.3 Brane Solutions Sourced by a Scalar Field with $V = 0$

In this section, we find exact $d + 2$ dimensional brane solutions ($\varepsilon = 0$) to Einstein-Maxwell-scalar gravity with identically null scalar potential, $V(\phi) = 0$. We follow the notation and conventions of Appendix A, and in this particular case, the field equations (A.8) reduce to

$$Y' + Y^2 = -\frac{2}{d}\,\phi'^2\,, \tag{3.4a}$$

$$(u\phi')' = 0\,, \tag{3.4b}$$

$$u'' - (d+2)\,(uY)' - 4Q^2\,\mathrm{e}^{-d\int Y} = 0\,, \tag{3.4c}$$

$$u'' - \frac{2(d-2)}{d}\,Q^2\,\mathrm{e}^{-d\int Y} = 0\,. \tag{3.4d}$$

Let us discuss separately the neutral and charged case.

### 3.3.1 Neutral Brane Solutions

One can easily check that flat branes with $R = r$ and $U = 1$ (corresponding to $u = r^d$ and $Y = 1/r$), are not solution of the field equations (3.4) with $Q = 0$. However, the system (3.4) with $Q = 0$ can be integrated exactly: we solve the trivial equation (3.4d), giving $u$ as a linear function of $r$; then we solve Eq. (3.4d) for $Y$; and finally we determine $\phi$ using Eq. (3.4b). The Riccati equation then gives just a constraint for the integration constants. The most general solution is:

$$U = \left(\frac{r}{r_0}\right)^{1-dw}\,, \quad R^2 = \left(\frac{r}{r_0}\right)^{2w}\,, \quad \phi = -\gamma\log\left(\frac{r}{r_0}\right) + \phi_0\,, \quad w - w^2 = \frac{2}{d}\,\gamma^2\,, \tag{3.5}$$

where $r_0$, $\gamma$, $w$ and $\phi_0$ are integration constants. The constraint implies the condition $0 \leqslant w \leqslant 1$. The solution (3.5) is invariant under the transformation $w \to 1 - w$, which maps solutions with $w \in [0, 1/2]$ into solutions with $w \in [1/2, 1]$. Neglecting the constant $\phi_0$, a trivial translation mode of the scalar, these solutions give a two-parameter family of brane solutions. In particular, $r_0$ represents a length scale, while $w$ is a dimensionless parameter. The solution (3.5) can be considered as the brane counterpart of the Janis-Newman-Winicour-Wyman spherical solutions.

For $w \neq 0, 1$ the solutions have a naked singularity at $r = 0$, in fact the scalar curvature is

$$\mathcal{R} = \frac{2\gamma^2}{r_0^2}\left(\frac{r_0}{r}\right)^{1+dw}\,. \tag{3.6}$$

Solutions (3.5) have non-standard asymptotics, thus — in principle — no-hair theorems, which forbid asymptotically flat black brane solutions when $V = 0$, do not apply. Nevertheless, one can easily check that Eqs. (3.4) do not allow for solutions with event horizons. Thus, the brane (3.5) is a zero temperature solution, which does not allow for finite temperature excitations.

In the two limiting cases $w = 0, 1$ the scalar is constant. For $w = 0$ the brane solution becomes

$$\mathrm{d}s^2 = -\frac{r}{r_0}\,\mathrm{d}t^2 + \frac{r_0}{r}\,\mathrm{d}r^2 + \mathrm{d}x_i\,\mathrm{d}x^i\,, \tag{3.7}$$

which is just $d + 2$ dimensional Minkowski space in a particular coordinate system; in fact, the $(r, t)$ sections of the metric can be brought in the Rindler form by a simple redefinition of the radial coordinate. For $w = 1$ the brane solution is

$$\mathrm{d}s^2 = -\left(\frac{r}{r_0}\right)^{1-d}\mathrm{d}t^2 + \left(\frac{r}{r_0}\right)^{d-1}\mathrm{d}r^2 + \left(\frac{r}{r_0}\right)^{2}\mathrm{d}x_i\,\mathrm{d}x^i\,, \tag{3.8}$$

a Ricci-flat manifold, which can be considered as the brane counterpart of the Schwarzschild black hole.

## Energy of the Brane

In the Euclidean action formalism [163], the variation of the boundary terms of the action consists of both a gravitational $\delta M_G$ and a scalar contribution $\delta M_\phi$:

$$\delta M_G = 8\pi\left[-\frac{d}{2}R^{d-1}R'\delta U + U'R^{d/2}\delta\left(R^{d/2}\right) - d\,U R^{d/2}\delta\left(R^{\frac{d-2}{2}}R'\right)\right]^{\infty}, \tag{3.9}$$

$$\delta M_\phi = -16\pi\left[R^d U\phi'\delta\phi\right]^{\infty}. \tag{3.10}$$

It follows that the total energy for the solution (3.5) is

$$M = \frac{4\pi}{r_0}dw\left[(2-d)w - 2\right]. \tag{3.11}$$

Taking into account the constraints on $w$ and $d$ (namely $0 \leqslant w \leqslant 1$ and $d \geqslant 2$), the energy vanishes only when $w = 0$, i.e. for Minkowski space, while for $0 < w \leqslant 1$ the sign of the energy is ruled by the sign of $r_0$ (negative for $r_0 > 0$ and positive for $r_0 < 0$). Taking $r > 0$, the solution (3.5) exists only for $r_0 > 0$, thus the brane has always a negative mass. This behaviour is quite different from the Janis-Newman-Winicour-Wyman solution, where the sign of the energy depends both on the value of the dimensionless parameter of the solutions and on $r_0$, see Section 2.2.

## Scaling Symmetries and Hyperscaling Violation

The brane metric (3.5) has remarkable scaling symmetries and can be put in the form (3.1) by the transformation of coordinates

$$\frac{r}{r_0} \to \left(\frac{r}{\tilde{r}_0}\right)^{2/[1+w(d-2)]}, \quad \tilde{r}_0 = \frac{2r_0}{1+w(d-2)}\,. \tag{3.12}$$

The hyperscaling violation parameter and the dynamical exponent are given by

$$z = \frac{2dw}{1 + w(d-2)}\,, \quad \vartheta = \frac{d(1+dw)}{1+w(d-2)}\,. \tag{3.13}$$

We observe that $z$ and $\vartheta$ are not independent but satisfy the relation

$$\vartheta = z + d\,. \tag{3.14}$$

From Eqs. (3.13) and Table 3.1, we infer that the brane solution (3.5) can neither describe an AdS nor a Lifšic spacetime. It can be either a domain wall for $w = 1/(d+2)$ or a conformal-Lifšic brane for $w \neq 1/(d+2)$. The relation (3.14) implies that the free energy of the dual QFT is constant. This is what we expect because owing to the absence of solutions with event horizons, our brane solution does not allow black brane excitations at finite temperature.

The null energy conditions for the bulk stress-energy tensor require [122]

$$(d-\vartheta)\,[d(z-1)-\vartheta] \geqslant 0\,, \quad (z-1)(d+z-\vartheta) \geqslant 0\,. \tag{3.15}$$

Taking into account that the constraint $0 \leqslant w \leqslant 1$ implies the condition $0 \leqslant z \leqslant 2d/(d-1)$, it is straightforward to check that the first inequality is always satisfied. The second one is saturated in our case, as expected because the source is a massless field.

### 3.3.2 Electrically Charged Brane Solutions in Four Dimensions

Let us now consider the case of non-vanishing electric charge. Taking for simplicity $d = 2$, Eqs. (3.4) become

$$Y' + Y^2 + \phi'^2 = 0\,, \quad (u\phi')' = 0\,, \quad u'' - 4(uY)' - 4Q^2\,\mathrm{e}^{-2\int Y} = 0\,, \quad u'' = 0\,. \tag{3.16}$$

Again, we first determine $u$ and $\phi$, then we solve the Riccati equation, and finally we use the third equation to express the charge $Q$ in terms of the integration constants:

$$U = \left(\frac{r}{r_0}\right)^{1-2w}\left[1 - \frac{r_0^2 Q^2}{(1-2w)^2}\left(\frac{r}{r_0}\right)^{1-2w}\right]^{-2}\,, \tag{3.17a}$$

$$R^2 = \left(\frac{r}{r_0}\right)^{2w}\left[1 - \frac{r_0^2 Q^2}{(1-2w)^2}\left(\frac{r}{r_0}\right)^{1-2w}\right]^{2}\,, \tag{3.17b}$$

$$\phi = -\gamma \log\left(\frac{r}{r_0}\right) + \phi_0\,, \tag{3.17c}$$

where $w(1-w) = \gamma^2$. These constraints imply $0 \leqslant w \leqslant 1$, with $w \neq 1/2$.

The solution (3.17) represents a three-parameter $(r_0,\, w,\, Q)$ family of brane solutions, with a naked singularity at $r = r_0\,(r_0^2Q^2/(1-2w)^2)^{(1/2w-1)}$ for all $w$ in the range $0 \leqslant w \leqslant 1$. In fact the scalar curvature is

$$\mathcal{R} = \frac{2\gamma^2}{r_0^2}\left(\frac{r}{r_0}\right)^{-1-2w}\left[1-\frac{r_0^2Q^2}{(1-2w)^2}\left(\frac{r}{r_0}\right)^{1-2w}\right]^{-2}. \tag{3.18}$$

For $w = 0, 1$ the solutions reduce to curved branes with vanishing scalar curvature $\mathcal{R} = 0$, sourced by a constant scalar field. In particular one has:

$$U = \frac{r}{r_0}\left(1-\frac{r_0Q^2r}{(1-2w)^2}\right)^{-2}, \quad R = 1-\frac{r_0Q^2r}{(1-2w)^2}\,, \qquad \text{for } w=0\,, \tag{3.19}$$

$$U = \frac{r_0}{r}\left(1-\frac{r_0^3Q^2}{(1-2w)^2r}\right)^{-2}, \quad R = \frac{r}{r_0}-\frac{r_0^2Q^2}{(1-2w)^2}\,, \qquad \text{for } w=1\,. \tag{3.20}$$

Both solutions represent a sort of Reissner-Nordström branes. Indeed, the metric part of the solutions can be written in the form $U = a/r + Q^2/r^2$, $R = r$, where $a$ is a constant, using a translation and a rescaling of the radial coordinate $r$

The general asymptotic behaviour of the solution (3.17) depends on the value of $w$, i.e. when $0 < w < 1/2$, we have for $r \to \infty$ (corresponding to $\phi \to -\infty$) at leading order:

$$U = \frac{(1-2w)^4}{r_0^4Q^4}\left(\frac{r}{r_0}\right)^{-1+2w}, \quad R^2 = \frac{r_0^4Q^4}{(1-2w)^4}\left(\frac{r}{r_0}\right)^{2-2w}, \quad \phi = -\gamma\log\frac{r}{r_0}\,, \tag{3.21}$$

while when $1/2 < w < 1$ one finds:

$$U = \left(\frac{r}{r_0}\right)^{1-2w}, \quad R^2 = \left(\frac{r}{r_0}\right)^{2w}, \quad \phi = -\gamma\log\frac{r}{r_0}\,. \tag{3.22}$$

Notice that in the latter case the asymptotic behaviour coincides with the neutral solution (3.5) with $d = 2$, discussed in the previous subsection. It is also easy to check that the two asymptotic forms (3.21) and (3.22) are mapped one into the other by the transformation $w \to 1-w$, that leaves invariant the constraint $w - w^2 = \gamma^2$.

## Energy of the Brane

Also in this case, we compute the total energy of the solution using the Euclidean action formalism [175]. The variation of the boundary terms of the action are:

$$\delta M = \delta M_G + \delta M_\phi - 16\pi\, Q\, \delta\Phi|^\infty\,, \tag{3.23}$$

where $\delta M_G$ and $\delta M_\phi$ are the gravitational and scalar contributions, corresponding to Eqs. (3.9) and (3.10) with $d = 2$, while the last term is the contribution due to the charge and $\Phi$ is the electric potential.

Evaluating the energy for our solution (3.17), we find that the electromagnetic contribution always vanishes at $r = \infty$, and the full result depends on the value of $w$. When $0 \leqslant w \leqslant 1/2$ we obtain

$$M = \frac{16\pi}{r_0}\left[-w + (2w-1)\log\frac{Q}{Q_0}\right], \tag{3.24}$$

where $Q_0$ is an integration constant. In this case the sign of the energy depends on the mutual values of $w$ and $Q$. When $1/2 \leqslant w \leqslant 1$ (where the asymptotic behaviour of the charged brane (3.17) coincides with the uncharged brane (3.5) for $d = 2$), one simply finds

$$M = -\frac{16\pi}{r_0}\,. \tag{3.25}$$

As expected, it coincides with the energy (3.11) of the uncharged solution with $d = 2$.

## Scaling Symmetries and Hyperscaling Violation

In order to study the scaling symmetries of the solution (3.17) in the ultraviolet regime, i.e. $r \to \infty$, we consider first the asymptotic form (3.21), describing the ultraviolet regime of the solution when $0 \leqslant w \leqslant 1/2$. Eq. (3.21) can be put in the form (3.1) by the transformation of coordinates

$$\frac{r}{r_0} \to \left(\frac{r}{\tilde{r}_0}\right)^2, \quad \tilde{r}_0 = \frac{2r_0^3Q^2}{(1-2w)^2}\,. \tag{3.26}$$

After this transformation, it is simple to extract the hyperscaling violation parameter and the dynamical exponent:

$$z = 4(1-w)\,, \quad \vartheta = 2(3-2w)\,. \tag{3.27}$$

We immediately notice that $\vartheta = 0$ for $w = 3/2$, which is outside the range of $w$. Hence, Table 3.1 tells us that the brane solution (3.17) cannot describe neither an AdS nor a Lifšic brane. The brane is either a domain wall for $w = 3/4$ or a conformal-Lifšic brane for $w \neq 3/4$. Notice also that hyperscaling violation parameter and the dynamical exponent are not independent but they satisfy the relation $\vartheta = z + 2$, the very same relation they satisfy in the neutral case in $d + 2$ dimensions, cf. Eq. (3.14). As a direct consequence, the free energy of the dual QFT is constant.

The null energy conditions for the bulk stress-energy tensor

$$(2-\vartheta)[2(z-1)-\vartheta] \geqslant 0\,, \quad (z-1)(2+z-\vartheta) \geqslant 0\,, \tag{3.28}$$

are satisfied. In particular, the second one is saturated.

Exploiting the symmetry of the asymptotic solutions (3.21) and (3.22) under $w \to 1-w$, we can easily derive the critical exponents $\vartheta$ and $z$ related to the scaling (3.22), which, as expected, are those of (3.13) with $d = 2$.

## 3.4 Classification of Brane Solutions Sourced by Scalar Fields

In this section we present a detailed physical classification of brane solutions sourced by a scalar field with a self-interaction potential $V(\phi)$, i.e. a classification of the brane solutions of the minimally coupled Einstein-Maxwell-scalar gravity theory described by the action (A.1). Obviously, the form of the brane solution will strongly depend on the form of the potential and a complete classification is without reach. On the other hand, having in mind holographic applications, we are not interested in generic solutions but on branes that respect some scaling symmetries, at least in some regions, say $r \to \infty$ and $r \to 0$. We can therefore build up a brane classification based on the scaling symmetries discussed in Section 3.2.

We will preliminary show that the scale-covariant solution (3.5) together with the solutions already known in the literature give all the possible brane solutions of minimally coupled Einstein-Maxwell-scalar gravity of the form (3.1). Using a reparametrisation of the radial coordinate $r$ we can easily write the metric (3.1) in the form (A.5) with $U \sim (r/r_0)^a$, $R \sim (r/r_0)^b$; inserting these expressions in the field equations (A.8) with $Q = 0$ one finds only three classes of solutions:

| | Metric function | Scalar field | Scalar potential |
|---|---|---|---|
| $AdS_{d+2}$ brane | $u \sim r^{d+2}$ | $\phi = \text{const}$ | $V = -\Lambda^2$ |
| Solution (3.5) | $u \sim r$ | $\phi \sim \log(r/r_0)$ | $V = 0$ |
| Domain Wall | $u \sim r^\eta, \eta \neq \{1, d+2\}$ | $\phi \sim \log(r/r_0)$ | $V \sim e^{\mu\phi}$ |

In our classification, we will distinguish between *elementary* solutions, i.e. solutions that respect some scaling symmetry, and *interpolating* solutions, i.e. solutions that approach to elementary branes only in the $r = 0$ infrared region and in the $r = \infty$ ultraviolet region. We will discuss separately these two types of solutions.

### 3.4.1 Elementary Solutions

Elementary solutions are defined as those solutions of minimally coupled Einstein-Maxwell-scalar theory which belong to one of the subclasses of Table 3.1. In principle, we should have four kinds of elementary branes, in correspondence with the four scale symmetries of Table 3.1. Yet, as a consequence of the previous demonstration, the Lifšic solution cannot be obtained if the source is a minimally coupled scalar field and we are therefore left with three classes of solutions:

(A) *AdS branes*, i.e. neutral solutions when the potential is a negative cosmological constant or has a local extremum. In this case we have a trivial scalar field.

(B) *Domain Walls*, i.e. neutral solutions when the potential is a pure exponential. Domain walls are sourced by a scalar behaving logarithmically.

(C) *Conformal-Lifšic branes*, i.e. neutral solutions for an identically null potential. For $Q \neq 0$ they appear as solutions of the theory for a purely exponential potential.

For finite $z$ and $\vartheta$ in Eq. (3.1), there are no other elementary brane solutions which can be sourced by a minimally coupled scalar field. However, in the $\vartheta = 0$, $z \to \infty$ limit, it is known that the Lifšic brane becomes the $\mathrm{AdS}_2 \times \mathbb{R}_d$ spacetime [126], and one could include this limiting case as the fourth kind of elementary brane solutions, namely the *$AdS_2 \times \mathbb{R}_d$ branes*. These spacetimes are charged solutions of Einstein-Maxwell-scalar theory when the potential is a negative cosmological constant or has a local extremum. Similarly to case (A), these branes are sourced by a constant scalar field.

### 3.4.2 Interpolating Solutions

Combining the three types of elementary brane solutions discussed above, one can construct different kinds of interpolating solutions, i.e. solutions that behave as elementary branes only in the ultraviolet and infrared regimes. These interpolating solutions are very useful for holographic applications, in particular for AdS/CFT and the gravity/condensed matter correspondence of Einstein-Maxwell-scalar gravity.

The recent literature dealing with this topic contains a multitude of such interpolating brane solutions derived in the context of the gravity theory (A.1) and its possible generalisations — covariant coupling between the $\mathrm{U}(1)$ gauge field and the scalar, coupling between the Maxwell tensor and the scalar, Einstein-Yang-Mills-scalar gravity, etc. Despite this variety of solutions and models, the simplest case described by the action (A.1) is extremely important for the crucial role played by the scalar field. In the dual QFT, the scalar field gives an order parameter triggering symmetry breaking and/or phase transitions. Moreover, the scalar field has a nice interpretation in terms of holographic renormalisation group equations describing the flow between ultraviolet/infrared fixed points, see e.g. Ref. [176].

The classification of the possible interpolating solutions of the theory (A.1) is simple because it is parametrised by a single function, the potential $V(\phi)$. It follows that the interpolating solutions are essentially determined by the behaviour of the potential in the infrared and ultraviolet region. This feature is not present in other, more complicated, models in which the presence of two or more coupling functions prevents a simple classification. In the following we will list all the known interpolating solutions and, in the case they have not been already discussed in the literature, we will discuss their possible existence.

AdS-AdS interpolating solutions. In general, solutions of this kind are present when the potential has a local maximum and a local minimum connected with continuity. The gravitational soliton bridges two AdS spacetimes whereas the dual field theory flows from a fixed point in the ultraviolet to another fixed point in the infrared. The two CFTs are connected by the

c-theorem, which gives well-defined predictions for the running of the central charge when running from the ultraviolet to the infrared. Interpolating solutions of this kind are typically numerical solutions and have been already discussed in the literature, see e.g. Ref. [177].

AdS-DW Interpolating solutions. Typically, these solutions are present when $Q = 0$ and the potential has an extremum at $\phi_0$ with $V(\phi_0) < 0$ in the ultraviolet (infrared), whereas it behaves exponentially in the infrared (ultraviolet). The gravitational soliton interpolates between an AdS spacetime at $r = \infty$ ($r = 0$) and a domain wall near $r = 0$ ($r = \infty$). The dual QFT flows from a fixed point in the ultraviolet (infrared) to an hyperscaling violating phase in the infrared (ultraviolet). Exact solutions of this kind are known, in the case of hyperscaling violation both in the infrared [111] and in the ultraviolet [113, 121]. Several numerical solutions are also known, see e.g. Ref. [114].

AdS-CL Interpolating solutions. Brane solutions of the theory (A.1) bridging an AdS spacetime in the ultraviolet (infrared) with a conformal-Lifšic solution in the infrared (ultraviolet) have not been discussed in the literature. Conversely, they are quite common in non-minimally coupled theories and in the case of holographic superconductors. In the context of the minimally coupled theory they are expected to show up in two cases: first, when $V(\phi)$ has an extremum in the ultraviolet (infrared), whereas in the infrared (ultraviolet) region the kinetic energy of the scalar dominates over its potential energy so that we can use $V \sim 0$; second, we have $Q \neq 0$ charged solutions, $V(\phi)$ has an extremum in the ultraviolet (infrared) whereas in the infrared (ultraviolet) region $V$ behaves exponentially. Obviously the existence of these solutions must be checked numerically.

DW-DW Interpolating solutions. Solutions interpolating between two domain wall branes are not known in the literature. However, we can easily find a form of the potential which is a good candidate for generating this kind of solution. One can start from a simple combination of exponentials: $V(\phi) = A\,\mathrm{e}^{\phi} + B\,\mathrm{e}^{-\phi}$, that obviously behaves as a single exponential in the two regimes $\phi \to \infty$ and $\phi \to -\infty$. We know that a simple exponential form of the potential leads, in the case of uncharged branes, to a domain wall solution [111]. Thus, the corresponding brane solutions of the model, if they exist, would give a soliton interpolating between two domain walls at $\phi = \pm\infty$.

DW-CL Interpolating solutions. Having in mind the features of the elementary solutions discussed in Section 3.4.1, one can expect this kind of solution to show up in the case of a potential which diverges exponentially in a region whereas approaches to zero in another region. Solutions of this type, although already known in the literature, had not been recognised as DW-CL interpolating solutions. We will show in Section 3.5 that, for an appropriate choice of the parameters, the solutions of Ref. [111] describe a DW-CL interpolating solution.

CL-CL Interpolating solutions. In order to generate this kind of branes one should consider a potential which vanishes in two distinct regions. Alternatively, one could consider charged solutions and a potential behaving exponentially. A mixed charged configuration is possible too: a vanishing potential in one region and an exponential one in the other region. Solutions of this type were known in the literature as well, but not recognised as CL-CL interpolating solutions. We will show in Section 3.6 that, for an appropriate choice of the parameters, the solutions of Ref. [111] describe a CL-CL interpolating solution.[2]

In the above classification of interpolating brane solutions, we have not considered the limiting case in which one of the elementary solution is $\mathrm{AdS}_2 \times \mathbb{R}_d$. Brane solutions interpolating between an elementary solution (A), (B) or (C) in the ultraviolet and $\mathrm{AdS}_2 \times \mathbb{R}_d$ in the infrared possibly exist whenever one considers charged branes and a potential $V$ behaving in the infrared as a negative cosmological constant. The simplest, well-known, example of this kind is obtained considering $V = -\Lambda^2$ identically. The charged brane solutions are simply given by the AdS-Reissner-Nordström black brane. In the extremal limit, when the BPS bound is saturated, we get a solitonic solution which interpolates between $\mathrm{AdS}_{d+2}$ in the $r \to \infty$ region and $\mathrm{AdS}_2 \times \mathbb{R}_d$ in the near-horizon region. The $\mathrm{AdS}_2 \times \mathbb{R}_d$ geometry and related interpolating solutions are of interest also because they may act as infrared regulators of the generic scale-covariant geometry (3.1) [126].

All the above interpolating solutions are considered as branes without event horizons, i.e. as zero temperature solutions. An important question, particularly in view of holographic applications, is whether they can be considered as the extremal limit of black brane solutions with non-trivial hair, i.e. solutions at finite temperature endowed with a non-trivial scalar field. There is no general answer to this question. Owing to no-hair theorems the existence of hairy solutions is related to global features of the potential $V(\phi)$. Nevertheless, in most examples discussed in the literature, the interpolating solutions appear as extremal limit of black brane solutions.

## 3.5 Domain-Wall/Conformal-Lifšic Interpolating Solutions

In this section we discuss exact solutions, which interpolate between a domain wall and a conformal-Lifšic brane. In the previous section we have seen that this kind of solution requires uncharged branes and a potential which diverges exponentially in a region, whereas approaches to zero in another region. We are therefore lead to consider $Q = 0$ solutions and the following simple potential ($0 \leqslant w \leqslant 1$)

$$V(\phi) = V_0\, dw\, [1 - w(d+2)] \exp\left(-\sqrt{\frac{8(1-w)}{dw}}\,\phi\right), \tag{3.29}$$

2. CL-CL interpolating solutions appear also in the context of non-minimally coupled Einstein-Maxwell-scalar gravity, see e.g. Sect. 8 of Ref. [178].

which diverges exponentially for $\phi \to -\infty$, while $V \to 0$ for $\phi \to \infty$. The general solution for the theory (A.1) with this potential is given by [111]

$$U = V_0\, R^2 - \alpha \left(\frac{r}{r_0}\right)^{1-dw}, \quad R^2 = \left(\frac{r}{r_0}\right)^{2w}, \quad \phi = \sqrt{\frac{d}{2}(w - w^2)}\, \log \frac{r}{r_0}\,, \tag{3.30}$$

where $0 \leqslant w \leqslant 1$ and $\alpha$ is an integration constant. Notice that when $V_0 = 0$, i.e. the potential is identically zero and the solution is sourced by the kinetic term of the scalar, the solution (3.30) becomes exactly the solution (3.5) if we set $\alpha = -1$.

When $\alpha > 0$ and $1/(d+2) < w \leqslant 1$, the solution (3.30) describes a black brane with an event horizon [111]. On the other hand, when $\alpha < 0$ the solution has no horizon and depending on the value of $w$ it has different asymptotic behaviour. For $0 \leqslant w < 1/(d+2)$, at $r \to \infty$ ($\phi \to \infty$) the second term in the metric function $U$ dominates over the first, the potential approaches zero and the solution becomes the conformal-Lifšic brane solution discussed in the previous section. Conversely, near $r = 0$ (corresponding to $\phi \to -\infty$), the potential diverges, the first term dominates over the second and the solution becomes a domain wall. Thus, the global solution (3.30) interpolates between a conformal-Lifšic brane in the ultraviolet and a domain wall in the infrared. Physically, this means that the ultraviolet behaviour is dominated by the kinetic energy of the scalar field, whereas the infrared behaviour is dominated by the potential energy of the scalar. Obviously, for $\alpha < 0$ and $1/(d+2) < w \leqslant 1$ the picture is reversed and we have a global solution that interpolates between a conformal-Lifšic in the infrared and a domain wall in the ultraviolet. The solution (3.30) in the $\alpha = 0$ extremal case, becomes the domain wall one obtains in the $r = 0$ region, and it has been extensively investigated in Ref. [178].

For $\alpha > 0$ and $1/(d+2) < w \leqslant 1$, we can compute the thermodynamical parameters of the black brane. The total mass in computed using Eqs. (3.9) and (3.10) and it reads

$$M = \frac{4\pi V_0\, dw\alpha}{r_0}\,, \tag{3.31}$$

while the temperature and the entropy are calculated using the well-known formulæ of Eq. (2.42)

$$T = \frac{V_0\,[(d+2)w - 1]}{4\pi r_0}\, \alpha^{(2w-1)[(d+2)w-1]}, \quad S = 16\pi^2 \alpha^{dw/[(d+2)w-1]}\,. \tag{3.32}$$

Using these equations it is easy to verify that the first principle $\mathrm{d}M = T\,\mathrm{d}S$ is satisfied.

## 3.6 Conformal-Lifšic/Conformal-Lifšic Interpolating Solutions

In Section 3.4.2 we have seen that CL-CL interpolating solutions require charged branes ($Q \neq 0$) and a potential having the same qualitative behaviour of (3.29). Considering for simplicity the four-dimensional case, $d = 2$, we take a non-vanishing electric charge and the potential

$$V(\phi) = \frac{2Q^2(1-w)}{1-3w}\, \exp\left(-4\sqrt{\frac{w}{1-w}}\,\phi\right). \tag{3.33}$$

The general brane solutions are given by [111]:

$$U = \frac{2Q^2 r_0^2}{(1-2w)(1-3w)} \left(\frac{r}{r_0}\right)^{2-4w} \left[1 - \beta \left(\frac{r}{r_0}\right)^{-1+2w}\right], \tag{3.34}$$
$$R^2 = \left(\frac{r}{r_0}\right)^{2w}, \quad \phi = \sqrt{w - w^2} \log \frac{r}{r_0}, \quad 0 \leqslant w \leqslant 1\,.$$

Also in this case, for $\beta > 0$ and $0 \leqslant w < 1/2$ (with $w \neq 1/3$) the solution (3.34) describes a black brane with an event horizon. For negative $\beta$ the brane has no horizon and it interpolates between two conformal-Lifšic elementary solutions in the infrared and ultraviolet regions. When $\beta < 0$ and $w > 1/2$, for $r \to \infty$ ($\phi \to \infty$) the potential approaches to zero and the solution gives an elementary conformal-Lifšic solution, which coincides with the asymptotic regime of the electrically charged brane (3.21) when $w > 1/2$. The solution reduces to an elementary conformal-Lifšic brane, also near $r = 0$, but with a different dynamical exponent. For $\beta < 0$ and $0 \leqslant w < 1/2$ ($w \neq 1/3$) we have the same limiting elementary conformal-Lifšic branes but with the infrared and ultraviolet regions exchanged. The $\beta = 0$ extremal limit describes conformal-Lifšic branes.

For $\beta > 0$ and $0 \leqslant w < 1/2$ (with $w \neq 1/3$) we can compute the thermodynamical parameters associated to the black brane:

$$M = \frac{8\pi\beta w}{r_0}, \quad T = \frac{(1-2w)}{4\pi r_0}\beta^{(1-4w)/(1-2w)}, \quad S = 16\pi^2 \beta^{2w/(1-2w)}, \tag{3.35}$$

and check that the first principle $\mathrm{d}M = T\,\mathrm{d}S$ is satisfied.

## 3.7 Summary and Conclusions

In this chapter, we have derived brane solutions of minimally coupled Einstein-Maxwell-scalar gravity in $d + 2$ dimensions in the case of an identically null potential. We have shown that these brane solutions belong to the broad class of scale-covariant metrics, which generate hyperscaling violation in the holographically dual QFT. Moreover, these solutions can be considered as the brane counterpart of the Janis-Newman-Winicour-Wyman spherical solutions of Einstein-scalar gravity. We have also explicitly shown that our brane solution, together with the AdS brane and the domain wall solution sourced by an exponential potential, give all the possible scale-covariant, hyperscaling violating, geometries of minimally coupled Einstein-Maxwell-scalar gravity with no Schrödinger isometries. Using this result, we have been able to give a classification of the brane solutions of the theory in terms of elementary and interpolating solutions. In particular, the interpolating solutions can find a broad field of holographic applications because the dual QFT describes the flow from different regimes (fixed points, hyperscaling violation, Lifšic) in the ultraviolet and infrared, characterised by different scaling symmetries.

In this context, it is important to stress that some of our solutions have curvature singularities at $r = 0$ (in the infrared of the dual QFT). The issue of the acceptability of naked singularities in the context of holographic models, and in particular in Einstein-Maxwell-scalar models, has been discussed in several papers [178–181]. A basic requirement for a solution with a naked singularity to be acceptable is that the scalar potential is bounded from above when evaluated at the solution [179]. This basic requirement is trivially satisfied for the brane solutions sourced by a scalar field with $V = 0$, discussed in Section 3.3. On the other hand, further requirements involving properties of the spectrum of small fluctuations near the solution must be imposed if the solution has to be considered physically acceptable. Alternatively, one can resolve the singularities looking for an infrared completion of the theory. From the bulk point of view, this completion can be realised using an infrared regular geometry such as $AdS_{d+2}$ [120] or $AdS_2 \times \mathbb{R}_d$ [126].

Chapter 4

# Inflation as de Sitter Instability

Inpired by holographic models of gravity, we consider a cosmological inflationary model in which inflation is generated by a scalar field slowly rolling off from a de Sitter maximum of its potential. Such models belong to the class of hilltop models and represent the most general model of this kind in which the scalar potential can be written as the sum of two exponentials. In the slow-roll approximation, our model reproduces correctly, for a wide range of its parameters, the most recent experimental data for the power spectrum of primordial perturbations. Moreover, it predicts inflation at energy scales of four to five orders of magnitude below the Planck scale. At the onset of inflation, the mass of the tachyonic excitation, i.e. of the inflaton, turns out to be seven to eight orders of magnitude smaller than the Planck mass.

Units: $c = \hbar = 1$.

This chapter is based on: M. Cadoni, E.F, and S. Mignemi. 'Inflation as de Sitter instability'. *Eur. Phys. J.* C76 (2016), 483. arXiv: 1510.04030.

## 4.1 Introduction

As we mentioned in Section 1.4, inflation is well described by a scalar field coupled to Einstein gravity. There exist a plethora of single-field inflationary models that can be classified according to the features of the scalar potential [182], but other alternatives include more scalar fields, as in the curvaton mechanism [183–185]. Nevertheless, the most recent data of the Planck satellite exclude non-Gaussian perturbations and give a striking experimental confirmation of the simplest single-field inflationary scenario [8, 186, 187], and in particular the Starobinsky model [149, 188, 189], or more in general, the so-called cosmological attractors [190–193], characterised by a 'red' power spectrum for primordial perturbations and a small tensor/scalar amplitude ratio.

The accuracy of the observational data concerning the power spectrum of primordial quantum fluctuations represents an efficient guide to select inflation models. But, despite the recent remarkable improvements, the important questions about the microscopic origin of the inflaton and the physics before inflation are still unanswered. This lack of knowledge does not allow one to single out a unique inflationary model, i.e. a specific form of the potential. In fact, although the Planck data can be used to strongly constrain the inflationary model, mainly through the values of the spectral index $n_s$ and the tensor/scalar amplitude ratio $r$, they are not sufficient to select a unique model.

In view of this situation, it is natural to look for hints coming from somewhere else in gravitational physics, for instance supergravity and string theory [194–197]. In Section 1.3, we mentioned

that there exists an 'analytical continuation' of the AdS/CFT correspondence, namely the domain wall/cosmology correspondence. The cosmological duals of solitons interpolating between AdS in the infrared and scale-covariant geometries in the ultraviolet generate inflation as the scalar field rolls down from a de Sitter spacetime [148]. In this context, inflation can be described as an instability of the de Sitter spacetime rolling down to a scaling solution. Such models are known as hilltop models [198, 199] and inflation is generated by a scalar field rolling off from a local maximum of the potential. In such a scenario, since inflation starts from a local maximum, the slow-roll conditions can be satisfied more easily. On the experimental side, hilltop models are a subset of the small-field models, which are characterised by a potential with negative curvature. This behaviour of the potential is typical of spontaneous symmetry breaking and phase transitions, e.g. quartic potentials, natural inflation models [200] and Coleman-Weinberg potentials [201]. Although hilltop models have been widely used to generate cosmological inflation, in most of them the potential is constructed using powers of the inflaton field. To our knowledge, little attention has been given to hilltop models in which the potential is built as a combination of two exponentials. In this chapter, we generalise a model proposed by Mignemi and Pintus [148] and we discuss the most general, holographically motivated, hilltop model, for which the potential can be written as the sum of two exponentials. We will show that although near the maximum our model has the well-known behaviour of hilltop models with a parabolic potential, at late times it gives predictions of the spectral parameters of the cosmic microwave background radiation, which are specific for a two-exponential potential.

## 4.2 The Model

The single-field models for inflation are described by the following action,

$$\mathcal{A} = \int \mathrm{d}^4x\sqrt{-g}\left(\frac{m_P^2}{16\pi}\,\mathcal{R} - \frac{1}{2}(\partial\phi)^2 - V(\phi)\right). \tag{4.1}$$

Here, we focus on inflation generated by a scalar field rolling off from a maximum of the scalar potential $V(\phi)$. This class of models is very natural from a physical point of view because inflation can be thought of just as an instability of the de Sitter spacetime, generated by a scalar perturbation.

Our first goal is to construct the general form of the potential belonging to this class. Without loss of generality we can assume that the maximum of the potential occurs at $\phi = 0$, so that the basic necessary conditions to be imposed on the potential read

$$V|_{\phi=0} > 0\,, \quad \left.\frac{\mathrm{d}V}{\mathrm{d}\phi}\right|_{\phi=0} = 0\,, \quad \left.\frac{\mathrm{d}^2V}{\mathrm{d}\phi^2}\right|_{\phi=0} < 0\,. \tag{4.2}$$

Obviously, the previous conditions are very loose and do not select any specific form of $V(\phi)$. We further constrain the form of the potential by requiring it to be a linear combination of two exponentials. This is a rather strong assumption, but is supported by several arguments. Exponential

potentials for scalar fields appear quite generically in a variety of situations: compactification of extra dimensions, $f(\mathcal{R})$ gravity theories (which on-shell are equivalent to Einstein-scalar gravity) and low-energy effective string theory. The double exponential potential appears in the context of dimensional reduction of gravity with non-trivial four-form flux on a maximally symmetric internal space [202]. Moreover, exponential potentials have been shown to be the source of brane solutions of Einstein-scalar gravity called domain walls [111, 113], which can be analytically continued into Friedmann-Robertson-Lamaître-Walker cosmological solutions [147, 148].

We are therefore led to consider the following general form of the inflation potential[1]

$$V(\phi) = \Lambda^2 \left( a_1 \, \mathrm{e}^{b_1 \mu \phi} + a_2 \, \mathrm{e}^{b_2 \mu \phi} \right) , \tag{4.3}$$

where $\Lambda$ and $\mu$ are some length scales, whose physical meaning will be clarified in short, and $a_{1,2},\ b_{1,2}$ are some dimensionless constants characterizing the model. They are constrained by Eqs. (4.2), giving

$$a_1 + a_2 > 0 \, , \quad a_1 b_1 = -a_2 b_2 \, , \quad a_1 b_1^2 + a_2 b_2^2 < 0 \, . \tag{4.4}$$

Modulo trivial symmetries interchanging the two exponentials in the potential, the most general solution of the previous equations is $a_1 > 0$, $a_2 < 0$, $b_2 > 0$, $b_1 > 0$ and $a_2/a_1 = -\beta^2$, where we have defined a new dimensionless parameter $\beta^2 \equiv b_1/b_2 < 1$. The parameter rescaling $\Lambda^2 \to 2\Lambda^2/(3a_2\gamma)$, $\mu \to \sqrt{3/(b_1 b_2)}\, \mu$ brings the potential in the form

$$V(\phi) = \frac{2\Lambda^2}{3\gamma} \left( \mathrm{e}^{\sqrt{3}\beta\mu\phi} - \beta^2 \, \mathrm{e}^{\sqrt{3}\mu\phi/\beta} \right) , \tag{4.5}$$

where $\gamma \equiv 1 - \beta^2$. The potential (4.5) is a two-scale generalisation of the model proposed in Refs. [113, 121], to which it reduces for the particular value of the parameter $\mu = 4\sqrt{\pi}\, l_P$. The cosmology of the particular model has been investigated in Ref. [148].[2] We will see in the next section that for generic values of the parameter $\mu \neq 4\sqrt{\pi}\, l_P$ the cosmological equations resulting from the model (4.5) do not give rise to an exactly integrable system.

The potential (4.5) is invariant both under the transformation $\beta \to 1/\beta$, which corresponds to interchanging the two exponentials, and under the transformation $\beta \to -\beta$, $\phi \to -\phi$. These symmetries allow us to limit our consideration to $0 < \beta < 1$. The two limiting cases $\beta = 0, 1$ correspond, respectively, to a pure exponential and to a potential behaving at leading order as

$$V(\phi) = \frac{2\Lambda^2}{3} \left( 1 - \sqrt{3}\mu\phi \right) \mathrm{e}^{\sqrt{3}\mu\phi} \, . \tag{4.6}$$

The potential $V(\phi)$ has a maximum at $\phi = 0$ corresponding to an unstable de Sitter solution with $V(0) = 2\Lambda^2/3$ and a corresponding tachyonic excitation, the inflaton.

The potential $V(\phi)$ is depicted in Fig. 4.1 for selected values of the parameters $\Lambda$, $\beta$ and $\mu$.

1. One could also consider a potential with an added constant term. This case will be discussed in Section 4.7.

2. Notice that our notation differs from that of Ref. [148] for the units used and for a rescaling of the parameter $\mu$ by a factor of 2.

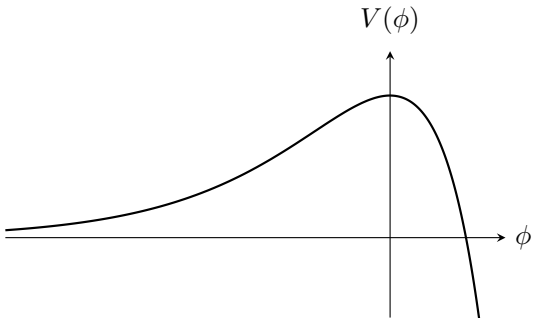


Figure 4.1: Plot of the potential (4.5) for $\Lambda = 2$, $\beta = 3/4$ and $\mu = \sqrt{3}/3$ in Planck units.

One can therefore use this model to describe inflation as generated by an unstable de Sitter solution. Inflation starts as a quantum fluctuation of the de Sitter solution and is initially driven by a tachyonic excitation of the de Sitter spacetime and proceeds as the scalar field rolls off from the maximum of the potential.

## Physical Scales

Besides the Planck length $l_P = 1/m_P$, the model is parametrised by the two length scales $\Lambda^{-1/2}$ and $\mu$ and by the dimensionless parameter $\beta$. The presence of two length scales is a characteristic feature of small-field models of inflation. In the present context, the two scales have a simple interpretation in terms of geometric properties of the function $V(\phi)$. They give, respectively, the height and the curvature of the $\phi = 0$ maximum of the function $V(\phi)$. Correspondingly, $\Lambda^{-1/2}$ and $\mu$ determine the two physical scales relevant for inflation: the vacuum energy $E_V$ at the beginning of inflation and the inflaton mass squared $M_I^2$. We have

$$M_I^2 = \left.\frac{\mathrm{d}^2 V}{\mathrm{d}\phi^2}\right|_{\phi=0} = -2\Lambda^2\mu^2 = -\frac{32\pi}{3}\frac{\lambda^4}{h^2}m_P^2\,, \tag{4.7}$$

$$E_V = [V(0)]^{1/4} = (2/3)^{1/4}\lambda\, m_P\,, \tag{4.8}$$

where we have introduced the two dimensionless parameters $h^{-1}$ and $\lambda$,

$$h = 4\sqrt{\frac{\pi}{3}}\left(\frac{l_P}{\mu}\right), \quad \lambda = \frac{\Lambda^{1/2}}{m_P}\,, \tag{4.9}$$

representing the measures of $\mu$ and $\Lambda^{1/2}$ in Planck units. In the following, instead of the negative quantity $M_I^2$, we use the inflaton mass defined as $m_I = \sqrt{-M_I^2}$.

Conversely, $\beta$ is a purely dimensionless parameter and plays a role which is drastically different from $\lambda$ and $h$. It is not linked to any physical scale of the model but quantifies the deviation of the potential from a pure exponential behaviour attained for $\beta$ near 0.

## 4.3 Cosmological Solutions

The cosmology of our model can be investigated using the usual Friedmann-Robertson-Lamaître-Walker parametrisation of the metric

$$\mathrm{d}s^2 = -\mathrm{d}t^2 + a^2(t)\,\mathrm{d}S^2_{(3)}\,. \tag{4.10}$$

The de Sitter spacetime with constant inflaton is an exact solution of the cosmological equations. The de Sitter solution has the usual exponential form, with the scale factor given by

$$a(t) = \exp\left(\frac{8\sqrt{\pi}\,l_P\,\Lambda\,t}{3}\right). \tag{4.11}$$

This solution describes a scalar field sitting forever at the maximum of the potential, generating an exact exponential expansion of the universe, i.e. never ending inflation.

The most interesting cosmological solutions are those in which inflation lasts for a finite amount of time. In this case, the scalar rolls off from the maximum of the potential, generating a quasi-exponential expansion of the universe as long as the potential energy of the scalar dominates over the kinetic one. This kind of solutions would be the cosmological counterpart of the solitonic solutions interpolating between an AdS spacetime in the infrared and a domain wall in the ultraviolet discussed in Refs. [113, 121].

Searching for these solutions, and following Ref. [148], one can try to find exact cosmological solutions by using a different parametrisation for the time variable and linear combinations of the fields in such way that the equations for the scalar field and the scale factor decouple. However, one can easily realise that the decoupling works only for the particular value of the parameter, i.e. $\mu = 4\sqrt{\pi}\,l_P$ (corresponding to $h = 1/\sqrt{3}$). For this value of $\mu$, the Einstein-scalar gravity models give rise to exactly integrable models both in the case of brane [113, 121] and cosmological solutions [148]. For generic values of the parameter $\mu$ the Einstein-scalar system does not decouple, is not exactly integrable and a cosmological solution cannot be found in analytic form.

Approximate solutions of the field equations can be found for some limiting cases. Of particular interest is the case of small $\beta$, for which the potential (4.5) behaves exponentially,

$$V(\phi) \sim -\frac{2\beta^2\Lambda^2}{3\gamma}\,\mathrm{e}^{\sqrt{3}\mu\phi/\beta}\,, \tag{4.12}$$

the system can be solved analytically and we have scaling (power-law) solutions, which are obtained from scale-covariant (domain wall) solutions using the transformation $t \to \mathrm{i}r$, $r \to \mathrm{i}t$ [111]. In the gauge (4.10) this scaling solution has the form

$$a(t) \sim t^{h^2\beta^2}\,, \quad \phi(t) \sim -\frac{h\beta}{2\sqrt{\pi}\,l_P}\log t\,. \tag{4.13}$$

## 4.4 Inflation and Slow-Roll Approximation

Lacking exact solutions to investigate the cosmology of our model (4.5), we work in the slow-roll approximation [203]. In this regime, the potential energy of the scalar field dominates over the kinetic energy and the universe has a quasi-exponential accelerated expansion as the scalar field slowly rolls off from the maximum of the potential. Following the usual approach, we introduce the slow-roll parameters $\epsilon$ and $\eta$,

$$\epsilon = \frac{m_P^2}{16\pi}\left(\frac{\mathrm{d}V/\mathrm{d}\phi}{V}\right)^2, \quad \eta = \frac{m_P^2}{8\pi}\frac{\mathrm{d}^2V/\mathrm{d}\phi^2}{V} - \epsilon\,. \tag{4.14}$$

Necessary conditions for the slow-roll approximation to be valid are $\epsilon, |\eta| \ll 1$. We have inflation as long as $0 \leqslant \epsilon < 1$. The parameter $\epsilon$ is zero on the maximum of the potential ($\phi = 0$) and the solution is exactly de Sitter, whereas inflation ends when $\epsilon = 1$.

The potential (4.5) and depicted in Fig. 4.1 is not a monotonic function of the scalar field: it goes to zero as $\phi \to -\infty$, has a maximum at $\phi = 0$, crosses the axis for $\phi = \phi_* \equiv -2\beta \log \beta/\sqrt{3}\gamma\mu$, and diverges to $-\infty$ as $\phi \to \infty$. Since slow-roll inflation cannot occur for a negative inflaton potential, our model is valid up to $\phi = \phi_*$ and the potential must be modified for values of $\phi$ greater than $\phi_*$. We have then two alternative branches that we can use to generate inflation, i.e. I: $0 \leqslant \phi \leqslant \phi_*$ and II: $-\infty < \phi \leqslant 0$. In the following, we investigate the first branch and in Section 4.5.3 we briefly discuss branch II and show that it cannot be compatible with observations.

Let us now introduce the variable

$$Y = \mathrm{e}^{\sqrt{3}\gamma\mu\phi/\beta}\,. \tag{4.15}$$

In this parametrisation the branch under consideration corresponds to $1 \leqslant Y \leqslant Y_* \equiv 1/\beta^2$.

As a function of $Y$, the slow-roll parameters $\epsilon$ and $\eta$ take the form

$$\epsilon = \frac{\beta^2}{h^2}\left(\frac{1-Y}{1-\beta^2 Y}\right)^2, \quad \eta = \frac{2}{h^2}\frac{\beta^2 - Y}{1-\beta^2 Y} - \epsilon\,. \tag{4.16}$$

The slow-roll parameter $\epsilon$ is zero for $Y = 1$, whereas $0 < \epsilon < 1$ for $1 < Y < Y_0$, where

$$Y_0 = \frac{\beta + h}{\beta + \beta^2 h}\,. \tag{4.17}$$

For $Y = Y_0$ we have $\epsilon = 1$ and the universe exits inflation. One can easily check that $Y_0 < 1/\beta^2$, so that during inflation we always have $1 < Y < 1/\beta^2$ and we can easily satisfy the first slow-roll condition $\epsilon \ll 1$. On the other hand, the parameter $\eta$, which gives a measure of the curvature of the potential, is not small, but we have $\eta = \mathcal{O}(h^{-2})$. It follows that the simplest way to satisfy the second slow-roll condition, $|\eta| \ll 1$, is to choose

$$h \gtrsim 10\,, \tag{4.18}$$

in this way we can have $\eta \approx 10^{-2}$ as well as $\epsilon \approx 10^{-2}$. As already noted, the model discussed in Ref. [148] does not satisfy Eq. (4.18) because it is characterised by $h = 1/\sqrt{3}$.

In the slow-roll regime, the universe expands quasi-exponentially and the number of e-folds $N = -\log a$, which determines the duration of inflation, is determined by

$$N = -\int \mathrm{d}t H = \frac{8\pi}{m_P^2} \int_{\phi_\mathrm{e}}^{\phi_\mathrm{b}} \mathrm{d}\phi \, \frac{V}{\mathrm{d}V/\mathrm{d}\phi} \,, \tag{4.19}$$

where $\phi_{\mathrm{e,b}}$ are the inflaton-field values at the end and beginning of inflation and $H \equiv \dot{a}/a$ is the Hubble parameter.

Using the definition (4.15) and the expression $Y_0$ for $Y$ at the end of inflation, Eq. (4.19) gives the function $Y(N)$ in implicit form,

$$\frac{Y^{1/\gamma}}{Y-1} = \mathrm{e}^{2N/h^2} A \,, \quad A := \frac{\beta}{\gamma} \left(\beta + \frac{1}{h}\right) \left(\frac{\beta + h}{\beta + \beta^2 h}\right)^{1/\gamma} . \tag{4.20}$$

In the case of the de Sitter solution (4.11) the scalar field remains constant (the inflaton sits on the top of the potential), and we have $N = \infty$, i.e. eternal inflation. Obviously this configuration is highly unstable. In fact, a small scalar perturbation starts the slow-roll of the inflaton along the slope and a finite value of $N$ is generated. If this fluctuation is small enough we can solve approximately Eq. (4.20) for $Y$ near $Y = 1$. We get at leading order,

$$Y = 1 + A^{-1} \, \mathrm{e}^{-2N/h^2} \,. \tag{4.21}$$

One can easily check that $0 \leqslant A^{-1} \leqslant 1$ with $A^{-1} \to 0$ for $\beta \to 1$ and $A^{-1} \to 1$ for $\beta \to 0$. Moreover, in the range $0 \leqslant \beta \leqslant 1$, $A^{-1}(\beta, h)$ is a monotonically decreasing function of $\beta$ which depends very weakly on $h$. It follows immediately that Eq. (4.21) is a good approximation for $\gamma$ not too close to 0, whenever $\mathrm{e}^{-2N/h^2} \ll 1$. When $\gamma \approx 0$ the approximation (4.21) holds irrespectively of the value of $N$.

## Perturbations and Spectral Parameters

One of the most striking predictions of inflation concerns the spectrum of tensor and scalar perturbations in the early universe [204–208]. During inflation the horizon shrinks and the primordial perturbations, which were causally connected are redshifted to superhorizon scales. Conversely, in the matter-radiation dominated era the horizon grows, the perturbations fall back on the horizon so that they can act as seeds for structure formation and anisotropy in the universe. The information as regards these primordial fluctuations is therefore encoded in the anisotropies of the cosmic microwave background.

Primordial quantum fluctuations are described in terms of two-point correlation functions for scalar and tensor modes in Fourier space and the associated power spectrum. In the slow-roll approximation, the power spectrum has a power-law behaviour and is usually characterised by four

parameters: the amplitudes of scalar perturbations $P_R$, the ratio $r$ of the amplitudes of tensor and scalar perturbations and their spectral indices $n_s$ and $n_T$. These parameters are functions of the number of e-folds $N$ and can be expressed in terms of the potential $V$ and the slow-roll parameters (4.16) as follows:

$$P_R^{1/2}(N) = \frac{4\sqrt{24\pi}}{3m_P^3} \left.\frac{V^{3/2}}{\mathrm{d}V/\mathrm{d}\phi}\right|_{\phi(N)}, \tag{4.22a}$$

$$r(N) = -8n_T(\phi(N)) = 16\epsilon(\phi(N)), \tag{4.22b}$$

$$n_s(N) = 1 - 4\epsilon(\phi(N)) + 2\eta(\phi(N)), \tag{4.22c}$$

where $\phi(N)$ is defined by Eq. (4.19).

Using Eqs. (4.15) and (4.16) we can express the spectral parameters as a function of $Y(N)$:

$$P_R^{1/2}(N) = \frac{4h\lambda^2}{3\beta\sqrt{\gamma}} \frac{[1-\beta^2 Y(N)]^{3/2}}{1-Y(N)} Y(N)^{\beta^2/2\gamma}, \tag{4.23a}$$

$$r(N) = \frac{16\beta^2}{h^2}\left(\frac{1-Y(N)}{1-\beta^2 Y(N)}\right)^2, \tag{4.23b}$$

$$n_s(N) = 1 - \frac{6\beta^2}{h^2}\left[\frac{1-Y(N)}{1-\beta^2 Y(N)}\right]^2 + \frac{4}{h^2}\frac{\beta^2 - Y(N)}{1-\beta^2 Y(N)}, \tag{4.23c}$$

where $Y(N)$ is defined, implicitly, by Eq. (4.20).

For $\mathrm{e}^{-2N/h^2} \ll 1$ we can use the approximate expansion for $Y$ given by Eq. (4.21) and we get, at leading order in the $\mathrm{e}^{-2N/h^2}$ expansion,

$$P_R^{1/2}(N) = \frac{4\gamma A}{3\beta} h\lambda^2 \,\mathrm{e}^{2N/h^2}, \tag{4.24a}$$

$$r(N) = \left(\frac{4\beta}{A\gamma h}\right)^2 \mathrm{e}^{-4N/h^2}, \tag{4.24b}$$

$$n_s(N) = 1 - \frac{4}{h^2}\left(1 + \frac{1+\beta^2}{A\gamma}\,\mathrm{e}^{-2N/h^2}\right). \tag{4.24c}$$

One important feature of Eqs. (4.24) is the exponential dependence on $N$. This must be compared with the typical behaviour of the Starobinsky model and more in general of cosmological attractor models, where one typically obtains $r \sim 1/N^2$ and $n_s - 1 \sim -1/N$ — see e.g. Ref. [193] and references therein.

It is easy to check that the exponential behaviour of the spectral parameters (4.24) is a universal feature of hilltop models characterised by a quadratic maximum. It is a consequence of the local behaviour of the potential near $\phi = 0$. In fact, Eqs. (4.24) can also be obtained by considering a potential $V(\phi) = 2\Lambda^2/3 + M_I^2\phi^2/2$, with $M_I^2$ given by Eq. (4.7). This is consistent with the fact that for $N/h^2$ very large, inflation occurs near to the maximum of the potential, where $V(\phi)$ can be approximated by the previous form.

Notice that the condition $h \gg 1$ alone does not guarantee the potential to be well approximated by the parabolic one. Since we need at least $h \gtrsim 10$, such limit is obtained for $N \gg 60$. For instance, for $h = 10$ and $N = 60$, we have $e^{-2N/h^2} \approx 0.54$. It follows that the approximate expressions (4.24) can only be used in a regime of very large $N$, for which we do not have direct access to observations, and, therefore, in the following, we will be using expressions (4.23).

## 4.5 Comparison with Observation

In this section we compare the theoretical results of our model for the spectral parameters $P_R$, $r$ and $n_s$ with the most recent results of observations, in particular the joint analysis of BICEP2/Keck Array and Planck data [186].

The spectral parameters are functions of the number of the e-folds $N$ and depend on the three dimensionless parameters $\lambda$, $h$ and $\beta$. Because $\lambda$ enters only in the normalisation of the power spectrum $P_R$, whereas $r$ and $n_s$ depend on $h$ and $\beta$ only we will use the following strategy: we will first determine using Eqs. (4.23b) and (4.23c) and the experimental results for $r$ and $n_s$, the allowed range of the parameters $h$ and $\beta$ for a given value of e-folds $N$. We will then use Eq. (4.23a) and the experimental results for $P_R$ to determine the corresponding values of the parameter $\lambda$. Finally we use Eqs. (4.7) and (4.8) to determine the vacuum energy $E_V$ and the inflaton mass $m_I$.

For $r$, $n_s$ and $P_R$ we use the most recent results [186], i.e. $r < 0.05$, $n_s = 0.965 \pm 0.006$ and $P_R^{1/2} \approx 10^{-5}$. Since the perturbations we are observing today with momentum of the order of the horizon radius exited the horizon during inflation at $N = [48, 60]$, we will consider only values of $N$ in this range.

The calculations have to be performed numerically because the function $Y(N)$ appearing in Eqs. (4.23) is not known, but it is defined implicitly by Eq. (4.20). As we said in the previous section, a possible way to avoid numerical computations is to work in a regime where $e^{-2N/h^2} \ll 1$ and then Eqs. (4.24) hold. But unfortunately, these expressions are valid in the large $N$ regime, not accessible to observations.

The results of our numerical computations are shown in the two sets of density plots in Figs. 4.2 and 4.3. Once we have chosen the value of $N$, the coloured region in such plots represent the range of values of $\beta$ and $h$ for which we have values of $r$ and $n_s$ compatible with the experimental measurements. Note that the allowed region of parameters $(\beta, h)$ is quite independent from $N$, at least for $N$ in the range $[48, 60]$.

### 4.5.1 Spectral Parameters

In Fig. 4.2 we show the numerical results obtained from Eqs. (4.23b) and (4.23c). We plot the tensor/scalar ratio $r$ (left) and the spectral index $n_s$ (right) as functions of $\beta$ and $h$ for four selected

values of $N = 48, 52, 56, 60$. The corresponding values of $r$ and $n_s$ are given in terms of the colour scale shown on the right of every plot.

In general, higher values of $n_s$ correspond to higher values of $h$. Moreover, when $\beta$ is not too close to zero, $n_s$ depends very weakly on $\beta$. For $\beta$ close to zero $h$ is allowed to vary from $h \sim 15$ up to $h \sim 1000$ and farther. As $\beta$ increases the allowed range of $h$ shrinks monotonically and is restricted to $[15, 50]$ for $\beta$ close to 1.

The tensor/scalar ratio $r$ shows a different pattern. For $\beta$ close to zero it depends strongly on $h$. Whereas for values of $\beta$ not too close to zero, it depends weakly on both parameters $\beta$ and $h$. Also in this case we observe the monotonic shrinking of the allowed values of $h$ for growing values of $\beta$.

### 4.5.2 Vacuum Energy and Inflaton Mass

In Fig. 4.3 we show the numerical results obtained from Eqs. (4.7) and (4.8). We plot the vacuum energy $E_V$ (left) and the inflaton mass $m_I$ (right) as functions of $\beta$ and $h$, again for $N = 48, 52, 56, 60$. The corresponding values of $E_V$ and $m_I$ are given in terms of the scale of colour shown on the right of every plot.

Since we do not have stringent experimental bounds on $E_V$ and $m_I$, we are interested just in the order of magnitude of these quantities. We observe that the order of magnitude of $E_V$ depends very weakly on $h$ and $N$. Also the dependence on $\beta$ is quite weak, as long as we take values of $\beta$ not too close to 0. Thus, for $\beta$ not too close to 0, the vacuum energy remains about $10^{-4}$ to $10^{-5}$ Planck masses. On the other hand, the inflaton mass is more sensitive to $\beta$. Its order of magnitude is between $10^{-7}$ and $10^{-8}$ Planck masses but for values of $\beta$ near to 0 we have smaller values of $m_I$.

### 4.5.3 The Other Branch of the Potential

Until now we have considered the slow-roll regime for branch I of the potential, i.e. $0 \leqslant \phi < \phi_*$. Let us briefly consider branch II, i.e. $-\infty < \phi \leqslant 0$. This might be interesting since the cosmological solutions one can obtain for the exact solvable model with $h = 1/\sqrt{3}$ are defined in this branch [148].

In terms of the parametrisation (4.15), branch II corresponds to $0 < Y \leqslant 1$. The slow-roll parameters $\epsilon$ and $\eta$ are still given by Eqs. (4.16) but now the condition for inflation $\epsilon \leqslant 1$ requires

$$\frac{\beta - h}{\beta(1 - \beta h)} \leqslant Y \leqslant 1\,,$$

which can be satisfied only if $h < \beta$. It follows that $h = \mathcal{O}(1)$. One can easily see from Eqs. (4.16) and Eqs. (4.23b) and (4.23c) that these values of $h$ are not only incompatible with the slow-roll condition $|\eta| \ll 1$, but are also completely ruled out by the experimental constraints on $n_s$.

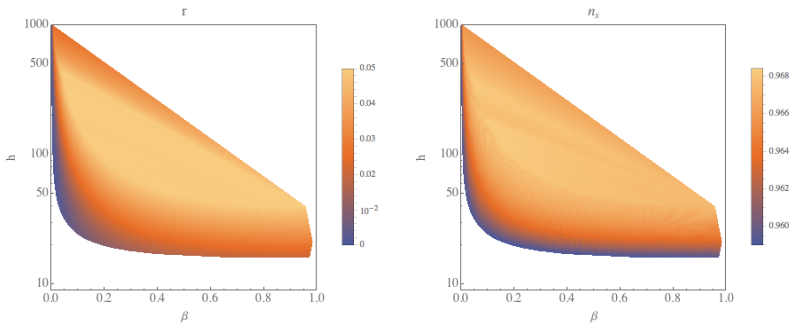


(a) $N = 48$

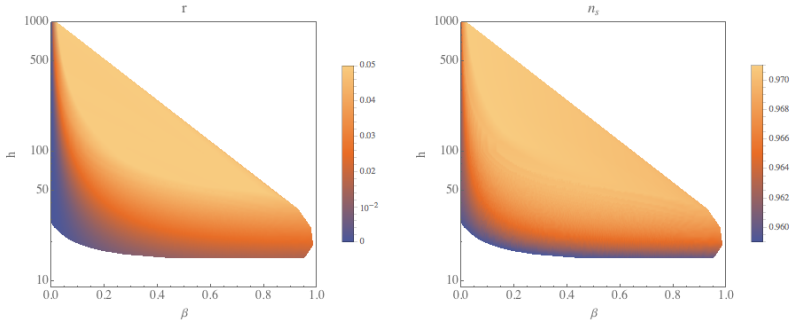


(b) $N = 52$

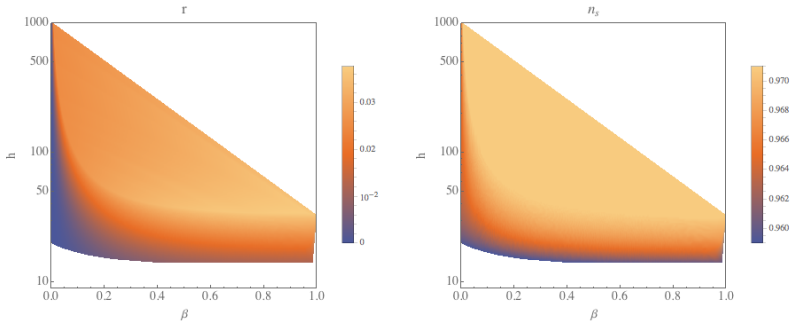


(c) $N = 56$

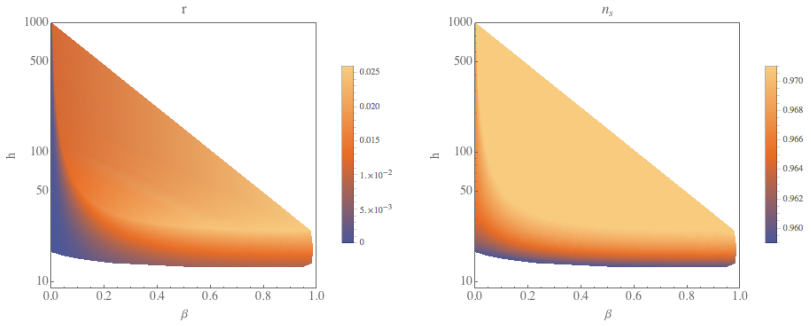


(d) $N = 60$

Figure 4.2: Region plots for the tensor/scalar ratio $r$ (left) and the spectral index $n_s$ (right) as functions of the parameters $\beta$ and $h$, for selected values of the number of e-folds $N$. The values of $r$ and $n_s$ are given in terms of the colour scale shown on the right of every plot.

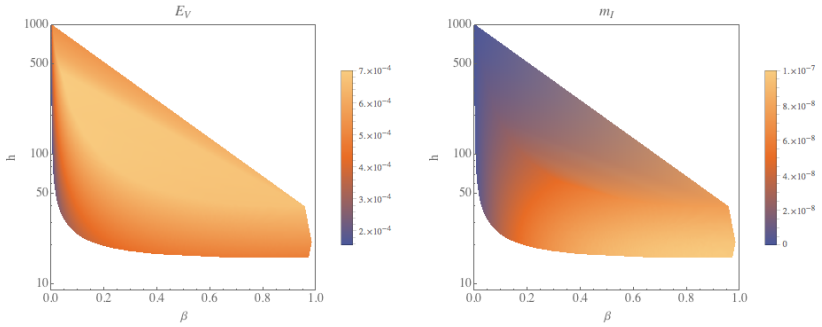


(a) $N = 48$

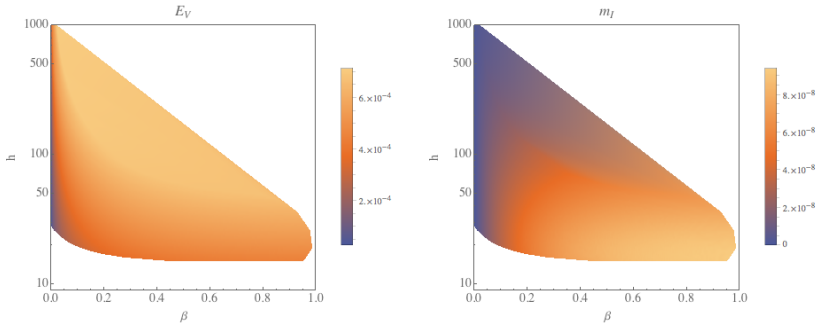


(b) $N = 52$

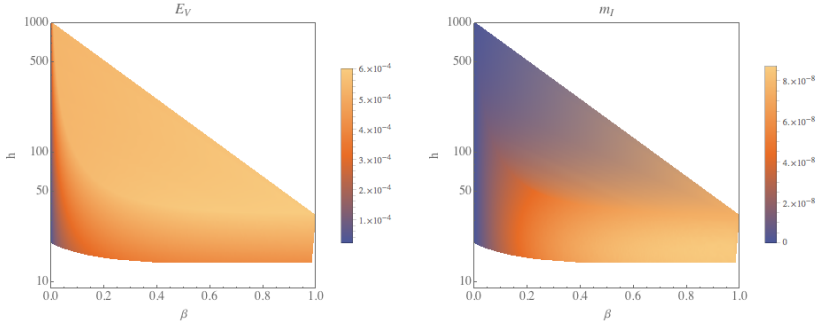


(c) $N = 56$

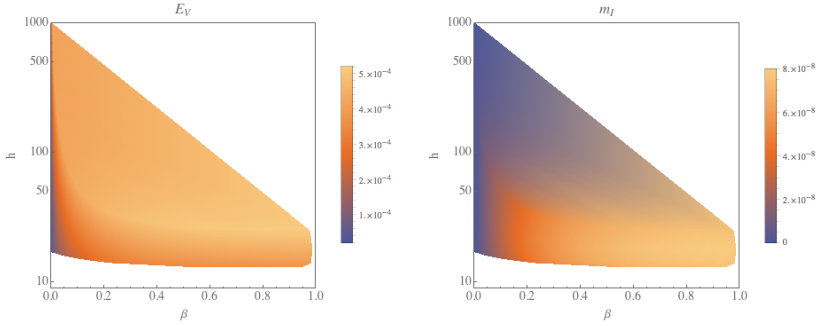


(d) $N = 60$

Figure 4.3: Region plots for the vacuum energy $E_V$ (left) and the mass of the inflaton $m_I$ (right), in Planck units, as functions of the parameters $\beta$ and $h$, for the selected values of the number of e-folds $N$. The values of $E_V$ and $m_I$ are given in terms of the colour scale shown on the right of every plot.

## 4.6 Summary and Conclusions

Inspired by holographic models used to describe hyperscaling violation, we have constructed the most general inflation potential given by the sum of two exponentials. In these models, inflation is generated by a scalar field rolling off from the de Sitter maximum of the potential. In the slow-roll approximation, our model reproduces correctly, for a wide range of its parameters, the most recent experimental data for the power spectrum of primordial perturbations. Moreover, it predicts inflation at energy scales of four to five orders of magnitude below the Planck scale, whereas the inflaton mass, at the onset of inflation, turns out to be seven to eight orders of magnitude smaller than the Planck mass. The proposed inflationary model belongs to the class of models in which the potential has a de Sitter regime, including the Starobinsky model and, more generally, the cosmological attractor models. Our model shares with those several features: (1) the potential is built as a combination of exponentials, it predicts (2) an energy scale of inflation four order of magnitude below the Planck mass, (3) a 'red' power spectrum and (4) a small tensor/scalar amplitude ratio. On the other hand, our model differs from the Starobinsky one in a crucial aspect: inflation is not generated, as in Starobinsky model, by a scalar field rolling off from an asymptotically constant potential, but rather from a local maximum of the potential. This property allows us to interpret the inflaton as a tachyonic excitation of the de Sitter vacuum and to introduce a second scale of energy in the theory, the mass scale $m_I$, which is 7–8 order of magnitude below the Planck mass. This hierarchy of scales opens the intriguing possibility that the origin of the inflaton could be explained by the physics at energy scales 7–8 order of magnitude below the Planck mass. Our model belongs to the general class of hilltop models and shares with the latter the local behaviour near the maximum of the potential. However, our scalar potential is the sum of two exponentials, therefore the global behaviour of our inflationary model is sensibly different from usual hilltop models constructed using powers of the inflaton. In particular, this results in different predictions for the spectral parameters $r$ and $n_s$ in the region of the e-folds $N$ accessible to observations.

We close with a brief comment about the reheating phase and the transition from inflation to the radiation/matter dominated era. During reheating, the energy is transferred from the inflaton to matter fields. This means that there must exist a region in which the kinetic energy of the inflaton dominates over its potential energy, e.g. a local minimum of the potential. It is evident from Fig. 4.1 that the potential (4.5) cannot be used to describe reheating. Thus, in order to describe reheating, our potential must be matched with continuity at the end of inflation with some other branch of a potential exhibiting a local minimum. This can be done very easily: in the $Y$-parametrisation, the point $Y_0$ given by Eq. (4.17), at which the universe exits inflation, is always on the left of the point $Y_* = 1/\beta^2$ at which the potential cuts the horizontal axis, i.e. $V(Y_0) > V(Y_*) = 0$ and $Y_0 < Y_*$. Since the slow-roll approximation is badly broken at $V = 0$, the matching with the branch of the potential with the local minimum must be performed at a point $Y_0 < Y < Y_*$.

## 4.7 Appendix: A Hyperbolic Cosine Model

The scalar potential (4.5) is the most general form of the potential one can obtain imposing the conditions (4.2) and assuming that it is built as a combination of two exponentials without an additive constant term. When such a constant term, $c$, is present, only the first equation in (4.4) has to be modified and becomes $c+a_1+a_2>0$, whereas the second and third equations remain unchanged. A general solution of the ensuing system is given by $a_1=-a_2(b_2/b_1)$, $a_1,a_2<0$, $b_1>0$, $b_2<0$ and $c>-a_1-a_2$. A simple example of this class of potentials is given by

$$V(\phi)=\Lambda^2\left(2-\cosh\mu\phi\right). \tag{4.25}$$

This potential gives a further example of inflation generated by an unstable de Sitter vacuum.[3] The potential (4.25) has a maximum at $\phi=0$, corresponding to an unstable de Sitter solution with $V(0)=\Lambda^2$, and a corresponding tachyonic excitation. For $\mu\phi\gg 1$, the potential behaves as a pure exponential. The vacuum energy and inflaton mass, expressed in terms of $h$ and $\lambda$, defined as in Eqs. (4.7) and (4.8), are

$$M_I^2=-\frac{16\pi}{3}\frac{\lambda^4}{h^2}\,m_P^2\,,\quad E_V=\lambda\,m_P\,. \tag{4.26}$$

Introducing the variable $Y=\mathrm{e}^{\mu\phi}$, the slow-roll parameters $\epsilon$ and $\eta$ take the form

$$\epsilon=\frac{1}{3h^2}\left(\frac{Y^2-1}{Y^2-4Y+1}\right)^2,\quad \eta=\frac{2}{3h^2}\frac{Y^2+1}{Y^2-4Y+1}-\epsilon\,. \tag{4.27}$$

The slow-roll parameter $\epsilon$ is zero on the maximum of the potential ($Y=1$). Moreover, we have $0\leqslant\epsilon\leqslant 1$ for $1\leqslant Y\leqslant Y_0$, where

$$Y_0=\frac{2\sqrt{3}h+\sqrt{1+9h^2}}{\sqrt{3}h+1}\,. \tag{4.28}$$

For $Y<Y_0$ we have inflation, whereas for $Y\geqslant Y_0$ we have $\epsilon\geqslant 1$ and the universe exits inflation. One can easily check that during inflation we always have $1\leqslant Y<2+\sqrt{3}$. Conversely, the parameter $\eta$, which gives a measure of the curvature of the potential, is not small in general, but is of order $h^{-2}$.

Also for these models the simplest way to satisfy the usual slow-roll conditions for inflation, $\epsilon,|\eta|\ll 1$, is to choose $h\gtrsim 10$, so that $\eta\approx 10^{-2}$ as well as $\epsilon\approx 10^{-2}$. The number of e-folds $N$ is given by

$$\frac{1+Y}{[Y(Y-1)]^{1/3}}=A\,\mathrm{e}^{2N/9h^2}\,,\quad A:=\frac{1+Y_0}{[Y_0(Y_0-1)]^{1/3}}\,. \tag{4.29}$$

3. Notice that a similar potential has been investigated in the context of constant-roll inflation, which reduces to slow-roll inflation when the rate of roll is small — see Ref. [209] and references therein.

In the slow-roll approximation the spectral parameters expressed in terms of $N$ are,

$$P_R^{1/2}(N) = 2h\lambda^2 \frac{(4Y - Y^2 - 1)^{3/2}}{(Y^2 - 1)Y^{1/2}}\,, \tag{4.30a}$$

$$r(N) = 16\epsilon(N) = \frac{16}{3h^2}\left(\frac{Y^2 - 1}{4Y - Y^2 - 1}\right)^2\,, \tag{4.30b}$$

$$n_s(N) = 1 - 4\epsilon(N) + 2\eta(N) = 1 - \frac{3}{8}r(N) + \frac{4}{3h^2}\frac{Y^2 + 1}{Y^2 - 4Y + 1}\,, \tag{4.30c}$$

where $Y = Y(N)$ is defined implicitly as a function of $N$ by Eq. (4.29).

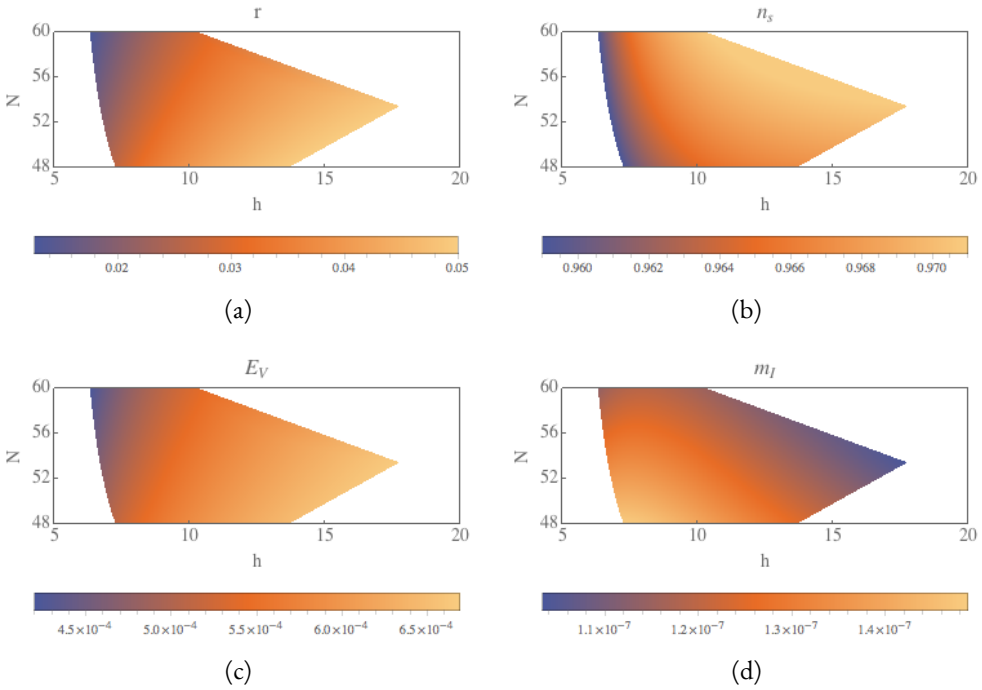


Figure 4.4: Region plots for (a) the tensor/scalar ratio $r$, (b) the spectral index $n_s$, (c) the vacuum energy $E_V$ and (d) the mass of the inflaton $m_I$ as functions of the scale parameter $h$ and the number of e-folds $N$. $E_V$ and $m_I$ are in Planck masses. The values of $r$, $n_s$, $E_V$ and $m_I$ are given in terms of the colour scale shown below every plot.

Fig. 4.4 shows that there exist values of $h$ for which the model correctly reproduces the results of observation [186] with $N = [48, 60]$. Moreover, it predicts the vacuum energy to be four orders of magnitude below the Planck scale and the mass of the inflaton seven orders of magnitude smaller than the Planck mass.

# Appendix A

# A Solution-Generating Method for Einstein-Maxwell-Scalar Theory

Units: $c = 1; G = 1/16\pi$; the kinetic scalar term is non-standard.

Minimally coupled Einstein-Maxwell-scalar gravity in $d+2$ dimensions is described by

$$\mathcal{A} = \int \mathrm{d}^{d+2}x\,\sqrt{-g}\left(\mathcal{R} - F^2 - 2(\partial\phi)^2 - V(\phi)\right), \tag{A.1}$$

and its field equations are

$$\mathcal{R}_{\mu\nu} - \tfrac{1}{2}g_{\mu\nu}\mathcal{R} = T^{\mathrm{EM}}_{\mu\nu} + T^{\phi}_{\mu\nu}\,, \quad \nabla_\mu F^{\mu\nu} = 0\,, \quad \nabla^2\phi = \frac{1}{4}\frac{\mathrm{d}V(\phi)}{\mathrm{d}\phi}\,, \tag{A.2}$$

where the electromagnetic and scalar energy-momentum tensor are,

$$T^{\mathrm{EM}}_{\mu\nu} = 2\left(F_{\mu\rho}F^{\rho}_{\nu} - \frac{1}{4}g_{\mu\nu}F^{\rho\sigma}F_{\rho\sigma}\right), \tag{A.3}$$

$$T^{\phi}_{\mu\nu} = 2\left(\partial_\mu\phi\,\partial_\nu\phi - \frac{1}{2}g_{\mu\nu}\partial^\rho\phi\,\partial_\rho\phi\right) - \frac{1}{2}g_{\mu\nu}V(\phi)\,. \tag{A.4}$$

Under certain assumptions upon the spacetime, the electromagnetic and scalar fields, Cadoni et al. [111] proposed a solution-generating technique to solve the field equations (A.2). With this procedure, they derived a large number of exact, static, asymptotically flat or AdS black hole and black brane solutions, whose holographic application might be useful to investigate condensed matter systems or strongly coupled quantum field theories. The method turns out to be particularly useful when the scalar profile is given, and the potential is not an input but rather an output of the theory.

They look for static, spherically symmetric solutions of the field equations, with line element in the Schwarzschild gauge:

$$\mathrm{d}s^2 = -U(r)\,\mathrm{d}t^2 + \frac{\mathrm{d}r^2}{U(r)} + R^2(r)\,\mathrm{d}\Omega^2_{(\varepsilon,d)}\,, \tag{A.5}$$

where $\mathrm{d}\Omega^2_{(\varepsilon,d)}$ is the line element of the $d$-dimensional transverse spacetime with constat curvature $\varepsilon = -1, 0, 1$, for hyperbolic, planar and spherical manifolds respectively.

They also assume that the scalar field is static and does not depend on the transverse coordinates, and they consider only purely electric solutions, characterised by the electric charge $Q$.[1] Then, the scalar field depends only on the radial coordinate and the only non-vanishing component of the Maxwell tensor is $F_{tr}$,

$$\phi = \phi(r)\,, \quad F_{tr} = \frac{Q}{R^d}\,. \tag{A.6}$$

Using Eqs. (A.5) and (A.6), the field equations take the form

$$\frac{R''}{R} = -\frac{2}{d}\phi'^2\,, \tag{A.7a}$$

$$(UR^d\phi')' = \frac{1}{4}R^d\frac{\mathrm{d}V}{\mathrm{d}\phi}\,, \tag{A.7b}$$

$$(UR^d)'' = \varepsilon d(d-1)R^{d-2} + \frac{2(d-2)}{d}\frac{Q^2}{R^d} - \frac{d+2}{d}R^d V\,, \tag{A.7c}$$

$$(UR^{d-1}R')' = \varepsilon(d-1)R^{d-2} - \frac{2}{d}\frac{Q^2}{R^d} - \frac{1}{d}R^d V\,. \tag{A.7d}$$

Of course, the solutions of these field equations (and their existence) depend on the class of potentials $V(\phi)$ considered. In any case, finding exact solutions is a very tough task, and might be impossible, even when the explicit form of the potential is given, or can be expressed in a simple form.

Usually, one must impose precise boundary conditions on the $r \to \infty$ asymptotic behaviour of the spacetime solution, which translate into boundary conditions for the scalar potential. For example, if we require an asymptotically flat spacetime, and assume without loss of generality that $\phi = 0$ as $r \to \infty$, it follows that $V(0) = 0$, while for asymptotically AdS spacetimes we have $V(0) = \Lambda$, with $\Lambda$ strictly negative. Typically, one also requires the existence of the Schwarzschild black hole (black brane) solution sourced by a constant scalar field $\phi = \phi_0$, implying $V'(\phi_0) = 0$, while the existence of black hole solutions sourced by a non-trivial scalar field, in general, is strongly constrained by no-hair theorems.

The field equations (A.7) can be written in a more convenient form by introducing the variables $R = \mathrm{e}^{\int Y}$ and $u = UR^d$,

$$Y' + Y^2 + \frac{2}{d}\,\phi'^2 = 0\,, \tag{A.8a}$$

$$(u\phi')' - \frac{1}{4}\frac{\mathrm{d}V}{\mathrm{d}\phi}\,\mathrm{e}^{d\int Y} = 0\,, \tag{A.8b}$$

$$u'' - (d+2)(uY)' + 2\varepsilon(d-1)\,\mathrm{e}^{(d-2)\int Y} - 4Q^2\,\mathrm{e}^{-d\int Y} = 0\,, \tag{A.8c}$$

$$u'' - \varepsilon d(d-1)\,\mathrm{e}^{(d-2)\int Y} - \frac{2(d-2)}{d}\,Q^2\,\mathrm{e}^{-d\int Y} + \frac{d+2}{d}\,V\,\mathrm{e}^{d\int Y} = 0\,. \tag{A.8d}$$

1. Notice that matter fields do not necessarily inherit spacetime symmetries, see e.g. Refs. [210–212].

Eq. (A.8a) is a first-order non-linear equation for $Y$, an example of the Riccati equation. Once the scalar profile $\phi(r)$ is given, solutions of the Riccati equation can be found. Then, Eq. (A.8c), which is linear in $u$, can be integrated to obtain

$$\frac{u}{R^{d+2}} = \int \left( 4Q^2 \int \frac{1}{R^d} - 2\varepsilon(d-1) \int R^{d-2} - C_1 \right) \frac{1}{R^{d+2}} + C_2 \,, \tag{A.9}$$

where $C_1$ and $C_2$ are integration constants. The potential is determined using Eq. (A.8d):

$$V = \frac{d^2(d-1)}{d+2} \frac{\varepsilon}{R^2} + \frac{2(d-2)}{d+2} \frac{Q^2}{R^{2d}} - \frac{d}{d+2} \frac{u''}{R^d} \,. \tag{A.10}$$

Notice that Eqs. (A.8a) and (A.8c) are universal, i.e. they do not depend on the potential.

# Part II

# Black Hole Perturbations and Gravitational Wave Emission

# Chapter 5

*Introduction to Part II*

# Black Hole Perturbations and Mimickers

Stellar black holes are thought to be the last stage in the evolution of massive stars and supermassive black holes can be found almost in the centre of each known galaxy. Many observative signatures of black holes can be analysed in perturbation theory. For this reason, we review some historical results in perturbation theory such as the Regge-Wheeler and Zerilli equations, quasi-normal modes, tidal effects and Love numbers. However, the dark compact object out there might be horizonless exotic objects that mimic black holes. Interesting examples of this kind, which we will discuss in this thesis are boson stars, traversable wormholes, gravastars and superspinars.

## 5.1 Introduction

The events GW150914 and GW151226 observed by the LIGO and Virgo collaborations have been interpreted as the gravitational waves emitted by a binary stellar-mass black holes merger. In particular, the LIGO observation of GW150914 has inaugurated the gravitational-wave astronomy era, a whole new instrument to explore the Universe with which we will have the possibility of testing gravity in extreme regimes. The existence of black holes is supported by various indirect observations in the electromagnetic band [213–220], but the detection of GW150914 and GW151226 can be acknowledged as the first direct observation. Also, the existence of event horizons might be proved only with gravitational-wave observations, as electromagnetic observations cannot prove the existence of event horizons, but only the existence of a light ring, i.e. a boundary within which photons can be trapped in circular orbits [221].

The gravitational-wave events observed by LIGO are characterised by three phases [222–226]: the inspiral, when the distance between the two companions is large, and it is well described by post-Newtonian theory; the merger, when the two objects coalesce, and which can only be described accurately through numerical simulations; and the ringdown, when the product of the merger relaxes to a stationary equilibrium configuration, with the emission of gravitational waves.

Most likely, the product of the collision of two black holes is another black hole, and then perturbed black holes are the most convincing sources of gravitational waves. For this reason, in this chapter, we review some basic concept of black hole perturbation theory.

Except that for rare exceptions (ideal configurations, high symmetries, not-that-natural assump-

tions) and in some approximations (weak-field, low velocities), Einstein's field equations can be impossible to solve analytically — even for the background! With the come of super-computers, it has become possible to solve numerically very complicated equations and then explore the strong-gravity regime in more realistic astrophysical scenarios. This new tool, known as numerical relativity [227], has allowed us testing gravity in regimes not reproducible in laboratory, e.g. gravitational collapse of black holes, inspiral phase and coalescence of binary black holes or neutron stars and generation of gravitational waves. Numerical relativity is a step beyond the post-Newtonian approximations and the general relativistic perturbations as it can control the full non-linear behaviour of general relativity.

On the other hand, there are some issues. For instance, coordinates in general relativity do not have a concrete meaning, what matters are distances and time intervals that can be defined only by the metric that, in turn, is the solution of the Einstein equations. This means that the choice of coordinates is crucial, to avoid coordinate singularities. In the case of black holes, one must pay attention also to physical singularities, where matter density and curvature become infinite. When one considers the gravitational-wave emission, the signal must be extracted at large distances while the signal is produced by a strong field source, hence optimisation is mandatory. In the world of numerical relativity, the 3+1 decomposition of spacetime is a way of writing the Einstein field equations such that they can be convenient for the alghorithms [228, 229]. The evolution of a system described by Einstein's equations can be viewed as a Cauchy problem: we specify the value of the metric and its derivatives at some initial time on a three-dimensional spacelike hypersurface. These metric components are then integrated forward in time.

However, although black holes are the simplest candidates for dark compact objects in the sky, signals similar to those detected by LIGO might also be produced by other compact objects — see Section 5.5. So, it is important and interesting to study these black hole mimickers and ask what piece of information we can obtain from gravitational-wave observations about the nature of the emitting object or the binary companions.

## 5.2 Black Hole Perturbations

In this section we consider perturbations about a black hole background. This work has begun back in 1957 by the pioneering paper by Regge and Wheeler [230], followed by the extensions of Zerilli [231–233] and Vishveshwara [234].

For defineteness we consider the most general static and spherically symmetric background in Schwarzschild-like coordinates,

$$g^{(0)}_{\mu\nu} = -\mathrm{e}^{\Gamma}\,\mathrm{d}t^2 + \mathrm{e}^{\Lambda}\,\mathrm{d}r^2 + r^2\left(\mathrm{d}\vartheta^2 + \sin^2\vartheta\,\mathrm{d}\varphi^2\right). \tag{5.1}$$

The quest for the stability of the Schwarzschild solution led Regge and Wheeler to consider linear

perturbations about the equilibrium equations, i.e.

$$g^{(0)}_{\mu\nu} \to g_{\mu\nu} = g^{(0)}_{\mu\nu} + h_{\mu\nu}\,, \tag{5.2}$$

where the perturbation $h_{\mu\nu}$ is small with respect to the background. The perturbation is then decomposed in (tensor) spherical harmonics, and for a given $\ell, m$ and parity $(-1)^{\ell+1}$ (odd) the most general perturbation can be written as,

$$h^{\rm odd}_{\mu\nu} = \begin{pmatrix} 0 & 0 & -h_0 \csc\vartheta\,\partial_\varphi & h_0 \sin\vartheta\,\partial_\vartheta \\ \star & 0 & -h_1 \csc\vartheta\,\partial_\varphi & h_1 \sin\vartheta\,\partial_\vartheta \\ \star & \star & h_2 \csc\vartheta\,\Delta_1 & -h_2 \sin\vartheta\,\Delta_2 \\ \star & \star & \star & -h_2 \sin\vartheta\,\Delta_1 \end{pmatrix} Y^{\ell m}\,, \tag{5.3}$$

while for parity $(-1)^{\ell}$ (even) one finds

$$h^{\rm even}_{\mu\nu} = \begin{pmatrix} \mathrm{e}^{\Gamma} H_0 & H_1 & h_0\,\partial_\vartheta & h_0\,\partial_\varphi \\ \star & \mathrm{e}^{\Lambda} H_2 & h_1\,\partial_\vartheta & h_1\,\partial_\varphi \\ \star & \star & r^2\,(K + G\,\partial^2_\vartheta) & r^2 G\,\Delta_1 \\ \star & \star & \star & r^2 \sin^2\vartheta\,[K + G\,(\partial^2_\vartheta - 2\Delta_2)] \end{pmatrix} Y^{\ell m}\,. \tag{5.4}$$

In Eqs. (5.3) and (5.4), the symbol $\star$ means symmetric, i.e. $h_{\mu\nu} = h_{\nu\mu}$, the perturbations $h_0$, $h_1$, $h_2$, $H_0$, $H_1$, $H_2$, $K$ and $G$ are functions of $t$ and $r$, and we have defined two angular operators as

$$\Delta_1 \equiv \partial_\varphi\,(\partial_\vartheta - \cot\vartheta)\,, \quad \Delta_2 \equiv \frac{1}{2}\left(\partial^2_\vartheta - \cot\vartheta\,\partial_\vartheta - \csc^2\vartheta\,\partial^2_\varphi\right). \tag{5.5}$$

Obviously, owing to the spherical symmetry of the spacetime the perturbation equations cannot mix terms that belong to different $\ell$ and parity. Moreover, $m$ can be set equal to zero since the resulting radial equation will not depend on $m$. In this way, the calculations are simplified, as the $\varphi$-dependence completely disappears.

### 5.2.1 The Regge-Wheeler Equation

Fortunately, out of the ten perturbation functions in Eqs. (5.3) and (5.4), some of them can be set to zero using a clever gauge transformation, today known as the Regge-Wheeler gauge. Such gauge transformation allows us to impose additional conditions on the perturbations function. In particular, they have eliminated the terms that contain the angular derivatives of highest order.

The final canonical form for a $\ell, m = 0$ odd wave is

$$h_{\mu\nu}^{\text{odd}} = \begin{pmatrix} 0 & 0 & 0 & h_0(r) \\ \star & 0 & 0 & h_1(r) \\ \star & \star & 0 & 0 \\ \star & \star & \star & 0 \end{pmatrix} \mathrm{e}^{\mathrm{i}\omega t} \sin\vartheta\, \partial_\vartheta P_\ell(\cos\vartheta)\,. \tag{5.6}$$

For the Schwarzschild spacetime, i.e. $\mathrm{e}^{\Gamma} = \mathrm{e}^{-\Lambda} = 1 - 2M/r$, plugging Eq. (5.6) into (5.2) and working out the Einstein field equations for the perturbation functions, one finds three non-trivial equations. In particular, it is possible to write $h_0$ as a function of $h_1$ and its derivative. Finally, we are left with a single second-order radial equation,

$$\frac{\mathrm{d}^2\psi(r)}{\mathrm{d}r_*^2} + \left(\omega^2 - V_{\text{RW}}(r)\right)\psi(r) = 0\,, \tag{5.7}$$

where $r_*$ is the tortoise coordinate defined by $\mathrm{d}r/\mathrm{d}r_* = 1 - 2M/r$, $\psi(r) = (1-2M/r)h_1(r)/r$, and $V_{\text{RW}}$ is the Regge-Wheeler potential,

$$V_{\text{RW}}(r) = \left(1 - \frac{2M}{r}\right)\left(\frac{\ell(\ell+1)}{r^2} - \frac{6M}{r^3}\right). \tag{5.8}$$

### 5.2.2 The Zerilli Equation

Similarly, the canonical form for a $\ell, m = 0$ even wave is

$$h_{\mu\nu}^{\text{even}} = \begin{pmatrix} \mathrm{e}^{\Gamma} H_0(r) & H_1(r) & 0 & 0 \\ \star & \mathrm{e}^{\Lambda} H_2(r) & 0 & 0 \\ \star & \star & r^2 K(r) & 0 \\ \star & \star & \star & r^2 \sin^2\vartheta\, K(r) \end{pmatrix} \mathrm{e}^{\mathrm{i}\omega t}\, P_\ell(\cos\vartheta)\,. \tag{5.9}$$

The Einstein field equations for the perturbation give seven non-trivial equations. First, we can eliminate either $H_0$ or $H_2$ as $H_2 = H_0 \equiv H$. Then, the derivatives of $K$ can be written in terms of $H$ and $H_1$. Finally, we are left with a second-order linear differential equation, which for the Schwarzschild black hole reads,

$$\frac{\mathrm{d}^2\psi(r)}{\mathrm{d}r_*^2} + \left(\omega^2 - V_{\text{Z}}(r)\right)\psi(r) = 0\,, \tag{5.10}$$

where $V_{\text{Z}}$ is the Zerilli potential,

$$V_{\text{Z}}(r) = 2\left(1 - \frac{2M}{r}\right)\frac{9M^3 + 9M^2 r\lambda + 3Mr^2\lambda^2 + r^3\lambda^2(1+\lambda)}{r^3(3M + r\lambda)^2}\,, \tag{5.11}$$

and the old metric functions can be written as functions of the new wavefunction as

$$K = \frac{6M^2 + 3\lambda M r + (\lambda+1)\lambda r^2}{r^2(3M+\lambda r)}\,\psi(r) + \left(1 - \frac{2M}{r}\right)\psi'(r)\,, \tag{5.12}$$

$$H_1 = \frac{\mathrm{i}\omega\,(3M^2 + 3\lambda M r - \lambda r^2)}{(r-2M)(3M+\lambda r)}\,\psi(r) - \mathrm{i}r\omega\,\psi'(r)\,, \tag{5.13}$$

$$H = \frac{\lambda r(r-2M) + M(r-3M) - r^4\omega^2}{(r-2M)(3M+\lambda r)}\,K + \frac{(\lambda+1)M - r^3\omega^2}{\mathrm{i}r\omega(3M+\lambda r)}\,H_1\,, \tag{5.14}$$

where $\lambda = (\ell-1)(\ell+2)/2$.

In this perturbative approach, it is also possible to study the gravitational radiation emitted by a point particle with mass $\mu_p \ll M$ falling into a Schwarzschild black hole [232]. For this problem, the choice of boundary conditions is essential: outgoing waves at infinity and ingoing waves at the horizon. In this case, the source term of the Einstein's equations is given by an integral of a delta-function over the world line of the particle,

$$T^{\mu\nu} = \mu_p \int \frac{\mathrm{d}\tau}{\sqrt{-g}}\, u_p^\mu u_p^\nu\, \delta\left(x^\mu - x_p^\mu(\tau)\right)\,, \tag{5.15}$$

where $u_p^\mu = \mathrm{d}x_p^\mu/\mathrm{d}\tau$ is the four-velocity of the particle. In order to study the perturbations, also the energy-momentum tensor must be expanded in spherical harmonics.

For a particle falling radially, there is no source term in the odd sector, while in the even sector, the right-hand side of Eq. (5.10) is no longer zero but it is sourced. This source term depends on the mass and the energy of the infalling particle and by its four-velocity components. We will give an explicit example of source term in Chapter 8.

## 5.3 Quasi-Normal Modes

In general relativity, quasi-normal modes arise in the study of linear perturbations of stellar or black hole spacetimes [235–237]. Quasi-normal mode oscillations have been found in perturbation calculations of particles falling into Schwarzschild and Kerr black holes and in the collapse of a star to form a black hole. Because of the emission of gravitational waves the oscillations are quasi-normal, i.e. complex.

As we have seen in the previous section, in most cases, the perturbation equations reduce to a linear second-order differential equation supplemented by boundary conditions at the horizon and at infinity. Quasi-normal modes are the complex eigenvalues of this equation, with the real part representing the actual frequency of the oscillation and the imaginary part representing the (inverse) damping time.

For black holes, the quasi-normal modes are deeply related to the boundary conditions required at the event horizon and at infinity. The effective potential in Eqs. (5.7) and (5.10) goes to zero as

$r \to 2M$ and $r \to \infty$, or in the tortoise coordinate $r_* \to -\infty$ and $r_* \to \infty$. For $V = 0$, the solutions behave as $\psi \sim \exp^{-\mathrm{i}\omega(t\pm r_*)}$. At the horizon we only have ingoing modes, while at infinity we only have outgoing modes,

$$\psi \sim \mathrm{e}^{-\mathrm{i}\omega(t-r_*)} \text{ at the horizon}, \qquad \psi \sim \mathrm{e}^{-\mathrm{i}\omega(t+r_*)} \text{ at infinity}. \tag{5.16}$$

In general, there exists a discrete infinity of quasi-normal modes that satisfy the boundary conditions. The quasi-normal frequencies are often labelled by an integer $n$ called the overtone number. The fundamental mode corresponds to $n = 0$ and is the less damped one.

In few exceptional cases, it is possible to solve analytically the wave equation. In general, quasi-normal mode frequencies are determined by numerical methods. However, solutions to the Regge-Wheeler equation can be given analytically in terms of the Heun functions [238].

For a Schwarzschild black hole, the quasi-normal mode spectra of even and odd perturbations are the same, i.e. they are isospectral [239, 240]. If we try to integrate the Zerilli equation with boundary conditions given by Eq. (5.16), we will run into numerical instabilities. We need to use an adeguate series expansion as

$$\psi = \mathrm{e}^{+\mathrm{i}\omega r_*} \sum_{j=0}^{\infty} \alpha_j (r-2M)^j \text{ at the horizon}, \quad \psi = \mathrm{e}^{-\mathrm{i}\omega r_*} \sum_{j=0}^{\infty} \frac{\beta_j}{r^j} \text{ at infinity}, \tag{5.17}$$

where the coefficients $\alpha_j$ and $\beta_j$ are determined by the series expansion of the Zerilli equation at the horizon and at infinity. The recipe of Chandrasekhar and Detweiler [240] is then as follows. For a given $\omega$ we integrate forwards from $-\infty$ and backwards from $+\infty$ to an intermediate value of $r_*$, which tipically coincides with the maximum of the potential, roughly at $3M$. Then we match the two solutions at the junction and we use a shooting method to determine the value of $\omega$, the quasi-normal mode, such that the Wronskian of the solutions is zero. In Table 5.1 we list the first two overtones for $\ell = 2$ and $\ell = 3$.

| | $\ell = 2$ | $\ell = 3$ |
|---|---|---|
| $n = 0$ | $0.374 - 0.089\mathrm{i}$ | $0.599 - 0.093\mathrm{i}$ |
| $n = 1$ | $0.348 - 0.275\mathrm{i}$ | $0.582 - 0.281\mathrm{i}$ |

Table 5.1: Fundamental and first overtone quasi-normal frequencies $\omega M$ for the Schwarzschild black hole.

For a Kerr black hole, the quasi-normal mode spectrum is richer [241–244] but entirely characterised only by the black hole mass and angular momentum. Thus, the detection of a few modes from the ringdown signal can allow for precision measurements of the black hole mass and spin [91], and possibly of higher multipole moments, which can be used to perform null-hypothesis tests of the no-hair theorems of general relativity [25].

## 5.4 Tidal Love Numbers

When we model the inspiral phase of a binary system, at large orbital separations (low frequencies) the tidal interaction is negligible. As the orbital separation decreases (higher frequencies), the tidal interaction becomes significant. These effects can be studied in perturbation theory as well and at first order, the relation between the tidal field and the induced moment is constant, and such a constant is known as the tidal Love number.[1] Tidal Love numbers have been studied first in Newtonian gravity [246]. Later, a fully relativistic theory has been developed to describe tidal effects in strong-gravity regimes, such as neutron stars and black holes [247–250].

Tidal Love numbers encode the information about the deformability of an object in a tidal environment and depend significantly on the object internal structure and the dynamics of the gravitational field. In fact, to define the relativistic Love numbers one only needs the vacuum exterior geometry, while to compute the Love numbers one needs to know the metric in the body interior, e.g. the equation of state.

An intriguing result in classical general relativity is the fact that the tidal Love numbers of a black hole are precisely zero. This property has been originally demonstrated for small tidal deformations of a Schwarzschild black hole and has been recently extended to arbitrarily strong tidal fields [251] and to the spinning case, at least in the axisymmetric case to quadratic order in the spin and generically to linear order in the spin [252–254].

A static, spherically symmetric compact object embedded in an external tidal field, is characterised by the symmetric and trace-free polar and axial tidal multipole moments of order $\ell$,

$$\mathcal{E}_{a_1\dots a_\ell} \equiv \frac{\langle C_{0a_10a_2;a_3\dots a_\ell}\rangle}{(\ell-2)!}\,, \quad \mathcal{B}_{a_1\dots a_\ell} \equiv \frac{\langle \epsilon_{a_1bc}\, C^{bc}_{a_20;a_3\dots a_\ell}\rangle}{\frac{2}{3}(\ell+1)(\ell-2)!}\,, \tag{5.18}$$

where $C_{abcd}$ is the Weyl tensor, a semicolon denotes a covariant derivative, $\epsilon_{abc}$ is the Levi-Civita symbol, the angular brackets denote symmetrisation of the indices $a_i$ and all traces are removed. The polar (axial) moments $\mathcal{E}_{a_1\dots a_\ell}$ ($\mathcal{B}_{a_1\dots a_\ell}$) can be decomposed in a basis of even (odd) parity spherical harmonics. We denote by $\mathcal{E}^{\ell m}$ and $\mathcal{B}^{\ell m}$ the amplitudes of the polar and axial components of the external tidal field with harmonic indices $(\ell, m)$, where $m$ is the azimuthal number, $|m| \leqslant \ell$. The structure of the external tidal field is entirely encoded in the coefficients $\mathcal{E}^{\ell m}$ and $\mathcal{B}^{\ell m}$.

We adopt the Geroch-Hansen definition of multipole moments [255, 256], equivalent [257] to the one by Thorne [258] in asymptotically mass-centered Cartesian coordinates. As a result of the external perturbation, the mass and current multipole moments — $M_\ell$ and $S_\ell$ — of the compact object are deformed and, in linear perturbation theory, these deformations are proportional to the applied tidal field. In the non-rotating case, mass (current) multipoles have even (odd) parity, and

1. When the orbital motion approaches a resonance, the relation between the induced quadrupole moment and the tidal field is no longer constant, and the tides become dynamical [245].

therefore they only depend on polar (axial) components of the tidal field.[2] Hence, we can define the polar and axial tidal Love numbers as [248, 250]

$$k_\ell^E \equiv -\frac{1}{2}\frac{\ell(\ell-1)}{M^{2\ell+1}}\sqrt{\frac{4\pi}{2\ell+1}}\frac{M_\ell}{\mathcal{E}_{\ell 0}}\,, \quad k_\ell^B \equiv -\frac{3}{2}\frac{\ell(\ell-1)}{(\ell+1)M^{2\ell+1}}\sqrt{\frac{4\pi}{2\ell+1}}\frac{S_\ell}{\mathcal{B}_{\ell 0}}\,, \tag{5.19}$$

where the numerical factor is conventional, $M$ is the mass of the object, whereas $\mathcal{E}_{\ell 0}$ ($\mathcal{B}_{\ell 0}$) is the amplitude of the axisymmetric component of the polar (axial) tidal field. Since we are considering only non-spinning objects in spherically symmetric spacetimes, we can define the tidal Love numbers in the axisymmetric $m = 0$ case, without loss of generality. The factor $1/M^{2\ell+1}$, that makes the Love numbers dimensionless, is non-standard. It is much more common to divide by powers of the object radius, but since the definition of radius for boson stars can be equivocal, we adopt this non-standard choice. Thus, our definition is related to those used by Hinderer, Binnington and Poisson through

$$k^{E,B}_{\ell\,\text{ours}} = \left(\frac{R}{M}\right)^{2\ell+1} k^{E,B}_{\ell\,\text{HBP}}\,. \tag{5.20}$$

Modified theories of gravity and exotic compact objects typically require the presence of extra fields which are (non) minimally coupled to the metric tensor, and therefore the definition of external applied fields. But, in astrophysical situations we expect the ratio of any external field to the gravitational tidal field to be small or negligible.

To compute the tidal Love numbers we need to calculate the induced mass and current moments as functions of the external tidal field. We consider static perturbations about a static spherically symmetric background spacetime (5.1), and we expand the metric in spherical harmonics.

Solving the appropriate field equations will give us expressions for the metric functions in (5.9) and (5.6). The multipole moments can be extracted from the asymptotic behaviour of the spacetime metric and fields:

$$g_{tt} = -1 + \frac{2M}{r} + h_{tt}\,, \quad g_{t\varphi} = \frac{2J}{r}\sin^2\vartheta + \sin\vartheta\, h_{t\varphi}\,, \tag{5.21}$$

where

$$h_{tt} = \sum_{\ell\geqslant 2}\left(\frac{2}{r^{\ell+1}}\sqrt{\frac{4\pi}{2\ell+1}}\,M_\ell\,Y^{\ell 0} + \mathcal{O}\left(\frac{1}{r^{\ell+2}}\right) - \frac{2r^\ell}{\ell(\ell-1)}\,\mathcal{E}_\ell\,Y^{\ell 0} + \mathcal{O}\left(r^{\ell-1}\right)\right), \tag{5.22}$$

$$h_{t\varphi} = \sum_{\ell\geqslant 2}\left(\frac{2}{r^{\ell}}\sqrt{\frac{4\pi}{2\ell+1}}\,\frac{S_\ell}{\ell}\,\partial_\vartheta\,Y^{\ell 0} + \mathcal{O}\left(\frac{1}{r^{\ell+1}}\right) + \frac{2r^{\ell+1}}{3\ell\,(\ell-1)}\,\mathcal{B}_\ell\,\partial_\vartheta\,Y^{\ell 0} + \mathcal{O}\left(r^{\ell}\right)\right), \tag{5.23}$$

An appropriate comparison between the solution of the field equations and the expansions (5.22) and (5.23) gives us a method to extract the multipole moments and consequently the tidal Love numbers.

2. This symmetry is broken if the compact object is spinning due to spin-tidal couplings. In such a case, there exists a series of selection rules that allow defining a wider class of 'rotational' tidal Love numbers [252–254, 259, 260].

## 5.5 Black Hole Mimickers

Black hole mimickers, or exotic compact objects, are possible alternatives to black holes as they are objects whose exterior geometry is the same as black holes but without an event horizon. Although most of them are unstable,[3] there exists no formation mechanism (yet), and might look as artificial solutions to Einstein's equations, they give rise to light rings, closed orbits where photons are confined, so that to an electromagnetic observer they would look as dark as black holes, and then indistinguishable. Gravitational-wave observations, on the other hand, can discriminate between a black hole and a mimicker. Beyond the interest on mimickers as themselves, their study is fundamental to test the presence of horizons observationally. In fact, even if some observational signatures of black holes, like ringdown signals [269] and shadows [270] are well reproduced by ultra-compact horizonless geometries, the details of gravitational-wave emission are different [271]. One can, for example, compare the gravitational-wave signature of a two exotic compact objects merger with that of more conventional compact object binaries consisting of black holes and neutron stars. At early times, the precise structure of the objects is almost irrelevant and the signatures are largely the same. However, for the late stages of the merger, the relative phase of the compact objects determines the gravitational wave signature. In Chapter 8, we discuss in detail the gravitational radiation emitted by a point-particle falling into a wormhole.

### 5.5.1 Boson Stars

Among exotic compact objects, boson stars might be the most realistic (or less exotic). They are stationary compact configurations made of fundamental bosonic fields coupled to gravity. We will discuss in more details this kind of stars in Chapter 6. Here we briefly comment boson stars as a black hole mimicker [272, 273]. Spherically symmetric minimal boson stars can mimic the power spectrum of a simple accretion disk model, due to a black hole of the same mass. On the other hand, interacting boson stars can mimic a broad spectrum of astrophysical black holes. Discrimination between black holes and boson stars can be possible via the gravitational lensing.

### 5.5.2 Wormholes

A wormhole is a hypothetical bridge between two remote spacetime regions. There exists a wormhole even in the Schwarzschild spacetime, but it would collapse faster than any particle could cross

3. Horizonless compact objects require exotic matter configurations and almost inevitably possess a *stable* light ring at $r < 3M$. The latter might be associated with various (linear and non-linear) instabilities, including fragmentation and collapse [261, 262] and ergoregion instability [263–268] when the object rotates sufficiently fast. The argument of instability can be circumvented by arguing that one could be observing exotic compact objects which are compact enough to agree with observations but not compact enough to go unstable. Besides, the instability could be present, but with an extremely large timescale.

and emerge on the other side. However, there exist traversable wormholes that can, in principle, be straddle in both ways [274, 275].

Using the thin-shell formalism, Visser [276, 277] constructed simple examples of traversable wormholes. These models are built by glueing together two Schwarzschild spacetimes in such a way that there is no event horizon, i.e. we take two copies of Schwarzschild, from which we remove the regions

$$D_{1,2} \equiv \{r_{1,2} \leqslant r_0 \,|\, r_0 > 2M\} \,. \tag{5.24}$$

Then we identify the boundaries of these manifold

$$\partial D_1 = \partial D_2 \equiv \{r_{1,2} = r_0 \,|\, r_0 > 2M\} \,, \tag{5.25}$$

such that the resulting spacetime is geodesically complete and possesses two asymptotically flat regions connected by a wormhole. Notice that $r_0 > 2M$ prevents the formation of a horizon.

The energy-momentum tensor is zero everywhere but at the throat, where the two universes are connected, and the non-zero energy-momentum tensor is proportional to a delta-function. The surgery at the throat requires a thin shell of matter with surface density and surface pressure

$$\sigma = -\frac{1}{2\pi r_0}\sqrt{1-\frac{2M}{r_0}} \,, \quad p = \frac{1}{4\pi r_0}\frac{1-M/r_0}{\sqrt{1-2M/r_0}} \,. \tag{5.26}$$

In general relativity, a traversable wormhole violates the weak energy condition [278]. On the other hand, the null and strong energy conditions are satisfied as long as the throat is within the light ring, i.e. $r_0 < 3M$. These energy conditions are no longer violated in modified theories of gravity, e.g. in Einstein-dilaton Gauss-Bonnet gravity, traversable wormholes satisfying all energy conditions exist [279].

Damour and Solodukhin [280] considered another simple example of traversable wormhole, described by the metric

$$\mathrm{d}s^2 = -\left(f(r)+\lambda^2\right)\mathrm{d}t^2 + \frac{\mathrm{d}r^2}{f(r)} + r^2\,\mathrm{d}\Omega^2 \,, \quad f(r) = 1-\frac{2M}{r} \,, \tag{5.27}$$

where $\lambda$ is a dimensionless parameter. They show that some observational features of black holes do not depend on the presence of an event horizon. In fact, the apparently irreversible accretion of matter down a hole, no-hair properties, quasi-normal mode ringing, and even dissipative properties of black hole horizons can be mimic by the wormhole (5.27) if the parameter $\lambda$ is exponentially small. To distinguish the two geometries, we should either observe a classical phenomenon such as matter accretion, or detect Hawking's radiation, which is way too weak to be detected for realistic black holes.

Recently, it has been argued that even mixed star-wormhole system could mimic some features of black holes [281].

### 5.5.3 Gravastars

Gravastars have been proposed as an alternative endpoint of gravitational collapse [282, 283]. The name is the *crasis* of "gravitational vacuum star". In the original model, in order to take into account quantum mechanics, the gravastar does not possess a horizon but rather a thin shell of ultra-relativistic fluid which satisfies the equation of state $\rho = p$. The interior region is a vacuum de Sitter space, whose equation of state is $\rho = -p$. The exterior region is described by the Schwarzschild geometry.

Mazur and Mottola claimed that these objects are stable since only the shell is non-vacuum. However, these objects develop a strong ergoregion instability when rapidly spinning [263, 265].

A simpler model is called thin-shell gravastar, and it is obtained when the thickness of the shell goes to zero [284]. The line element for this model is as in Eq. (5.1) with

$$\mathrm{e}^{\Gamma} = \mathrm{e}^{-\Lambda} = \begin{cases} 1 - \frac{2M}{r} & r > R\,, \\ 1 - 2C\frac{r^2}{L^2} & r < R\,, \end{cases} \tag{5.28}$$

where $R$ is the radius of the gravastar, $C$ its compactness, and $L$ the de Sitter length.

### 5.5.4 Superspinars

Superspinars are another kind of black hole mimickers [285]. In string theory, it is possible to violate the Kerr bound, i.e. the ratio between their angular momentum and mass can be greater than one. For this reason, they have no event horizon. Although finding such super-spinning objects (for instance in active galactic nuclei or as sources of gamma ray bursts) could be interpreted as a piece of evidence for string theory, they have been shown to be unstable for multiple reasons [265–268].

# Chapter 6

# Boson Stars

We review boson stars and in particular mini boson stars and their stability. Next, we show that mini boson stars in five spacetime dimensions are dynamically unstable. Then, we investigate boson star solutions built from various scalars with different masses, we provide strong evidence that these stars are stable at least in part of the parameter space, and we provide quantitative criteria for instability. These solutions share a lot of features with the well-known single-boson stars.

Units: $c = G = \hbar = 1$.

Note: This chapter contains new results not published elsewhere.

## 6.1 Introduction

Boson stars are built coupling a complex scalar field to gravity,[1] i.e. they are self-gravitating solutions made of massive bosonic fields. This subject has been broadly reviewed [287–294], and here we summarize only the fundamental features.

The energy of the scalar field — which can be either a stable fundamental bosonic particle or an unstable particle with decay/inverse-decay in equilibrium — gravitates holding the star together, and the gravitational collapse is not inevitable. Sometimes, it is said that boson stars are held in equilibrium by the Heisenberg uncertainty principle, because the Klein-Gordon wave equation which describes the scalar field tends to disperse fields, the same dispersion which underlies the Heisenberg uncertainty principle.

Gravity is necessary to build a boson star, but we will need an oscillating complex scalar field, as Derrick's theorem [295] states that no regular, static, nontopological localised scalar field solutions are stable in three-dimensional (spatial) flat space. Even if the scalar is no longer static, the spacetime remains static.

Boson stars could be astrophysical stellar objects. As neutron stars, they have a maximum mass (inversely proportional to the mass of the constituent scalar field) across which the configuration is no longer stable. Differently, they do not have a surface. If we make a correspondence, we could say that to different equations of state for neutron stars correspond different potentials for boson stars, with the advantage that boson stars are easier to evolve than neutron star models.

1. It is not possible to find time-independent, spacetime solutions for a real scalar field. However, there are non-singular, time-dependent near-equilibrium configurations of self-gravitating real scalar fields, which are known as oscillatons [286].

Boson stars have often been invoked as generic dark matter candidates [288], to explain dark matter halos [296, 297], and to model accretion of dark matter into stars [298, 299].

For a fixed boson mass $\mu$, boson stars can come under a variety of sizes and compactnesses, a maximum mass that scales like $M_{\rm max} \approx 0.633\, m_P^2/\mu$, where $m_P$ is the Planck mass, for minimally coupled scalars, and a compactness that can be negligibly small or very close to that of black holes. For this reason, high-compactness boson stars have been proposed as black hole mimickers [272, 273]. Black holes and their mimickers are indistinguishable to electromagnetic telescopes, and the potential electromagnetic differences can be tweaked by adjusting the boson star potential. In fact, a boson star can be a non-interacting compact object, as long as we do not include any explicit coupling to any electromagnetic or other fields. However, the observation of gravitational waves from such objects may be able to distinguish black holes from boson stars.

The possibility of detecting boson stars — through gravitational redshift, (micro-)lensing, emission of gravitational waves, or, in the case of a giant boson star, its dark matter contribution to the rotation curves of galactic halos — is discussed, e.g., in Ref. [293].

However, there are two objections against invoking boson stars as the compact, dark objects seen in our universe. The first is the issue of instability, a common problem to all ultra-compact objects, as discussed in Section 5.5. The second objection argues that a single scalar of mass $\mu$ will fix, once and for all, the maximum mass of very compact objects. In such scenario, it would be hard to explain the variety of masses that black hole candidates are observed to have. Such arguments can be evaded by invoking a large number of different bosonic fields to be present. However, in Section 6.5, we show that even with only two different scalars we can obtain stable multi-boson star solutions with different maximum masses.

## 6.2 Review on Boson Stars

In this section we review some general properties of general relativistic boson stars, whose general action is

$$\mathcal{A} = \int \mathrm{d}^4x\,\sqrt{-g}\left(\frac{\mathcal{R}}{16\pi} - |\partial\phi|^2 - V\left(|\phi|^2\right)\right), \tag{6.1}$$

and the Einstein-Klein-Gordon equations are

$$R_{\mu\nu} - \frac{\mathcal{R}}{2}\,g_{\mu\nu} = 8\pi\,T_{\mu\nu}\,, \tag{6.2}$$

$$\frac{1}{\sqrt{-g}}\,\partial_\mu\left(\sqrt{-g}\,g^{\mu\nu}\,\partial_\nu\phi\right) = \frac{\mathrm{d}V}{\mathrm{d}|\phi|^2}\phi\,, \tag{6.3}$$

where the energy-momentum tensor is given by,

$$T_{\mu\nu} = \frac{1}{2}\left[\left(\partial_\mu\phi\,\partial_\nu\phi^* + \partial_\mu\phi^*\,\partial_\nu\phi\right) - g_{\mu\nu}\left(|\partial\phi|^2 + V\left(|\phi|^2\right)\right)\right]. \tag{6.4}$$

As a consequence of Noether's theorem, the invariance of the Lagrangian in (6.1) under global U(1) transformations, $\phi \to e^{i\alpha}\phi$, implies the existence of a conserved current $J^\mu$ and the spatial integral of the time-component of the current defines the conserved Noether charge: the boson number $\mathcal{N}$,

$$J_\mu = \frac{i}{2}\left(\phi^*\nabla_\mu\phi - \phi\nabla_\mu\phi^*\right), \qquad \mathcal{N} = \int d^3x\,\sqrt{-g}\,J^0\,. \tag{6.5}$$

Boson stars are often classified according to their scalar potential. The three most common models are summerised in Table 6.1, togheter with the scaling of the maximum mass.

| Model | Potential $V(\lvert\phi\rvert^2)$ | Maximum mass $M_{\rm max}/M_\odot$ |
|---|---|---|
| Minimal | $\mu^2\lvert\phi\rvert^2$ | $8\times10^{-11}\left(\frac{\rm eV}{\mu}\right)$ |
| Massive | $\mu^2\lvert\phi\rvert^2 + \frac{\alpha}{4}\lvert\phi\rvert^4$ | $5\sqrt{\alpha}\left(\frac{0.1\,\rm GeV}{\mu}\right)^2$ |
| Solitonic | $\mu^2\lvert\phi\rvert^2\left(1-\frac{2\lvert\phi\rvert^2}{\sigma_0^2}\right)^2$ | $\frac{(7\times10^5\,\rm GeV)^3}{\mu\,\sigma_0^2}$ |

Table 6.1: Scalar potential and maximum mass for the three most common models of boson stars. $\mu$ is the mass of the bosonic field, $\alpha$ is a dimensionless parameter and $\sigma_0$ is a constant of the same order of $\mu$. For massive boson stars, the maximum mass holds in the $\alpha \gg 1$ limit.

The simplest potential is the free-field case, or mini boson star, characterized by a massive potential [300, 301]. This model and its stability will be discussed better in Section 6.3. It has a maximum mass configuration of $M_{\rm max} \approx 0.663\,m_P^2/\mu$, known as the Kaup limit. Except for very light bosons, $\mu \sim 10^{-11}$ eV, this limit is way below the Chandrasekhar limit for fermion stars, i.e. $M_{\rm Ch}/M_\odot \sim (1\,{\rm GeV}/\mu)^2$.

This model can be easily extended by adding a quartic interaction term in addition to the massive term [302]. It is now known as massive boson star model because, depending on the value of $\alpha$, the total mass can reach values compatible with the Chandrasekhar limit.

A third common model is the solitonic one [303–305]. This model supports confined nondispersive solutions with finite mass and allows for supermassive configurations of order $10^6 M_\odot$ even for very heavy bosons, e.g. $\mu \sim \sigma_0 \sim 1$ TeV.

A more comprehensive list of boson star models can be found in Ref. [294]. Other models and extensions include e.g. rotating boson stars [306, 307] and mixed fermion-boson stars [308, 309]. Boson stars can also be built in alternative theories of gravity, by introducing Maxwell or Yang-Mills terms the action (6.1), and considering a vector field instead of a scalar field [310].

## 6.3 Mini Boson Stars

Mini boson stars, characterised by the potential $V(|\phi|^2) = \mu^2|\phi|^2$, have been introduced by Kaup [300] as the Klein-Gordon counterpart of John Wheeler's geons [311]. In this section we review the equilibrium solutions and their stability. This will be useful to compare with what happens for boson stars in higher dimensions (Section 6.4) and boson stars built with various scalars (Section 6.5).

### 6.3.1 Equilibrium Solutions

We consider a spherically symmetric spacetime in Schwarzschild-like coordinates, and a harmonic ansatz for the scalar field,

$$\mathrm{d}s^2 = -\mathrm{e}^{\Gamma(r)}\,\mathrm{d}t^2 + \mathrm{e}^{\Lambda(r)}\,\mathrm{d}r^2 + r^2\,\mathrm{d}\Omega^2\,, \quad \phi(t,r) = \frac{1}{\sqrt{8\pi}}\,\phi_0(r)\,\mathrm{e}^{-\mathrm{i}\omega t}\,. \tag{6.6}$$

The relevant Einstein and Klein-Gordon equilibrium equations are,

$$\Lambda' = \frac{1-\mathrm{e}^{\Lambda}}{r} + r\left(\omega^2\mathrm{e}^{\Lambda-\Gamma}\phi_0^2 + \phi_0'^2 + \mathrm{e}^{\Lambda}V_0\right), \tag{6.7}$$

$$\Gamma' = \frac{\mathrm{e}^{\Lambda}-1}{r} + r\left(\omega^2\mathrm{e}^{\Lambda-\Gamma}\phi_0^2 + \phi_0'^2 - \mathrm{e}^{\Lambda}V_0\right), \tag{6.8}$$

$$\phi_0'' = \left(\frac{\Lambda'-\Gamma'}{2} - \frac{2}{r}\right)\phi_0' + \mathrm{e}^{\Lambda}\left(\frac{\mathrm{d}V}{\mathrm{d}|\phi|^2} - \omega^2\mathrm{e}^{-\Gamma}\right)\phi_0\,, \tag{6.9}$$

where $V_0 \equiv V\left(\phi_0^2\right)$, e.g. for a mini boson star $V_0 = \mu^2\phi_0^2$. Notice that after the change of variables $r \to \mu r$ and $\omega \to \omega/\mu$, Eqs. (6.7) to (6.9) do not depend on $\mu$. For simplicity, henceforth we set $\mu = 1$. In order to have a physical solution we have to impose regular boundary conditions at the origin,[2]

$$\Gamma(0) = \Gamma_c\,, \quad \Lambda(0) = 0\,, \quad \phi_0(0) = \phi_c\,, \quad \phi_0'(0) = 0\,, \tag{6.10}$$

while at infinity we require the scalar field to vanish and the spacetime to be asymptotically flat,

$$\lim_{r\to\infty}\phi_0(r) = 0\,, \quad \lim_{r\to\infty}\mathrm{e}^{\Gamma(r)} = \lim_{r\to\infty}\mathrm{e}^{-\Lambda(r)} = 1\,. \tag{6.11}$$

For each value of the scalar field central value $\phi_c$, the background equations form an eigenvalue problem for the frequency $\omega$, which we solve using a standard shooting method. In general, the boundary conditions are satisfied by a discrete set of eigenfrequencies; here we focus on the lowest eigenfrequency, which corresponds to a boson star in the ground state and to a scalar profile with no nodes — see Fig. 6.1. The higher frequencies correspond to excited states that will decay to the ground

2. Actually, to increase the accuracy of the numerical integration, it is customary to consider a higher-order expansion near the origin which reduces to Eq. (6.10) at first order.

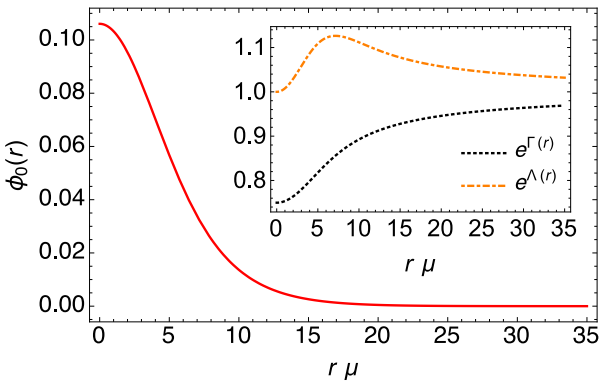


Figure 6.1: Scalar profile and metric functions (inset) as functions of the radial coordinate for the $\phi_c \approx 0.106$ configuration. The total mass for this configuration is $M \approx 0.542/\mu$.

state through emission of gravitational and scalar radiation [312]. The value $\Gamma_c$ can be arbitrary, it can always be tweaked by a time-redefinition in order to achieve (6.11), i.e. asymptotic flatness.

The total mass of the configuration is defined as the $r \to \infty$ limit of

$$M(r) = \frac{r}{2}\left(1 - \frac{1}{e^{\Lambda(r)}}\right), \tag{6.12}$$

in analogy with the total mass of the Schwarzschild solution.

Then, by following the procedure described above, we obtain a family of solutions parametrised by the central value of the scalar field $\phi_c$. In Fig. 6.2 we plot the total mass versus $\phi_c$ and we observe that, in our units, the maximum mass value, $M_{\rm max} \approx 0.663\, m_P^2/\mu$ is attained for $\phi_c \approx 0.27$.

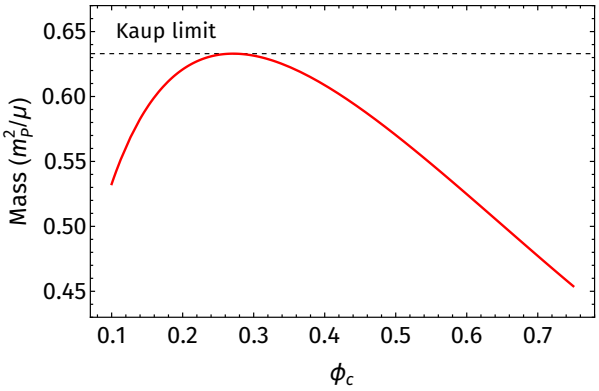


Figure 6.2: Total mass as function of the scalar field central value for mini boson stars. The Kaup limit is attained for $\phi_c \approx 0.27$.

Boson stars do not have a hard surface, as the scalar is spread out all over the radial direction. However, the configuration is highly localized in a radius $\sim 1/\mu$ and it is customary to define the effective radius $R$ as the radius within which the 99% (sometimes the 90%) of the total mass is contained, i.e. $M(R) = 0.99M$.

### 6.3.2 Stability of Mini Boson Stars

A maximum mass usually indicates a point of marginal stability [313] and we now discuss whether the background solutions of the previous subsection are stable. A common approach is to consider small fluctuations about the equilibrium configurations such that we can work in linear perturbation theory [314, 315]. However, a solution can be linearly stable and yet have a non-linear instability. In such a case, other methods are needed, e.g. full numerical evolutions of the Einstein-Klein-Gordon equations.

Assuming the linear perturbations to be only in the radial direction [316, 317], we introduce four perturbation fields and we expand about the equilibrium configuration,

$$\begin{aligned}
\Lambda(t,r) &= \Lambda_0(r) + \delta\Lambda(t,r)\,,\\
\Gamma(t,r) &= \Gamma_0(r) + \delta\Gamma(t,r)\,,\\
\phi(t,r) &= \frac{1}{\sqrt{8\pi}}\left[\phi_0(r)\,\mathrm{e}^{-\mathrm{i}\omega t} + \delta\psi_1(t,r) + \mathrm{i}\,\delta\psi_2(t,r)\right].
\end{aligned}$$

The resulting Einstein-Klein-Gordon equations for the perturbations can be manipulated to get rid off $\delta\Gamma$ and $\delta\psi_2$, and in the end we are left with two equations in two unknowns,

$$\begin{aligned}
\delta\psi_1'' =& -\mathrm{e}^{\Lambda_0}\left(\frac{1}{r^2\phi_0} - r\phi_0^2\phi_0' + \frac{\phi_0'}{r} - 2\phi_0\right)\delta\Lambda - \frac{\delta\Lambda'}{r\phi_0} - \left(\frac{\Gamma_0' - \Lambda_0'}{2} - \frac{2\phi_0'}{\phi_0} + \frac{2}{r}\right)\delta\psi_1'\\
&+ \mathrm{e}^{\Lambda_0-\Gamma_0}\,\delta\ddot{\psi}_1 + \left(\omega^2\mathrm{e}^{\Lambda_0-\Gamma_0} + 2r\mathrm{e}^{\Lambda_0}\phi_0\phi_0' + 3\mathrm{e}^{\Lambda_0}\right)\delta\psi_1\,, \qquad (6.13)\\
\delta\Lambda'' =& \left(\frac{2}{r^2} + \Lambda_0'' - \frac{(\Gamma_0' - \Lambda_0')^2}{2} - \frac{\Lambda_0' + 2\Gamma_0'}{r} + 4\phi_0'^2\right)\delta\Lambda - \frac{3}{2}\left(\Gamma_0' - \Lambda_0'\right)\delta\Lambda'\\
&+ 4r\mathrm{e}^{\Lambda_0}\phi_0\left(\frac{2\Gamma_0' + \Lambda_0'}{2} + \frac{\phi_0'}{\phi_0}\right)\delta\psi_1 + \mathrm{e}^{\Lambda_0-\Gamma_0}\,\delta\ddot{\Lambda} - 4\left(2\phi_0' - r\mathrm{e}^{\Lambda_0}\phi_0\right)\delta\psi_1'\,. \qquad (6.14)
\end{aligned}$$

For the stability analysis, we assume harmonic time dependence,

$$\delta\psi_1 = \delta\psi_1(r)\,\mathrm{e}^{\mathrm{i}\sigma t}\,, \quad \delta\Lambda = \delta\Lambda(r)\,\mathrm{e}^{\mathrm{i}\sigma t}\,. \qquad (6.15)$$

The system (6.13) and (6.14) defines a characteristic value problem for $\sigma^2$. It can be shown that the system is self-adjoint [316] and hence the values of $\sigma^2$ must be real. To determine stability or instability we just need to determine whether $\sigma^2$ is positive or negative. Negative values of $\sigma^2$ correspond to perturbations that will grow, which means that the boson star is unstable against radial oscillations.

In Fig. 6.5, the red solid line represents the value of $\sigma^2$ for different background configurations. We observe that it is positive for $\phi_c \lesssim 0.27$, the very same value for which we have the maximum mass. This means that configurations on the left of the maximum in Fig. 6.2 are stable against linear radial perturbation, while configurations on the right are not.

The procedure for calculating the frequency $\sigma^2$ is as follows. Once we have an equilibrium solution, we solve Eqs. (6.13) and (6.14) along regular boundary conditions at the origin,[3]

$$\delta\Lambda(0) = \delta\Lambda'(0) = 0\,, \quad \delta\Lambda''(0) = \delta\Lambda_c\,, \tag{6.16}$$

$$\delta\psi_1(0) = \delta\psi_c\,, \quad \delta\psi_1'(0) = 0\,, \quad \delta\psi_1''(0) = \frac{3 + \mathrm{e}^{-\Gamma_c}(\sigma^2 - \omega^2)}{6}\delta\psi_c - \frac{\delta\Lambda_c}{2\phi_c}\,, \tag{6.17}$$

asymptotic flatness at infinity,

$$\lim_{r\to\infty} \delta\Lambda(r) = \lim_{r\to\infty} \delta\psi_1(r) = 0\,, \tag{6.18}$$

and with the condition that the boson number $\mathcal{N}$ must be conserved. Notice that, since the system is linear, the value of $\delta\psi_c$ is arbitrary. We begin with considering perturbations very close to the configuration which corresponds to the maximum mass, where $\sigma^2 = 0$. Then we shoot for $\Lambda_c$ until the boundary conditions are satisfied. For more general configurations ($\sigma^2 \neq 0$), we simultaneously shoot for $\Lambda_c$ and $\sigma^2$.

### 6.3.3 Binding-Energy Criterion

The binding-energy criterion is an alternative method for studying stability proposed by Kusmartsev et al. [318]. As a general fact, stable systems are expected to have negative binding-energy, defined as $E_{\text{bind}} = M - \mu\mathcal{N}$, while positive binding-energy signals an instability. However, negative binding-energy is a necessary but not sufficient condition for stability.

The method consists of investigating the critical points of a mapping and the construction of bifurcation diagrams of the binding-energy versus the boson number.

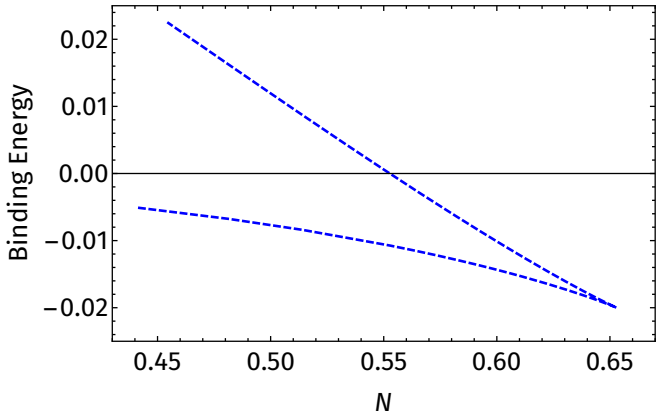


Figure 6.3: Bifurcation diagrams of the binding-energy versus the total boson number.

3. Actually, to increase the accuracy of the numerical integration, it is customary to consider a higher-order expansion near the origin which reduces to Eqs. (6.16) and (6.17) at first order.

The mapping is between the two-dimensional subspace of the dynamical variables of the boson field, and space of the integrals of motion, such as the gravitational mass $M$ and the total particle number $\mathcal{N}$. Using catastrophe theory to classify the singularities of such mapping, it is possible to derive general criteria for the stability of the star. The results agree with those of linear perturbation theory.

In Fig. 6.3 we plot the bifurcation diagram for mini boson stars. The lower branch of the bifurcation diagram corresponds to a stable configuration and the cusp occurs at precisely the location of the $\phi_c$ corresponding to the maximum mass. The upper branch corresponds to solutions with larger $\phi_c$, and eventually reaches a positive binding-energy.

## 6.4 Boson Stars in Higher Dimensions

In this section we show that mini boson stars in five dimensions are always unstable against radial oscillations. This is a new result, not published elsewhere, that also proves an assertion made recently by Brihaye and Hartmann [319], who showed that these stars always have a positive binding-energy.

We consider the most general time-dependent, spherically symmetric line element in five dimensions,

$$\mathrm{d}s^2 = -\mathrm{e}^{\Gamma(t,r)}\,\mathrm{d}t^2 + \mathrm{e}^{\Lambda(t,r)}\,\mathrm{d}r^2 + r^2\left(\mathrm{d}\vartheta_1^2 + \sin^2\vartheta_1\,\mathrm{d}\vartheta_2^2 + \sin^2\vartheta_1\sin^2\vartheta_2\,\mathrm{d}\varphi^2\right), \tag{6.19}$$

and we decompose the scalar field in two real scalars

$$\phi(t,r) = \frac{1}{\sqrt{8\pi}}\left[\psi_1(t,r) + \mathrm{i}\,\psi_2(t,r)\right]\mathrm{e}^{-\mathrm{i}\omega t}\,. \tag{6.20}$$

The Einstein-Klein-Gordon background equations are obtained by setting $\Lambda(t,r) = \Lambda_0(r)$, $\Gamma(t,r) = \Gamma_0(r)$, $\psi_1(t,r) = \phi_0(r)$ and $\psi_2(t,r) = 0$, and they read

$$\Lambda_0' = \frac{2r}{3}\left(\mathrm{e}^{\Lambda_0-\Gamma_0}\omega^2\phi_0^2 + \mathrm{e}^{\Lambda_0}\phi_0^2 + \phi_0'^2\right) + \frac{2-2\mathrm{e}^{\Lambda_0}}{r}\,, \tag{6.21}$$

$$\Gamma_0' = \frac{2r}{3}\left(\mathrm{e}^{\Lambda_0-\Gamma_0}\omega^2\phi_0^2 - \mathrm{e}^{\Lambda_0}\phi_0^2 + \phi_0'^2\right) + \frac{2\mathrm{e}^{\Lambda_0}-2}{r}\,, \tag{6.22}$$

$$\phi_0'' = \left(\frac{\Lambda_0'-\Gamma_0'}{2} - \frac{3}{r}\right)\phi_0' + \mathrm{e}^{\Lambda_0}\left(1-\mathrm{e}^{-\Gamma_0}\omega^2\right)\phi_0\,, \tag{6.23}$$

along with regular boundary conditions at the origin,[4]

$$\Gamma_0(0) = \Gamma_c\,, \quad \Lambda_0(0) = 0\,, \quad \phi_0(0) = \phi_c\,, \quad \phi_0'(0) = 0\,, \tag{6.24}$$

4. Actually, to increase the accuracy of the numerical integration, it is customary to consider a higher-order expansion near the origin which reduces to Eq. (6.24) at first order.

while at infinity we require the scalar field to vanish and the spacetime to be asymptotically flat,

$$\lim_{r\to\infty}\phi_0(r)=0\,,\qquad \lim_{r\to\infty}\mathrm{e}^{\Gamma_0(r)}=\lim_{r\to\infty}\mathrm{e}^{-\Lambda_0(r)}=1\,. \tag{6.25}$$

The total mass in five dimension is the $r\to\infty$ limit of

$$M(r)=\frac{3\pi r^2}{8}\left(1-\frac{1}{\mathrm{e}^{\Lambda_0(r)}}\right). \tag{6.26}$$

As in the four-dimensional case, for each value of the scalar field central value, we use a shooting method to find the lowest frequency $\omega$ which solves the background equations. In Fig. 6.4 we plot the total mass as function of the central value of the scalar field and we observe that there is no local maximum.

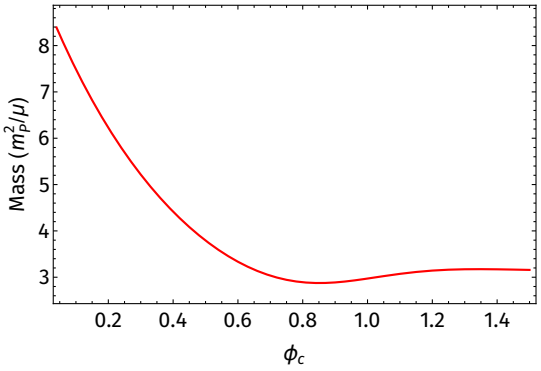


Figure 6.4: Total mass as function of the scalar field central value for five-dimensional mini boson stars.

In order to study linear stability, following the analysis of Gleiser and Watkins [316] and Hawley and Choptuik [317], we introduce four perturbation fields and we expand about the equilibrium configuration. The four equations for the perturbed quantities can be manipulated such that we are left with two equations in two unknowns,

$$\begin{aligned}\delta\psi_1''=&-\mathrm{e}^{\Lambda_0}\left(\frac{3}{r^2\phi_0}-\frac{2r\phi_0^2\phi_0'}{3}+\frac{2\phi_0'}{r}-2\phi_0\right)\delta\Lambda-\frac{3}{2r\phi_0}\delta\Lambda'+\mathrm{e}^{\Lambda_0-\Gamma_0}\ddot{\delta\psi}_1\\&-\left(\frac{\Gamma_0'-\Lambda_0'}{2}-\frac{2\phi_0'}{\phi_0}+\frac{3}{r}\right)\delta\psi_1'+\mathrm{e}^{\Lambda_0}\left(\mathrm{e}^{-\Gamma_0}\omega^2+\frac{4r\phi_0\phi_0{}'}{3}+3\right)\delta\psi_1\,,\end{aligned} \tag{6.27}$$

$$\begin{aligned}\delta\Lambda''=&\left(\frac{4}{r^2}+\Lambda_0''-\frac{(\Gamma_0'-\Lambda_0')^2}{2}-\frac{\Lambda_0'+4\Gamma_0'}{r}+4\phi_0'^2\right)\delta\Lambda-\left(\frac{3\,(\Gamma_0'-\Lambda_0')}{2}+\frac{1}{r}\right)\delta\Lambda'\\&+\mathrm{e}^{\Lambda_0-\Gamma_0}\ddot{\delta\Lambda}-8\left(\phi_0'-\frac{r\,\mathrm{e}^{\Lambda_0}\phi_0}{3}\right)\delta\psi_1'+\frac{4r\,\mathrm{e}^{\Lambda_0}\phi_0}{3}\left(\Lambda_0'+2\Gamma_0'+\frac{2\phi_0'}{\phi_0}\right)\delta\psi_1\,.\end{aligned} \tag{6.28}$$

For the stability analysis, we assume harmonic time dependence

$$\delta\psi_1(t,r)=\delta\psi_1(r)\,\mathrm{e}^{i\sigma t}\,,\qquad \delta\Lambda(t,r)=\delta\Lambda(r)\,\mathrm{e}^{i\sigma t}\,. \tag{6.29}$$

The boundary conditions at $r = 0$ are[5]

$$\delta\Lambda(0) = \delta\Lambda'(0) = 0\,, \quad \delta\Lambda''(0) = \delta\Lambda_c\,, \tag{6.30}$$

$$\delta\psi_1(0) = \delta\psi_c\,, \quad \delta\psi_1'(0) = 0\,, \quad \delta\psi_1''(0) = \frac{\mathrm{e}^{-\Gamma_c}(\sigma^2-\omega^2)+3}{8}\,\delta\psi_c - \frac{3\delta\Lambda_c}{4\phi_c}\,. \tag{6.31}$$

At infinity the perturbations vanish,

$$\lim_{r\to\infty}\delta\Lambda(r) = \lim_{r\to\infty}\delta\psi_1(r) = 0\,. \tag{6.32}$$

As in the four-dimensional case, the system (6.27) and (6.28) along with the condition that the boson number must be conserved, defines a characteristic value problem for $\sigma^2$. In order to determine stability or instability we just need to determine whether $\sigma^2$ is positive or negative. To solve the system (6.27) and (6.28) for a given $\phi_c$ we begin by solving the respective background solution and then we shoot for $\sigma^2$ and $\delta\Lambda_c$. Notice that, since the system is linear, the value of $\delta\psi_c$ is arbitrary.

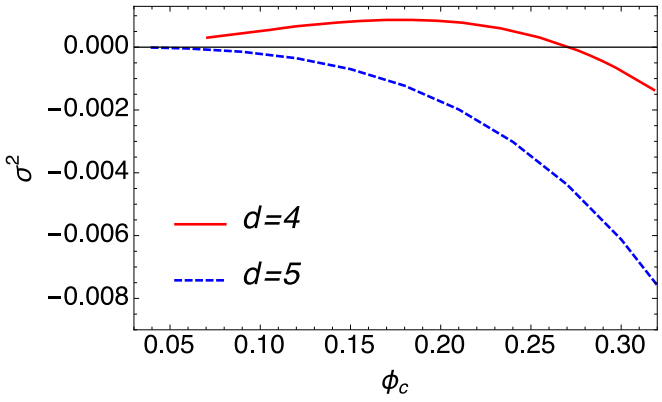


Figure 6.5: Distribution for the squared frequency $\sigma^2$ with respect to the central value of the scalar $\phi_c$. In four dimensions $\sigma^2$ crosses zero, while in five dimensions it is always negative.

The dependence of the squared frequency $\sigma^2$ on the value of the scalar at the origin, $\phi_c$, is plotted in Fig. 6.5, together with the corresponding four-dimensional case. We observe that $\sigma^2$ is always negative in the five-dimensional (and presumably, higher-dimensional) case, contrary to the four-dimensional case [317], implying that mini boson star solutions in five spacetime dimensions are always unstable against radial perturbations.

## 6.5 Multi-Scalar Boson Stars

In this section we construct boson stars built with various scalars and we investigate their stability.

5. Actually, to increase the accuracy of the numerical integration, it is customary to consider a higher-order expansion near the origin which reduces to Eqs. (6.30) and (6.31) at first order.

### 6.5.1 Setup

We consider Einstein gravity minimally coupled with $N$ massive complex scalars, i.e. an $N$-boson star, described by the following action,

$$\mathcal{A} = \int \mathrm{d}^4x\,\sqrt{-g}\left[\frac{\mathcal{R}}{16\pi} - \sum_{n=1}^{N}\left(|\partial_\mu\Phi_n|^2 + \mu_n^2|\Phi_n|^2\right)\right]. \tag{6.33}$$

As in the single-boson star case, we consider a time-independent and spherically symmetric spacetimes, and harmonic ansätze for the scalar fields,

$$\mathrm{d}s^2 = -\mathrm{e}^{\Gamma(r)}\,\mathrm{d}t^2 + \mathrm{e}^{\Lambda(r)}\,\mathrm{d}r^2 + r^2\,\mathrm{d}\Omega^2\,, \quad \Phi_n(t,r) = \frac{1}{\sqrt{8\pi}}\,\phi_n(r)\,\mathrm{e}^{-\mathrm{i}\omega_n t}\,. \tag{6.34}$$

In Einstein's equations the total energy-momentum tensor $T_{\mu\nu}$ is given by the sum of the energy-momentum tensors of each scalar,[6]

$$T_{\mu\nu} = \frac{1}{2}\sum_n\left[\left(\partial_\mu\Phi_n\,\partial_\nu\Phi_n^* + \partial_\mu\Phi_n^*\,\partial_\nu\Phi_n\right) - g_{\mu\nu}\left(g^{\alpha\beta}\,\partial_\alpha\Phi_n^*\,\partial_\beta\Phi_n + \mu_n^2\Phi_n^*\Phi_n\right)\right]. \tag{6.35}$$

The relevant field equations are

$$\frac{\mathrm{e}^{\Lambda}-1}{r^2} + \frac{\Lambda'}{r} = \frac{1}{2}\sum_n\left[\mathrm{e}^{\Lambda}\left(\mathrm{e}^{-\Gamma}\omega_n^2 + \mu_n^2\right)\phi_n^2 + \phi_n'^2\right], \tag{6.36}$$

$$\frac{1-\mathrm{e}^{\Lambda}}{r^2} + \frac{\Gamma'}{r} = \frac{1}{2}\sum_n\left[\mathrm{e}^{\Lambda}\left(\mathrm{e}^{-\Gamma}\omega_n^2 - \mu_n^2\right)\phi_n^2 + \phi_n'^2\right]. \tag{6.37}$$

Similarly, the Klein-Gordon equation for each scalar

$$\frac{1}{\sqrt{-g}}\,\partial_\mu\left(\sqrt{-g}\,g^{\mu\nu}\,\partial_\nu\Phi_n\right) = \mu_n^2\Phi_n\,, \tag{6.38}$$

(and its complex conjugate) is

$$\phi_n'' + \left(\frac{\Gamma'-\Lambda'}{2} + \frac{2}{r}\right)\phi_n' + \mathrm{e}^{\Lambda}\left(\mathrm{e}^{-\Gamma}\omega_n^2 - \mu_n^2\right)\phi_n = 0\,. \tag{6.39}$$

The Noether charges (particle number) associated to the $\mathrm{U}(1)$ invariance of each mode of the action (6.33) are:

$$\mathcal{N}_n = \frac{\omega_n}{2}\int \mathrm{d}r\,r^2\exp\left(\frac{\Lambda-\Gamma}{2}\right)\phi_n^2\,. \tag{6.40}$$

6. The same energy-momentum tensor appears in the multistate boson star models [320, 321], where $\Phi_n$ are the eigenstates of *one* scalar field with the same mass. In our model, each $\Phi_n$ is a different bosonic field, in its ground state and with its own mass.

### 6.5.2 Equilibrium Solutions

In this section we construct spherically symmetric, time-independent boson stars by integrating numerically (6.36), (6.37) and (6.39) along with boundary conditions. We impose regularity at the origin,[7]

$$\Gamma(0) = \Gamma_c\,, \quad \Lambda(0) = 0\,, \quad \phi_n(0) = \phi_{nc}\,, \quad \phi_n'(0) = 0\,, \tag{6.41}$$

whereas at infinity we impose the metric to be Minkowski and the scalar fields to vanish.

$$\lim_{r\to\infty} \phi_n(r) = 0\,, \quad \lim_{r\to\infty} \mathrm{e}^{\Gamma(r)} = \lim_{r\to\infty} \mathrm{e}^{-\Lambda(r)} = 1\,. \tag{6.42}$$

The problem is then reduced to an eigenvalue problem for the frequencies $\omega_n$, which we solve using a standard shooting method. In general, the boundary conditions are satisfied by a discrete set of frequencies. We focus here on the ground state, corresponding to a scalar field with no nodes (see Fig. 6.6).

We will restrict our study by considering only two scalars, i.e. $N = 2$ and $\mu_2 = 2\mu_1$. The complete specification of the equilibrium solution requires the mode content, i.e., the relative amplitude between the $\phi_n$ at the centre of the star, which is unspecified *a priori*.

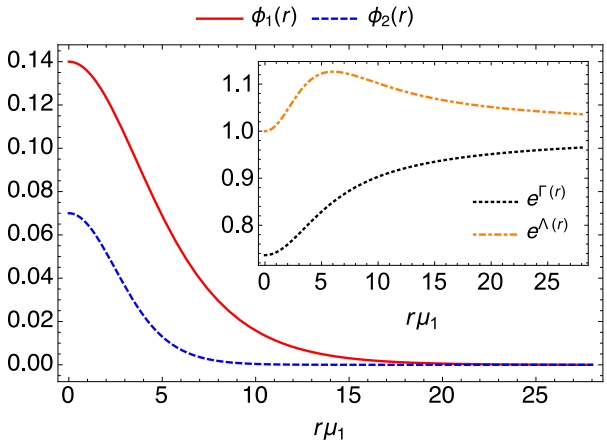


Figure 6.6: Scalar profiles and metric functions (inset) for the two-boson star with relative amplitude $\phi_{2c}/\phi_{1c} = 1/2$. The central value for the first scalar is $\phi_{1c} = 0.14$. The total mass for this configuration is $M \approx 0.488/\mu_1$.

Typical scalar-field and metric profiles are shown in Fig. 6.6 for $\phi_{1c} = 0.14 = 2\phi_{2c}$, in units of $\mu_1 = 1$. The scalar and metric profile resemble those of the purely single-boson stars and approach their asymptotic values at infinity exponentially fast [322]. For this particular set of parameters, the ADM mass of the configuration is $M \approx 0.488/\mu_1$.

7. Actually, to increase the accuracy of the numerical integration, it is customary to consider a higher-order expansion near the origin which reduces to Eq. (6.41) at first order.

A useful and relevant information is how the total mass of boson stars changes with the central value of the scalar field or with the effective radius $R$. This is summarised in Fig. 6.7 for two representative mode content. As expected, these stars have a maximum mass, still of order $\sim 1/\mu_i$. The maximum mass, when measured in units of the lightest mode in the problem, is smaller when the second mode has a larger amplitude. In the limit that the second mode dominates completely, the maximum mass should be one-half of its Kaup limit $M_{\rm max} \approx 0.633/\mu_1$.

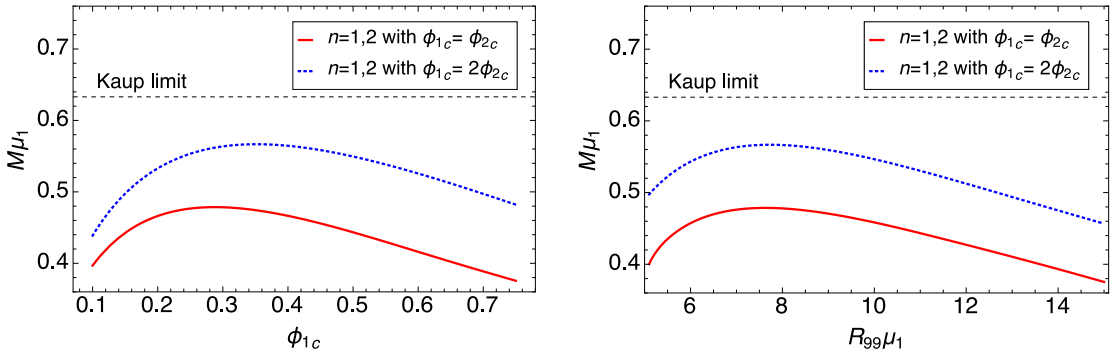


Figure 6.7: Left Panel: Total mass of the two-boson stars as a function of the central value of the first mode, for different mode content. The lower, solid (red) line corresponds to two scalars with the same value at the origin; The second line (blue, dotted) corresponds to two scalars with relative amplitude at the origin of 1/2. Right Panel: Total mass as a function of the effective radius.

The total mass of the two-boson stars is shown in the contour plot in Fig. 6.8 for a wide range of central values of the fields. In this plot, we can observe the same behaviour shown in Fig. 6.7: the

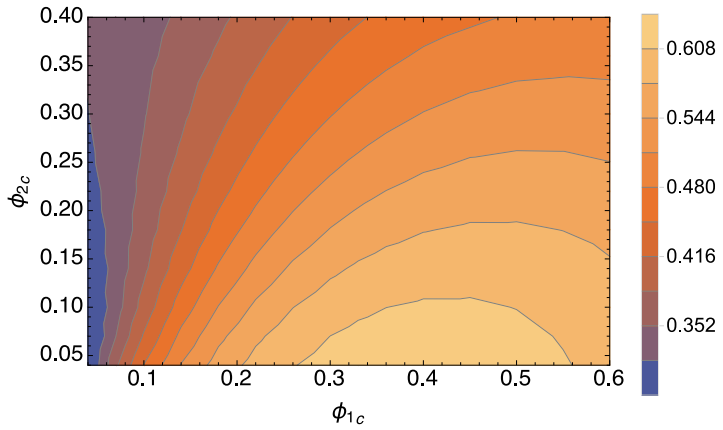


Figure 6.8: Contour plot of the total mass of the two-boson stars as a fuction of the central value of the scalars. The value of $M$ is given in terms of the scale of colour on the right.

total mass increases, reaches a local maximum and then decreases. This is evident for small values of $\phi_{2c}$, while as $\phi_{2c}$ gets bigger the total mass value does not drop fast enough to be noted in the plot. We also observe that the maximum total mass tends to the Kaup limit as $\phi_{2c} \to 0$, i.e., when our solution reduces to the single-boson star.

We also find that the compactness of these boson stars decreases with radius, i.e., boson stars with a large radius $R$ (fixed masses $\mu_i$, corresponding to small values of the scalar at the origin) have a small total mass $M \sim 1/R$. In essence, in the large $R$ regime these are quasi-Newtonian, extremely dilute configurations.

### 6.5.3 Stability

In analogy with the single-boson star, the existence of a maximum mass is a hint of marginal stability. Ideally, the stability properties are studied via an analysis of how the system behaves under small fluctuations. Unfortunately, a dynamical analysis for multi-scalar boson stars can become very cumbersome due to the large number of equations to solve.

However, a stability criterion for solutions that depend on two parameters has been introduced studying the stability of fermion-boson stars [323, 324]. At a critical point (a point that separates stable from unstable configurations) there must be a direction $\mathfrak{n}$ such that the directional derivatives of $\{M, \mathcal{N}_1, \mathcal{N}_2\}$ vanish, implying that at the stability boundary $\mathfrak{n}$ is tangential to the level curves of constant $M$, $\mathcal{N}_1$, and $\mathcal{N}_2$. The critical equilibrium configurations correspond to the extreme values of the boson numbers $\mathcal{N}_1$ and $\mathcal{N}_2$ when surveyed along a level curve of constant total mass. In Ref. [324] the authors validated the results by numerical evolutions, and they showed that only the stars on one side of such a critical point are stable against perturbations. On the other side of the critical point, the solutions are unstable and can, depending on the initial perturbation, either evolve to a stable star or collapse to a black hole.

We have repeated the analysis for the two-boson stars under study. In Fig. 6.9 we consider the particular case $M \approx 0.485/\mu_1$, in which the critical configuration is obtained when $\mathcal{N}_1 \approx 0.299$ and $\mathcal{N}_2 \approx 0.101$ for $\phi_{1_c} \approx 0.294$, or equivalently, $\phi_{2_c} \approx 0.279$. Notice that, for positive $\phi_{1_c}$ ($\phi_{2_c}$), the boson number $\mathcal{N}_1$ decreases, reaches a minimum and then increases. Since the mass is kept fixed the boson number $\mathcal{N}_2$ has a complementary behaviour.

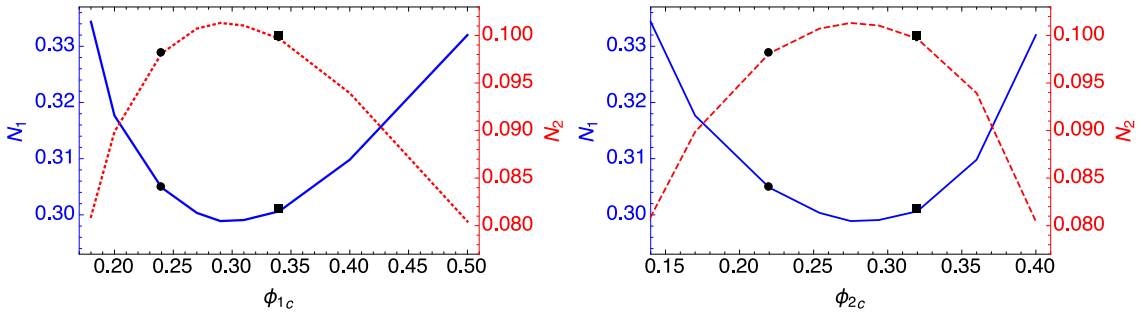


Figure 6.9: The boson numbers $\mathcal{N}_1$ (blue solid line) and $\mathcal{N}_2$ (red dashed line) for the equilibrium configurations as function of $\phi_{1_c}$ (Left Panel) and $\phi_{2_c}$ (Right Panel) when $M \approx 0.485/\mu_1$. The position of the extrema corresponds to the critical point which divides stable from unstable configurations.

As an example, let us consider the points $\phi_{1c} = 0.24$ (black circles) and $\phi_{1c} = 0.34$ (black squares) in Fig. 6.9, respectively on the left and the right of the critical point, and the subset with relative amplitude $\phi_{2c}/\phi_{1c} = 11/12$. For such solutions, the maximum mass is $M_{\rm max} \approx 0.491/\mu_1$, reached when $\phi_{1c}$ ($\phi_{2c}$) is equal (up to numerical errors) to the value corresponding to the minimum (maximum) of $\mathcal{N}_1$ ($\mathcal{N}_2$). Hence, these two configurations are also on the left and on the right of the maximum mass. Configurations with boson number $\mathcal{N}_1$ ($\mathcal{N}_2$) on the left of the minimum (maximum) are stable configurations, while those on the right side are unstable.

Once we fix the central value of one field or their relative amplitude, the stability of the solutions can also be studied by means of the binding-energy stability criterion discussed in Section 6.3.3.

We generalise the criterion to multi-scalar boson stars by defining the binding-energy and the total boson number as,

$$E_{\rm bind} = M - \sum_n \mu_n \mathcal{N}_n \,, \quad \mathcal{N}_{\rm tot} = \sum_n \mathcal{N}_n \,. \tag{6.43}$$

The binding-energy as a function of total boson number is shown in Fig. 6.10 for some relative amplitudes of the central values and shows a lot of similarity with Fig. 6.3.

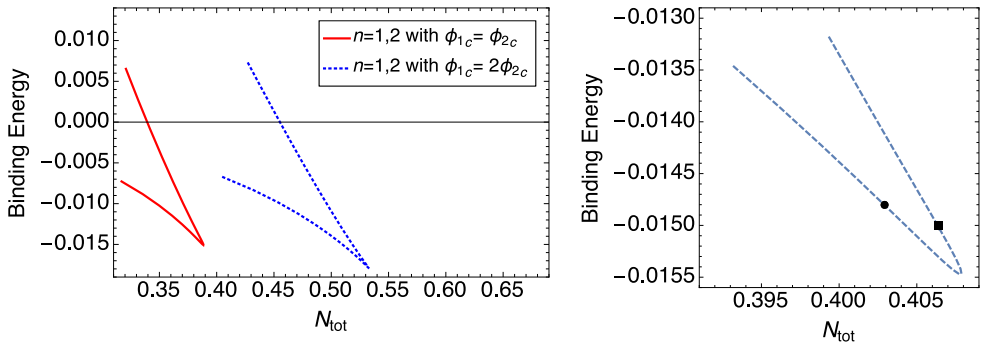


Figure 6.10: Bifurcation diagrams of the binding-energy versus the total boson number. Left Panel: The first curve from left (red, solid) corresponds to two scalars with the same value at the origin; The second curve (blue, dotted) corresponds to two scalars with relative amplitude at the origin of 1/2. Right Panel: Two bosons with relative amplitude at the origin of 12/11; The black circle corresponds to $\phi_{1c} = 0.24$, while the black square corresponds to $\phi_{1c} = 0.34$. Notice how the first point is on the stable part of the branch, while the second is on the unstable, in agreement with the analysis of Fig. 6.9.

This cuspy diagram has interesting features. The cusp occurs at precisely (to within numerical uncertainties) the location of the maximum mass. The line branching off at that point, with steeper slope, corresponds to boson stars with a large value of the scalar at the origin, and eventually reaches a positive binding-energy. The single-boson case shows that the cusp marks the onset of stability. The binding energy diagram for the configurations studied in Fig. 6.9 are shown in the right panel of figure 6.10; Both results are consistent. In summary, combining the two stability criteria, the lower branch of each cusp (central values of the fields smaller than the critical value) corresponds to stable boson star configurations while the upper branch (central values of the fields bigger than the

critical value) corresponds to unstable configurations. There is therefore compelling evidence that multi-scalar boson stars are also marginally stable at the point of maximum mass.

Chapter 7

# Tidal Deformations and Love Numbers for Exotic Compact Objects

The tidal Love numbers encode the deformability of a self-gravitating object immersed in a tidal environment and depend significantly both on the object's internal structure and the dynamics of the gravitational field. In general relativity, all the Love numbers of black holes are exactly zero. We extend this result aiming at testing the nature of compact objects: we compute the tidal Love numbers of exotic compact objects within the framework of general relativity, including different families of boson stars, gravastars, wormholes, and other toy models for quantum corrections at the horizon scale; in the black hole limit, we find a universal logarithmic dependence of the tidal Love numbers on the location of the surface, making the tidal Love numbers of these objects small, but not desperately small to measure. We assess the ability of present and future gravitational-wave detectors to measure the tidal Love numbers of these objects, including the first analysis of tidal Love numbers with LISA. Both LIGO, the Einstein Telescope and LISA can impose interesting constraints on boson stars, while LISA is able to probe even extremely compact objects. The fact that these numbers are generically non-zero provides a piece of evidence for new physics at the horizon scale. We argue that future gravitational-wave measurements of the tidal Love numbers of compact objects in a binary system provide a novel way to test black holes and general relativity in the strong-field regime.

Units: $c = G = 1$.

This chapter is based on: V. Cardoso, E.F, A. Maselli, P. Pani, and G. Raposo. 'Testing strong-field gravity with tidal Love numbers'. (2017). arXiv: 1701.01116.

## 7.1 Introduction

Tidal interactions have several implications in different branches of physics: from geophysics, in the description of oceanic tides and seismic effects, to astrophysics, in the description of ordinary and neutron stars up to galaxies. Tidal interactions are fundamental in the interpretation of tidal tails and binary systems [325, 326] and they can give rise to extreme phenomena, e.g. tidal disruptions, in strong regimes.

Tidal Love numbers measure the deformability of a self-gravitating object immersed in an external tidal field [12, 327]. These tidal effects can leave a detectable imprint in the gravitational-wave signal emitted by a neutron-star binary in the late stages of its orbital evolution [248, 328, 329]. So far, a relativistic extension [248–250] of the Newtonian theory of tidal deformability has been

mostly motivated by the prospect of measuring the tidal Love numbers of neutron stars through gravitational-wave detections and, in turn, understanding the behaviour of matter at ultra-nuclear densities [330–336]. In this chapter, we use tidal effects to explore more fundamental questions about the nature of compact objects and the behaviour of gravity in the strong-field regime.

The intriguing general relativistic result that the tidal Love numbers of black holes vanish poses a problem of 'naturalness' [337, 338], analogous to the strong CP problem and the hierarchy problem in particle physics, or to the cosmological constant problem. The resolution of this naturalness problem could lead to a huge piece of evidence for new physics, which is accessible in gravitational-wave data.

In this chapter, we explore a possible solution to this problem. New physics effects could manifest themselves as unexpectedly large quantum back-reactions or changes in the equation of state, and as a consequence black holes might simply not be formed, and other objects might be the end product of gravitational collapse. These exotic compact objects include boson stars, gravastars, wormholes, and various toy models describing quantum corrections at the horizon scale, like superspinars, fuzzballs [339], '2-2 holes' [340] and others [341–346]. These objects might be formed from the collapse of exotic fields or by quantum effects at the horizon scale, and represent the prototypical example of exotic gravitational wave sources [322, 347, 348] which might be searched for with Earth- or space-based detectors.

There exists another related solution to the naturalness problem. We do not delve into it here and we refer to the paper upon which this chapter is based. The argument is as follows. General relativity might not be a good description of the geometry close to horizons. Black holes other than Kerr arise in theories beyond general relativity which are motivated by both theoretical arguments and by alternative solutions to the dark matter and dark energy problems. Arguably, the simplest hairy black holes arise in Einstein-Maxwell theory and are described by the Reissner-Nordström solution. Although astrophysical black holes are expected to be electrically neutral, Reissner-Nordström black holes can be studied as a proxy of black holes beyond vacuum general relativity and could also emerge naturally in models of minicharged dark matter and dark photons [349]. In several scalar-tensor theories, black holes are uniquely described by the Kerr solution, as in general relativity [350]. However, these theories introduce a scalar degree of freedom (non-minimally) coupled to gravity and the response of black holes to external perturbations is generically richer [351]. In theories with several or with complex bosons, hairy black hole solutions might exist that can be seen as boson stars with a black hole at the center [88, 352]. These solutions are natural endpoints of the superradiant instability of the Kerr geometry, and may even describe metastable states when a single real field is present [353, 354]. Finally, in higher-curvature theories of gravity, the Einstein-Hilbert action is considered as the first term of a possibly infinite expansion containing all curvature invariants. To leading order in the curvature corrections, stationary black holes in these theories belong to only two families [355, 356], i.e. the Einstein-dilaton-Gauss-Bonnet solution [357–359] and the dynamical Chern-Simons solution [360, 361].

The observational determination of the tidal properties of compact objects will also help answering the fundamental question about the existence of event horizon and their possible tests with gravitational-wave data. In Chapter 8 we will show that ultracompact horizonless geometries can mimic very well the last phases of the coalescence of two black holes, when they merge to form a single distorted black hole, ringing down to its final Kerr geometry. In this scenario, horizonless geometries would show up as *echoes* in the gravitational waveforms at very late times [362]. The exclusion of echoes up to some instant $t$ after the merger rules out the structure of the spacetime down to a region $r/r_+ - 1 \sim \exp(-t/r_+)$, with $r_+$ the Schwarzschild radius of the spacetime. Thus, more sensible detectors will probe regions closer and closer to the horizon. The above picture refers to the final, post-merger state. On the other hand, the inspiral signal may contain imprints of the structure of the inspiralling objects. This piece of information is encoded in the way each of these objects reacts to the gravitational field created by the other, i.e. their tidal Love numbers. As we will show, the tidal Love numbers of all exotic compact objects vanish in the black hole limit, logarithmically. Thus, observational bounds on the tidal Love numbers will provide constraints on the compactness of the inspiralling objects.

Using the perturbative formalism described in Chapter 5 and following the notation introduced in Section 5.4, we compute the lowest quadrupolar and octupolar polar and axial tidal Love numbers for various models of spherically symmetric and static exotic compact objects, under the assumption that the only surviving tide at large distances is gravitational.

One of our main results is that the tidal Love numbers of several exotic compact objects display a logarithmic dependence in the black hole limit, i.e. when the compactness of the object approaches that of a black hole,

$$C := M/r_0 \to 1/2\,, \tag{7.1}$$

where $M$ and $r_0$ are the mass and the radius of the object. As shown in Table 7.2, this property holds for wormholes, thin-shell gravastars, and for a simple toy model of a static object with a perfectly reflecting surface [341, 342]. It is natural to conjecture that this logarithmic behaviour is model-independent and will hold for any exotic compact object whose exterior spacetime is arbitrarily close to that of a black hole in the $r_0 \to 2M$ limit. Furthermore, this mild dependence implies that even the tidal Love numbers of an object with $r_0 - 2M \approx l_P$ are not extremely small, contrarily to what one could expect. Indeed, we estimate that the dimensionless tidal Love numbers defined in Eq. (5.19) are

$$k_2^{E,B} \approx \mathcal{O}\left(10^{-3}\right), \quad k_3^{E,B} \approx \mathcal{O}\left(10^{-4}\right), \tag{7.2}$$

for an exotic compact object in the entire mass range $M \in [1, 100]\, M_\odot$. Note that all tidal Love numbers of ultracompact exotic objects listed in Table 7.2 have the opposite sign relative to the neutron-star case.

The accuracy with which gravitational-wave detectors can estimate the tidal Love numbers of compact objects is shown in Fig. 7.6 for three boson star models, where the two inspiralling objects are assumed to be equal. In moderately optimistic scenarios, a gravitational-wave detection of a compact-binary coalescence with LIGO can place an upper bound on the tidal Love numbers of the two objects at the level of $k_2^E \sim 10$, whereas the future Einstein Telescope [363] can potentially improve this constraint by a factor of ten. Interestingly, the future space interferometer LISA [364] has the ability to set much tighter constraints (see also Fig. 7.4) and to rule out several candidates of supermassive exotic compact objects. In essence, both Earth- and space-based detectors are able to discriminate even the most compact boson stars, by imposing stringent bounds on their tidal Love numbers. By contrast, as we show in Section 7.4, only LISA is able to probe the regime of very compact exotic compact objects, describing geometries which are microscopic corrections at the horizon scale, for which the compactness $C = 0.48$ or higher.

## 7.2 Tidal Love Numbers of Boson Stars

In this section, we compute tidal Love numbers for representative models of boson stars — see Chapter 6 and in particular Section 6.2. We consider spherically symmetric minimal, massive and solitonic boson stars, with background metric and background scalar field given by (6.6), whose Einstein-Klein-Gordon background equations are provided by Eqs. (6.7) to (6.9).

By using the procedure described in Section 6.3 for mini boson stars, *mutatis mutandis*, we can compute a sequence of background solutions characterised by the value of the scalar at the centre of the star, $\phi_c$. Notice that, contrary to the minimal and massive case — in which the scalar profile decays exponentially — in the solitonic model, the scalar profile has a very steep profile which makes the numerical integration of the background equations very challenging, requiring very fine-tuned shooting parameters. But the steepness of the scalar profile is also a benefit as it makes the definition of the radius more natural.

In Fig. 7.1, we show the gravitational mass $M$ against its effective radius $R$ (left panel) and the compactness $C = M/R$ as a function of the mass (right panel).

For minimal and interacting boson stars, we observe a maximum which separates stable (on the right) from unstable (on the left) configurations. On the other hand, solitonic boson stars display a completely different behaviour: there exists a stable branch for high values of $R$ and small masses (bottom-right part of the left panel in Fig. 7.1), an unstable branch that starts after the first maximum roughly at $R\mu \sim 50$, and then a second stable branch which starts at $R\mu \sim 10$ up to the maximum on the top-right part of the plot. As shown in the right panel of Fig. 7.1, for minimal and massive boson stars the compactness is typically of $\mathcal{O}\left(10^{-2}\right)$. On the other hand, solitonic boson stars can be almost as compact as black holes (i.e. $C \approx 1/2$), meaning that their radius can be of the order of the Schwarzschild light ring. Even though boson stars have a wide range of compactness, interactions

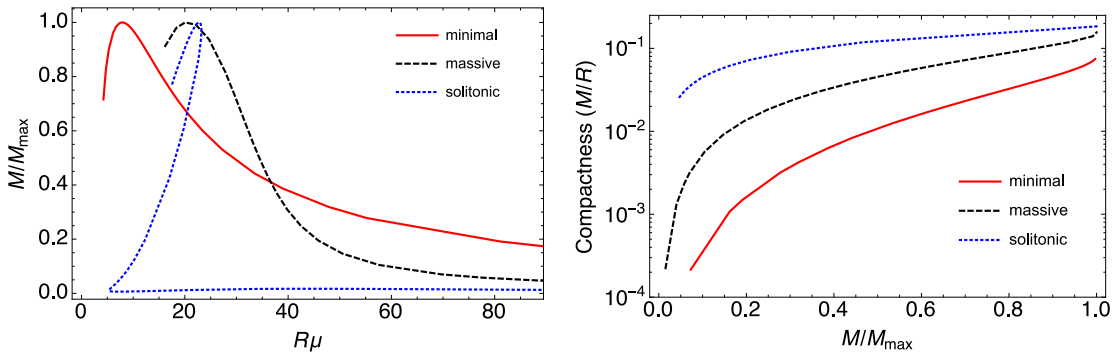


Figure 7.1: Left panel: ADM mass as a function of the effective radius $R$ for different models of boson stars, including some unstable configurations. Right panel: Compactness of the models in the stable branch as a function of the mass. For the massive and solitonic model we have considered three cases: $\alpha = 10^4\,\mu^2$ and $\sigma_0 = 0.05$ respectively.

between boson stars typically lead to a net weight gain, clustering old boson stars close to the mass peak [299], which also coincides with the peak of compactness.

The details of the numerical procedure to find the tidal Love numbers *à la* Hinderer [248] are given in Sections 7.2.1 and 7.2.2. The tidal Love numbers are shown in Fig. 7.2 as a function of the total mass $M$, for different boson star models. We only show static configurations in the stable branch, i.e. with a mass smaller than $M_{\rm max}$. For minimal boson stars and the $\ell = 2$ polar tidal Love number, our results agree with those recently obtained in Ref. [365]. In addition, we also present the results for $\ell = 2$ and $\ell = 3$, for both axial and polar tidal Love numbers, and for the three boson star models previously discussed.

The behaviour of the tidal Love numbers of boson stars is in qualitative agreement with that of neutron stars. For a given boson star model with a given mass, the magnitude of the polar tidal Love number is larger than that of an axial tidal Love number with the same $\ell$. Furthermore, in the Newtonian regime ($M \to 0$) the tidal Love numbers scale as $k^E_\ell \sim 1/C^{2\ell+1}$, $k^B_\ell \sim -1/C^{2\ell}$, in agreement with the neutron star case.

### 7.2.1 Polar Perturbations

The metric perturbation is given by Eq. (5.9) with $H_1 = 0$, and we write the scalar perturbation as

$$\delta\Phi = \frac{1}{\sqrt{8\pi}}\, \mathrm{e}^{-\mathrm{i}\omega t}\phi_1(r)\, P_\ell(\cos\vartheta)\,. \tag{7.3}$$

The linearized Einstein-Klein-Gordon equations imply $H_0 = H_2 \equiv H$, while $K$ can be written as a function of $H$, $\phi_1$ and the background functions. We are then left with a radial equation for the perturbation function $H$, coupled to the perturbed Klein-Gordon equation for the scalar

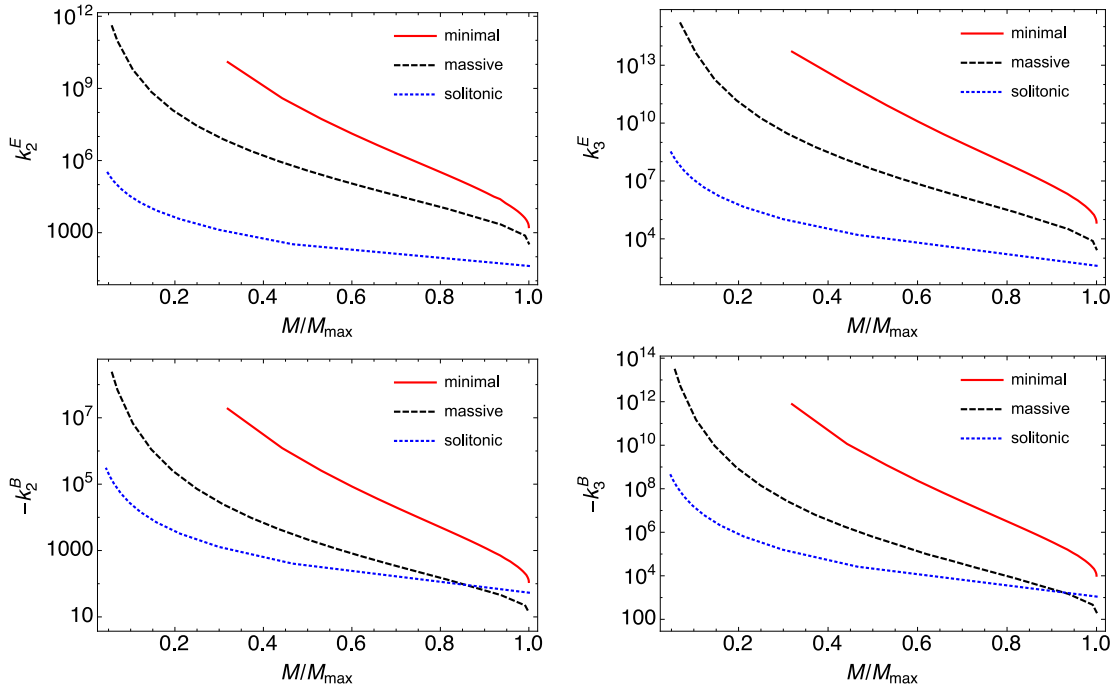


Figure 7.2: Polar (top panels) and axial (bottom panels) tidal Love numbers for minimal, massive and solitonic boson stars. For the massive and solitonic model we have considered $\alpha = 10^4\,\mu^2$ and $\sigma_0 = 0.05$, respectively. With these values, the maximum mass scales approximately as shown in Table 6.1. Left and right panels refers to $\ell = 2$ and $\ell = 3$, respectively. The numerical data are available online. These plots include only stars in the stable branch.

| | Neutron star | Boson star |
|---|---|---|
| $k_2^E$ | 210 | 41 |
| $k_2^B$ | 11 | $-14$ |
| $k_3^E$ | 1300 | 403 |
| $k_3^B$ | 70 | $-212$ |

Table 7.1: Tidal Love numbers of neutron and boson stars. We provide the lowest value for the polar Love numbers found in our exploration of solitonic boson stars, and correspond to $M\mu \approx 3.12553$ (i.e. to a compactness $C \approx 0.18$). In the axial case, the lowest number corresponds to a massive boson star with $M\mu \approx 3.1235$ (i.e. $C \approx 0.16$) and $\alpha = 10^4\,\mu^2$. As a comparison, we also provide the order of magnitude of the tidal Love numbers for static neutron stars with compactness $C \approx 0.2$ (the precise number depends on the neutron-star equation of state).

perturbation $\phi_1$,

$$H'' + \left(\frac{2}{r} - r\omega^2\phi_0^2\,\mathrm{e}^{\Lambda-\Gamma} + \Gamma' - r\phi_0'^2\right) H' + 4\left[\phi_0'' - \left(\frac{\Lambda'+\Gamma'}{2} - \frac{2}{r}\right)\phi_0' - \omega^2\phi_0\,\mathrm{e}^{\Lambda-\Gamma}\right]\phi_1 + \left[\Gamma'^2 - \frac{2\Gamma'}{r} - 6\omega^2\phi_0^2\,\mathrm{e}^{\Lambda-\Gamma} + 2\phi_0'^2 + \frac{\mathrm{e}^{\Lambda}(\ell^2+\ell+2)-2}{r^2}\right] H = 0\,, \tag{7.4}$$

$$\phi_1'' + \left(\frac{2}{r} - r\omega^2\phi_0^2\,\mathrm{e}^{\Lambda-\Gamma} + \Gamma' - r\phi_0'^2\right)\phi_1' + \left[\phi_0'' - \left(\frac{\Lambda'+\Gamma'}{2} - \frac{2}{r}\right)\phi_0' - \omega^2\phi_0\,\mathrm{e}^{\Lambda-\Gamma}\right] H - \left[\frac{\phi_0''}{\phi_0} + \left(\frac{\Gamma'-\Lambda'}{2} + \frac{2}{r}\right)\frac{\phi_0'}{\phi_0} + 4\phi_0'^2 + \frac{\ell(\ell+1)\mathrm{e}^{\Lambda}}{r^2}\right]\phi_1 - \frac{\mathrm{d}\delta V}{\mathrm{d}|\phi^2|}\,\mathrm{e}^{\Lambda}\phi_0 = 0\,. \tag{7.5}$$

We now solve the perturbation system supplied by regular boundary conditions at the origin,[1]

$$H \approx H^{(\ell)} r^{\ell} + \mathcal{O}\left(r^{\ell+2}\right), \quad \phi_1 \approx \phi_1^{(\ell)} r^{\ell} + \mathcal{O}\left(r^{\ell+2}\right). \tag{7.6}$$

Since the system (7.4) and (7.5) is linear, the value of $H^{(\ell)}$ can be set to 1, and the correct value can be recovered *a posteriori*. The value of $\phi_1^{(\ell)}$ is determined using a shooting method by requiring that $\phi_1 \to 0$ as $r \to \infty$.

At distances greater than the boson star effective radius, Eq. (7.4) reduces to

$$H'' + \frac{2(r-M)}{r(r-2M)} H' - \frac{4M^2 - 2\ell(\ell+1)Mr + l(\ell+1)r^2}{r^2(r-2M)^2} H = 0\,, \tag{7.7}$$

which has a general solution in terms of the associate Legendre functions $P_\ell^2$ and $Q_\ell^2$. Using their asymptotic behaviour and comparing with (5.22) we find (for $\ell = 2$ and $\ell = 3$)

$$\begin{aligned} k_2^E = \frac{8}{5}\Big((1-2\mathcal{C})^2[2\mathcal{C}(y-1)-y+2]\Big)\Big(2\mathcal{C}\left[4\mathcal{C}^4(y+1)+2\mathcal{C}^3(3y-3)+2\mathcal{C}^2(13-11y)\right. \\ \left. +\ 3\mathcal{C}(5y-8)-3(y-2)\right]+3(1-2\mathcal{C})^2[2\mathcal{C}(y-1)-y+2]\log(1-2\mathcal{C})\Big)^{-1}, \end{aligned} \tag{7.8}$$

$$\begin{aligned} k_3^E = \frac{6}{7}\Big((1-2\mathcal{C})^2\left[2\mathcal{C}^2(y-1)-3\mathcal{C}(y-2)+y-3\right]\Big)\Big(2\mathcal{C}\left[4\mathcal{C}^5(y+1)\right. \\ \left. +\ 2\mathcal{C}^4(9y-2)-20\mathcal{C}^3(7y-9)+5\mathcal{C}^2(37y-72)-45\mathcal{C}(2y-5)+15(y-3)\right] \\ +\ 15(1-2\mathcal{C})^2\left(2\mathcal{C}^2(y-1)-3\mathcal{C}(y-2)+y-3\right)\log(1-2\mathcal{C})\Big)^{-1}. \end{aligned} \tag{7.9}$$

where $\mathcal{C} = M/R_{\rm ext}$ and $y = rH'/H$ evaluated at $R_{\rm ext}$. The values of $k_\ell^E$ are independent of the extraction radius $R_{\rm ext}$ if the latter is sufficiently large.

### 7.2.2 Axial Perturbations

In this case, the metric perturbation is given by Eq. (5.6), while the scalar perturbation is still (7.3). The perturbed Einstein-Klein-Gordon equations imply $h_1 = \phi_1 = 0$, and we are left with a single radial equation for the perturbed function $h_0$,

$$h_0'' - \frac{\Lambda' + \Gamma'}{2} h_0' + \frac{r(\Lambda' + \Gamma') - (\ell^2 + \ell - 2)e^{\Lambda} - 2}{r^2} h_0 = 0\,, \tag{7.10}$$

that we solve along with regular boundary conditions at the origin,

$$h_0 \approx h_0^{(\ell+1)} r^{\ell+1} + \mathcal{O}\left(r^{\ell+3}\right). \tag{7.11}$$

Notice that the value of $h_0^{(\ell+1)}$ is not given but it can be fixed arbitrarily to 1 and corrected *a posteriori* once the intensity of the tidal field is known.

1. As usual, to increase the accuracy of the numerical integration, we consider a higher-order expansion near the origin which reduce to Eq. (7.6) at first order.

Outside the star, Eq. (7.10) reduces to the simple diffential equation

$$h_0'' + \frac{4M - \ell(\ell+1)r}{r^2(r-2M)}\, h_0 = 0\,, \tag{7.12}$$

whose general solution can be written in terms of the hypergeometric functions. By matching its asymptotic behaviour to (5.23), we find (for $\ell = 2$ and $\ell = 3$)

$$\begin{aligned} k_2^B = \frac{8}{5}\Big(2\mathcal{C}(y-2) - y + 3\Big)\Big(2\mathcal{C}\left[2\mathcal{C}^3(y+1) + 2\mathcal{C}^2 y + 3\mathcal{C}(y-1) - 3y + 9\right] \\ + 3[2\mathcal{C}(y-2) - y + 3]\log(1-2\mathcal{C})\Big)^{-1}\,, \end{aligned} \tag{7.13}$$

$$\begin{aligned} k_3^B = \frac{8}{7}\Big(8\mathcal{C}^2(y-2) - 10\mathcal{C}(y-3) + 3(y-4)\Big)\Big(2\mathcal{C}\left[4\mathcal{C}^4(y+1) + 10\mathcal{C}^3 y\right. \\ + \left. 30\mathcal{C}^2(y-1) - 15\mathcal{C}(7y-18) + 45(y-4)\right] \\ + 15\left[8\mathcal{C}^2(y-2) - 10\mathcal{C}(y-3) + 3(y-4)\right]\log(1-2\mathcal{C})\Big)^{-1}\,, \end{aligned} \tag{7.14}$$

where again $\mathcal{C} = M/R_{\rm ext}$ but now $y = rh_0'/h_0$ evaluated at $R_{\rm ext}$. Even in this case, the values of $k_\ell^B$ are independent of the extraction radius $R_{\rm ext}$ if the latter is sufficiently large.

## 7.3 Models of Microscopic Corrections at the Horizon Scale

Several phenomenological models of quantum black holes introduce a Planck-scale modification near the horizon. In this section, we consider three toy models for microscopic corrections at the horizon scale, namely a wormhole, a Schwarzschild geometry with a perfectly reflective surface near the horizon [341, 342], and a thin-shell gravastar. The exterior spacetime of these models is described by the Schwarzschild metric, and the perturbation formalism is identical to the one developed in Section 5.2. On the other hand, the interior is either vacuum or de Sitter and the junction/boundary conditions at the radius $r_0$ are model dependent. As a result of these properties, the tidal Love numbers of these models can be computed in closed analytical form. The qualitative features are the same and, especially in the black hole limit, do not depend strongly on the details of the models. In Table 7.2 we present explicit formulas for the black hole limit, while (cumbersome) expressions for generic compactness are provided online. The details of the computation are given in Sections 7.3.2 and 7.3.3.

Wormholes. We consider a traversable wormhole built with two copies of the Schwarzschild spacetime, as described in Section 5.5.2. In Fig. 7.3a, we show the wormhole Love numbers as functions of $\xi$ and we notice that they have the opposite sign to those of a neutron star. In the Newtonian limit they behave as $k_\ell^{E,B} \sim -1/C^{2\ell+1}$. Interestingly, the scaling for polar Love numbers agrees with that of neutron stars, but that for the axial Love numbers is different.

Perfect Mirror. Thermodynamical arguments suggest that any horizonless microscopic model of black holes should act as a mirror, at least for long wavelength perturbations. Motivated by this scenario, we consider a Schwarzschild geometry with a perfect mirror at $r = r_0 > 2M$ and impose Dirichlet boundary conditions on the Regge-Wheeler and Zerilli functions, for the axial and polar sectors, respectively. Thus, our strategy is to consider the stationary limit of generically dynamical perturbations (in the Fourier space, where $\omega$ is the frequency of the perturbation) of a Schwarzschild geometry. The tidal Love numbers for this model as functions of $\xi$ are shown in Fig. 7.3b. Close to the black hole limit, the polar and axial Love numbers for the same multipolar order are almost identical and the respective curves overlap as we can see in the inset. Also for this model, all tidal Love numbers are negative and $k_\ell^{E,B} \sim -1/C^{2\ell+1}$ in the Newtonian limit.

Gravastars. For thin-shell gravastars, like those introduced in Section 5.5.3, tidal Love numbers can be computed analytically [345, 346]. We consider a gravastar whose thin shell is described by a fluid with zero energy density and negative pressure. The Newtonian regime of a gravastar is peculiar due to the de Sitter interior and its tidal Love numbers scale as $k_\ell^{E,B} \sim -1/C^{2\ell}$. This scaling of the polar tidal Love numbers is different from that of an ordinary neutron star and the other models of microscopic corrections at the horizon scale, whereas the scaling of the axial tidal Love numbers is the same as that for wormholes and a perfect mirror model. The behaviour of the tidal Love numbers as functions of $\xi$ is shown in Fig. 7.3c. Also in this case, the polar and axial Love numbers are negative. Similar to the perfectly reflective mirror case, close to the black hole limit, the polar and axial Love numbers for the same multipolar order are almost identical and the respective curves overlap as we can see in the inset.

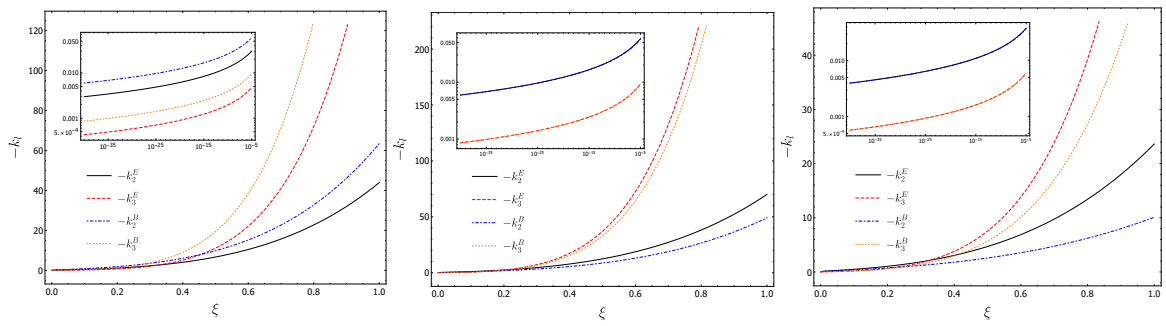


(a) Wormhole (b) Perfect Mirror (c) Gravastar

Figure 7.3: The $\ell = 2,\ 3$ polar and axial tidal Love numbers for (a) a wormhole constructed by patching two Schwarzschild spacetimes at the throat radius $r_0 > 2M$; (b) a toy model of Schwarzschild metric with a perfectly reflective surface at $r_0 > 2M$; (c) a thin-shell gravastar with zero energy density. The tidal Love numbers are negative and all vanish in the black hole limit, $\xi := r_0/(2M) - 1 \to 0$.

### 7.3.1 On the Universal Black Hole Limit

It is remarkable that the models described above display a very similar behaviour in the black hole limit, as summarised in Table 7.2. Indeed, although all tidal Love numbers vanish in this limit, they have a logarithmic dependence.

| | Wormhole | Perfect Mirror | Gravastar |
|---|---|---|---|
| $k_2^E$ | $\frac{4}{5(8+3\log\xi)}$ | $\frac{8}{5(7+3\log\xi)}$ | $\frac{16}{5(23-6\log 2+9\log\xi)}$ |
| | $-3\times10^{-3}$ | $-6\times10^{-3}$ | $-4\times10^{-3}$ |
| $k_2^B$ | $\frac{16}{5(31+12\log\xi)}$ | $\frac{32}{5(25+12\log\xi)}$ | $\frac{32}{5(43-12\log 2+18\log\xi)}$ |
| | $-6\times10^{-3}$ | $-6\times10^{-3}$ | $-4\times10^{-3}$ |
| $k_3^E$ | $\frac{8}{105(7+2\log\xi)}$ | $\frac{8}{35(10+3\log\xi)}$ | $\frac{16}{35(31-6\log 2+9\log\xi)}$ |
| | $-4\times10^{-4}$ | $-9\times10^{-4}$ | $-6\times10^{-4}$ |
| $k_3^B$ | $\frac{16}{7(209+60\log\xi)}$ | $\frac{32}{7(197+60\log\xi)}$ | $\frac{32}{7(307-60\log 2+90\log\xi)}$ |
| | $-9\times10^{-4}$ | $-9\times10^{-4}$ | $-6\times10^{-4}$ |

Table 7.2: Tidal Love numbers of some exotic compact objects. We provide expressions for very compact configurations where the surface $r_0$ sits at $r_0 \sim 2M$ and is parametrized by $\xi := r_0/(2M) - 1$ (modulo subleading terms of $\mathcal{O}\left(\xi/(\log\xi)^2\right)$), and its numerical value when $r_0 - 2M \sim l_P \approx 1.6\times10^{-33}$ cm. This value is roughly valid in the entire mass range $M \in [1, 100]\, M_\odot$ due to the mild logarithmic dependence. All Love numbers vanish in the black hole limit, $\xi \to 0$.

Due to this mild dependence, the tidal Love numbers are not extremely small, as one would have naively expected if the scaling with $\xi$ were polynomial. Indeed, in the Planckian case ($r_0 - 2M \sim l_P \approx 1.6\times10^{-33}$ cm) the order of magnitude of the tidal Love numbers is the same for all models, and it is only five orders of magnitude smaller than those a typical neutron star. This logarithmic dependence implies that the deviations from zero are relatively large even when the throat is located just a Planck length away from the would-be horizon.

On the light of our results, it is natural to conjecture that this logarithmic dependence is a generic feature of ultracompact exotic objects, and will hold true for any exotic compact object whose exterior spacetime is arbitrarily close to that of a black hole in the $r_0 \to 2M$ limit. These putative deviations from the 'zero-Love' rule of black holes in general relativity might be within reach future detections.

### 7.3.2 Polar Perturbations

In the exterior spacetime, Einstein's equations for static polar-type perturbations of the Schwarzschild metric reduce to Eq. (7.7), whose general solution for any $\ell$ is

$$H^{\rm ext} = C_1\, P^2_\ell(r/M-1) + C_2\, Q^2_\ell(r/M-1)\,, \tag{7.15}$$

where $C_1$ and $C_2$ are two integration constants. The term proportional to $C_1$ diverges at large distances and is identified with the external tidal field, whereas the term proportional to $C_2$ is the body response. The other metric function $K$ is

$$K = \left(1+\frac{4M(r-M)}{(\ell^2+\ell-2)\,r(r-2M)}\right)H - \frac{2M}{\ell^2+\ell-2}\,H'\,. \tag{7.16}$$

The interior spacetime depends on the model under consideration. In the wormhole model, we consider that the other universe is an exact copy of exterior metric, so that polar perturbations are described by Eq. (7.15) with two independent constants, $C_3$ and $C_4$. On the 'other side' of the wormhole, we require that there are no tidal fields, i.e. $C_3 = 0$.

In the perfect mirror model, perturbations do not penetrate the surface and the interior solution is irrelevant.

In the gravastar model the interior solution for any $\ell$ which is regular at the origin reads

$$H^{\rm int} \sim \frac{r^\ell}{3-\Lambda r^2}\,{}_2F_1\left(\frac{\ell-1}{2},\frac{\ell}{2};\ell+\frac{3}{2};\frac{2Cr^2}{r_0^2}\right). \tag{7.17}$$

In the wormhole and the gravastar cases, the interior and the exterior solutions are described by three independent constants, whereas the perfect mirror model is described by two constants. Since the problem is linear, an overall amplitude is irrelevant so we need to impose two junction conditions at $r = r_0$ in the wormhole and gravastar cases, and one boundary condition at $r = r_0$ in the perfect mirror case.

In the former cases, we can impose the Darmois-Israel junction conditions [366], which relate the discontinuity of the extrinsic curvature across the radius with the properties of a thin shell of matter located at $r = r_0$. By adapting the formalism developed in Ref. [347], we find that $[[K]] = 0$ and $[[{\rm d}K/{\rm d}r_*]] = -8\pi\sqrt{1-2M/r_0}\,\delta\Sigma$, where $\delta\Sigma$ is the perturbation of the surface energy density of the thin shell. The symbol '$[[\,\cdot\,]]$' denotes the 'jump' of a given quantity across the spherical shell, i.e. $[[A]] \equiv \lim_{\epsilon\to 0} A(r\to r_0+\epsilon) - A(r\to r_0-\epsilon)$. For simplicity, we assume that the thin-shell matter is stiff, so that $\delta\Sigma \sim 0$. Therefore, in the polar sector we impose $[[K]] = 0$ and $[[{\rm d}K/{\rm d}r_*]] = 0$. These two conditions completely specify the matching between the interior and the exterior solution in the wormhole and gravastar cases.

In the perfect mirror case, we will impose a $Z_2$ symmetry on the surface and, therefore, the wavefunction vanishes at $r = r_0$. In the static limit, one can solve analitically the Zerilli equation and

then reconstruct the metric function $H_0$ thorugh

$$H = \frac{\lambda r^2 - 3M^2 - 3\lambda M r}{r(3M+\lambda r)}\,\psi_{\rm Z}' + \frac{9M^3 + 9\lambda M^2 r + 3\lambda^2 M r^2 + \lambda^2(\lambda+1)r^3}{r^2(3M+\lambda r)^2}\,\psi_{\rm Z}\,, \tag{7.18}$$

where $\lambda = (\ell-1)(\ell+2)/2$. By imposing the Dirichlet boundary condition $\psi_{\rm Z} = 0$, the ratio $C_1/C_2$ in Eq. (7.15) is completely specified.

Finally, once the perturbation equations are completely specified (modulo an overall amplitude) through the junction/boundary conditions, it is straightforward to compare the analytical expression for $H_0$ at large distance with Eq. (5.22), extract the multipole moments and the tidal field amplitudes, and finally compute the polar tidal Love numbers by using Eq. (5.19).

### 7.3.3 Axial Perturbations

In the exterior spacetime, Einstein's equations for static axial perturbations of the Schwarzschild metric reduce to Eq. (7.12), whose general solution for any $\ell$ is

$$h_0^{\rm ext} = C_1\, r^2\, {}_2F_1\left(1-\ell,\ell+2;4;\frac{r}{2M}\right) + C_2\, G^{2,0}_{2,2}\left(\frac{r}{2M}\,\middle|\,\begin{matrix}1-\ell,\ell+2\\ -1,2\end{matrix}\right), \tag{7.19}$$

where $G^{2,0}_{2,2}$ is the Meijer function and ${}_2F_1$ is one of the hypergeometric functions. The terms proportional to $C_1$ and $C_2$ are identified with the external tidal field and with the body response, respectively. The above solution reduces to simply expressions for integer values of $\ell$, which can be written in terms of polynomial and logarithmic functions.

Also in the axial case, the interior spacetime is model dependent. In the wormhole case we consider the same solution as in Eq. (7.19) but with zero tidal field, namely $C_1 = 0$.

In the gravastar case, the interior solution which is regular for any $\ell$ near the origin reads

$$h_0^{\rm int} \sim r^{\ell+1}\, {}_2F_1\left(\frac{\ell-1}{2},\frac{\ell+2}{2};\ell+\frac{3}{2};\frac{2Cr^2}{r_0^2}\right). \tag{7.20}$$

As in the polar case, the interior solution of the perfect mirror model is irrelevant to the purposes of computing the tidal Love numbers.

The junction conditions for axial perturbations are easier because they do not couple to the matter of a putative thin shell. Therefore, regularity of the axial perturbations across the shell imposes that $h_0$ and its derivative with respect to $r_*$ be smooth. Thus, for the wormhole and gravastar cases in the axial sector we impose $[[h_0]] = 0$ and $[[{\rm d}h_0/{\rm d}r_*]] = 0$.

For the perfect mirror model, we impose a Dirichlet condition on the Regge-Wheeler function evaluated at $r = r_0$. This function is defined through[2]

$$h_0 = \frac{\mathrm{d}(r\psi_{\rm RW})}{\mathrm{d}r_*}\,, \qquad h_1 = \frac{-\mathrm{i}\omega r}{1-2M/r}\psi_{\rm RW}\,, \tag{7.21}$$

and satisfies the Regge-Wheeler equation (5.7) which can be solved analytically in the static limit. Again, the ratio of the two integration constants in Eq. (7.19) is fixed by imposing $\psi_{\rm RW} = 0$.

After that the perturbations are fully specified through the junction/boundary conditions, the axial tidal Love numbers can be computed by comparing the large-distance behaviour of $h_0$ with Eq. (5.23), extracting the multipole moments, and finally using the definition (5.19).

## 7.4 Detectability

To estimate the detectability of the tidal Love numbers through gravitational wave observations, we use a Fisher matrix approach, given parametrized models of the waveforms, and assuming detector noise of known distribution [367].

The tidal Love numbers enter the phase of the gravitational-wave signal as a fifth-order post-Newtonian (5PN) correction. The contribution due to tidal effects $\psi_{\rm T}$ adds linearly to the point-particle contribution $\psi_{\rm PP}$,

$$\tilde{h}(f) = \mathcal{A}(f)\exp\left[\mathrm{i}\left(\psi_{\rm PP}+\psi_{\rm T}\right)\right], \tag{7.22}$$

and it depends on the polar $\ell = 2$ tidal Love numbers through the constant [248, 328]

$$\lambda := \frac{2}{3}\,M^5 k_2^E\,. \tag{7.23}$$

The contribution of higher multipole and axial Love numbers is subleading.

In our analysis, we will use the so-called TaylorF2 approximant of the gravitational-wave template in the frequency domain [368], which is 3.5PN accurate in the point-particle phase and 2PN accurate in the tidal term [333, 369].

For binary systems for which $\lambda_{i=1,2} \neq 0$, finite-size effects are described in terms of the average deformability,

$$\Lambda = \frac{1}{26}\left[(1+12q)\lambda_1 + \frac{q+12}{q}\lambda_2\right], \tag{7.24}$$

where $q := m_1/m_2 \geqslant 1$ is the mass ratio. For non-spinning objects, the waveform depends on 6 parameters i.e. the amplitude $\mathcal{A}$, the phase $\phi_c$ and time $t_c$ at the coalescence, the chirp mass

2. Note that our definition differs from the standard one by a factor $\omega$, which has been included so that $h_1 \to 0$ in the static limit, whereas $h_0$ remains finite, as expected.

$\mathcal{M} = \nu^{3/5}(m_1 + m_2)$, the symmetric mass ratio $\nu = m_1 m_2/(m_1 + m_2)^2$ and the average tidal deformability $\Lambda$ defined in Eq. (7.24). Nonetheless, the amplitude is completely uncorrelated with the other variables, and therefore we will restrict our analysis by performing derivatives only with respect to the remaining parameters, leading to a $5 \times 5$ Fisher matrix.

The detector properties are encoded in the noise spectral density $S_h(f)$. We perform the analysis both for terrestrial and space interferometers. For the Earth-based detectors, we consider (i) AdLIGO with its anticipated design sensitivity curve `ZERO_DET_high_P` [370] and (ii) the Einstein telescope (ET) design configuration, with noise described by the analytic fit provided in Ref. [371]. As space-based detector, we consider the most optimistic LISA configuration, namely the `N2A5` model defined in Ref. [372], with a $5 \times 10^6$ km arm-length and an observing time of $T_{\rm obs} = 5$ yr.

To compute the errors on the tidal deformability, we numerically integrate the Fisher information matrix within the frequency range $[f_{\rm min}, f_{\rm max}]$, where $f_{\rm min}^{\rm AdLIGO} = 20$ Hz, $f_{\rm min}^{\rm ET} = 1$ Hz, and $f_{\rm min}^{\rm LISA} = \max[10^{-5}, 4.149 \times 10^{-5}(10^{-6}\mathcal{M})^{-5/8} T_{\rm obs}^{-3/8}]$ Hz [373]. For the upper frequency we choose $f_{\rm max}^{\rm AdLIGO} = (6^{3/2}m\pi)^{-1}$, while for LISA $f_{\rm max}^{\rm LISA} = \min[1\,{\rm Hz}, (6^{3/2}m\pi)^{-1}]$, being $m = m_1 + m_2$ the total mass of the system.

### 7.4.1 Model-Independent Tests with Gravitational Waves

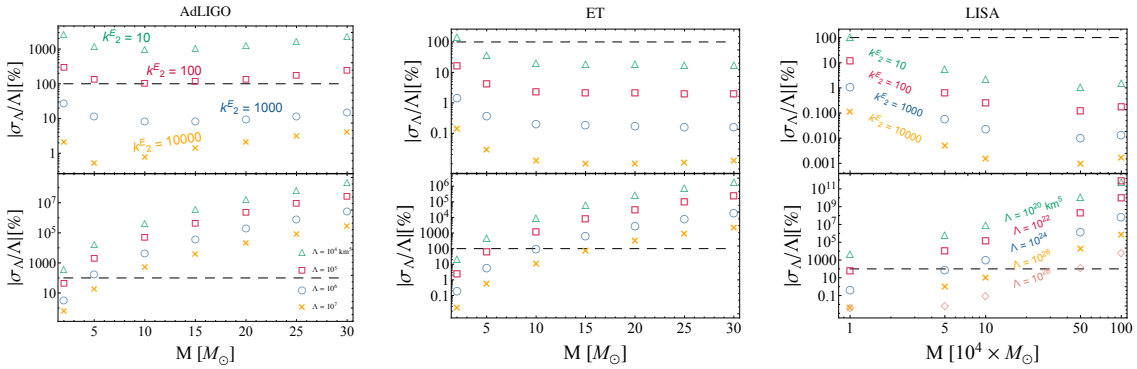


Figure 7.4: Relative percentage errors on the average tidal deformability $\Lambda$ for equal-mass binaries at 100 Mpc (for AdLIGO and ET, left and middle panel, respectively) and at 500 Mpc (for LISA, right panel) as functions of the mass of the single object and for different values of the tidal Love number $k_2^E$ (top panels) and of $\Lambda$ (bottom panels) of the two objects. The horizontal dashed line identifies the upper bound $\sigma_\Lambda/\Lambda = 1$.

Before discussing the detectability for different families of exotic compact objects, it is instructive to analyze the impact of the tidal Love numbers on the gravitational wave signal in a more general framework. Figure 7.4 shows the relative uncertainty $\sigma_\Lambda/\Lambda$ for equal-mass binaries at $d = 100$ Mpc (for AdLIGO and ET) and at $d = 500$ Mpc (for LISA), as a function of the mass of the objects and for different values of the tidal Love numbers $k_2^E$ (top panels) and of the average tidal deformability $\Lambda$ (bottom panels). In the panels of Fig. 7.4, the dashed horizontal line denotes the upper bound $\sigma_\Lambda = \Lambda$. Therefore, each point above that line is indistinguishable from a black hole-black hole

binary in general relativity ($\Lambda = k_2^E = 0$) within the errors, whereas a measurement of the tidal Love numbers for systems which lie below the threshold line would be incompatible to zero and, therefore, the exotic compact objects can be distinguished from black holes in this case.

It is worth remarking that — motivated by the prospect of measuring the tidal Love numbers of neutron stars through gravitational wave detections — several efforts have been devoted to investigate the detectability of $\Lambda$ for objects with $M \lesssim 2M_\odot$. The latter represents the mass range in which terrestrial interferometers will provide new information on matter at supranuclear densities from neutron-star binaries. On the other hand, our results shown in Fig. 7.4 do not assume any specific model and extend the analysis of the detectability of the tidal Love numbers to a regime unexplored so far, where more massive exotic compact objects can contribute to the gravitational wave signal through finite-size effects. Likewise, to the best of our knowledge, this work presents the first analysis on the detectability of tidal effects with LISA.

From the bottom panels of Fig. 7.4 we note that, for a fixed $\Lambda$, the detectability is favored for low-mass systems, as the tidal phase scales with the inverse of the total mass $\psi_{\rm T} \propto \Lambda\, m^{-10/3}(1+q)^2/q$. Moreover, for $2M_\odot \lesssim M \lesssim 5M_\odot$, AdLIGO will constrain the tidal Love numbers for small compactness only (i.e. for large $\Lambda$). This picture improves for ET, which leads to an upper bound $\sigma_\Lambda/\Lambda = 1$ up to $M \simeq 15M_\odot$. Therefore, as far as terrestrial interferometers are considered, the high-compactness regime for exotic compact objects seems to be available only for the third generation of detectors. This result is also evident from the top panels of the left and middle plots in Fig. 7.4, which show that AdLIGO will not be able to set any significant constraint below $k_2^E \simeq 100$, regardless the exotic compact object mass.

On the other hand, space interferometers open a completely new window onto finite-size effects. The top-right panel of Fig. 7.4 shows that LISA is capable to bound the Love numbers with a relative accuracy $\sigma_\Lambda/\Lambda \lesssim 10\%$ in almost the entire mass range $M \in [10^4, 10^6]\, M_\odot$. In other words, binary systems made of intermediate-mass compact objects will provide interesting constraints on the tidal Love numbers, with $k_2^E \simeq 10$ and above, and therefore also on the nature of these objects. The exquisite precision of LISA can be traced back on the dependence of the tidal deformability (which is the physical parameter entering the waveform) on the exotic compact object mass, i.e. $\Lambda \propto M^5$, which amplifies the tidal effect on the gravitational wave signal. This is confirmed by the right-bottom panel of Fig. 7.4, where the upper bound on $\Lambda = 10^{24}\,\mathrm{km}^5$ for $M = 5 \times 10^4 M_\odot$ corresponds to $k_2^E \sim 0.7$.

### 7.4.2 Detectability of Exotic Compact Objects

We discuss the detectability of the exotic compact objects investigated in the previous sections. As a general setup, we consider equal-mass binaries at distances $d = 100\,\mathrm{Mpc}$ with $M \in [2, 30] M_\odot$ for AdLIGO/ET, and at $d = 500\,\mathrm{Mpc}$ with $M \in [10^4, 10^6] M_\odot$ for LISA. The gravitational wave signal is proportional to $1/d$, and therefore the error on $\Lambda$ scales linearly with the distance.

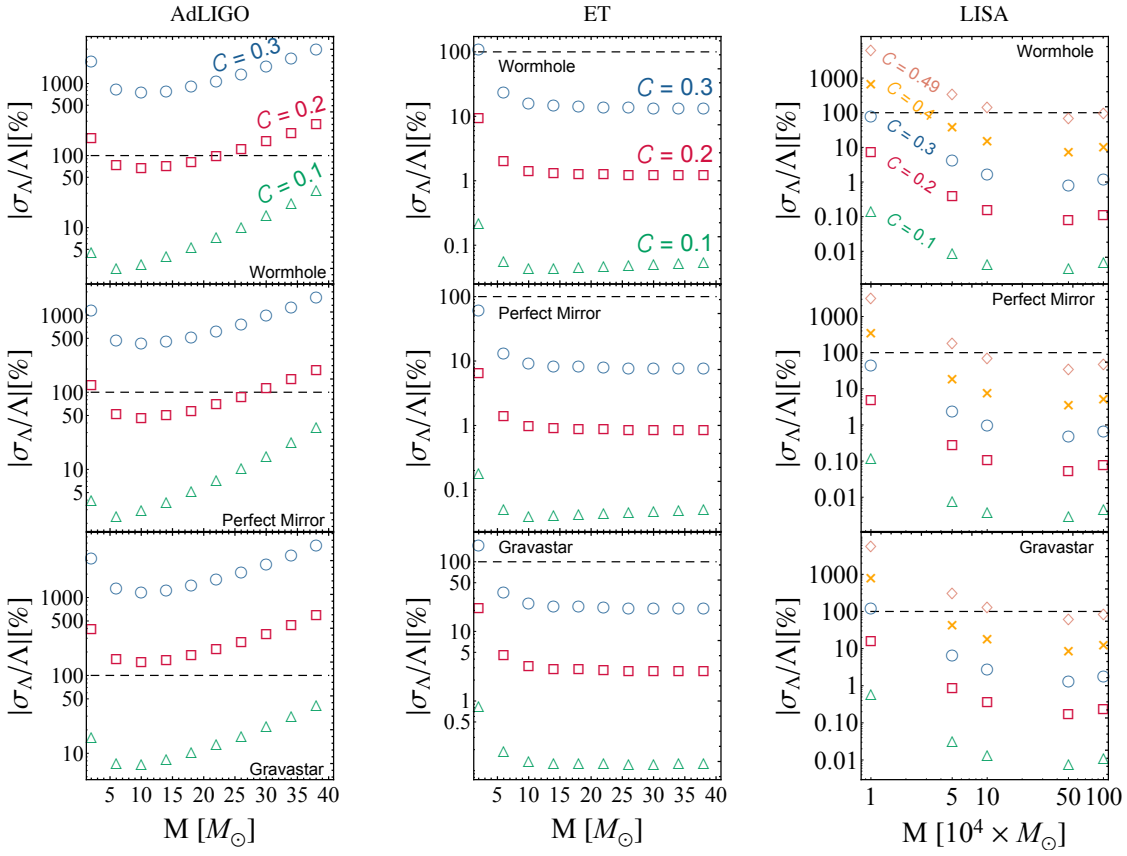


Figure 7.5: Relative percentage errors on the tidal deformability for binaries observed by AdLIGO (left panels), ET (middle panels), and LISA (right panels), as functions of the exotic compact object mass and for different values of the compactness. For terrestrial interferometers we consider prototype binaries at $d = 100$ Mpc, while for LISA we set the source at $d = 500$ Mpc. Top, middle and bottom panels refer to wormholes, perfect-mirror models, and gravastars, respectively.

In Fig. 7.5 we show the percentage relative errors $\sigma_\Lambda/\Lambda$ for models of wormholes, perfect mirrors and gravastars, as a function of the mass of the object and for different values of its compactness. Some qualitative results are independent of the nature of the exotic compact object: the left panels confirm that AdLIGO would be able to constrain the tidal deformability only for small values of the compactness, namely $C \lesssim 0.2$. As the errors scale with the distance, an upper bound $\sigma_\Lambda/\Lambda \sim 1$ for $C = 0.3$, would require a source located at a distance $\sim 10$ Mpc.

Furthermore, the relative errors decrease for larger masses, reach a minimum, and then increase again. This behavior can be explained by looking at the functional form of Eq. (7.23). For a fixed compactness (i.e. for fixed $k_2^E$), the average tidal deformability grows with the exotic compact object mass, thus making the tidal part of the gravitational waveform easier to be detected. However, since the template is truncated at the last stable orbit, $f_{\rm max} \sim m^{-1}$, increasing the mass also reduces the number of effective cycles spent into the detector's bandwidth. This is particular penalizing for tidal effects, which enter the gravitational wave signal as high-PN/high-frequency corrections.

It is worth noticing that a network of advanced interferometers would improve these results, even though it will not drastically change the upper bound on the compactness of these objects. Indeed, if we consider that the experiments are all independent, the Fisher matrices computed for each detector simply sum up, and the overall error on $\Lambda$ is given by the inverse of the total $\Gamma_{ab}$. Assuming five detectors with the same sensitivity of AdLIGO, the relative error $\sigma_\Lambda$ would decrease roughly by a factor $\sqrt{5}$ which, from our results in Fig. 7.5, is still not enough to constrain objects much more compact than $C \sim 0.2$.

Third-generation ground-based detectors, like ET (middle panels of Fig. 7.5), hold more promising results. In this case, the relative errors $\sigma_\Lambda/\Lambda$ decrease roughly by one order of magnitude relative to AdLIGO. A gravitational wave detection of an exotic compact object binary at $d = 100\,\mathrm{Mpc}$ would allow to distinguish the system from a black hole-black hole binary (by the sole detection of the tidal Love numbers) up to compactness $C \sim 0.3$.

This scenario improves drastically for space-based detectors such as LISA (right panels of Fig. 7.5). Within the considered mass range, tidal effects may be measured for exotic compact objects with $C \lesssim 0.3$ up to 1% of accuracy. Moreover, LISA will be able to put strong constraints even for more compact objects: for $M \gtrsim 10^5 M_\odot$ it would be possible to set an upper bound $\sigma_\Lambda/\Lambda = 1$ in the entire parameter space. As discussed in the previous section, these results rely on the magnitude of the exotic compact object mass, which strengthens the effect of tidal interactions in the waveform. The right panels of Fig. 7.5 show indeed that for all the considered exotic compact object models, LISA leads the analysis to nearly explore the black hole limit $C \to 1/2$.

It is worth remarking that, as finite-size effects develop during the late inspiral, eventually leading to complex phenomena like the excitations of modes [245], a more accurate template which extends the frequency domain of the waveform up to the merger phase, would improve this analysis.

### 7.4.3 Detectability of Boson Stars

For each model of boson stars, we focus on the most compact configuration in the stable branch. In Fig. 7.6, we show the results of the Fisher matrix analysis for an equal-mass boson star-boson star binary as a function of the boson star mass, obtained by considering the most compact configuration and by varying the parameters of the potential. Since, for each model, we consider the maximum compactness allowed in the non-spinning case, our results can be seen as conservative, since less compact configurations are easier to discriminate.

The forecast for detecting boson star-boson star binaries by using gravitational wave tidal effects are more promising than for other exotic compact objects, because the compactness of boson stars is at most $C \lesssim 0.3$ and, in turn, their tidal Love numbers are larger. AdLIGO will be able to discriminate between minimal boson stars and black holes in all the mass range. These errors worsen for massive objects. However, for all the models analyzed, second-generation detectors will set a strong upper bound on the tidal deformability, unless solitonic boson star are considered. Results

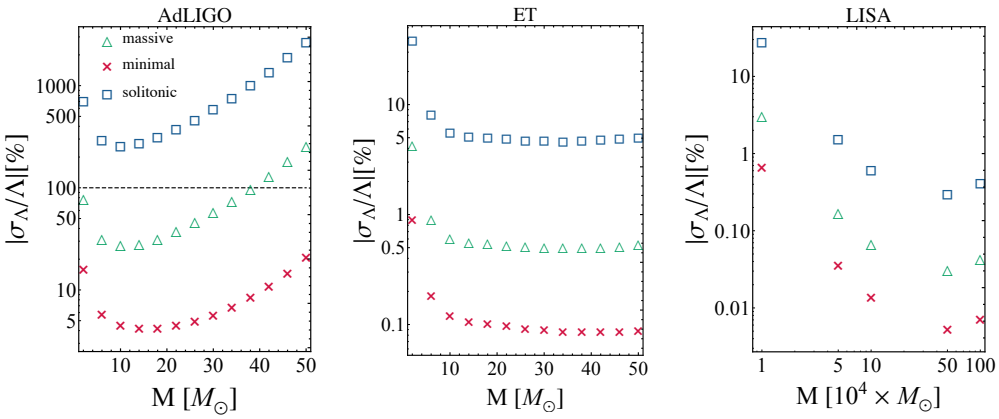


Figure 7.6: Relative percentage errors on the average tidal deformability $\Lambda$ for boson star-boson star binaries observed by AdLIGO (left panel), the Einstein Telescope (ET) (middle panel), and LISA (right panel), as a function of the boson star mass and for different boson star models considered in this chapter. For each model we considered the most compact configuration in the stable branch. For terrestrial interferometers we assume a prototype binary at $d = 100\,\mathrm{Mpc}$, while for LISA the source is located at $d = 500\,\mathrm{Mpc}$. The horizontal dashed line identifies the upper bound $\sigma_\Lambda/\Lambda = 1$. Roughly speaking, a measurement of the tidal Love numbers for systems which lie below the threshold line would be incompatible with zero and, therefore, the corresponding boson stars can be distinguished from black holes. Here $\Lambda$ is given by Eq. (7.24), the two inspiralling objects have the same mass, and $\sigma_\Lambda/\Lambda \sim \sigma_{k_2^E}/k_2^E$.

in Fig. 7.6 suggest that models of minimal and massive boson stars can be distinguished from black holes through AdLIGO detections, whereas discriminating between black holes and more compact boson stars such as solitonic models will require future detectors like ET. Again, the uncertainties significantly decrease with LISA, especially in the high-mass regime, where relative errors are below 1% for every binary configuration with $M \gtrsim 5 \times 10^4 M_\odot$.

## 7.5 Summary and Conclusions

In this chapter we have used the theory of tidal deformations to explore fundamental questions about the nature of event horizons, the existence of exotic compact objects and the behaviour of gravity in the strong-field regime.

In particular, we have shown that within the framework of general relativity, the tidal Love numbers of exotic compact objects are generically non-zero. Some exotic compact objects can be as compact as a black hole, and in this limit, all tidal Love numbers vanish *logarithmically*. This result holds for all models of exotic compact object we have considered. It is therefore natural to conjecture that this logarithmic dependence is a generic feature of ultra-compact exotic objects.

We have explored the detectability of these tidal effects in some details, both for ground- and for space-based detectors. Ground-based detectors such as AdLIGO and ET can constrain exotic compact object models with compactness $C \lesssim 0.2$ and $C \lesssim 0.3$, respectively, whereas a LISA-like

mission can constrain supermassive exotic compact objects up to $C \lesssim 0.49$. Interestingly, AdLIGO can set stringent constraints on various boson star models, and both ET and LISA will be able to discriminate a boson star binary from a black hole binary just by measuring the tidal Love numbers of the binary components.

The prospects for testing deviations from general relativity are less promising. Results not included in this chapter indicate that the tidal Love numbers of Reissner-Nordström and uncharged static Brans-Dicke black holes vanish, as in general relativity. However, the tidal Love numbers of black holes are non-zero in other interesting extensions. In particular, the axial tidal Love numbers of a Schwarzschild black hole in Chern-Simons gravity and the tidal Love numbers of static black holes in Einstein-dilaton-Gauss-Bonnet gravity. While the tidal Love numbers of black holes beyond general relativity are different from zero, their effect in the gravitational wave signal is small and typically subleading relative to other, point-particle, beyond general relativity effects such as dipolar emission. Nevertheless, the non-vanishing of the black hole tidal Love numbers remains a piece of evidence of deviations from general relativity and its phenomenological implications are under investigation.

# Chapter 8

# The Ringdown of a Black Hole Mimicker

We investigate the gravitational radiation of a particle falling into a black hole mimicker, in particular a traversable wormhole. We show that if the mimicker is compact enough, the initial ringdown signal is almost indistinguishable from that of a black hole with the same mass. This result suggests that the initial ringdown signal is not the conclusive proof for event horizons. Each very compact object will display a similar ringdown followed by the proper modes of vibration of the object itself, i.e. its quasi-normal modes.

Units: $c = G = 1$.

This chapter is based on: V. Cardoso, E.F, and P. Pani. 'Is the gravitational-wave ringdown a probe of the event horizon?' *Phys. Rev. Lett.* 116 (2016), 171101. arXiv: 1602.07309. Erratum: *ibid.* 117 (2016), 089902.

## 8.1 Introduction

The gravitational-wave detection of the events GW150914 and GW151226 have been interpreted as the merger of two black holes and the product of the coalescence is another black hole [374]. Far from claiming that this interpretation is not correct and that the product of the merger might be something more exotic, in this chapter, we would like to answer a matter of principle: is there any evidence for event horizons in the detected signals?

With a few rare exceptions [269, 280, 375], the ringdown waveform is commonly associated to the quasi-normal modes of the final object which, in turn, are closely related to the peculiar boundary conditions required at the event horizon, namely the absence of outgoing waves — see Section 5.3. That being the case, the gravitational wave ringdown signal provides a way to prove the existence of an event horizon in dark, compact objects. Here, we stress that, in general, the ringdown modes do *not* coincide with the quasi-normal mode frequencies.

If the final object does not possess a horizon, the boundary conditions change completely, thus drastically affecting the quasi-normal mode structure. On the other hand, the ringdown waves of the distorted compact object are closely related to the null, unstable, geodesics in the spacetime [236, 376–379], their frequency and damping time being associated with the orbital frequency and with the instability timescale of circular null geodesics, respectively. Thus, in principle, the ringdown phase should not depend on the presence of a horizon as long as the final object has a light ring.

If the final object is a black hole, its quasi-normal modes incidentally also describe the ringdown phase, as the ingoing condition at the horizon simply takes the ringdown waves and 'carries' them

inside the black hole.

To sum up, if there is no horizon or the horizon is replaced by a surface of different nature (as, e.g. in the firewall [40] or in the gravastar proposals) the relaxation of the corresponding horizonless compact object should then consist on the usual light-ring ringdown modes (which are no longer quasi-normal modes), followed by the proper modes of vibration of the object itself. The former are insensitive to the boundary conditions and similar to the black hole case, whereas the latter, defined by different boundary conditions, can differ dramatically from their black hole counterpart and are usually identified as quasi-normal modes.

## 8.2 Setup

To the best of our knowledge, the above picture has never been verified in the context of gravitational wave tests of an event horizon. Here we perform such analysis by considering the ringdown signal and the quasi-normal modes associated with a horizonless compact object with a light ring. For definiteness, we focus on the gravitational radiation emitted by a point particle in radial motion towards a traversable wormhole — see Fig. 8.1 for an illustration. The main qualitative features of our analysis are independent of the specific horizonless object and apply also to spherical shells of matter, gravastars, compact boson stars and others [262, 269, 380, 381].

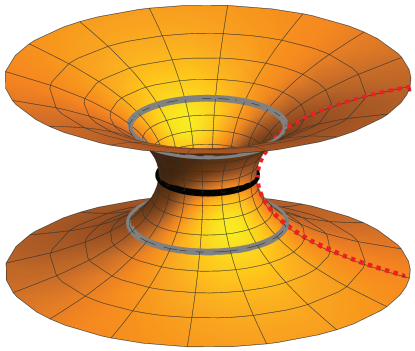

Figure 8.1: Illustration of a dynamical process involving a compact horizonless object. A point particle plunges radially (red dashed curve) in a wormhole spacetime, and emerges in another 'universe'. The black curve denotes the wormhole's throat, the two grey curves are the light rings. When the particle crosses each of these curves, it excites characteristic modes which are trapped between the light-ring potential wells, see Figs. 8.3 and 8.4.

The specific solution is obtained by identifying two Schwarzschild metrics with the same mass $M$ at the throat $r = r_0 > 2M$, as described in Section 5.5.2. In Schwarzschild coordinates, the two metrics are identical and described by

$$\mathrm{d}s^2 = -f(r)\,\mathrm{d}t^2 + \frac{\mathrm{d}r^2}{f(r)} + r^2\,\mathrm{d}\Omega^2\,, \qquad f(r) = 1 - \frac{2M}{r}\,. \tag{8.1}$$

Because Schwarzschild's coordinates do not extend to $r < 2M$, we use the tortoise coordinate $\mathrm{d}r/\mathrm{d}r_* = \pm f$, where henceforth the upper and lower signs refer to the two different universes connected at the throat. Without loss of generality we assume $r_*(r_0) = 0$, so that one domain is $r_* > 0$ whereas the other domain is $r_* < 0$.

The four-velocity of a particle with mass $\mu_p \ll M$ and conserved energy $E$ in this spacetime reads $u_p^\mu := \mathrm{d}x_p^\mu/\mathrm{d}\tau = \left(E/f, \mp\sqrt{E^2 - f}, 0, 0\right)$, where $\tau$ is the proper time, and the coordinate time $t_p$ is governed by

$$t_p'(r) = \mp \frac{E}{f\sqrt{E^2 - f}} \,. \tag{8.2}$$

A particle falling from infinity reaches the throat in finite time (we set $t_p(r_0) = 0$) and emerges in the other universe. In the point-particle limit, Einstein's equations sourced by the stress-energy tensor (5.15) reduce to a pair of Zerilli equations,

$$\frac{\mathrm{d}^2\psi_\ell(\omega, r)}{\mathrm{d}r_*^2} + \left(\omega^2 - V_{\rm Z}(r)\right)\psi_\ell(\omega, r) = S_\ell \,, \tag{8.3}$$

with the effective potential $V_{\rm Z}$ given by Eq. (5.11) and

$$S_\ell = \frac{2\sqrt{2}\,\mu_p E(9 + 8\lambda)^{1/4}\,\mathrm{e}^{\mathrm{i}\omega t_p}}{f(3M + r\lambda)^2\omega t_p'} \left[f^2 t_p' \left(2\mathrm{i}\lambda + (3M + r\lambda)\omega t_p'\right) - (3M + r\lambda)\omega\right] , \tag{8.4}$$

where $\lambda = (\ell - 1)(\ell + 2)/2$ and $\ell \geqslant 2$ is the index of the spherical-harmonic expansion. The source term is different in the two universes due to the presence of $t_p(r)$. The time-domain wavefunction can be recovered via

$$\hat{\psi}_\ell(t, r) = \frac{1}{\sqrt{2\pi}} \int \mathrm{d}\omega\, \mathrm{e}^{-\mathrm{i}\omega t}\psi_\ell(\omega, r) \,. \tag{8.5}$$

With the master equation in both universes at hand, we only miss the junction conditions for $\psi_\ell$ at the throat. The latter depend on the properties of the matter confined in the thin shell [347]. For simplicity, here we assume that the microscopic properties of the shell are such that $\psi_\ell$ and $\mathrm{d}\psi_\ell/\mathrm{d}r_*$ are continuous at $r_* = 0$. This assumption is not crucial and can be modified without changing our qualitative results.

Finally, the energy flux emitted in gravitational waves reads [232]

$$\frac{\mathrm{d}E}{\mathrm{d}\omega} = \frac{1}{32\pi} \sum_{\ell \geqslant 2} \frac{(\ell + 2)!}{(\ell - 2)!}\, \omega^2 |\psi_\ell(\omega, r \to \infty)|^2 \,, \tag{8.6}$$

and the solution $\psi_\ell$ can be obtained through the standard Green's function as

$$\psi_\ell(r) = \frac{\psi_+}{W} \int_{-\infty}^{r} \mathrm{d}r_*\, S_\ell\, \psi_- + \frac{\psi_-}{W} \int_{r}^{\infty} \mathrm{d}r_*\, S_\ell\, \psi_+ \,, \tag{8.7}$$

where $\psi_\pm$ are the solutions of the corresponding homogeneous problem with correct boundary conditions at $r_* \to \pm\infty$, and the Wronskian $W = \psi_- \mathrm{d}\psi_+/\mathrm{d}r_* - \psi_+ \mathrm{d}\psi_-/\mathrm{d}r_*$ is constant by virtue of the field equations. We validated the results presented below by comparing this procedure with a direct integration of the master equation through a shooting method, obtaining the same results up to numerical accuracy.

## 8.3 Quasi-Normal Mode Spectrum

The quasi-normal modes of the wormhole are defined by the eigenvalue problem associated with the master equation above with $S_\ell = 0$ and supplemented by regularity boundary conditions. We require $\psi_\ell \sim \mathrm{e}^{\pm \mathrm{i}\omega r_*}$ at the asymptotic boundaries of both universes. Note that, because $r_* \to \pm r$ at infinity, in Schwarzschild coordinates both homogeneous equations and boundary conditions are the same. At the throat we impose continuity of $\mathrm{d}\psi_\ell/\mathrm{d}r_*$ which — given the symmetry of the problem and the homogeneity of the master equation — can be achieved only in two ways: by imposing either $\mathrm{d}\psi_\ell(0)/\mathrm{d}r_* = 0$ or $\psi_\ell(0) = 0$. Correspondingly, we find two families of quasi-normal modes that can be obtained by a straightforward direct integration supplied by a high-order asymptotic expansion of the solution [382] in either of the two domains.

A representative example of the polar quasi-normal mode spectrum is shown in Fig. 8.2, while the values of the fundamental quasi-normal mode for the first family are listed in Table 8.1.

| Black Hole $\omega_{\rm BH} M$ | Wormhole $\omega_{\rm WH} M$ | | |
|---|---|---|---|
| | $r_0 = 2.001M$ | $r_0 = 2.0001M$ | $r_0 = 2.00001M$ |
| $0.374 - 0.089\mathrm{i}$ | $0.141 - 8.68 \cdot 10^{-7}\mathrm{i}$ | $0.102 - 5.35 \cdot 10^{-8}\mathrm{i}$ | $0.079 - 6.93 \cdot 10^{-9}\mathrm{i}$ |

Table 8.1: Fundamental QNM for the Schwarzschild black hole and for a wormhole with different $r_0$.

Remarkably, in the black hole limit, $r_0 \to 2M$, the spectrum is dramatically different from that of a Schwarzschild black hole: the quasi-normal modes of the wormhole approach the real axis and become long-lived. In fact, as $r_0 \to 2M$ the deviations from the black hole quasi-normal modes are arbitrarily large.

This behaviour can be understood by investigating the effective potential shown in Fig. 8.3. Due to the presence of the throat at $r_* = 0$, the effective potential is $Z_2$-symmetric and develops another barrier at $r_* < 0$. Therefore, for any $r_0 \lesssim 3M$, wormholes can support long-lived modes trapped between the two potential wells near the light rings. These modes are analog to the 'slowly-damped' modes of ultracompact stars [383–385].

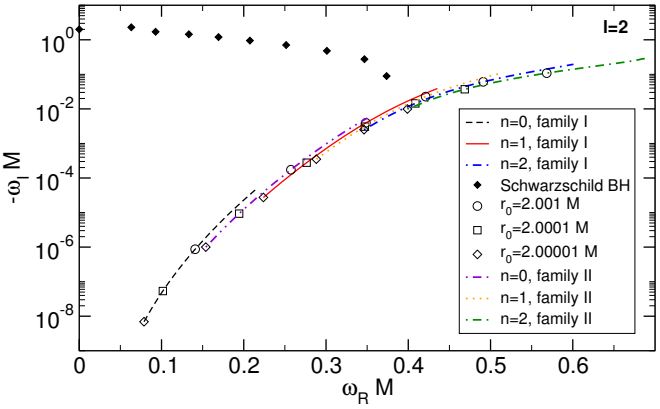


Figure 8.2: The first three tones ($n = 0, 1, 2$) for the two families of polar $\ell = 2$ quasi-normal modes of a wormhole parametrically shown in the complex plane for different values of the throat location $r_0$, and compared to the first quasi-normal modes of a Schwarzschild black hole. In the black hole limit ($r_0 \to 2M$) all quasi-normal modes of the wormhole approach the real axis.

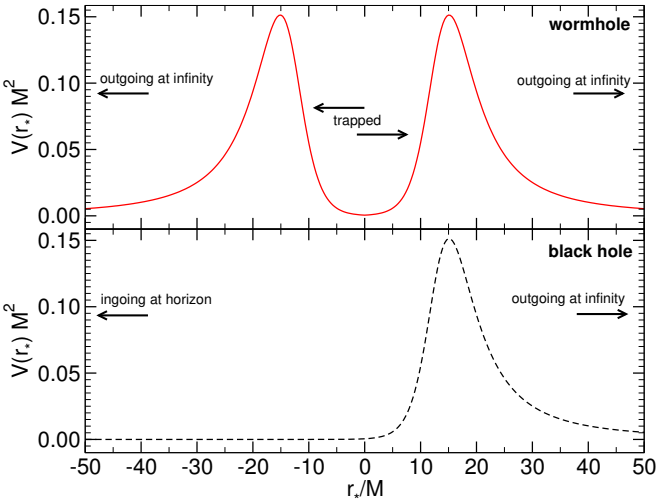


Figure 8.3: Effective $\ell = 2$ potential in tortoise coordinates for a static traversable wormhole (top panel) with $r_0 = 2.001M$ and for a Schwarzschild black hole (bottom panel).

## 8.4 Excitation of Light-Ring Modes vs Quasi-Normal Modes

Given the drastically different quasi-normal mode spectrum of a wormhole relative to the black hole case, one might be tempted to expect an entirely different ringdown signal in actual dynamical processes. This expectation seems to be confirmed by the energy spectrum shown in the left panel of Fig. 8.4 and compared to the case of a particle plunging into a Schwarzschild black hole. The spectra coincide only at low frequencies, but are generically very different. Furthermore, in the black hole limit, the long-lived quasi-normal modes of the wormhole can be excited and correspond to narrow, Breit-Wigner resonances in the spectrum [386, 387].

However, as previously discussed, the black hole quasi-normal modes are light-ring modes and

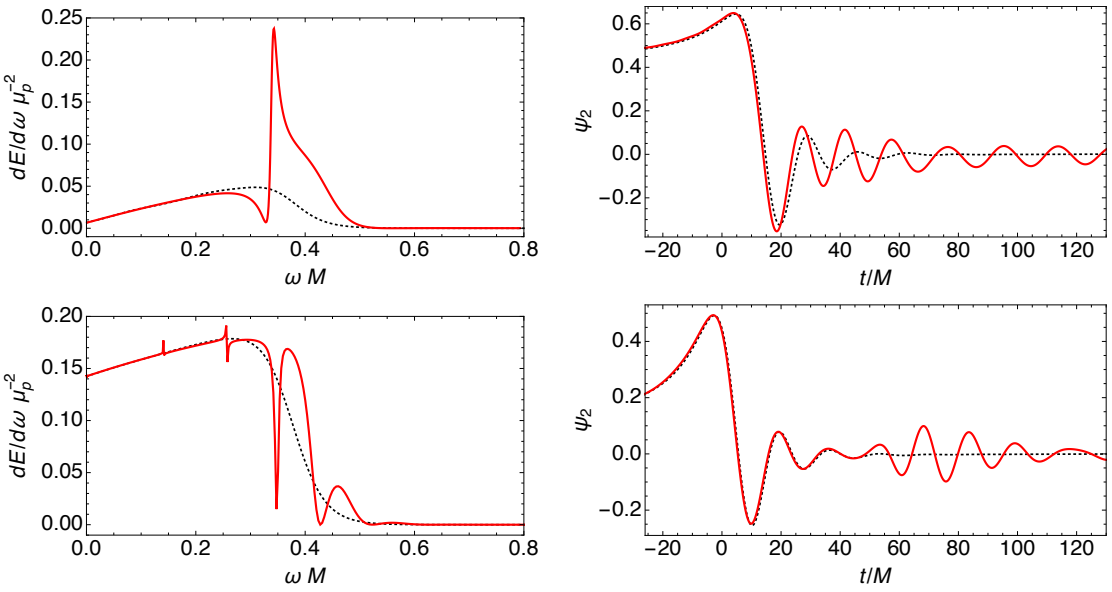


Figure 8.4: Left panels: quadrupolar gravitational wave energy spectrum for a point particle crossing a traversable wormhole (red solid line) and compared to the case of a particle plunging into a Schwarzschild black hole (dotted black line) with the same energy $E$. Top and bottom panels refer to $r_0 = 2.1M$, $E = 1.01$ and to $r_0 = 2.001M$, $E = 1.5$, respectively (different parameters give qualitatively similar results). Right panels: the corresponding gravitational wave waveforms compared to the black hole case. The black hole waveform was shifted in time by $\Delta t$, see Eq. (8.8), to account for the dephasing due to the light travel time from the throat to the light ring.

should play a role for any object with a light ring. In fact, the striking difference in the energy spectra does not leave a trace in the initial ringdown waveform. This is shown in the right panel of Fig. 8.4 for the time-domain wavefunction $\hat{\psi}_2(t, r)$ extracted at infinity as a function of time. As the wormhole approaches the black hole limit, $r_0 \to 2M$, the initial ringdown is precisely the same as in the Schwarzschild case: the waveform oscillates with the same fundamental quasi-normal mode of a Schwarzschild black hole, although the quasi-normal mode spectrum of the wormhole is completely different from that of the black hole. We stress that the fundamental black hole quasi-normal mode does *not* appear as a pole of the corresponding Green's function of the wormhole, but nevertheless dominates the ringdown.

The quasi-normal modes of the wormhole contain low energy and get excited only at late times, namely after the particle crosses the throat in the characteristic timescale

$$\Delta t = \int_{r_0}^{3M} \frac{\mathrm{d}r}{f(r)} \sim -2M \log\left(\frac{\delta}{M}\right), \tag{8.8}$$

where in the last step we considered $r_0 = 2M + \delta$ with $\delta \ll M$. Finally, in the black hole limit ($\delta \to 0$) all quasi-normal modes are long-lived and have similar frequencies (see Fig. 8.2), which gives rise to a peculiar beating pattern at late times.

## 8.5 Summary and Conclusions

Our results give strong evidence for a highly counter-intuitive phenomenon: in the post-merger phase of a compact binary coalescence, the initial ringdown signal chiefly depends on the properties of the light ring of the final object rather than its quasi-normal modes. If the final object is arbitrarily close to a black hole, the ringdown modes will correspond to the black hole quasi-normal modes, even if the object does not possess a horizon. In particular, this also means that mass (and probably spin) estimates from current ringdown templates perform well even if the compact object is horizonless. The actual quasi-normal modes of the object are excited only at late times and typically do not contain a significant amount of energy. Therefore, they play a subdominant role in the merger waveforms, but will likely dominate over Price's power-law tails [388].

Clearly, our model is heuristic and could be extended in several ways, e.g. by including rotation, finite-size and self-force effects, and more generic orbits. None of these effects is expected to change the qualitative picture discussed above. Environmental effects (such as accretion disks, magnetic fields, dark matter distributions or a cosmological constant) are typically negligible [269] and should not affect the waveform significantly. In particular, the motion of the particle before crossing the innermost-stable circular orbit is irrelevant for the ringdown signal, which depends almost entirely on the subsequent plunge and the particle's motion after crossing the light ring. It would be interesting to extend our analysis by performing a numerical simulation of a compact binary merger producing a horizonless compact object.

Our results are relevant to test possible consequences of quantum effects at the horizon scale, e.g. the firewall and the gravastar proposals. In these models the quasi-normal mode spectrum might considerably differ from the Kerr case, but this will not prevent gravitational-wave observatories from detecting their ringdown signal using standard black hole-based templates. For various black hole mimickers the horizon is removed by a quantum phase transition, which would naturally occur on Planckian length scales $\delta$ [40, 269, 280, 283, 389]. In this case, the changes to the quasi-normal mode spectrum are more dramatic and, if detected, they will provide a piece of incontrovertible evidence for quantum corrections at the horizon scale. In the $\delta \ll M$ limit we expect that our results will be qualitatively valid for any model. Interestingly, Eq. (8.8) shows that the delay $\Delta t$ for the quasi-normal modes to appear after the main burst of radiation produced at the light ring depends only logarithmically on $\delta$. For a final object with mass roughly sixty solar masses, $\Delta t \sim 16\tau_{\rm BH}$ ($\tau_{\rm BH} \approx 3\,$ms being the fundamental damping time of a Schwarzschild black hole with the same mass) even if the length scale is Planckian, $\delta \sim l_p = 2 \times 10^{-33}\,$cm. For $\delta \sim \sqrt{2 l_p M} \sim 10^{-13}\,$cm, as in the original gravastar model, such delay is only halved.

Our results suggest that future gravitational wave detections by LIGO [390], Virgo [391] and KAGRA [392] should focus on extracting the late-time ringdown signal, where the actual quasi-normal modes of the final object are eventually excited. Even in the absence of a horizon, these modes are expected to be in the same frequency range of the black hole quasi-normal modes and

therefore might be detectable with advanced gravitational-wave interferometers. Furthermore, their extremely long damping time might be used to enhance the signal through long-time integrations, even if the energy contained in these modes is weak. Estimating the signal-to-noise ratio required for such precise measurements is an important extension of our work.

As discussed in Section 5.5, black hole mimickers are generically unstable. Therefore, while our results are generic, the viability of a black hole mimicker depends on the specific model, especially on its compactness and spin [393].

At the moment, the post-merger signal leaves room for alternative theories of gravity [394, 395], dark particles [348] and exotic compact objects, such as gravastars and empty shells [362, 396]. Our results show that only late-time ringdown detections might be used to rule out exotic alternatives to black holes and to test quantum effects at the horizon scale. As it stands, the events GW150914 and GW151226 do not provide the final evidence for horizons, but strongly support the existence of light rings, itself a genuinely general relativistic effect.

# Conclusions

In this thesis we have investigated topics of black hole physics with the aim of bridging different aspects of this research field. We have chosen to focus our research on two key concepts, which we believe very promising for future developments: scalar sources and black hole perturbation theory.

As we have stressed several times in this thesis, scalar fields play a crucial role in different sectors of gravitational and particle physics. Nevertheless, their status is still not completely clear. Do they always correspond to fundamental microscopic fields as the recent discovery of the Higgs boson indicates, or may also represent just an effective description of unknown physics? We think that an answer to this fundamental question requires critical thinking about the role that scalar fields play in three different areas of gravitational physics — standard black holes and no-hair theorems, holographic description of gravity and cosmology. This thesis represents a step in this direction.

Perturbation theory of gravitational configurations is a transversal concept too. It plays an essential role in several areas of gravitational physics — e.g. stability, calculation of transport coefficients in the holographic set-up, cosmology and gravitational wave emission. In this thesis we have used it for different purposes: the issue of stability of boson stars, the calculation of tidal deformations of black hole mimickers and for a critical discussion on recent gravitational-wave data from black hole merging.

Here we give a list of the most important results of this thesis and prospects for future investigations. In the first part, we have discussed three different models in which general relativity is coupled to a real scalar field. We have considered a massless or asymptotically massless scalar, and we have found a new family of asymptotically flat black holes and exact brane solutions conformal to the Lifšic spacetime whose dual gauge theory is characterised by hyperscaling violation. Then we have studied an inflationary model whose scalar potential is motivated by holographic arguments. In the second part, we have considered several different black hole mimickers and we have investigated their possible astrophysical signatures in gravitational waves. We have studied the stability of mini boson star in five spacetime dimensions and we have constructed mini boson stars built with more than one scalar. We have computed the tidal Love numbers for various black hole mimickers and we have discussed their possible detection. Finally we have shown that the gravitational radiation emitted by a particle falling into a black hole mimicker is almost indistinguishable if the mimickers is sufficiently compact.

In Chapter 2 we have derived a two-parameter family of exact, asymptotically flat, spherically

symmetric, black hole solutions sourced by a non-trivial scalar field which decays asymptotically as $1/r$. The scalar potential near $\phi = 0$ behaves as $V(\phi) \sim \phi^5$ meaning that it is not renormalisable from the quantum field theory point of view, and our model could at least give an effective description. Our solutions violate the assumptions of no-hair theorems both in their old and recent formulation: the potential is not convex and the masses are not positive definite, meaning violation of the positive energy theorem. The thermodynamics of our solutions is the same of the Schwarzschild solution in the large mass limit, whereas the infrared behaviour of the mass spectrum of the black hole, depending on the value of the parameters, is characterised by the presence of a mass gap. What we have not addressed in this chapter and would be important to study is the issue of the stability of our black hole solutions in more details. We also plan to investigate the rotating case.

Chapter 3 is the 'brane counterpart' of Chapter 2 plus charge, i.e. we have derived brane solutions of minimally coupled Einstein-Maxwell-scalar gravity for an identically null potential. These solutions are scale-covariant metrics, and their interest is motivated by holography, as the dual QFT of these solutions is characterised by hyperscaling violation. We have given a general classifications of all brane solutions of minimally coupled Einstein-Maxwell-scalar which are relevant for holographic applications with no Schrödinger isometries.

In Chapter 4 we have studied an inflationary model whose two-exponential scalar potential is inspired by the same holographic models that motivate the topics tackled in the previous chapters. Inflation begins when the inflaton starts rolling off from the maximum of the potential, caused by a de Sitter instability. In the slow-roll approximation, our model reproduces correctly, for a wide range of its parameters, the most recent experimental data for the power spectrum of primordial perturbations. Moreover, it predicts inflation at energy scales of four to five orders of magnitude below the Planck scale, whereas the inflaton mass, at the onset of inflation, turns out to be seven to eight orders of magnitude smaller than the Planck mass. In this chapter we have not discussed the reheating phase and the transition from inflation to the radiation/matter dominated era. Our model can be extended by modifying the potential, and some progress has already been made.

In Chapter 6 we have studied two aspects of boson stars. We have studied the existence and the stability of mini boson stars in five dimensions and we have confirmed a recent claim showing that five-dimensional — and presumably, higher-dimensional — mini boson stars are unstable against linear radial perturbations. Then we have investigated boson stars built from various scalars with different masses and we have discussed similarities and differences with the single-boson star case. We have provided strong evidence that these stars are stable at least in part of the parameter space, studying their stability with two different criteria and we have provided quantitative criteria for instability.

In Chapter 7 we have compute the tidal Love numbers of exotic compact objects within the framework of general relativity. In the black hole limit, all the Love numbers vanish logarithmically,

but they are in general non-zero. Future gravitational-wave measurements of the tidal Love numbers of compact objects in a binary system will provide a novel way to test black holes and general relativity in the strong-field regime. Future developments and extensions of this work include: consider the presence of electromagnetic or scalar tidal fields and hence the definition of new families of Love numbers; consider rotating objects, in fact, although the spin of the individual components of a neutron star binary system are typically small, but this might not be the case for exotic compact objects and for black holes; consider extra charges, e.g. static black holes in Einstein-dilaton-Gauss-Bonnet theory or spinning black holes in Chern-Simons gravity. Some of them are already work in progress.

In Chapter 8 we have presented an important and counter-intuitive phenomenon: the initial ringdown signal depends on the light ring modes rather than the quasi-normal modes. For a black hole, its quasi-normal modes also describe the ringdown phase by accident. For another horizonless object, its quasi-normal modes appear at later times. Hence, only late-time ringdown detections might be used to rule out exotic alternatives to black holes and to test quantum effects at the horizon scale. The model discussed in this chapter has already been extended in Ref. [362], but other extensions are possible, e.g. by including rotation, finite-size and self-force effects, and more generic orbits. However, none of these effects is expected to qualitatively change the result.

# Bibliography


[1] LIGO Scientific and Virgo collaborations, B. P. Abbott et al. 'Observation of Gravitational Waves from a Binary Black Hole Merger'. *Phys. Rev. Lett.* 116 (2016), 061102. arXiv: 1602.03837.

[2] LIGO Scientific and Virgo collaborations, B. P. Abbott et al. 'GW151226: Observation of Gravitational Waves from a 22-Solar-Mass Binary Black Hole Coalescence'. *Phys. Rev. Lett.* 116 (2016), 241103. arXiv: 1606.04855.

[3] A. Einstein. 'Grundgedanken der allgemeinen Relativitätstheorie und Anwendung dieser Theorie in der Astronomie'. *Sitzungsber. Preuss. Akad. Wiss. Berlin* (1915), 315.

[4] A. Einstein. 'Zur allgemeinen Relativitätstheorie'. *Sitzungsber. Preuss. Akad. Wiss. Berlin* (1915), 778, 799.

[5] A. Einstein. 'Erklärung der Perihelbewegung des Merkur aus der allgemeinen Relativitätstheorie '. *Sitzungsber. Preuss. Akad. Wiss. Berlin* (1916), 831.

[6] A. Einstein. 'Feldgleichungen der Gravitation'. *Sitzungsber. Preuss. Akad. Wiss. Berlin* (1916), 844.

[7] K. Schwarzschild. 'Über das Gravitationsfeld eines Massenpunktes nach der Einsteinschen Theorie'. *Sitzungsber. Preuss. Akad. Wiss. Berlin* 7 (1916), 189.

[8] Planck collaboration, P. A. R. Ade et al. 'Planck 2015 Results. XX. Constraints on inflation'. *Astronom. Astrophys.* 594 (2016), A20. arXiv: 1502.02114.

[9] C. M. Will. 'The Confrontation between General Relativity and Experiment'. *Living Rev. Relat.* 17 (2014), 4. arXiv: 1403.7377.

[10] K. S. Stelle. 'Renormalization of Higher Derivative Quantum Gravity'. *Phys. Rev.* D16 (1977), 953.

[11] S. W. Hawking and R. Penrose. 'The Singularities of Gravitational Collapse and Cosmology'. *Proc. R. Soc.* A314 (1970), 529.

[12] E. Poisson and C. M. Will. *Gravity. Newtonian, Post-Newtonian, Relativistic*. Cambridge, UK: CUP, 2014. 792 pp.

[13] C. Brans and R. H. Dicke. 'Mach's principle and a relativistic theory of gravitation'. *Phys. Rev.* 124 (1961), 925.

[14] G. W. Horndeski. 'Second-order scalar-tensor field equations in a four-dimensional space'. *Int. J. Theor. Phys.* 10 (1974), 363.

[15] T. Damour and G. Esposito-Farèse. 'Tensor multiscalar theories of gravitation'. *Class. Quantum Grav.* 9 (1992), 2093.

[16] Y. Fujii and K.-i. Maeda. *The scalar-tensor theory of gravitation*. Monographs on Mathematical Physics. Cambridge, UK: CUP, 2007.

[17] T. P. Sotiriou and V. Faraoni. '$f(\mathcal{R})$ Theories Of Gravity'. *Rev. Mod. Phys.* 82 (2010), 451. arXiv: 0805.1726.

[18] A. De Felice and S. Tsujikawa. '$f(\mathcal{R})$ theories'. *Living Rev. Relat.* 13 (2010), 3. arXiv: 1002.4928.

[19] S. Nojiri and S. D. Odintsov. 'Unified cosmic history in modified gravity: from $f(\mathcal{R})$ theory to Lorentz non-invariant models'. *Phys. Rept.* 505 (2011), 59. arXiv: 1011.0544.

[20] K. Hinterbichler. 'Theoretical Aspects of Massive Gravity'. *Rev. Mod. Phys.* 84 (2012), 671. arXiv: 1105.3735.

[21] T. Clifton, P. G. Ferreira, A. Padilla, and C. Skordis. 'Modified Gravity and Cosmology'. *Phys. Rept.* 513 (2012), 1. arXiv: 1106.2476.

[22] S. Capozziello and M. De Laurentis. 'Extended Theories of Gravity'. *Phys. Rept.* 509 (2011), 167. arXiv: 1108.6266.

[23] C. de Rham. 'Massive Gravity'. *Living Rev. Relat.* 17 (2014), 7. arXiv: 1401.4173.

[24] N. Yunes and X. Siemens. 'Gravitational-Wave Tests of General Relativity with Ground-Based Detectors and Pulsar Timing-Arrays'. *Living Rev. Relat.* 16 (2013), 9. arXiv: 1304.3473.

[25] E. Berti et al. 'Testing General Relativity with Present and Future Astrophysical Observations'. *Class. Quantum Grav.* 32 (2015), 243001. arXiv: 1501.07274.

[26] LIGO Scientific and Virgo collaborations, B. P. Abbott et al. 'Tests of general relativity with GW150914'. *Phys. Rev. Lett.* 116 (2016), 221101. arXiv: 1602.03841.

[27] N. Yunes, K. Yagi, and F. Pretorius. 'Theoretical Physics Implications of the Binary Black-Hole Mergers GW150914 and GW151226'. *Phys. Rev.* D94 (2016), 084002. arXiv: 1603.08955.

[28] S. Bird, I. Cholis, J. B. Muñoz, Y. Ali-Haïmoud, M. Kamionkowski, E. D. Kovetz, A. Raccanelli, and A. G. Riess. 'Did LIGO Detect Dark Matter?' *Phys. Rev. Lett.* 116 (2016), 201301. arXiv: 1603.00464.

[29] M. Sasaki, T. Suyama, T. Tanaka, and S. Yokoyama. 'Primordial Black Hole Scenario for the Gravitational-Wave Event GW150914'. *Phys. Rev. Lett.* 117 (2016), 061101. arXiv: 1603.08338.

[30] S. A. Hartnoll, C. P. Herzog, and G. T. Horowitz. 'Building a Holographic Superconductor'. *Phys. Rev. Lett.* 101 (2008), 031601. arXiv: 0803.3295.

[31] G. T. Horowitz and M. M. Roberts. 'Holographic Superconductors with Various Condensates'. *Phys. Rev.* D78 (2008), 126008. arXiv: 0810.1077.

[32] C. P. Herzog. 'Lectures on Holographic Superfluidity and Superconductivity'. *J. Phys.* A42 (2009), 343001. arXiv: 0904.1975.

[33] G. T. Horowitz. 'Introduction to Holographic Superconductors'. In: *From Gravity to Thermal Gauge Theories: The AdS/CFT Correspondence*. Ed. by E. Papantonopoulos. Lecture Notes in Physics 828. Berlin; Heidelberg: Springer, 2011, p. 313. arXiv: 1002.1722.

[34] P. Kovtun, D. T. Søn, and A. O. Starinets. 'Holography and hydrodynamics: Diffusion on stretched horizons'. *J. High Energy Phys.* 0310 (2003), 064. arXiv: hep-th/0309213.

[35] P. Kovtun, D. T. Søn, and A. O. Starinets. 'Viscosity in Strongly Interacting Quantum Field Theories from Black Hole Physics'. *Phys. Rev. Lett.* 94 (2005), 111601. arXiv: hep-th/0405231.

[36] A. Strominger and C. Vafa. 'Microscopic origin of the Bekenstein-Hawking entropy'. *Phys. Lett.* B379 (1996), 99. arXiv: hep-th/9601029.

[37] O. Lunin and S. D. Mathur. 'AdS/CFT duality and the black hole information paradox'. *Nucl. Phys.* B623 (2002), 342. arXiv: hep-th/0109154.

[38] O. Lunin and S. D. Mathur. 'Statistical interpretation of Bekenstein entropy for systems with a stretched horizon'. *Phys. Rev. Lett.* 88 (2002), 211303. arXiv: hep-th/0202072.

[39] S. D. Mathur. 'The Information Paradox: A Pedagogical Introduction'. In: *Proceedings of the CERN Winter School on Strings, Supergravity and Gauge Theories*. (Geneva, Switzerland, Feb. 9–13, 2009). *Class. Quantum Grav.* 26 (2009), 224001. arXiv: 0909.1038.

[40] A. Almheiri, D. Marolf, J. Polchinski, and J. Sully. 'Black Holes: Complementarity or Firewalls?' *J. High Energy Phys.* 1302 (2013), 062. arXiv: 1207.3123.

[41] S. Ryu and T. Takayanagi. 'Holographic Derivation of Entanglement Entropy from the anti de Sitter Space/Conformal Field Theory Correspondence'. *Phys. Rev. Lett.* 96 (2006), 181602. arXiv: hep-th/0603001.

[42] T. Nishioka, S. Ryu, and T. Takayanagi. 'Holographic entanglement entropy: An overview'. *J. Phys.* A42 (2009), 504008. arXiv: 0905.0932.

[43] T. P. Sotiriou. 'Gravity and Scalar Fields'. In: *Proceedings of the 13th International Conference on Topics in Astroparticle and Underground Physics*. (Asilomar, CA, USA, Sept. 8–13, 2013). Ed. by E. Papantonopoulos. Lecture Notes in Physics 892. Cham, Switzerland: Springer, 2015, p. 3. arXiv: 1404.2955.

[44] T. P. Sotiriou. 'Black Holes and Scalar Fields'. *Class. Quantum Grav.* 32 (2015), 214002. arXiv: 1505.00248.

[45] V. Sahni. 'Dark matter and dark energy'. In: *The physics of the early universe. Proceedings of the 2nd Aegean School*. (Ermoupolis, Greece, Sept. 22–30, 2003). Ed. by E. Papantonopoulos. Lecture Notes in Phys. 653. Berlin; Heidelberg: Springer, 2004, p. 141. arXiv: astro-ph/0403324.

[46] ATLAS collaboration, G. Aad et al. 'Observation of a new particle in the search for the Standard Model Higgs boson with the ATLAS detector at the LHC'. *Phys. Lett.* B716 (2012), 1. arXiv: 1207.7214.

[47] CMS collaboration, S. Chatrchyan et al. 'Observation of a new boson at a mass of 125 GeV with the CMS experiment at the LHC'. *Phys. Lett.* B716 (2012), 30. arXiv: 1207.7235.

[48] R. Ruffini and J. A. Wheeler. 'Introducing the black hole'. *Phys. Today* 24 (1971), 30.

[49] R. P. Kerr. 'Gravitational field of a spinning mass as an example of algebraically special metrics'. *Phys. Rev. Lett.* 11 (1963), 237.

[50] H. Reissner. 'Über die Eigengravitation des elektrischen Feldes nach der Einsteinschen Theorie'. *Ann. Phys.* 355 (1916), 106.

[51] G. Nordström. 'On the Energy of the Gravitational Field in Einstein's Theory'. *Verhandl. Koninkl. Ned. Akad. Wetenschap., Afdel. Natuurk., Amsterdam* 26 (1918), 1201.

[52] E. T. Newman, R. Couch, K. Chinnapared, A. Exton, A. Prakash, and R. Torrence. 'Metric of a Rotating, Charged Mass'. *J. Math. Phys.* 6 (1965), 918.

[53] J. M. Bardeen, B. Carter, and S. W. Hawking. 'The four laws of black hole mechanics'. *Commun. Math. Phys.* 31 (1973), 161.

[54] R. M. Wald. 'The thermodynamics of black holes'. *Living Rev. Relat.* 4 (2001), 6. arXiv: gr-qc/9912119.

[55] S. W. Hawking. 'Gravitational radiation from colliding black holes'. *Phys. Rev. Lett.* 26 (1971), 1344.

[56] J. D. Bekenstein. 'Black holes and entropy'. *Phys. Rev.* D7 (1973), 2333.

[57] S. W. Hawking. 'Particle Creation by Black Holes'. *Commun. Math. Phys.* 43 (1975), 199. Erratum: *ibid.* 46 (1976), 206.

[58] W. Israel. 'Event horizons in static vacuum space-times'. *Phys. Rev.* 164 (1967), 1776.

[59] W. Israel. 'Event horizons in static electrovac space-times'. *Commun. Math. Phys.* 8 (1968), 245.

[60] B. Carter. 'Axisymmetric Black Hole Has Only Two Degrees of Freedom'. *Phys. Rev. Lett.* 26 (1971), 331.

[61] R. M. Wald. 'Final states of gravitational collapse'. *Phys. Rev. Lett.* 26 (1971), 1653.

[62] D. C. Robinson. 'Uniqueness of the Kerr black hole'. *Phys. Rev. Lett.* 34 (1975), 905.

[63] J. D. Bekenstein. 'Black hole hair: 25 years after'. In: *Proceedings of the 2nd International Sakharov Conference*. (Moscow, Russia, May 20–24, 1996). Ed. by I. M. Dremin and A. M. Semikhatov. Singapore: World Scientific, 1997, p. 216. arXiv: gr-qc/9605059.

[64] M. S. Volkov. 'Hairy black holes in the XX-th and XXI-st centuries'. (2016). arXiv: 1601.08230.

[65] M. S. Volkov and D. V. Gal'tsov. 'NonAbelian Einstein Yang-Mills black holes'. *J. Exp. Theor. Phys. Lett.* 50 (1989), 346. *Pis'ma Zh. Eksp. Teor. Fiz.* 50 (1989), 312.

[66] P. Bizon. 'Colored black holes'. *Phys. Rev. Lett.* 64 (1990), 2844.

[67] S. Droz, M. Heusler, and N. Straumann. 'New black hole solutions with hair'. *Phys. Lett.* B268 (1991), 371.

[68] K.-M. Lee, V. P. Nair, and E. J. Weinberg. 'A Classical instability of Reissner-Nordstrom solutions and the fate of magnetically charged black holes'. *Phys. Rev. Lett.* 68 (1992), 1100. arXiv: hep-th/9111045.

[69] B. R. Greene, S. D. Mathur, and C. M. O'Neill. 'Eluding the no hair conjecture: Black holes in spontaneously broken gauge theories'. *Phys. Rev.* D47 (1993), 2242. arXiv: hep-th/9211007.

[70] T. Torii and K.-i. Maeda. 'Black holes with non-Abelian hair and their thermodynamical properties'. *Phys. Rev.* D48 (1993), 1643.

[71] P. T. Chruściel, J. Lopes Costa, and M. Heusler. 'Stationary Black Holes: Uniqueness and Beyond'. *Living Rev. Relat.* 15 (2012), 7. arXiv: 1205.6112.

[72] J. D. Bekenstein. 'Nonexistence of baryon number for static black holes'. *Phys. Rev.* D5 (1972), 1239.

[73] J. D. Bekenstein. 'Novel 'no scalar hair' theorem for black holes'. *Phys. Rev.* D51 (1995), 6608.

[74] D. Sudarsky. 'A Simple proof of a no hair theorem in Einstein Higgs theory,' *Class. Quantum Grav.* 12 (1995), 579.

[75] G. W. Gibbons and K.-i. Maeda. 'Black Holes and Membranes in Higher Dimensional Theories with Dilaton Fields'. *Nucl. Phys.* B298 (1988), 741.

[76] D. Garfinkle, G. T. Horowitz, and A. Strominger. 'Charged black holes in string theory'. *Phys. Rev.* D43 (1991), 3140.

[77] M. Cadoni and S. Mignemi. 'Dilatonic black holes in theories with moduli fields'. *Phys. Rev.* D48 (1993), 5536. arXiv: hep-th/9305107.

[78] S. Monni and M. Cadoni. 'Dilatonic black holes in a S-duality model'. *Nucl. Phys.* B466 (1996), 101. arXiv: hep-th/9511067.

[79] M. J. Duff and J. T. Liu. 'Anti-de Sitter black holes in gauged $N = 8$ supergravity'. *Nucl. Phys.* B554 (1999), 237. arXiv: hep-th/9901149.

[80] T. Torii, K. Maeda, and M. Narita. 'Scalar hair on the black hole in asymptotically anti-de Sitter space-time'. *Phys. Rev.* D64 (2001), 044007.

[81] T. Hertog. 'Towards a Novel no-hair Theorem for Black Holes'. *Phys. Rev.* D74 (2006), 084008. arXiv: gr-qc/0608075.

[82] E. Witten. 'A Simple Proof of the Positive Energy Theorem'. *Commun. Math. Phys.* 80 (1981), 381.

[83] P. K. Townsend. 'Positive Energy and the Scalar Potential in Higher Dimensional (Super) Gravity Theories'. *Phys. Lett.* B148 (1984), 55.

[84] A. Anabalón. 'Exact Black Holes and Universality in the Backreaction of non-linear Sigma Models with a potential in (A)dS4'. *J. High Energy Phys.* 1206 (2012), 127. arXiv: 1204.2720.

[85] A. Anabalón and J. Oliva. 'Exact Hairy Black Holes and their Modification to the Universal Law of Gravitation'. *Phys. Rev.* D86 (2012), 107501. arXiv: 1205.6012.

[86] A. Anabalón and N. Deruelle. 'On the mechanical stability of asymptotically flat black holes with minimally coupled scalar hair'. *Phys. Rev.* D88 (2013), 064011. arXiv: 1307.2194.

[87] A. Anabalón, D. Astefanesei, and R. Mann. 'Exact asymptotically flat charged hairy black holes with a dilaton potential'. *J. High Energy Phys.* 1310 (2013), 184. arXiv: 1308.1693.

[88] C. A. R. Herdeiro and E. Radu. 'Kerr black holes with scalar hair'. *Phys. Rev. Lett.* 112 (2014), 221101. arXiv: 1403.2757.

[89] C. Charmousis, T. Kolyvaris, E. Papantonopoulos, and M. Tsoukalas. 'Black Holes in Bi-scalar Extensions of Horndeski Theories'. *J. High Energy Phys.* 1407 (2014), 085. arXiv: 1404.1024.

[90] C. A. R. Herdeiro and E. Radu. 'Ergosurfaces for Kerr black holes with scalar hair'. *Phys. Rev.* D89 (2014), 124018. arXiv: 1406.1225.

[91] E. Berti, V. Cardoso, and C. M. Will. 'On gravitational-wave spectroscopy of massive black holes with the space interferometer LISA'. *Phys. Rev.* D73 (2006), 064030. arXiv: gr-qc/0512160.

[92] E. Berti, J. Cardoso, V. Cardoso, and M. Cavaglia. 'Matched-filtering and parameter estimation of ringdown waveforms'. *Phys. Rev.* D76 (2007), 104044. arXiv: 0707.1202.

[93] S. Gossan, J. Veitch, and B. S. Sathyaprakash. 'Bayesian model selection for testing the no-hair theorem with black hole ringdowns'. *Phys. Rev.* D85 (2012), 124056. arXiv: 1111.5819.

[94] V. Cardoso and L. Gualtieri. 'Testing the black hole "no-hair" hypothesis'. *Class. Quantum Grav.* 33 (2016), 174001. arXiv: 1607.03133.

[95] G. 't Hooft. 'Dimensional reduction in quantum gravity'. In: *Salamfestschrift. A Collection of Talks from the Conference on Highlights of Particle and Condensed Matter Physics*. (Trieste, Italy, Mar. 8–12, 1993). Ed. by A. Ali, J. Ellis, and S. Randjbar-Daemi. River Edge, NJ, USA: World Scientific, 1994, p. 284. arXiv: gr-qc/9310026.

[96] L. Susskind. 'The World as a Hologram'. *J. Math. Phys.* 36 (1995), 6377. arXiv: hep-th/9409089.

[97] O. Aharony, S. S. Gubser, J. M. Maldacena, H. Ooguri, and Y. Oz. 'Large $N$ field theories, string theory and gravity'. *Phys. Rept.* 323 (2000), 183. arXiv: hep-th/9905111.

[98] G. T. Horowitz and J. Polchinski. 'Gauge/gravity duality'. In: *Approaches to Quantum Gravity. Toward a New Understanding of Space, Time and Matter*. Ed. by D. Oriti. Cambridge: CUP, 2009, p. 169. arXiv: gr-qc/0602037.

[99] P. C. Argyres. 'Introduction to the AdS/CFT Correspondence'. In: *From Gravity to Thermal Gauge Theories: The AdS/CFT Correspondence*. Ed. by E. Papantonopoulos. Lecture Notes in Physics 828. Berlin; Heidelberg: Springer, 2011, p. 57.

[100] J. M. Maldacena. 'The Large $N$ limit of superconformal field theories and supergravity'. *Int. J. Theor. Phys.* 38 (1999), 1113. arXiv: hep-th/9711200. Also in: *Adv. Theor. Math. Phys.* 2 (1998), 231.

[101] E. Witten. 'Anti-de Sitter space and holography'. *Adv. Theor. Math. Phys.* 2 (1998), 253. arXiv: hep-th/9802150.

[102] S. S. Gubser, I. R. Klebanov, and A. M. Polyakov. 'Gauge theory correlators from noncritical string theory'. *Phys. Lett.* B428 (1998), 105. arXiv: hep-th/9802109.

[103] P. Breitenlohner and D. Z. Freedman. 'Positive Energy in anti-De Sitter Backgrounds and Gauged Extended Supergravity'. *Phys. Lett.* B115 (1982), 197.

[104] R.-G. Cai and Y.-Z. Zhang. 'Black plane solutions in four-dimensional spacetimes'. *Phys. Rev.* D54 (1996), 4891. arXiv: gr-qc/9609065.

[105] C. J. Gao and S. N. Zhang. 'Dilaton black holes in de Sitter or Anti-de Sitter universe'. *Phys. Rev.* D70 (2004), 124019. arXiv: hep-th/0411104.

[106] C. Charmousis, B. Goutéraux, and J. Soda. 'Einstein-Maxwell-Dilaton theories with a Liouville potential'. *Phys. Rev.* D80 (2009), 024028. arXiv: 0905.3337.

[107] S. S. Gubser and F. D. Rocha. 'Peculiar properties of a charged dilatonic black hole in $AdS_5$'. *Phys. Rev.* D81 (2010), 046001. arXiv: 0911.2898.

[108] K. Goldstein, S. Kachru, S. Prakash, and S. P. Trivedi. 'Holography of Charged Dilaton Black Holes'. *J. High Energy Phys.* 1008 (2010), 078. arXiv: 0911.3586.

[109] S. Mignemi. 'Exact solutions of dilaton gravity with (anti)-de Sitter asymptotics'. *Mod. Phys. Lett.* A29 (2014), 1450010. arXiv: 0907.0422.

[110] G. Bertoldi, B. A. Burrington, A. W. Peet, and I. G. Zadeh. 'Lifshitz-like black brane thermodynamics in higher dimensions'. *Phys. Rev.* D83 (2011), 126006. arXiv: 1101.1980.

[111] M. Cadoni, M. Serra, and S. Mignemi. 'Exact solutions with AdS asymptotics of Einstein and Einstein-Maxwell gravity minimally coupled to a scalar field'. *Phys. Rev.* D84 (2011), 084046. arXiv: 1107.5979.

[112] B. Goutéraux, J. Smolic, M. Smolic, K. Skenderis, and M. Taylor. 'Holography for Einstein-Maxwell-dilaton theories from generalized dimensional reduction'. *J. High Energy Phys.* 1201 (2012), 089. arXiv: 1110.2320.

[113] M. Cadoni, M. Serra, and S. Mignemi. 'Black brane solutions and their solitonic extremal limit in Einstein-scalar gravity'. *Phys. Rev.* D85 (2012), 086001. arXiv: 1111.6581.

[114] M. Cadoni, P. Pani, and M. Serra. 'Infrared Behavior of Scalar Condensates in Effective Holographic Theories'. *J. High Energy Phys.* 1306 (2013), 029. arXiv: 1304.3279.

[115] M. Cadoni, G. D'Appollonio, and P. Pani. 'Phase transitions between Reissner-Nordström and dilatonic black holes in 4D AdS spacetime'. *J. High Energy Phys.* 1003 (2010), 100. arXiv: 0912.3520.

[116] M. Cadoni and P. Pani. 'Holography of charged dilatonic black branes at finite temperature'. *J. High Energy Phys.* 1104 (2011), 049. arXiv: 1102.3820.

[117] S. S. Gubser and F. D. Rocha. 'The gravity dual to a quantum critical point with spontaneous symmetry breaking'. *Phys. Rev. Lett.* 102 (2009), 061601. arXiv: 0807.1737.

[118] B. Goutéraux and E. Kiritsis. 'Generalized Holographic Quantum Criticality at Finite Density'. *J. High Energy Phys.* 1112 (2011), 036. arXiv: 1107.2116.

[119] B. Goutéraux and E. Kiritsis. 'Quantum critical lines in holographic phases with (un)broken symmetry'. *J. High Energy Phys.* 1304 (2013), 053. arXiv: 1212.2625.

[120] M. Cadoni and M. Serra. 'Hyperscaling violation for scalar black branes in arbitrary dimensions'. *J. High Energy Phys.* 1211 (2012), 136. arXiv: 1209.4484.

[121] M. Cadoni and S. Mignemi. 'Phase transition and hyperscaling violation for scalar black branes'. *J. High Energy Phys.* 1206 (2012), 056. arXiv: 1205.0412.

[122] X. Dong, S. Harrison, S. Kachru, G. Torroba, and H. Wang. 'Aspects of holography for theories with hyperscaling violation'. *J. High Energy Phys.* 1206 (2012), 041. arXiv: 1201.1905.

[123] K. Narayan. 'On Lifshitz scaling and hyperscaling violation in string theory'. *Phys. Rev.* D85 (2012), 106006. arXiv: 1202.5935.

[124] E. Perlmutter. 'Hyperscaling violation from supergravity'. *J. High Energy Phys.* 1206 (2012), 165. arXiv: 1205.0242.

[125] M. Ammon, M. Kaminski, and A. Karch. 'Hyperscaling-Violation on Probe D-Branes'. *J. High Energy Phys.* 1211 (2012), 028. arXiv: 1207.1726.

[126] J. Bhattacharya, S. Cremonini, and A. Sinkovics. 'On the IR completion of geometries with hyperscaling violation'. *J. High Energy Phys.* 1302 (2013), 147. arXiv: 1208.1752.

[127] M. Alishahiha and H. Yavartanoo. 'On Holography with Hyperscaling Violation'. *J. High Energy Phys.* 1211 (2012), 034. arXiv: 1208.6197.

[128] P. Dey and S. Roy. 'Lifshitz metric with hyperscaling violation from NS5-D$p$ states in string theory'. *Phys. Lett.* B720 (2013), 419. arXiv: 1209.1049.

[129] J. Sadeghi, B. Pourhasan, and F. Pourasadollah. 'Thermodynamics of Schrödinger black holes with hyperscaling violation'. *Phys. Lett.* B720 (2013), 244. arXiv: 1209.1874.

[130] M. Alishahiha, E. Ó Colgáin, and H. Yavartanoo. 'Charged Black Branes with Hyperscaling Violating Factor'. *J. High Energy Phys.* 1211 (2012), 137. arXiv: 1209.3946.

[131] B. S. Kim. 'Hyperscaling violation: a unified frame for effective holographic theories'. *J. High Energy Phys.* 1211 (2012), 061. arXiv: 1210.0540.

[132] M. Edalati, J. F. Pedraza, and W. Tangarife Garcia. 'Quantum Fluctuations in Holographic Theories with Hyperscaling Violation'. *Phys. Rev.* D87 (2013), 046001. arXiv: 1210.6993.

[133] J. Gath, J. Hartong, R. Monteiro, and N. A. Obers. 'Holographic Models for Theories with Hyperscaling Violation'. *J. High Energy Phys.* 1304 (2013), 159. arXiv: 1212.3263.

[134] S. Cremonini and A. Sinkovics. 'Spatially Modulated Instabilities of Geometries with Hyperscaling Violation'. *J. High Energy Phys.* 1401 (2014), 099. arXiv: 1212.4172.

[135] M. Hassaïne. 'New black holes of vacuum Einstein equations with hyperscaling violation and Nil geometry horizons'. *Phys. Rev.* D91 (2015), 084054. arXiv: 1503.01716.

[136] M. Bravo-Gaete, S. Gómez, and M. Hassaïne. 'Towards the Cardy formula for hyperscaling violation black holes'. *Phys. Rev.* D91 (2015), 124038. arXiv: 1505.00702.

[137] G. Kofinas. 'Hyperscaling violating black holes in scalar-torsion theories'. *Phys. Rev.* D92 (2015), 084022. arXiv: 1507.07434.

[138] A. Salvio. 'Holographic Superfluids and Superconductors in Dilaton-Gravity'. *J. High Energy Phys.* 1209 (2012), 134. arXiv: 1207.3800.

[139] D. Roychowdhury. 'Hydrodynamics from scalar black branes'. *J. High Energy Phys.* 1504 (2015), 162. arXiv: 1502.04345.

[140] N. Ogawa, T. Takayanagi, and T. Ugajin. 'Holographic Fermi Surfaces and Entanglement Entropy'. *J. High Energy Phys.* 1201 (2012), 125. arXiv: 1111.1023.

[141] K. Narayan, T. Takayanagi, and S. P. Trivedi. 'AdS plane waves and entanglement entropy'. *J. High Energy Phys.* 1304 (2013), 051. arXiv: 1212.4328.

[142] K. Narayan. 'Non-conformal brane plane waves and entanglement entropy'. *Phys. Lett.* B726 (2013), 370. arXiv: 1304.6697.

[143] S. Cremonini and X. Dong. 'Constraints on renormalization group flows from holographic entanglement entropy'. *Phys. Rev.* D89 (2014), 065041. arXiv: 1311.3307.

[144] K. Skenderis and P. K. Townsend. 'Hidden supersymmetry of domain walls and cosmologies'. *Phys. Rev. Lett.* 96 (2006), 191301. arXiv: hep-th/0602260.

[145] K. Skenderis, P. K. Townsend, and A. van Proeyen. 'Domain-wall/cosmology correspondence in AdS/dS supergravity'. *J. High Energy Phys.* 0708 (2007), 036. arXiv: 0704.3918.

[146] E. Shaghoulian. 'FRW cosmologies and hyperscaling-violating geometries: higher curvature corrections, ultrametricity, Q-space/QFT duality, and a little string theory'. *J. High Energy Phys.* 1403 (2014), 011. arXiv: 1308.1095.

[147] M. Cadoni and M. Ciulu. 'Dark Energy from holographic theories with hyperscaling violation'. *J. High Energy Phys.* 1405 (2014), 089. arXiv: 1311.4098.

[148] S. Mignemi and N. Pintus. 'An exactly solvable inflationary model'. *Gen. Rel. Gravit.* 47 (2015), 51. arXiv: 1404.4720.

[149] A. A. Starobinsky. 'A New Type of Isotropic Cosmological Models Without Singularity'. *Phys. Lett.* B91 (1980), 99.

[150] A. H. Guth. 'The Inflationary Universe: A Possible Solution to the Horizon and Flatness Problems'. *Phys. Rev.* D23 (1981), 347.

[151] K. Sato. 'First Order Phase Transition of a Vacuum and Expansion of the Universe'. *Mon. Not. R. Astron. Soc.* 195 (1981), 467.

[152] A. D. Linde. 'A New Inflationary Universe Scenario: A Possible Solution of the Horizon, Flatness, Homogeneity, Isotropy and Primordial Monopole Problems'. In: *Proceeding of the 2nd Seminar on Quantum Gravity*. (Moscow, USSR, Oct. 13–15, 1981). Ed. by M. A. Markov and P. C. West. New York, NY, USA: Plenum Press, 1984, p. 185. *Phys. Lett.* B108 (1982), 389.

[153] A. Albrecht and P. J. Steinhardt. 'Cosmology for Grand Unified Theories with Radiatively Induced Symmetry Breaking'. *Phys. Rev. Lett.* 48 (1982), 1220.

[154] A. D. Linde. 'Inflationary Cosmology'. In: *Proceedings of the 22nd IAP Colloquium "Inflation+25"*. (Paris, France, June 26–30, 2006). Ed. by M. Lemoine, J. Martin, and P. Peter. Lecture Notes in Physics 738. Berlin; Heidelberg: Springer, 2007, p. 1. arXiv: 0705.0164.

[155] A. D. Linde. 'Chaotic Inflation'. *Phys. Lett.* B129 (1983), 177.

[156] S. Dodelson. *Modern Cosmology*. San Diego, CA, USA: Academic Press, 2003. 440 pp.

[157] V. Mukhanov. *Physical Foundations of Cosmology*. Cambridge, UK: CUP, 2005. 421 pp.

[158] A. I. Janis, E. T. Newman, and J. Winicour. 'Reality of the Schwarzschild Singularity'. *Phys. Rev. Lett.* 20 (1968), 878.

[159] M. Wyman. 'Static Spherically Symmetric Scalar Fields in General Relativity'. *Phys. Rev.* D24 (1981), 839.

[160] K. S. Virbhadra. 'Janis-Newman-Winicour and Wyman solutions are the same'. *Int. J. Mod. Phys.* A12 (1997), 4831. arXiv: gr-qc/9701021.

[161] A. Sadhu and V. Suneeta. 'A naked singularity stable under scalar field perturbations'. *Int. J. Mod. Phys.* D22 (2013), 1350015. arXiv: 1208.5838.

[162] C. Barceló and M. Visser. 'Traversable wormholes from massless conformally coupled scalar fields'. *Phys. Lett.* B466 (1999), 127. arXiv: gr-qc/9908029.

[163] C. Martínez, R. Troncoso, and J. Zanelli. 'Exact black hole solution with a minimally coupled scalar field'. *Phys. Rev.* D70 (2004), 084035. arXiv: hep-th/0406111.

[164] T. Hertog and G. T. Horowitz. 'Designer gravity and field theory effective potentials'. *Phys. Rev. Lett.* 94 (2005), 221301. arXiv: hep-th/0412169.

[165] A. Eichhorn, H. Gies, J. Jaeckel, T. Plehn, M. M. Scherer, and R. Sondenheimer. 'The Higgs Mass and the Scale of New Physics'. *J. High Energy Phys.* 1504 (2015), 022. arXiv: 1501.02812.

[166] P. Burda, R. Gregory, and I. Moss. 'Gravity and the stability of the Higgs vacuum'. *Phys. Rev. Lett.* 115 (2015), 071303. arXiv: 1501.04937.

[167] D. T. Son. 'Toward an AdS/cold atoms correspondence: A Geometric realization of the Schrödinger symmetry'. *Phys. Rev.* D78 (2008), 046003. arXiv: 0804.3972.

[168] K. Balasubramanian and J. McGreevy. 'Gravity duals for non-relativistic CFTs'. *Phys. Rev. Lett.* 101 (2008), 061601. arXiv: 0804.4053.

[169] C. Duval, M. Hassaïne, and P. A. Horváthy. 'The Geometry of Schrödinger symmetry in gravity background/non-relativistic CFT'. *Ann. Phys.* 324 (2009), 1158. arXiv: 0809.3128.

[170] T. Andrade, C. Keeler, A. Peach, and S. F. Ross. 'Schrödinger holography with $z = 2$'. *Class. Quantum Grav.* 32 (2015), 085006. arXiv: 1412.0031.

[171] J. Hartong, E. Kiritsis, and N. A. Obers. 'Schrödinger Invariance from Lifshitz Isometries in Holography and Field Theory'. *Phys. Rev.* D92 (2015), 066003. arXiv: 1409.1522.

[172] J. Hartong, E. Kiritsis, and N. A. Obers. 'Lifshitz space–times for Schrödinger holography'. *Phys. Lett.* B746 (2015), 318. arXiv: 1409.1519.

[173] H. J. Boonstra, K. Skenderis, and P. K. Townsend. 'The domain-wall/QFT correspondence'. *J. High Energy Phys.* 9901 (1999), 003. arXiv: hep-th/9807137.

[174] I. Kanitscheider and K. Skenderis. 'Universal hydrodynamics of non-conformal branes'. *J. High Energy Phys.* 0904 (2009), 062. arXiv: 0901.1487.

[175] C. Martínez and R. Troncoso. 'Electrically charged black hole with scalar hair'. *Phys. Rev.* D74 (2006), 064007. arXiv: hep-th/0606130.

[176] J. de Boer. 'The Holographic renormalization group'. In: *Proceedings of the Workshop on the quantum structure of space-time and the geometrical nature of fundamental interactions.* (Berlin, Germany, Oct. 4–10, 2000). Ed. by E. A. Bergshoeff, A. Ceresole, C. Kounnas, D. Lust, and A. Sevrin. *Fortsch. Phys.* 49 (2001), 339. arXiv: hep-th/0101026.

[177] S. S. Gubser, S. S. Pufu, and F. D. Rocha. 'Quantum critical superconductors in string theory and M-theory'. *Phys. Lett.* B683 (2010), 201. arXiv: 0908.0011.

[178] C. Charmousis, B. Goutéraux, B. S. Kim, E. Kiritsis, and R. Meyer. 'Effective Holographic Theories for low-temperature condensed matter systems'. *J. High Energy Phys.* 1011 (2010), 151. arXiv: 1005.4690.

[179] S. S. Gubser. 'Curvature singularities: The Good, the bad, and the naked'. *Adv. Theor. Math. Phys.* 4 (2000), 679. arXiv: hep-th/0002160.

[180] U. Gürsoy, E. Kiritsis, and F. Nitti. 'Exploring improved holographic theories for QCD: Part II'. *J. High Energy Phys.* 0802 (2008), 019. arXiv: 0707.1349.

[181] U. Gürsoy, E. Kiritsis, L. Mazzanti, and F. Nitti. 'Holography and Thermodynamics of 5D Dilaton-gravity'. *J. High Energy Phys.* 0905 (2009), 033. arXiv: 0812.0792.

[182] S. Dodelson, W. H. Kinney, and E. W. Kolb. 'Cosmic microwave background measurements can discriminate among inflation models'. *Phys. Rev.* D56 (1997), 3207. arXiv: astro-ph/9702166.

[183] K. Enqvist and M. S. Sloth. 'Adiabatic CMB perturbations in pre-Big Bang string cosmology'. *Nucl. Phys.* B626 (2002), 395. arXiv: hep-ph/0109214.

[184] D. H. Lyth and D. Wands. 'Generating the curvature perturbation without an inflaton'. *Phys. Lett.* B524 (2002), 5. arXiv: hep-ph/0110002.

[185] T. Moroi and T. Takahashi. 'Effects of cosmological moduli fields on cosmic microwave background'. *Phys. Lett.* B522 (2001), 215. arXiv: hep-ph/0110096. Erratum: *ibid.* B539 (2002), 303.

[186] BICEP2/Keck and Planck collaborations, P. A. R. Ade et al. 'Joint Analysis of BICEP2/*Keck Array* and *Planck* Data'. *Phys. Rev. Lett.* 114 (2015), 101301. arXiv: 1502.00612.

[187] Planck collaboration, P. A. R. Ade et al. 'Planck 2015 Results. XVII. Constraints on primordial non-Gaussianity'. *Astronom. Astrophys.* 594 (2016), A17. arXiv: 1502.01592.

[188] A. A. Starobinsky. 'The Perturbation Spectrum Evolving from a Nonsingular Initially de Sitter Cosmology and the Microwave Background Anisotropy'. *Sov. Astron. Lett.* 9 (1983), 302.

[189] B. Whitt. 'Fourth Order Gravity as General Relativity Plus Matter'. *Phys. Lett.* B145 (1984), 176.

[190] S. Downes, B. Dutta, and K. Sinha. 'Attractors, Universality and Inflation'. *Phys. Rev.* D86 (2012), 103509. arXiv: 1203.6892.

[191] R. Kallosh, A. Linde, and D. Roest. 'Universal Attractor for Inflation at Strong Coupling'. *Phys. Rev. Lett.* 112 (2014), 011303. arXiv: 1310.3950.

[192] R. Kallosh, A. Linde, and D. Roest. 'Superconformal Inflationary $\alpha$-Attractors'. *J. High Energy Phys.* 1311 (2013), 198. arXiv: 1311.0472.

[193] A. Linde. 'Inflationary Cosmology after Planck 2013'. In: *Post-Planck Cosmology*. Ed. by C. Deffayet, P. Peter, B. Wandelt, M. Zaldarriaga, and L. F. Cugliandolo. Lecture Notes of the Les Houches Summer School 2013. Oxford, UK: OUP, 2015, p. 231. arXiv: 1402.0526.

[194] C. P. Burgess, M. Cicoli, and F. Quevedo. 'String Inflation After Planck 2013'. *J. Cosmol. Astropart. Phys.* 1311 (2013), 003. arXiv: 1306.3512.

[195] R. Kallosh and A. Linde. 'Universality Class in Conformal Inflation'. *J. Cosmol. Astropart. Phys.* 1307 (2013), 002. arXiv: 1306.5220.

[196] P. Fré, A. Sagnotti, and A. S. Sorin. 'Integrable Scalar Cosmologies I. Foundations and links with String Theory'. *Nucl. Phys.* B877 (2013), 1028. arXiv: 1307.1910.

[197] P. Binetruy, E. Kiritsis, J. Mabillard, M. Pieroni, and C. Rosset. 'Universality classes for models of inflation'. *J. Cosmol. Astropart. Phys.* 1504 (2015), 033. arXiv: 1407.0820.

[198] L. Boubekeur and D. Lyth. 'Hilltop inflation'. *J. Cosmol. Astropart. Phys.* 0507 (2005), 010. arXiv: hep-ph/0502047.

[199] K. Kohri, C.-M. Lin, and D. H. Lyth. 'More hilltop inflation models'. *J. Cosmol. Astropart. Phys.* 0712 (2007), 004. arXiv: 0707.3826.

[200] K. Freese, J. A. Frieman, and A. V. Olinto. 'Natural inflation with pseudo Nambu-Goldstone bosons'. *Phys. Rev. Lett.* 65 (1990), 3233.

[201] A. D. Linde. 'Coleman-Weinberg Theory and a New Inflationary Universe Scenario'. *Phys. Lett.* B114 (1982), 431.

[202] L. Järv, T. Mohaupt, and F. Saueressig. 'Quintessence cosmologies with a double exponential potential'. *J. Cosmol. Astropart. Phys.* 0408 (2004), 016. arXiv: hep-th/0403063.

[203] A. R. Liddle and D. H. Lyth. *Cosmological inflation and large scale structure*. Cambridge, UK: CUP, 2000. 416 pp.

[204] A. A. Starobinsky. 'Spectrum of relict gravitational radiation and the early state of the universe'. *J. Exp. Theor. Phys. Lett.* 30 (1979), 682. *Pis'ma Zh. Eksp. Teor. Fiz.* 30 (1979), 719.

[205] V. F. Mukhanov and G. V. Chibisov. 'Quantum Fluctuation and Nonsingular Universe'. *J. Exp. Theor. Phys. Lett.* 33 (1981), 532. *Pis'ma Zh. Eksp. Teor. Fiz.* 33 (1981), 549.

[206] H. Kodama and M. Sasaki. 'Cosmological Perturbation Theory'. *Prog. Theor. Phys. Suppl.* 78 (1984), 1.

[207] V. F. Mukhanov, H. A. Feldman, and R. H. Brandenberger. 'Theory of cosmological perturbations'. *Phys. Rept.* 215 (1992), 203.

[208] V. Mukhanov. 'Quantum Cosmological Perturbations: Predictions and Observations'. *Eur. Phys. J.* C73 (2013), 2486. arXiv: 1303.3925.

[209] H. Motohashi, A. A. Starobinsky, and J. Yokoyama. 'Inflation with a constant rate of roll'. *J. Cosmol. Astropart. Phys.* 1509 (2015), 018. arXiv: 1411.5021.

[210] I. Smolić. 'Symmetry inheritance of scalar fields'. *Class. Quantum Grav.* 32 (2015), 145010. arXiv: 1501.04967.

[211] M. Cvitan, P. Dominis Prester, and I. Smolić. 'Does three dimensional electromagnetic field inherit the spacetime symmetries?' *Class. Quantum Grav.* 33 (2016), 077001. arXiv: 1508.03343.

[212] I. Smolić. 'Constraints on the symmetry noninheriting scalar black hole hair'. *Phys. Rev.* D95 (2016), 024016. arXiv: 1609.04013.

[213] K. Menou, E. Quataert, and R. Narayan. 'Astrophysical evidence for black hole event horizons'. In: *Gravitation and Relativity: At the Turn of the Millennium, Proceedings of the GR-15 Conference*. (Pune, India, Dec. 16–21, 1997). Ed. by N. Dahdich and J. Narlikar. Pune, India: IUCAA, 1998, p. 43. arXiv: gr-qc/9803057.

[214] M. J. Rees. 'Astrophysical Evidence for Black Holes'. In: *Black Holes and Relativistic Stars. Proceedings of the Symposium dedicated to the memory of Subrahmanyan Chandrasekhar*. (Chicago, USA, Dec. 14–15, 1996). Ed. by R. M. Wald. Chicago; London: University of Chicago Press, 1998, p. 79. arXiv: astro-ph/9701161.

[215] R. Narayan, M. R. Garcia, and J. McClintock. 'X-ray Novae and the Evidence for Black Hole Event Horizons'. In: *Proceedings of the 9th Marcel Grossmann meeting*. (Rome, Italy, July 2–8, 2000). Ed. by V. G. Gurzadyan, R. T. Jantzen, and R. Ruffini. Singapore; River Edge, NJ: World Scientific, 2000, p. 405. arXiv: astro-ph/0107387.

[216] J. E. McClintock, R. Narayan, and G. B. Rybicki. 'On the lack of thermal emission from the quiescent black hole XTE J1118+480: Evidence for the event horizon'. *Astrophys. J.* 615 (2004), 402. arXiv: astro-ph/0403251.

[217] R. Narayan. 'Black holes in astrophysics'. *New J. Phys.* 7 (2005), 199. arXiv: gr-qc/0506078.

[218] A. E. Broderick and R. Narayan. 'On the nature of the compact dark mass at the galactic center'. *Astrophys. J.* 638 (2006), L21. arXiv: astro-ph/0512211.

[219] A. Müller. 'Experimental evidence of black holes'. In: *School on Particle Physics, Gravity and Cosmology*. (Dubrovnik, Croatia, Aug. 21–Sept. 2, 2006). Ed. by L. Bonora, R. Iengo, D. Klabucar, S. Pallua, and I. Picek. Vol. PoS (P2GC). Proceedings of Science. Trieste, Italy: SISSA, 2006, p. 017. arXiv: astro-ph/0701228.

[220] J. E. McClintock and R. A. Remillard. 'Black hole binaries'. In: *Compact Stellar X-Ray Sources*. Ed. by W. H. G. Lewin and M. van der Klis. Cambridge Astrophysics Series 39. Cambridge; New York: Cambridge University Press, 2006, p. 157. arXiv: astro-ph/0306213.

[221] M. A. Abramowicz, W. Kluzniak, and J.-P. Lasota. 'No observational proof of the black hole event-horizon'. *Astron. Astrophys.* 396 (2002), L31. arXiv: astro-ph/0207270.

[222] F. Pretorius. 'Evolution of binary black hole spacetimes'. *Phys. Rev. Lett.* 95 (2005), 121101. arXiv: gr-qc/0507014.

[223] A. Buonanno, G. B. Cook, and F. Pretorius. 'Inspiral, merger and ring-down of equal-mass black-hole binaries'. *Phys. Rev.* D75 (2007), 124018. arXiv: gr-qc/0610122.

[224] E. Berti, V. Cardoso, J. A. Gonzalez, U. Sperhake, M. Hannam, S. Husa, and B. Bruegmann. 'Inspiral, merger and ringdown of unequal mass black hole binaries: A multipolar analysis'. *Phys. Rev.* D76 (2007), 064034. arXiv: gr-qc/0703053.

[225] U. Sperhake, E. Berti, and V. Cardoso. 'Numerical simulations of black-hole binaries and gravitational wave emission'. *C. R. Acad. Sci.* 14 (2013), 306. arXiv: 1107.2819.

[226] L. Blanchet. 'Gravitational Radiation from Post-Newtonian Sources and Inspiralling Compact Binaries'. *Living Rev. Relat.* 17 (2014), 2. arXiv: 1310.1528.

[227] T. Baumgarte and S. Shapiro. *Numerical Relativity. Solving Einstein's Equations on the Computer*. Cambridge, UK: CUP, 2010. 698 pp.

[228] E. Gourgoulhon. *3+1 formalism and bases of numerical relativity*. Lecture notes. 2007. arXiv: gr-qc/0703035.

[229] M. Alcubierre. *Introduction to 3+1 Numerical Relativity*. International Series of Monographs on Physics. Oxford, UK: OUP, 2008. 444 pp.

[230] T. Regge and J. A. Wheeler. 'Stability of a Schwarzschild singularity'. *Phys. Rev.* 108 (1957), 1063.

[231] F. J. Zerilli. 'Effective potential for even parity Regge-Wheeler gravitational perturbation equations'. *Phys. Rev. Lett.* 24 (1970), 737.

[232] F. J. Zerilli. 'Gravitational field of a particle falling in a Schwarzschild geometry analyzed in tensor harmonics'. *Phys. Rev.* D2 (1970), 2141.

[233] F. J. Zerilli. 'Perturbation analysis for gravitational and electromagnetic radiation in a Reissner-Nordström geometry'. *Phys. Rev.* D9 (1974), 860.

[234] C. V. Vishveshwara. 'Stability of the Schwarzschild metric'. *Phys. Rev.* D1 (1970), 2870.

[235] K. D. Kokkotas and B. G. Schmidt. 'Quasinormal modes of stars and black holes'. *Living Rev. Relat.* 2 (1999), 2. arXiv: gr-qc/9909058.

[236] E. Berti, V. Cardoso, and A. O. Starinets. 'Quasinormal modes of black holes and black branes'. *Class. Quantum Grav.* 26 (2009), 163001. arXiv: 0905.2975.

[237] R. A. Konoplya and A. Zhidenko. 'Quasinormal modes of black holes: From astrophysics to string theory'. *Rev. Mod. Phys.* 83 (2011), 793. arXiv: 1102.4014.

[238] P. P. Fiziev. 'Exact solutions of Regge-Wheeler equation and quasi-normal modes of compact objects'. *Class. Quantum Grav.* 23 (2006), 2447. arXiv: gr-qc/0509123.

[239] S. Chandrasekhar. 'On the Equations Governing the Perturbations of the Schwarzschild Black Hole'. *Proc. R. Soc. Lond.* A343 (1975), 289.

[240] S. Chandrasekhar and S. L. Detweiler. 'The quasi-normal modes of the Schwarzschild black hole'. *Proc. R. Soc. Lond.* A344 (1975), 441.

[241] S. L. Detweiler. 'Black Holes and Gravitational Waves. III. The Resonant Frequencies of Rotating Holes'. *Astrophys. J.* 239 (1980), 292.

[242] E. W. Leaver. 'An analytic representation for the quasi normal modes of Kerr black holes'. *Proc. R. Soc. Lond.* A402 (1985), 285.

[243] H. Onozawa. 'A detailed study of quasinormal frequencies of the Kerr black hole'. *Phys. Rev.* D55 (1997), 3593. arXiv: gr-qc/9610048.

[244] E. Berti, V. Cardoso, K. D. Kokkotas, and H. Onozawa. 'Highly damped quasinormal modes of Kerr black holes'. *Phys. Rev.* D68 (2003), 124018. arXiv: hep-th/0307013.

[245] J. Steinhoff, T. Hinderer, A. Buonanno, and A. Taracchini. 'Dynamical Tides in General Relativity: Effective Action and Effective-One-Body Hamiltonian'. *Phys. Rev.* D94 (2016), 104028. arXiv: 1608.01907.

[246] A. E. H. Love. *Some Problems of Geodynamics*. Cambridge: CUP, 1911. 210 pp.

[247] H. Fang and G. Lovelace. 'Tidal coupling of a Schwarzschild black hole and circularly orbiting moon'. *Phys. Rev.* D72 (2005), 124016. arXiv: gr-qc/0505156.

[248] T. Hinderer. 'Tidal Love numbers of neutron stars'. *Astrophys. J.* 677 (2008), 1216. arXiv: 0711.2420. Erratum: *ibid.* 697 (2009), 964.

[249] T. Damour and A. Nagar. 'Relativistic tidal properties of neutron stars'. *Phys. Rev.* D80 (2009), 084035. arXiv: 0906.0096.

[250] T. Binnington and E. Poisson. 'Relativistic theory of tidal Love numbers'. *Phys. Rev.* D80 (2009), 084018. arXiv: 0906.1366.

[251] N. Gürlebeck. 'No-hair theorem for Black Holes in Astrophysical Environments'. *Phys. Rev. Lett.* 114 (2015), 151102. arXiv: 1503.03240.

[252] E. Poisson. 'Tidal deformation of a slowly rotating black hole'. *Phys. Rev.* D91 (2015), 044004. arXiv: 1411.4711.

[253] P. Pani, L. Gualtieri, A. Maselli, and V. Ferrari. 'Tidal deformations of a spinning compact object'. *Phys. Rev.* D92 (2015), 024010. arXiv: 1503.07365.

[254] P. Landry and E. Poisson. 'Tidal deformation of a slowly rotating material body. External metric'. *Phys. Rev.* D91 (2015), 104018. arXiv: 1503.07366.

[255] R. P. Geroch. 'Multipole moments. II. Curved space'. *J. Math. Phys.* 11 (1970), 2580.

[256] R. O. Hansen. 'Multipole moments of stationary space-times'. *J. Math. Phys.* 15 (1974), 46.

[257] Y. Gürsel. 'Multipole moments for stationary systems: The equivalence of the Geroch-Hansen formulation and the Thorne formulation'. *Gen. Rel. Gravit.* 15 (1983), 737.

[258] K. S. Thorne. 'Multipole Expansions of Gravitational Radiation'. *Rev. Mod. Phys.* 52 (1980), 299.

[259] P. Pani, L. Gualtieri, and V. Ferrari. 'Tidal Love numbers of a slowly spinning neutron star'. *Phys. Rev.* D92 (2015), 124003. arXiv: 1509.02171.

[260] P. Landry and E. Poisson. 'Dynamical response to a stationary tidal field'. *Phys. Rev.* D92 (2015), 124041. arXiv: 1510.09170.

[261] J. Keir. 'Slowly decaying waves on spherically symmetric spacetimes and ultracompact neutron stars'. *Class. Quantum Grav.* 33 (2016), 135009. arXiv: 1404.7036.

[262] V. Cardoso, L. C. B. Crispino, C. F. B. Macedo, H. Okawa, and P. Pani. 'Light rings as observational evidence for event horizons: long-lived modes, ergoregions and nonlinear instabilities of ultracompact objects'. *Phys. Rev.* D90 (2014), 044069. arXiv: 1406.5510.

[263] J. L. Friedman. 'Ergosphere instability'. *Comm. Math. Phys.* 63 (1978), 243.

[264] G. Dotti, R. Gleiser, and J. Pullin. 'Instability of charged and rotating naked singularities'. *Phys. Lett.* B644 (2007), 289. arXiv: gr-qc/0607052.

[265] V. Cardoso, P. Pani, M. Cadoni, and M. Cavaglià. 'Ergoregion instability of ultracompact astrophysical objects'. *Phys. Rev.* D77 (2008), 124044. arXiv: 0709.0532.

[266] G. Dotti, R. J. Gleiser, I. F. Ranea-Sandoval, and H. Vucetich. 'Gravitational instabilities in Kerr space times'. *Class. Quantum Grav.* 25 (2008), 245012. arXiv: 0805.4306.

[267] V. Cardoso, P. Pani, M. Cadoni, and M. Cavaglià. 'Instability of hyper-compact Kerr-like objects'. *Class. Quantum Grav.* 25 (2008), 195010. arXiv: 0808.1615.

[268] P. Pani, E. Barausse, E. Berti, and V. Cardoso. 'Gravitational instabilities of superspinars'. *Phys. Rev.* D82 (2010), 044009. arXiv: 1006.1863.

[269] E. Barausse, V. Cardoso, and P. Pani. 'Can environmental effects spoil precision gravitational-wave astrophysics?' *Phys. Rev.* D89 (2014), 104059. arXiv: 1404.7149.

[270] F. H. Vincent, Z. Meliani, P. Grandclément, E. Gourgoulhon, and O. Straub. 'Imaging a boson star at the Galactic center'. *Class. Quantum Grav.* 33 (2016), 105015. arXiv: 1510.04170.

[271] C. F. B. Macedo, P. Pani, V. Cardoso, and L. C. B. Crispino. 'Into the lair: gravitational-wave signatures of dark matter'. *Astrophys. J.* 774 (2013), 48. arXiv: 1302.2646.

[272] E. W. Mielke and F. E. Schunck. 'Boson stars: Alternatives to primordial black holes?' *Nucl. Phys.* B564 (2000), 185. arXiv: gr-qc/0001061.

[273] F. S. Guzmán and J. M. Rueda-Becerril. 'Spherical boson stars as black hole mimickers'. *Phys. Rev.* D80 (2009), 084023. arXiv: 1009.1250.

[274] H. G. Ellis. 'Ether flow through a drainhole. A particle model in general relativity'. *J. Math. Phys.* 14 (1973), 104.

[275] M. Visser. *Lorentzian wormholes. From Einstein to Hawking*. Woodbury, USA: AIP, 1996. 412 pp.

[276] M. Visser. 'Traversable wormholes: Some simple examples'. *Phys. Rev.* D39 (1989), 3182. arXiv: 0809.0907.

[277] M. Visser. 'Traversable wormholes from surgically modified Schwarzschild space-times'. *Nucl. Phys.* B328 (1989), 203. arXiv: 0809.0927.

[278] M. S. Morris, K. S. Thorne, and U. Yurtsever. 'Wormholes, Time Machines, and the Weak Energy Condition'. *Phys. Rev. Lett.* 61 (1988), 1446.

[279] P. Kanti, B. Kleihaus, and J. Kunz. 'Wormholes in Dilatonic Einstein-Gauss-Bonnet Theory'. *Phys. Rev. Lett.* 107 (2011), 271101. arXiv: 1108.3003.

[280] T. Damour and S. N. Solodukhin. 'Wormholes as black hole foils'. *Phys. Rev.* D76 (2007), 024016. arXiv: 0704.2667.

[281] V. Dzhunushaliev, V. Folomeev, B. Kleihaus, and J. Kunz. 'Can mixed star-plus-wormhole systems mimic black holes?' *J. Cosmol. Astropart. Phys.* 1608 (2016), 030. arXiv: 1601.04124.

[282] P. O. Mazur and E. Mottola. 'Gravitational condensate stars: An alternative to black holes'. (2001). arXiv: gr-qc/0109035.

[283] P. O. Mazur and E. Mottola. 'Gravitational vacuum condensate stars'. *Proc. Nat. Acad. Sci.* 101 (2004), 9545. arXiv: gr-qc/0407075.

[284] M. Visser and D. L. Wiltshire. 'Stable gravastars: An alternative to black holes?' *Class. Quantum Grav.* 21 (2004), 1135. arXiv: gr-qc/0310107.

[285] E. G. Gimon and P. Hořava. 'Astrophysical violations of the Kerr bound as a possible signature of string theory'. *Phys. Lett.* B672 (2009), 299. arXiv: 0706.2873.

[286] E. Seidel and W. M. Suen. 'Oscillating soliton stars'. *Phys. Rev. Lett.* 66 (1991), 1659.

[287] T. D. Lee and Y. Pang. 'Nontopological solitons'. *Phys. Rept.* 221 (1992), 251.

[288] P. Jetzer. 'Boson stars'. *Phys. Rept.* 220 (1992), 163.

[289] N. Straumann. 'Fermion and boson stars'. In: *Proceedings of the 81st WE-Heraeus-Seminar*. (Bad Honnef, Germany, Sept. 2–6, 1991). Ed. by J. Ehlers and G. Schäfer. Lecture Notes in Physics 410. Berlin; New York: Springer, 1992, p. 267.

[290] A. R. Liddle and M. S. Madsen. 'The structure and formation of boson stars'. *Int. J. Mod. Phys.* D1 (1992), 101.

[291] E. W. Mielke and F. E. Schunck. 'Boson stars: Early history and recent prospects'. In: *Proceedings of the 8th Marcel Grossmann meeting*. (Jerusalem, Israel, June 22–27, 1997). Ed. by T. Piran and R. Ruffini. Singapore: World Scientific, 1999, p. 1607. arXiv: gr-qc/9801063.

[292] E. W. Mielke and F. E. Schunck. 'Boson and axion stars'. In: *Proceedings of the 9th Marcel Grossmann meeting*. (Rome, Italy, July 2–8, 2000). Ed. by V. G. Gurzadyan, R. T. Jantzen, and R. Ruffini. Singapore: World Scientific, 2002, p. 581.

[293] F. E. Schunck and E. W. Mielke. 'General relativistic boson stars'. *Class. Quantum Grav.* 20 (2003), R301. arXiv: 0801.0307.

[294] S. L. Liebling and C. Palenzuela. 'Dynamical Boson Stars'. *Living Rev. Relat.* 15 (2012), 6. arXiv: 1202.5809.

[295] G. H. Derrick. 'Comments on nonlinear wave equations as models for elementary particles'. *J. Math. Phys.* 5 (1964), 1252.

[296] R. Sharma, S. Karmakar, and S. Mukherjee. 'Boson star and dark matter'. (2008). arXiv: 0812.3470.

[297] J.-W. Lee. 'Is dark matter a BEC or scalar field?' *J. Korean Phys. Soc.* 54 (2009), 2622. arXiv: 0801.1442.

[298] R. Brito, V. Cardoso, and H. Okawa. 'Accretion of dark matter by stars'. *Phys. Rev. Lett.* 115 (2015), 111301. arXiv: 1508.04773.

[299] R. Brito, V. Cardoso, C. F. B. Macedo, H. Okawa, and C. Palenzuela. 'Interaction between bosonic dark matter and stars'. *Phys. Rev.* D93 (2016), 044045. arXiv: 1512.00466.

[300] D. J. Kaup. 'Klein-Gordon Geon'. *Phys. Rev.* 172 (1968), 1331.

[301] R. Ruffini and S. Bonazzola. 'Systems of selfgravitating particles in general relativity and the concept of an equation of state'. *Phys. Rev.* 187 (1969), 1767.

[302] M. Colpi, S. L. Shapiro, and I. Wasserman. 'Boson Stars: Gravitational Equilibria of Selfinteracting Scalar Fields'. *Phys. Rev. Lett.* 57 (1986), 2485.

[303] T. D. Lee. 'Soliton Stars and the Critical Masses of Black Holes'. *Phys. Rev.* D35 (1987), 3637.

[304] R. Friedberg, T. D. Lee, and Y. Pang. 'Mini-soliton stars'. *Phys. Rev.* D35 (1987), 3640.

[305] R. Friedberg, T. D. Lee, and Y. Pang. 'Scalar Soliton Stars and Black Holes'. *Phys. Rev.* D35 (1987), 3658.

[306] F. E. Schunck and E. W. Mielke. 'Rotating boson stars'. In: *Proceedings of the 152nd WE-Heraeus-Seminar*. (Bad Honnef, Germany, Sept. 18–22, 1995). Ed. by F. W. Hehl, R. Puntigam, and H. Ruder. Berlin; New York: Springer, 1996, p. 138.

[307] S. Yoshida and Y. Eriguchi. 'Rotating boson stars in general relativity'. *Phys. Rev.* D56 (1997), 762.

[308] A. B. Henriques, A. R. Liddle, and R. G. Moorhouse. 'Combined Boson-Fermion Stars'. *Phys. Lett.* B233 (1989), 99.

[309] A. B. Henriques, A. R. Liddle, and R. G. Moorhouse. 'Combined Boson-Fermion Stars: Configurations and Stability'. *Nucl. Phys.* B337 (1990), 737.

[310] R. Brito, V. Cardoso, C. A. R. Herdeiro, and E. Radu. 'Proca stars: Gravitating Bose-Einstein condensates of massive spin 1 particles'. *Phys. Lett.* B752 (2016), 291. arXiv: 1508.05395.

[311] J. A. Wheeler. 'Geons'. *Phys. Rev.* 97 (1955), 511.

[312] R. Ferrell and M. Gleiser. 'Gravitational Atoms. I. Gravitational Radiation From Excited Boson Stars'. *Phys. Rev.* D40 (1989), 2524.

[313] M. Gleiser. 'Stability of Boson Stars'. *Phys. Rev.* D38 (1988), 2376. Erratum: *ibid.* D39 (1989), 1257.

[314] T. D. Lee and Y. Pang. 'Stability of Mini-Boson Stars'. *Nucl. Phys.* B315 (1989), 477.

[315] P. Jetzer. 'Dynamical Instability of Bosonic Stellar Configurations'. *Nucl. Phys.* B316 (1989), 411.

[316] M. Gleiser and R. Watkins. 'Gravitational Stability of Scalar Matter'. *Nucl. Phys.* B319 (1989), 733.

[317] S. H. Hawley and M. W. Choptuik. 'Boson stars driven to the brink of black hole formation'. *Phys. Rev.* D62 (2000), 104024. arXiv: gr-qc/0007039.

[318] F. V. Kusmartsev, E. W. Mielke, and F. E. Schunck. 'Gravitational stability of boson stars'. *Phys. Rev.* D43 (1991), 3895. arXiv: 0810.0696.

[319] Y. Brihaye and B. Hartmann. 'Minimal boson stars in 5 dimensions: classical instability and existence of ergoregions'. *Class. Quantum Grav.* 33 (2016), 065002. arXiv: 1509.04534.

[320] S. H. Hawley and M. W. Choptuik. 'Numerical evidence for 'multi-scalar stars''. *Phys. Rev.* D67 (2003), 024010. arXiv: gr-qc/0208078.

[321] A. Bernal, J. Barranco, D. Alic, and C. Palenzuela. 'Multi-state Boson Stars'. *Phys. Rev.* D81 (2010), 044031. arXiv: 0908.2435.

[322] C. F. B. Macedo, P. Pani, V. Cardoso, and L. C. B. Crispino. 'Astrophysical signatures of boson stars: quasinormal modes and inspiral resonances'. *Phys. Rev.* D88 (2013), 064046. arXiv: 1307.4812.

[323] A. B. Henriques, A. R. Liddle, and R. G. Moorhouse. 'Stability of boson-fermion stars'. *Phys. Lett.* B251 (1990), 511.

[324] S. Valdez-Alvarado, C. Palenzuela, D. Alic, and L. A. Ureña-López. 'Dynamical evolution of fermion-boson stars'. *Phys. Rev.* D87 (2013), 084040. arXiv: 1210.2299.

[325] A. Toomre and J. Toomre. 'Galactic bridges and tails'. *Astrophys. J.* 178 (1972), 623.

[326] W. H. Press and S. A. Teukolsky. 'On formation of close binaries by two-body tidal capture'. *Astrophys. J.* 213 (1977), 183.

[327] C. Murray and S. Dermott. *Solar System Dynamics*. Cambridge, UK: CUP, 1999. 592 pp.

[328] É. É. Flanagan and T. Hinderer. 'Constraining neutron star tidal Love numbers with gravitational wave detectors'. *Phys. Rev.* D77 (2008), 021502. arXiv: 0709.1915.

[329] T. Hinderer et al. 'Effects of neutron-star dynamic tides on gravitational waveforms within the effective-one-body approach'. *Phys. Rev. Lett.* 116 (2016), 181101. arXiv: 1602.00599.

[330] J. Lattimer and M. Prakash. 'The physics of neutron stars'. *Science* 304 (2004), 536. arXiv: astro-ph/0405262.

[331] T. Hinderer, B. D. Lackey, R. N. Lang, and J. S. Read. 'Tidal deformability of neutron stars with realistic equations of state and their gravitational wave signatures in binary inspiral'. *Phys. Rev.* D81 (2010), 123016. arXiv: 0911.3535.

[332] S. Postnikov, M. Prakash, and J. M. Lattimer. 'Tidal Love Numbers of Neutron and Self-Bound Quark Stars'. *Phys. Rev.* D82 (2010), 024016. arXiv: 1004.5098.

[333] J. Vines, É. É. Flanagan, and T. Hinderer. 'Post-1-Newtonian tidal effects in the gravitational waveform from binary inspirals'. *Phys. Rev.* D83 (2011), 084051. arXiv: 1101.1673.

[334] T. Damour, A. Nagar, and L. Villain. 'Measurability of the tidal polarizability of neutron stars in late-inspiral gravitational-wave signals'. *Phys. Rev.* D85 (2012), 123007. arXiv: 1203.4352.

[335] W. Del Pozzo, T. G. F. Li, M. Agathos, C. Van Den Broeck, and S. Vitale. 'Demonstrating the feasibility of probing the neutron star equation of state with second-generation gravitational wave detectors'. *Phys. Rev. Lett.* 111 (2013), 071101. arXiv: 1307.8338.

[336] A. Maselli, L. Gualtieri, and V. Ferrari. 'Constraining the equation of state of nuclear matter with gravitational wave observations: Tidal deformability and tidal disruption'. *Phys. Rev.* D88 (2013), 104040. arXiv: 1310.5381.

[337] R. A. Porto. 'The effective field theorist's approach to gravitational dynamics'. *Phys. Rept.* 633 (2016), 1. arXiv: 1601.04914.

[338] R. A. Porto. 'The Tune of Love and the Nature(ness) of Spacetime'. *Fortsch. Phys.* 64 (2016), 723. arXiv: 1606.08895.

[339] K. Skenderis and M. Taylor. 'The fuzzball proposal for black holes'. *Phys. Rept.* 467 (2008), 117. arXiv: 0804.0552.

[340] B. Holdom and J. Ren. 'Not quite a black hole'. (2016). arXiv: 1612.04889.

[341] M. Saravani, N. Afshordi, and R. B. Mann. 'Empty black holes, firewalls, and the origin of Bekenstein-Hawking entropy'. *Int. J. Mod. Phys.* D23 (2015), 1443007. arXiv: 1212.4176.

[342] J. Abedi, H. Dykaar, and N. Afshordi. 'Echoes from the Abyss: Evidence for Planck-scale structure at black hole horizons'. (2016). arXiv: 1612.00266.

[343] S. B. Giddings. 'Possible observational windows for quantum effects from black holes'. *Phys. Rev.* D90 (2014), 124033. arXiv: 1406.7001.

[344] N. Uchikata and S. Yoshida. 'Slowly rotating thin shell gravastars'. *Class. Quantum Grav.* 33 (2016), 025005. arXiv: 1506.06485.

[345] P. Pani. 'I-Love-Q relations for gravastars and the approach to the black-hole limit'. *Phys. Rev.* D92 (2015), 124030. arXiv: 1506.06050.

[346] N. Uchikata, S. Yoshida, and P. Pani. 'Tidal deformability and I-Love-Q relations for gravastars with polytropic thin shells'. *Phys. Rev.* D94 (2016), 064015. arXiv: 1607.03593.

[347] P. Pani, E. Berti, V. Cardoso, Y. Chen, and R. Norte. 'Gravitational wave signatures of the absence of an event horizon. I. Nonradial oscillations of a thin-shell gravastar'. *Phys. Rev.* D80 (2009), 124047. arXiv: 0909.0287.

[348] G. F. Giudice, M. McCullough, and A. Urbano. 'Hunting for Dark Particles with Gravitational Waves'. *J. Cosmol. Astropart. Phys.* 1610 (2016), 001. arXiv: 1605.01209.

[349] V. Cardoso, C. F. B. Macedo, P. Pani, and V. Ferrari. 'Black holes and gravitational waves in models of minicharged dark matter'. *J. Cosmol. Astropart. Phys.* 1605 (2016), 054. arXiv: 1604.07845.

[350] T. P. Sotiriou and V. Faraoni. 'Black holes in scalar-tensor gravity'. *Phys. Rev. Lett.* 108 (2012), 081103. arXiv: 1109.6324.

[351] E. Barausse and T. P. Sotiriou. 'Perturbed Kerr Black Holes can probe deviations from General Relativity'. *Phys. Rev. Lett.* 101 (2008), 099001. arXiv: 0803.3433.

[352] C. Herdeiro, E. Radu, and H. Runarsson. 'Kerr black holes with Proca hair'. *Class. Quantum Grav.* 33 (2016), 154001. arXiv: 1603.02687.

[353] R. Brito, V. Cardoso, and P. Pani. 'Black holes as particle detectors: evolution of superradiant instabilities'. *Class. Quantum Grav.* 32 (2015), 134001. arXiv: 1411.0686.

[354] R. Brito, V. Cardoso, and P. Pani. 'Superradiance'. *Lecture Notes in Physics* 906 (2015), 1. arXiv: 1501.06570.

[355] N. Yunes and L. C. Stein. 'Non-Spinning Black Holes in Alternative Theories of Gravity'. *Phys. Rev.* D83 (2011), 104002. arXiv: 1101.2921.

[356] P. Pani, C. F. B. Macedo, L. C. B. Crispino, and V. Cardoso. 'Slowly rotating black holes in alternative theories of gravity'. *Phys. Rev.* D84 (2011), 087501. arXiv: 1109.3996.

[357] S. Mignemi and N. R. Stewart. 'Charged black holes in effective string theory'. *Phys. Rev.* D47 (1993), 5259. arXiv: hep-th/9212146.

[358] P. Kanti, N. E. Mavromatos, J. Rizos, K. Tamvakis, and E. Winstanley. 'Dilatonic black holes in higher curvature string gravity'. *Phys. Rev.* D54 (1996), 5049. arXiv: hep-th/9511071.

[359] P. Pani and V. Cardoso. 'Are black holes in alternative theories serious astrophysical candidates? The Case for Einstein-Dilaton-Gauss-Bonnet black holes'. *Phys. Rev.* D79 (2009), 084031. arXiv: 0902.1569.

[360] N. Yunes and F. Pretorius. 'Dynamical Chern-Simons Modified Gravity. I. Spinning Black Holes in the Slow-Rotation Approximation'. *Phys. Rev.* D79 (2009), 084043. arXiv: 0902.4669.

[361] S. Alexander and N. Yunes. 'Chern-Simons Modified General Relativity'. *Phys. Rept.* 480 (2009), 1. arXiv: 0907.2562.

[362] V. Cardoso, S. Hopper, C. F. B. Macedo, C. Palenzuela, and P. Pani. 'Echoes of ECOs: gravitational-wave signatures of exotic compact objects and of quantum corrections at the horizon scale'. *Phys. Rev.* D94 (2016), 084031. arXiv: 1608.08637.

[363] M. Punturo et al. 'The Einstein Telescope: A third-generation gravitational wave observatory'. In: *Proceedings of the 14th Workshop on Gravitational wave data analysis*. (Rome, Italy, Jan. 26–29, 2010). Class. Quantum Grav. 27. 2010, p. 194002.

[364] P. Amaro-Seoane, S. Aoudia, S. Babak, P. Binetruy, E. Berti, et al. 'Low-frequency gravitational-wave science with eLISA/NGO'. *Class. Quantum Grav.* 29 (2012), 124016. arXiv: 1202.0839.

[365] R. F. P. Mendes and H. Yang. 'Tidal deformability of dark matter clumps'. (2016). arXiv: 1606.03035.

[366] W. Israel. 'Singular hypersurfaces and thin shells in general relativity'. *Nuovo Cim.* B44 (1966), 1. Erratum: *ibid.* B48 (1967), 463.

[367] M. Vallisneri. 'Use and abuse of the Fisher information matrix in the assessment of gravitational wave parameter estimation prospects'. *Phys. Rev.* D77 (2008), 042001. arXiv: gr-qc/0703086.

[368] T. Damour, B. R. Iyer, and B. S. Sathyaprakash. 'Frequency domain *P*-approximant filters for time truncated inspiral gravitational wave signals from compact binaries'. *Phys. Rev.* D62 (2000), 084036. arXiv: gr-qc/0001023.

[369] D. Bini, T. Damour, and G. Faye. 'Effective action approach to higher-order relativistic tidal interactions in binary systems and their effective one body description'. *Phys. Rev.* D85 (2012), 124034. arXiv: 1202.3565.

[370] LIGO collaboration, D. Shoemaker. *Advanced LIGO anticipated sensitivity curves*. Tech. rep. T0900288-v3. 2010. URL: https://dcc.ligo.org/LIGO-T0900288/public.

[371] B. S. Sathyaprakash and B. F. Schutz. 'Physics, Astrophysics and Cosmology with Gravitational Waves'. *Living Rev. Relat.* 12 (2009), 2. arXiv: 0903.0338.

[372] A. Klein, E. Barausse, A. Sesana, A. Petiteau, E. Berti, S. Babak, J. Gair, S. Aoudia, I. Hinder, F. Ohme, and B. Wardell. 'Science with the space-based interferometer eLISA: Supermassive black hole binaries'. *Phys. Rev.* D93 (2016), 024003. arXiv: 1511.05581.

[373] E. Berti, A. Buonanno, and C. M. Will. 'Estimating spinning binary parameters and testing alternative theories of gravity with LISA'. *Phys. Rev.* D71 (2005), 084025. arXiv: gr-qc/0411129.

[374] LIGO Scientific and Virgo collaboration, B. P. Abbott et al. 'Binary Black Hole Mergers in the first Advanced LIGO Observing Run'. *Phys. Rev.* X6 (2016), 041015. arXiv: 1606.04856.

[375] V. Ferrari and K. D. Kokkotas. 'Scattering of particles by neutron stars: Time evolutions for axial perturbations'. *Phys. Rev.* D62 (2000), 107504. arXiv: gr-qc/0008057.

[376] W. H. Press. 'Long Wave Trains of Gravitational Waves from a Vibrating Black Hole'. *Astrophys. J.* 170 (1971), L105.

[377] C. J. Goebel. 'Comments on the "vibrations" of a black hole'. *Astrophys. J.* 172 (1972), L95.

[378] V. Ferrari and B. Mashhoon. 'New approach to the quasinormal modes of a black hole'. *Phys. Rev.* D30 (1984), 295.

[379] V. Cardoso, A. S. Miranda, E. Berti, H. Witek, and V. T. Zanchin. 'Geodesic stability, Lyapunov exponents and quasinormal modes'. *Phys. Rev.* D79 (2009), 064016. arXiv: 0812.1806.

[380] P. T. Leung, Y. T. Liu, W. M. Suen, C. Y. Tam, and K. Young. 'Quasinormal modes of dirty black holes'. *Phys. Rev. Lett.* 78 (1997), 2894. arXiv: gr-qc/9903031.

[381] E. Barausse, V. Cardoso, and P. Pani. 'Environmental Effects for Gravitational-wave Astrophysics'. *J. Phys. Conf. Ser.* 610 (2015), 012044. arXiv: 1404.7140.

[382] P. Pani. 'Advanced Methods in Black-Hole Perturbation Theory'. *Int. J. Mod. Phys.* A28 (2013), 1340018. arXiv: 1305.6759.

[383] S. Chandrasekhar and V. Ferrari. 'On the non-radial oscillations of a star. III: A reconsideration of the axial modes'. *Proc. R. Soc.* A434 (1991), 449.

[384] S. Chandrasekhar and V. Ferrari. 'On the non-radial oscillations of a star. IV: An application of the theory of Regge poles'. *Proc. R. Soc.* A437 (1992), 133.

[385] M. A. Abramowicz, M. Bruni, S. Sonego, N. Andersson, and P. Ghosh. 'Gravitational waves from ultracompact stars: The optical geometry view of trapped modes'. *Class. Quantum Grav.* 14 (1997), L189.

[386] J. A. Pons, E. Berti, L. Gualtieri, G. Miniutti, and V. Ferrari. 'Gravitational signals emitted by a point mass orbiting a neutron star: Effects of stellar structure'. *Phys. Rev.* D65 (2002), 104021. arXiv: gr-qc/0111104.

[387] E. Berti, V. Cardoso, and P. Pani. 'Breit-Wigner resonances and the quasinormal modes of anti-de Sitter black holes'. *Phys. Rev.* D79 (2009), 101501. arXiv: 0903.5311.

[388] R. H. Price. 'Nonspherical perturbations of relativistic gravitational collapse. I. Scalar and gravitational perturbations'. *Phys. Rev.* D5 (1972), 2419.

[389] S. B. Giddings. 'Gravitational wave tests of quantum modifications to black hole structure – with post-GW150914 update'. *Class. Quantum Grav.* 33 (2016), 235010. arXiv: 1602.03622.

[390] LIGO Scientific collaboration, J. Aasi et al. 'Advanced LIGO'. *Class. Quantum Grav.* 32 (2015), 074001. arXiv: 1411.4547.

[391] Virgo collaboration, F. Acernese et al. 'Advanced Virgo: a second-generation interferometric gravitational wave detector'. *Class. Quantum Grav.* 32 (2015), 024001. arXiv: 1408.3978.

[392] KAGRA collaboration, K. Somiya. 'Detector configuration of KAGRA: The Japanese cryogenic gravitational-wave detector'. *Class. Quantum Grav.* 29 (2012), 124007. arXiv: 1111.7185.

[393] C. B. M. H. Chirenti and L. Rezzolla. 'On the ergoregion instability in rotating gravastars'. *Phys. Rev.* D78 (2008), 084011. arXiv: 0808.4080.

[394] R. Konoplya and A. Zhidenko. 'Detection of gravitational waves from black holes: Is there a window for alternative theories?' *Phys. Lett.* B756 (2016), 350. arXiv: 1602.04738.

[395] J. L. Blázquez-Salcedo, C. F. B. Macedo, V. Cardoso, V. Ferrari, L. Gualtieri, F. S. Khoo, J. Kunz, and P. Pani. 'Perturbed black holes in Einstein-dilaton-Gauss-Bonnet gravity: Stability, ringdown, and gravitational-wave emission'. *Phys. Rev.* D94 (2016), 104024. arXiv: 1609.01286.

[396] C. Chirenti and L. Rezzolla. 'Did GW150914 produce a rotating gravastar?' *Phys. Rev.* D94 (2016), 084016. arXiv: 1602.08759.